



January 2019

Characterization Of Dopamine Transporter Amino Terminal Palmitoylation And Neurotoxic Substrate Activity

Daniel Jacob Stanislawski

Follow this and additional works at: <https://commons.und.edu/theses>

Recommended Citation

Stanislawski, Daniel Jacob, "Characterization Of Dopamine Transporter Amino Terminal Palmitoylation And Neurotoxic Substrate Activity" (2019). *Theses and Dissertations*. 2867.
<https://commons.und.edu/theses/2867>

This Dissertation is brought to you for free and open access by the Theses, Dissertations, and Senior Projects at UND Scholarly Commons. It has been accepted for inclusion in Theses and Dissertations by an authorized administrator of UND Scholarly Commons. For more information, please contact zeineb.yousif@library.und.edu.

CHARACTERIZATION OF DOPAMINE TRANSPORTER AMINO TERMINAL
PALMITOYLATION AND NEUROTOXIC SUBSTRATE ACTIVITY

by

Daniel Jacob Stanislawski

Bachelor of Science, University of North Dakota, 2012

A Dissertation

Submitted to the Graduate Faculty

of the

University of North Dakota

in partial fulfillment of the requirements

for the degree of

Doctor of Philosophy

Grand Forks, North Dakota

December

2019

Copyright 2019 Daniel J. Stanislawski

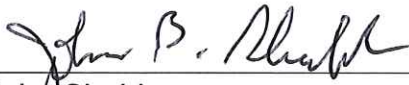
This dissertation, submitted by Daniel J. Stanislawski in partial fulfillment of the requirements for the Degree of Doctor of Philosophy from the University of North Dakota, has been read by the Faculty Advisory Committee under whom the work has been done and is hereby approved.



James D. Foster, Chairperson


Roxanne A. Vaughan


L. Keith Henry


Eric Murphy


John Shabb


Manu Manu

This dissertation is being submitted by the appointed advisory committee as having met all of the requirements of the school of Graduate Studies at the University of North Dakota and is hereby approved.


Dean of the School of Graduate Studies

11/22/19
Date

PERMISSION

Title: Characterization of dopamine transporter amino terminal palmitoylation and neurotoxic substrate activity

Department: Biochemistry and Molecular Biology

Degree: Doctor of Philosophy

In presenting this dissertation in partial fulfillment of the requirements for a graduate degree from the University of North Dakota, I agree that the library of this University shall make it freely available for inspection. I further agree that permission for extensive copying for scholarly purposes may be granted by the professor who supervised my dissertation work or, in his absence, by the Chairperson of the department or the dean of the School of Graduate Studies. It is understood that any copying or publication or other use of this dissertation or part thereof for financial gain shall not be allowed without my written permission. It is also understood that due recognition shall be given to me and to the University of North Dakota in any scholarly use which may be made of any material in my dissertation.

Daniel J. Stanislowski

December, 2019

TABLE OF CONTENTS

LIST OF FIGURES	ix
LIST OF TABLES	xiii
ACKNOWLEDGEMENTS.....	xiv
ABSTRACT	xviii
CHAPTER	
1. INTRODUCTION.....	1
Dopamine	1
Preface – The Modern Soma.....	1
Pavlov, Skinner, Learning, Behavior, and...Advertising?	5
Synthesis, Exocytotic Release, and Receptors	12
The Dopamine Transporter	17
Structure and Mechanism of DA Transport.....	17
Regulation	24
DAT-Mediated DA Efflux.....	32
DAT Disease Association	32
S-Palmitoylation	36
Overview.....	36
The Acyl-Biotinyl Exchange	41
DAT Palmitoylation	43
2. DAT N-TERMINAL PALMITOYLATION AND THIS MODIFICATION'S EFFECT ON DOPAMINE EFFLUX.....	47

Abstract	47
Introduction.....	48
Results	52
Acyl-Biotinyl Exchange Analysis of Cys to Ala Point Mutant Palmitoylation	52
Palmitoylation of Single Intracellular Cys rDATs.....	53
Palmitoylation of DATs with or without the Putative Palmitoylation Sites	56
In Vivo Palmitoylation of the rDAT N-terminal Peptide	56
Cyanogen Bromide (CNBr) Digestion and ABE Analysis of the rDAT N-terminus	58
CNBr Proteolytic Mapping of Cys to Ala rDATs Expressed in LLC _{PK} ₁ Cells	62
Analysis of Cys90 Palmitoylation	65
Surface Expression Analysis of Palmitoylation- Deficient rDATs.....	65
DA Uptake Saturation Kinetics of Palmitoylation Deficient rDATs.....	69
Global Palmitoylation Inhibition with 2BP Effect on DA Uptake	75
Palmitoylation Deficient rDATs Display Altered DA efflux	77
Global Palmitoylation Inhibition by 2BP Effect on DA Efflux.....	81
Discussion	82
Methods.....	98
Cell Culture and Site Directed Mutagenesis	98
Transfection	98
SDS-PAGE and Western Blotting	99
Plasma Membrane Preparation	100
Synaptosome Preparation	100
Asp-N Endoproteinase Proteolysis	101

	CNBr Chemical Proteolysis	101
	Acyl-Biotinyl Exchange	102
	2BP DA Uptake Assay.....	104
	DA Efflux Assay	104
	DA Uptake Saturation Analysis.....	105
	Surface Biotinylation	105
3.	THE EFFECTS OF THE PARKINSON-INDUCING NEUROTOXINS MPP ⁺ AND 6-OHDA ON THE DOPAMINE TRANSPORTER'S MODIFICATION AND FUNCTION	107
	Abstract	107
	Introduction.....	109
	Results	114
	6-OHDA and MPP ⁺ Competitively Inhibit DAT- mediated DA Uptake.....	114
	6-OHDA and MPP ⁺ Induce Downregulation of DAT Activity	116
	Incubation of 6-OHDA and MPP ⁺ on DAT-Expressing Cells Affects DA Uptake and Requires Functional DATs.....	118
	Neurotoxin Effects on DAT-Mediated Reverse DA Transport	120
	Inhibiting PKC Reduces Neurotoxin-Induced DA Efflux.....	123
	Neurotoxin Effect on DAT Phosphorylation	129
	Neurotoxin Effect on DAT Palmitoylation	132
	Discussion	134
	Methods.....	139
	Cell Culture	139
	Generation of DAT-Expressing LLCPK ₁ Cells	139
	SDS-PAGE and Western Blotting.....	140
	Neurotoxin Dose-Response Assay on Inhibition of DA Uptake	141
	DA Uptake Downregulation Assay.....	141

	Neurotoxin Pre-incubation DA Uptake Assay	142
	Neurotoxin DA Efflux Assay.....	143
	Dopamine Transporter Phosphorylation Assay	143
	Plasma Membrane Preparation	145
	Acyl-Biotinyl Exchange	145
4.	DISCUSSION.....	148
	Limitations of the Work Presented in this Dissertation	148
	Future Studies	149
	Summary Conclusions.....	150
5.	REFERENCES.....	152

LIST OF FIGURES

Chapter 1:

Figure	Page
1. Pavlovian and Skinnerian conditioning compared	6
2. Major dopamine pathways in the brain	8
3. Firing of DA neurons encodes reward prediction error	9
4. How does this sell bacon cheeseburgers?!?.....	11
5. Synthesis and release of DA.....	14
6. Protein mechanisms in vesicular-plasma membrane fusion and pore formation.....	15
7. Dopamine receptor effector proteins and signaling cascades.....	18
8. Secondary structure of DAT based on the LeuT crystal structure.....	20
9. X-ray crystal structure of dDAT	22
10. Alternating access mechanism of substrate transport	25
11. Na ⁺ involvement in the neurotransmitter transport process	26
12. DAT Binding Partner Interactions	29
13. Phosphorylation of the dopamine transporter	31
14. 2D topological diagram of location of hDAT coding variants.....	35
15. Mechanism of protein S-palmitoylation	37
16. Structure of human DHHC20	38

17. Functional consequences of protein palmitoylation	40
18. The ABE method	42
19. Dopamine transporter palmitoylation mechanisms	45

Chapter 2:

Figure	Page
1. Palmitoylation levels of WT and mutant rDATs measured by ABE	54
2. ABE analysis of WT and multiple Cys to Ala mutants of rDAT	55
3. Palmitoylation analysis of mutant DATs containing only the Cys residues suspected of being palmitoylated or containing all Cys residues except the suspected palmitoylation sites	57
4. Asp-N schematic proteolytic profile of rDAT	59
5. Asp-N proteolysis of rat striatal synaptosomes and subsequent detection of palmitoylated rDAT N-terminus by ABE	60
6. Depiction of N-terminal rDAT displaying N-terminal methionine residues, the primary aspartic acid cleavage site by Asp-N, and relative locations of intracellular cysteines potentially accessible for S-palmitoylation	61
7. CNBr digestion of rat striatal synaptosomes and subsequent detection of palmitoylated rDAT N-terminus by ABE	63
8. CNBr digestion of WT, Cys6Ala, Cys135Ala rDATs in LLCPK ₁ cells	64
9. Palmitoylation characterization of Cys90Ala rDAT	66
10. Surface biotinylation analysis of Cys90Ala rDATs' surface expression ...	68
11. Saturation analyses of Cys6Ala rDAT	70
12. Saturation analyses of Cys580Ala rDAT	71

13. Saturation analyses of Cys6/580Ala rDAT	72
14. Saturation analyses of Cys90Ala rDAT	73
15. 2BP downregulation of DA uptake decreases with palmitoylation-deficient rDATs.....	76
16. Significant correlation between 2BP-induced DAT downregulation and number of DAT palmitoylation sites	78
17. Cys6 and Cys580 impose opposite effects on DA reverse transport	80
18. 2BP affects DA efflux.....	83
19. Schematic of Cys6 palmitoylation tethering DAT's N-terminus to the plasma membrane	90

Chapter 3:

Figure	Page
1. Chemical structures of 6-OHDA and MPP ⁺	112
2. Known neurotoxic mechanisms of 6-OHDA and MPP ⁺	113
3. MPP ⁺ has a 16-fold greater potency than 6-OHDA for the inhibition of DA uptake.....	115
4. 6-OHDA induces DAT downregulation to a significantly lesser extent than DA or MPP ⁺	117
5. Neurotoxin downregulation of DAT requires their DAT-mediated transport.....	119
6. 20 μ M MPP ⁺ induces DA efflux.....	121
7. IC ₅₀ concentration of neurotoxin effect on DA Efflux.....	122
8. 6-OHDA blunts DA efflux from WT hDATs.....	124

9. PKC inhibition effect on 6-OHDA DA efflux signature.....	126
10. PKC inhibition reduces MPP ⁺ -induced DA efflux	127
11. PKC inhibition reduces AMPH-stimulated DA efflux	128
12. 6-OHDA inhibits basal and attenuates PMA-induced DAT phosphorylation	130
13. Total DAT protein expression is unchanged after neurotoxin treatment	131
14. Neurotoxin effect on DAT palmitoylation.....	133

LIST OF TABLES

Table	Page
1. Summary of palmitoylation deficient rDATs DA transport kinetics <i>versus</i> WT	74

ACKNOWLEDGEMENTS

I wish to extend my warmest thanks to everyone involved in my graduate education. First I would like to thank my mentor, Dr. James Foster. It has been an absolute pleasure to train under a highly skilled biochemist since my latter undergraduate days. From day one it was clear he had the best interests of his students at heart when he became an adjunct professor of chemistry so I would be able to complete my chemistry capstone in his lab. It is in his lab where the bulk of my graduate learning occurred and from him I have gained insight into pursuing answers to scientific problems in a research setting. I thank him for always being open-minded and receptive to new research ideas and free thought, and for the many trips, lunches, and conversations. Most importantly, I would like to thank him for this life-changing opportunity during which he has helped me to grow both personally and professionally. Thank you! I look forward to many years of friendship!

I would next like to thank Dr. Roxanne Vaughan and Dr. Keith Henry for critiquing my work over the years and for helping to elevate my expectations to their high standards to which I tried to perform each experiment. I thank Dr. Eric Murphy for the wonderful classes and several stimulating discussions these last six years. I thank Dr. John Shabb for his tutelage during the final stages of my undergraduate education, helping me get into graduate school, and the teaching opportunities he afforded me. I thank Dr. Manu Manu for his intriguing

bioinformatics course and for serving as the at large member of my advisory committee.

I thank my most loving family for being there through the many ups and few downs I've experienced during my graduate school experience. I thank my mother, Diane, for her counsel, strength, and wisdom. I thank her for her exemplary life, the last two decades of which were assaulted by the gale force winds of adversity which she suffered with the disposition of both a kind-hearted benefactor and a military general. I thank my sweet wife, Diane, for her effulgent love and support. She is the most nurturing person I have ever met and I am truly blessed to have the honor of being married to such an angel. I thank my three babies, Jane, Thomas, and Dorothy, on whom I have come to depend for love and inspiration more and more every day. I thank my brother, James, for his advice, insight, and not letting me get too up or too down. I thank all my wonderful in-laws for their unwavering loving support.

During the course of my graduate education I have had the pleasure of meeting and working with several great people, some of whom have become dear friends. I thank Dr. FNU Pramod Akula Bala for his insatiable curiosity and unique insight, and Christopher Brown for his unequivocal loyalty and passion for truth – I thank them both for their friendship. I thank all lab colleagues I've worked with over the years: Margaret Smith, Dr. Danielle Bolland, Dr. Rejwi Acharya, Dr. Sathyavathi Challasivakanaka, Madhur Shetty, Michael Tomlinson, and many more. In particular I'd like to thank Moriah Hovde for her friendship and many thought-provoking discussions, and Garret Larson for his friendship and being an

easy to teach, intelligent, and industrious young man. I thank Jennifer Hershey, Julie Horn, and Joyce Rice for their administrative assistance – I needed a lot of it.

I thank God, the Blessed Virgin Mary, and the Catholic Church. I would be despairingly lost without you. Thank you, thank you, thank you.

For my first true love and the strongest person I've ever known,
my mother

Requiescat In Pace

ABSTRACT

The projects described in this dissertation revolve around the functional consequences experienced by the transport protein for the neurotransmitter dopamine resulting from alterations to its palmitoylation condition or exposure to Parkinson disease-inducing transport substrates. This membrane-resident transport protein, pragmatically termed the dopamine transporter, relocates dopamine from extracellular areas of receptor sites of action to intracellular sequestration; the dopamine transporter is a powerful mediator of dopamine signaling. As such, genetic, toxicant, or chronic breakdown of dopamine transporter function is associated with multiple psychological abnormalities. Biomedical research has produced several pharmacotherapies for maladies like depression, attention deficit/hyperactivity disorder, and addiction, some of which produce their therapeutic profiles by modulating dopamine transporter function. The potential for pharmacological manipulation of the dopamine transporter is, however, not without its dark side. Dopamine's critical role in the neurotransmission of reward and pleasure render the dopamine transporter a favorite target of illicit, addictive drugs of abuse like cocaine and several flavors of amphetamine. All of these factors make intimate understanding of the many mechanisms involved in the dopamine transporter's function relevant not only to mental, but also societal health. This dissertation explores aspects of dopamine transporter mechanistic regulation which, once more thoroughly understood, may

be modified to allow finer control over transporter operation, generating novel approaches to mental health treatment.

The first study investigates site identification and functional characterization of post-translational modification of the dopamine transporter by a lipid moiety, palmitic acid. Palmitic acid, hexadecanoic acid in IUPAC nomenclature, is a saturated 16 carbon fatty acid whose attachment to proteins is termed S-palmitoylation. This lipidation process is executed by an array of enzymes belonging to the acyl transferase class of the gene name *zDHHC*. Importantly, S-palmitoylation is reversible: a protein's palmitoylation status can change in response to cell stimuli or the palmitoylated protein's activation. As palmitate is of an aliphatic nature, its attachment creates a hydrophobic protein microenvironment around the site of its augmentation which propitiates its insertion into likewise hydrophobic loci – usually membranes – which induces a protein-specific functional outcome. A combination of dopamine transporter proteolysis, site-directed mutagenesis, acyl-biotinyl exchange, surface biotinylation, and forward and reverse dopamine transport assays implicate two N-terminal cysteine residues as sites of palmitate incorporation, in addition to the previously analyzed C-terminal site, and reveal a role for this lipid modification in dopamine transporter-mediated dopamine efflux.

The second project seeks to further understand the dopamine transporter's contribution to Parkinson disease. The hallmark of this disease is a loss of motor coordination precipitated by selective death of nigro-striatal dopamine neurons and concomitant depletion of dopamine neurotransmission in the movement planning

and execution region of the brain – the striatum. The selective loss of these neurons directly correlates with dopamine transporter expression; indeed, even amongst dopamine neuronal pathways, the nigro-striatal fiber, which is lost to the greatest extent of these, has the highest transporter expression. It is for this reason the dopamine transporter has been a focus of Parkinson disease research. This study utilizes the dopamine transporter substrates 6-hydroxydopamine and 1-methyl-4-phenylpyridinium, which induce cell death through a panoply of biochemical mechanisms and are used to generate Parkinsonian symptoms in animal models, to probe for aberrant dopamine transporter function and post-translational modification. This inquiry revealed that, though these compounds induce cell death through similar mechanisms, their dopamine transporter-specific effects are quite different. Interestingly, 1-methyl-4-phenylpyridinium is a strong inducer of dopamine uptake downregulation and dopamine efflux, a phenomenon now implicated in Parkinson disease onset, while 6-hydroxydopamine mitigates this efflux event as well as attenuates transporter phosphorylation.

Overall, this dissertation argues for the existence of N-terminal palmitoylation of the dopamine transporter, that palmitoylation is an additional contributor to the dopamine efflux paradigm, that transporter-mediated efflux may contribute to Parkinson disease onset, and that some of the transporter-specific effects of 6-hydroxydopamine may be exploited to alleviate neuropsychiatric maladies associated with aberrant dopamine efflux.

CHAPTER 1

INTRODUCTION

Dopamine

Preface – The Modern Soma

In the ancient Vedic religious text, *Rig Veda*, is described a deity who is both deity and ritual – the immortal and the means of immortality – Soma¹. One seeking interlocution with the Soma entity ingests the Soma plant or Soma plant liquid extract during the ‘Soma-sacrifice’ ceremony to achieve the desired transcendence¹. The psychotropic ambrosia derived from this god/plant/libation induces stimulant, hedonic, hallucinogenic, entactogenic, and euphoric experiences and is thought to grant the participant longevity, vitality, and resurrection². The identity of the Soma plant described in the 9th Mandala of the *Rig Veda* has long been a subject of scholarly debate³⁻⁵, yet over the epochs a multitude of vines, herbs, and flowers has likely been used in the Soma ritual as all the plants in question contain mind-altering compounds like ibogaine, L-DOPA, ephedrine, tryptamines, or monoamine oxidase inhibitors⁶. The altar is erected, the fire kindled, the Soma berries crushed, the celebrant exults.

Is this not, in some sense, the experience of the drug abuser? Is he not after some form of transcendence? Some attempt, albeit misguided, to escape the banality and disappointment of everyday life? Are there more innocuous

manifestations of this practice? What of the avid social media user who seeks but is, for some reason, unable to find what he is searching for after the hours of mindless scrolling? Is it the same exhilaration sensed at the first like of his first post he seeks? Or, perhaps, is it the perpetual self-affirmation attained from those glimpses into a former lover's socially sanitized, filtered, and photo shopped faux reality where she is still unable to hide those acne blemishes? For what is the television watcher searching during the hours of mass consumption of vicarious experience through his favorite streaming television dispensary? Happiness? Maybe sought after but never achieved. Enlightenment? Surely not. What of sports? What, exactly, is the function of *ESPN*? What of *E! Entertainment Television*? How many human lifetimes are obliterated in trivialities and vacuous curiosity? How much ingenuity, innovation, and intellectual and scientific breakthrough have been expunged by visions of Harry Potter, Mickey Mouse, and Michael Jordan? Television programming, indeed. What about the individual overcome by ubiquitous hyper-sexualization and his concomitant descent into depths of deviance and diminishing returns associated with sex addiction? Is the purpose of his existence achievement of sexual gratification? Of course not, but why does his brain insist it is so? How much culpability lies at the feet of society and circumstance and how much at his? Or the chronic eater-of-feelings whose brain is now wired to interpret that dust sprinkled dehydrated cardboard as food but is completely oblivious that it is that very dust doing the wiring and the dehydrated cardboard is anything but food?

How does a civilization's art degenerate from Franz Schubert to Cardi B?

Aldous Huxley was a preeminent philosopher, author, and scientist of his generation. In his most famous, far ahead of its time, and prophetic work, *Brave New World*⁷, Huxley details life in a future totalitarian technocracy which maintains absolute control through advanced social, psychological, and biological engineering which aims to keep all citizens distracted and contented. This control technique is typified in use by all citizens, regardless of socio-economic status, of the perfect drug: Soma. It is described⁷:

“Two thousand pharmacologists and bio-chemists were subsidized in A.P. 178... Six years later it was being produced commercially. The perfect drug... Euphoric, narcotic, pleasantly hallucinant... Take a holiday from reality whenever you like, and come back without so much as a headache or a mythology... One cubic centimetre cures ten gloomy sentiments... Now-such is progress-the old men work, the old men copulate, the old men have no time, no leisure from pleasure, not a moment to sit down and think- or if ever by some unlucky chance such a crevice of time should yawn in the solid substance of their distractions, there is always soma, delicious soma.”

This Soma is consumed to eschew concern, negative emotion, cognitive dissonance, and especially sentiments of rebellion and change. How does one think, let alone imagine, beyond a matrix of inculcated pleasure-seeking? If one is contented and saturated with creature comforts will he be able to break his pleasure-inducing fetters? Is there any similitude between Huxley’s dystopian drug use and a phenomenon of the modern lifestyle? It seems so: drugs of abuse^{8–12}, sex^{13–17}, food^{18–21}, video games²², television²³, and social media²⁴, all elicit dopamine-potentiated rewarding properties and are capable of producing addiction^{25–32} – a prime mover of which is dopamine (DA) neurotransmission^{33–35}. Activation of the DA reward pathway has achieved a coup d’état of motivation for

human behavior, or, more likely, a coup d'état of the DA reward pathway has achieved dominion over human behavior. This is the modern Soma and it is of the *Brave New World* category rather than the transcendent Vedic form. The former produces somnolence while the latter is an attempted step in the journey for truth.

The sociological and anthropological impact of dopamine reward seeking behavior is utterly mind-boggling. There are not many greater influences on human behavior (perhaps money or religion) and the pleasure principle as the end to which behavior is directed will increase in influence as newer thrill-inducing technologies captivate wider swaths of youth and adult populations (television to video games to virtual reality to what?). So, how has the archetypal instantiations represented by Cardi B come to predominate over the Franz Schuberts? The former is saturated with several forms of sensual appeal to the so called 'reptilian' brain and directs the mind's eye toward immediate gratification (pleasure) in place of future rewards of greater purpose to which the latter harkens. The net result of choosing more and more of the 'Cardi Bs' across all sensory input manifestations (TV, food, sex, etc.) is the detachment of purposeful action from the reward satiation, producing rampant inaction; the release of dopamine-directed reward as an end in and of itself. It keeps the user plumbed into the La-Z-Boy rather than working to effect change and producing some good in the 'real world' and certainly not questioning anything. And with the stunning array of new gadgets, toys, movies, media platforms, pornography, bands, TV shows, video games, 'news' programs, sporting events, etc., etc., one ends up floundering in a Pavlovian-Skinnerian abyss of highly personalized dopamine-guided behavioral patterns.

When one gets a tattoo of the DA molecule, is he truly aware of how he is branding himself? How has this come to be?

Pavlov, Skinner, Learning, Behavior, and... Advertising?

Reinforcement learning³⁶ (RL) is a process by which learned behavior is either supported (positive reinforcement) or opposed (negative reinforcement) by environmental stimuli. Pavlovian conditioning (RL)³⁷ occurs when an unconditioned stimulus (US), classically a food reward, is predicted by a conditioned stimulus (CS), classically a ringing bell, which produces a conditioned response (CR), classically salivation, after repeated CS-US trials. This type of RL conditions reflexive or involuntary behaviors. The Skinnerian³⁶ advancement of Pavlov's paradigm was to induce a subject's voluntary behavior in eliciting reward or avoiding noxious stimuli. In this paradigm, the experimental subject operates on its environment (hence 'operant' conditioning) such that a behavior, like lever pressing (the lever being the environmental stimulus which cues the behavior), produces a food reward, which, after repetition, becomes a behavior-reinforcing stimulus pairing. The subject learns that lever pressing produces the food reward. Thus, behavior can be conditioned through stimulus-response learning and a subject's voluntary and involuntary behavior can be conditioned to attain reward and avert punishment through environmental stimuli (Figure 1).

The neurobiological mechanism by which RL occurs is activation of DA neurons^{38,39}. The primary neuronal DA tract activated by rewarding stimuli is the

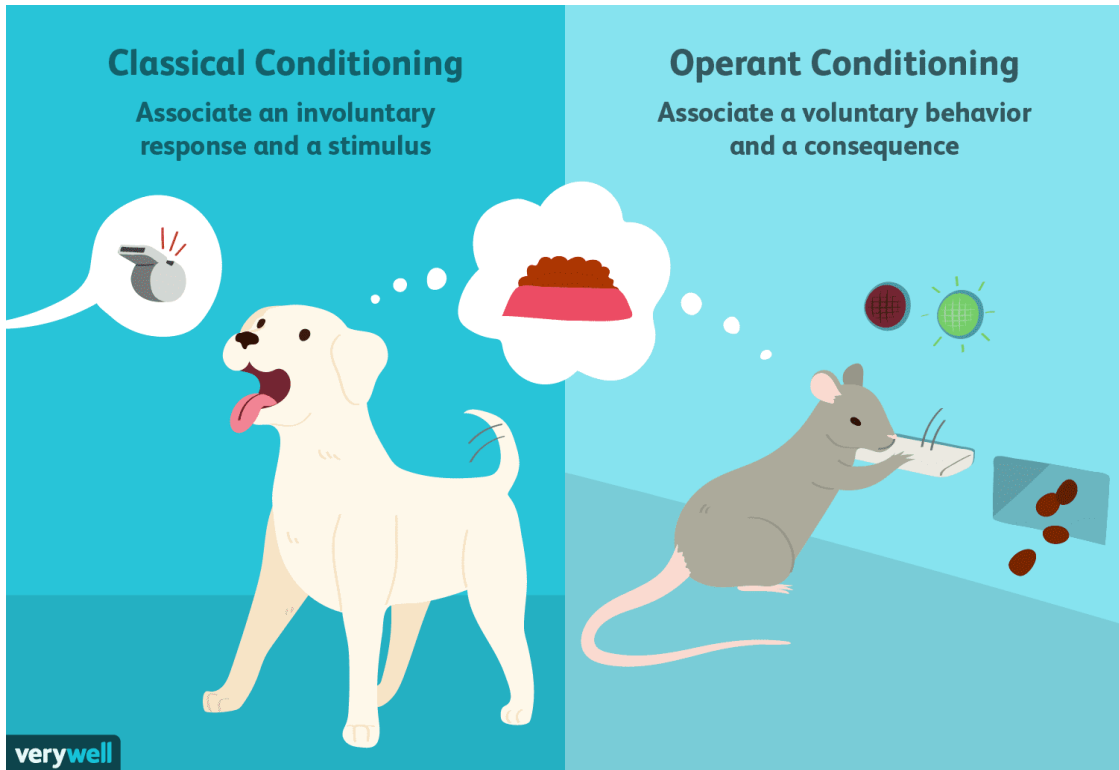


Figure 1. Pavlovian and Skinnerian conditioning compared. Simple schematic comparison of classical conditioning of a dog's conditioned involuntary response (panting, excitement, tail wagging) to the conditioned stimulus (whistle) in expectation of an unconditioned stimulus (food reward) to operant conditioning of a mouse's voluntary response (operation of the lever) to elicit the behavior reinforcing food reward. Image courtesy of [https://fthmb.tqn.com/eKmmGPsmUZvy7k68o36Lq1LUeHg=/1500x1000/filter:s:fill\(ABEAC3,1\)/2794861-classical-vs-operant-conditioning-5afc42a343a10300370da76f.png](https://fthmb.tqn.com/eKmmGPsmUZvy7k68o36Lq1LUeHg=/1500x1000/filter:s:fill(ABEAC3,1)/2794861-classical-vs-operant-conditioning-5afc42a343a10300370da76f.png), with permission.

mesolimbic DA pathway whose nexus is the ventral tegmental area (VTA) and which ultimately innervates the nucleus accumbens (NAc) of the ventral striatum^{40,41} (Figure 2). Rewarding stimuli activate phasic DAergic neuron responses⁴² while punishments actually inhibit their firing^{43,44}. Amazingly, after conditioning by Pavlov's system, activation of these DA neurons transfers from the reception of the US to the presentation of the CS⁴⁵. This process occurs through DA coding of prediction error (PE) and determination of incentive salience. A PE occurs when an individual's subjective estimation about a future outcome is incorrect, resulting in an outcome that is either greater than anticipated (positive PE) or worse than expected (negative PE)^{46,47} (Figure 3). In fact, the amount of excited quantal DA release is directly proportional to the subject's prediction of the reward value^{48,49} and probability of receiving the reward⁵⁰. As more and more stimulus-response iterations are experienced and their respective values are coded for by DA NAc neurons, the stimulus which is associated with the greatest DA release will achieve incentive salience, or the highest motivational value, to which end the subject's behavior becomes directed⁵¹⁻⁵³. Indeed, NAc DAergic signals are essential for the attribution of incentive salience ('wanting'), but is not required for the hedonic impact of reward ('liking')^{34,54,55}, which is mediated through opioid^{56,57} and endocannabinoid⁵⁸ accumbens transmission.

Though it is the primary neurological system for RL⁵⁹, the DA-mediated attribution of incentive salience becomes more complex and individualized in higher order species, with, quite obviously, humans being the most complex and

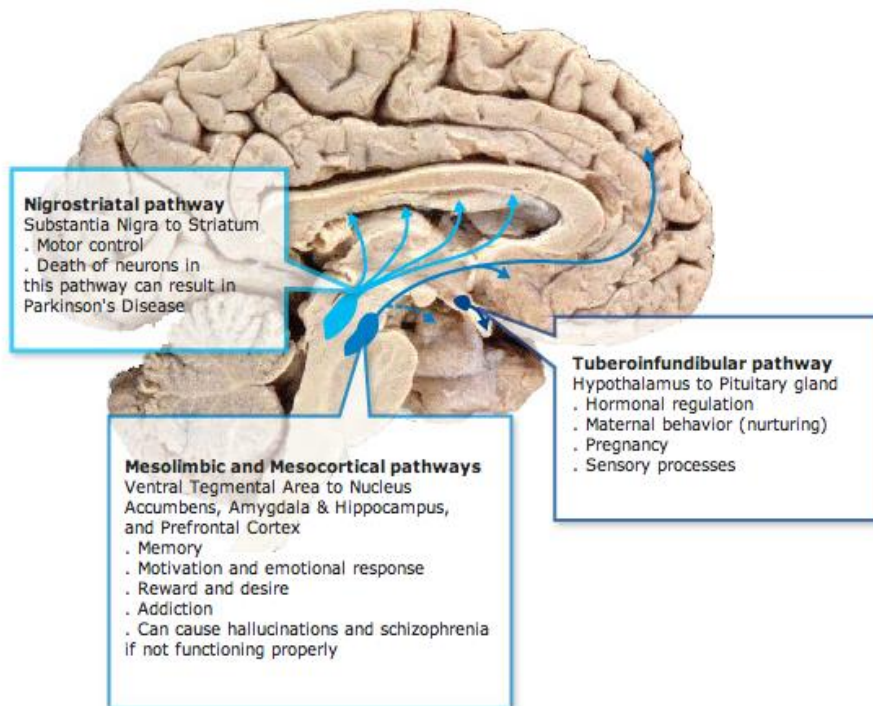
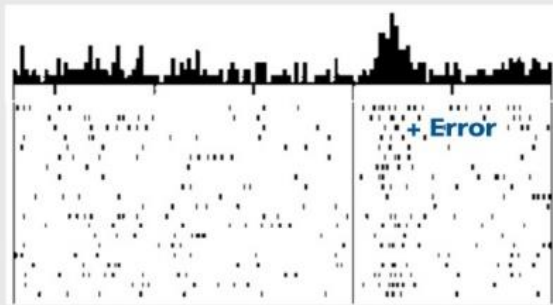


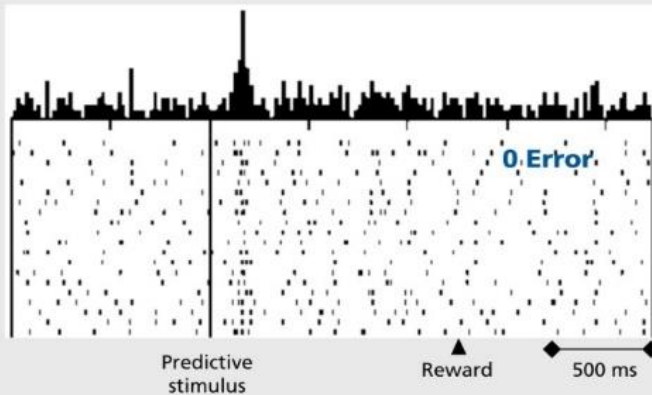
Figure 2. Major dopamine pathways in the brain. Schematic diagram of the brain's DA tracts. The nigrostriatal pathway originates in the substantia nigra and innervates the striatum and coordinates movement (discussed in greater detail in chapter III). The mesolimbic fiber runs from the VTA to the NAc and is involved in reward. The mesocortical tract also begins in the VTA and terminates in multiple regions of the prefrontal cortex and contributes to cognitive control and emotion. The tuberoinfundibular pathway cell bodies reside in the hypothalamus and send processes to the pituitary gland where DA secretion controls prolactin release. Image courtesy of <http://medlibes.com/uploads/Screen%20shot%202010-07-15%20at%2010.48.11%20PM.png>, with permission.

No prediction
Reward occurs



Reward

Reward predicted
Reward occurs

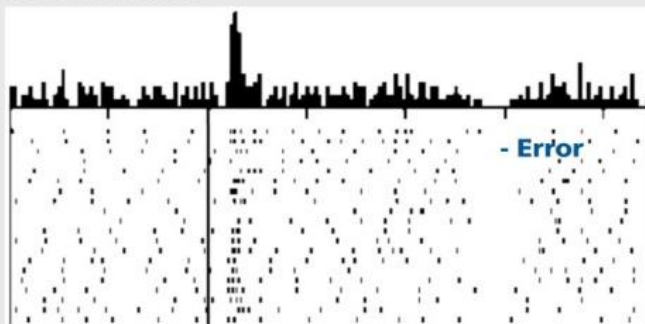


Predictive
stimulus

Reward

500 ms

Reward predicted
No reward occurs



Predictive
stimulus

(no reward)

Figure 3. Firing of DA neurons encodes reward prediction error. Reception of an unexpected rewarding stimulus induces burst firing of DA neurons, positive prediction error (top). Application of a conditioned stimulus induces phasic neuron stimulation, but the reception of the reward does not alter basal DA neuron firing pattern, no prediction error (middle). Conditioned stimulus induces expected neuronal excitation, but the absence of reward ablates even tonic firing of DA neurons, negative prediction error (bottom). Adapted from ref #46, with permission.

individualized. Perturbations in attribution of incentive salience are associated with two prevalent human diseases: depression can be a result of deficits of incentive salience attribution wherein the depressed individual assigns subnormal motivational value to rewarding tasks^{60–62}, and addiction coincides with excessive attribution of incentive salience to behavior which negatively affects one's life, producing chronic alterations to DA-mediated motivation systems^{63,64}. It is the usurpation of the DA-incentive salience system that results in addiction⁶⁵, yet it is also a takeover of this mechanism which marketing and advertising is hoping to achieve – with every advertisement, all the time. The advertiser's tactics are sometimes subtle^{66–68} and sometimes overt (Figure 4)^{69,70}, but the end result is a ruthless, shameless attempt to subvert the target audience's (you) incentive salience attribution capacity – to instill, using an amalgamation of Skinnerian and Pavlovian RL schemas⁷¹, irrational desire for a product one does not need, and, ultimately, to habituate the purchase and use of the marketed product⁷². Thus an effective advertisement (like the one in Figure 4) supplies the CS that stimulates involuntary NAc DA signaling (the strength of which depends on the amount and subjective significance of pleasure modalities it appeals to) in the viewer's brain which alters his perception of the product (reality, really) such that he values the product higher than what it is actually worth, generating an illogical desire for its attainment. Advertising contributes to several addiction-associated disorders including alcoholism⁷³, compulsive buying⁷⁴, and obesity^{75–77}. We learn by the modern soma, we survive by the modern soma, we behave according to the

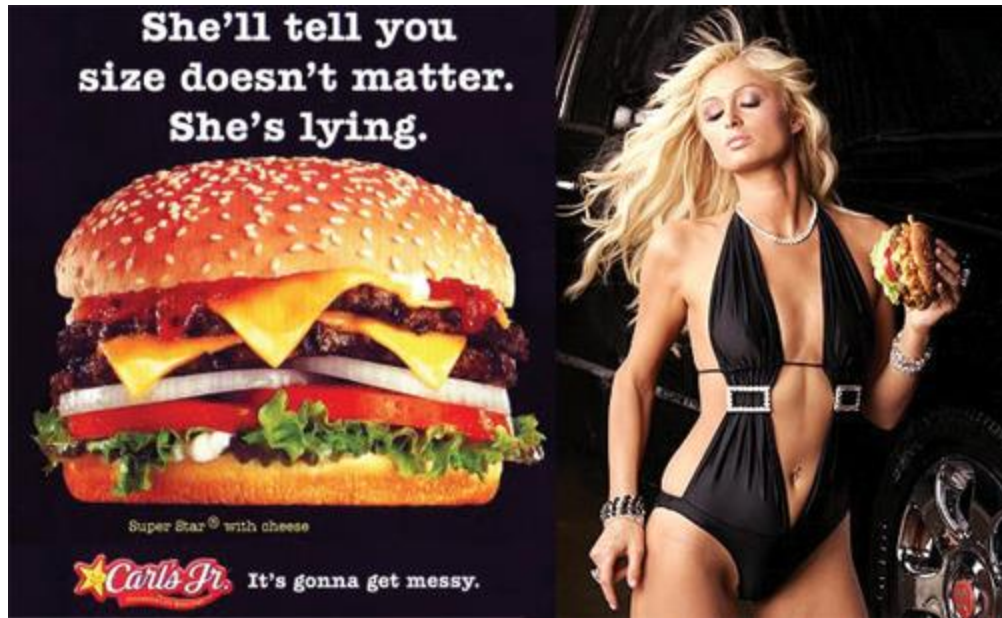


Figure 4. How does this sell bacon cheeseburgers?!? This conditioned stimulus (advertisement) appeals to multiple aspects of male psychology, producing a manipulated DAergic reaction which biases the inflicted individual's attribution of incentive salience and subsequent behavior toward ingestion of Carl's Jr. rather than Burger King (probably) because....sex. What a time to be alive!!

modern soma, but we do not thrive on the modern soma. The ubiquity of DA science extends from pharmacological through the sociological disciplines, and, after analysis of our epoch by scholars of millennia to come, it will be of anthropological and historical significance.

Synthesis, Exocytotic Release, and Receptors

In the central nervous system, DA executes numerous physiological functions. In addition to the previously described learning and rewarding properties of DA neurotransmission, emotion, cognition, movement, memory, and sensory processes all involve DA signaling. Intriguingly, DA has been demonstrated to perform peripheral functions as well: DA is synthesized and secreted by pancreatic β -cells whereby it regulates insulin release^{78–80}, and it is likewise produced and released by immune cells to modulate several aspects of their function, including cytokine synthesis and secretion^{81–83}. DA is a catecholamine transmitter which relates that its structure possesses a benzene ring from which project two hydroxyl functional groups and ethylamine (Chapter 3 Figure 1). DA is synthesized from its amino acid precursor L-Tyrosine (Tyr) which is transported across the blood brain barrier (BBB) by large neutral amino acid transporter (LAT1)⁸⁴ and enters DA neurons. The sequential enzymatic reactions of tyrosine hydroxylase (TH) and aromatic L-amino acid decarboxylase (AADC) cooperate to produce DA from Tyr. TH requires tetrahydrobiopterin, iron (Fe^{2+}) and molecular oxygen to catalyze the rate-limiting step of DA synthesis to further hydroxylate Tyr's aromatic ring. The molecular product of this reaction is L-dihydroxyphenylalanine (L-DOPA) which, like Tyr, passes the BBB *via* LAT1 activity⁸⁴ and is therefore a standard treatment

for the DA-deficient disorder, Parkinson disease (PD)⁸⁵. TH function is increased by neuron depolarization-induced extracellular signal-regulated protein kinase (ERK) and cAMP-dependent protein kinase (PKA) phosphorylation of Serine (Ser) residues 19, 31, and 40^{86,87}. AADC removes the carboxylic acid moiety from L-DOPA's α -carbon, creating 3,4-dihydroxyphenethylamine or dopamine (DA). DA can be converted to norepinephrine by dopamine beta hydroxylase which can be further modified to epinephrine by phenylethanolamine-N-methyltransferase in neurons expressing these enzymes⁸⁸. Cytosolic DA is tightly controlled as it can transform into cytotoxic reactive oxygen species and is thus rapidly deaminated by monoamine oxidase enzymes or methylated by catechol-o-methyl transferase⁸⁹.

After synthesis, DA is sequestered into vesicles through the vesicular membrane transport protein, vesicular monoamine transporter (VMAT2)⁹⁰ (Figure 5). VMAT2 packages DA into vesicles in opposition to the DA concentration gradient through its pairing with proton antiport congruent with the H⁺ gradient. Low vesicular pH is maintained by vesicular H⁺-ATPase activity. Once loaded with transmitter, vesicles undergo anterograde trafficking along microtubule filaments by ATP-dependent kinesin function^{91,92}. Once docked in the axon terminal 'active zone', priming of the vesicle, fusion of the vesicular and plasma membranes, and egress of the vesicle cargo is carried out by soluble N-ethylmaleimide sensitive factor attachment protein receptor (SNARE) machinery⁹³⁻⁹⁵ (Figure 6). SNARE proteins belong to two broad categories: vesicle (v)-SNAREs which are present on granule membranes, and target (t)-SNAREs which reside in the nerve terminal plasma membrane. Conformational adjustment of the α -helical t-SNARE syntaxin

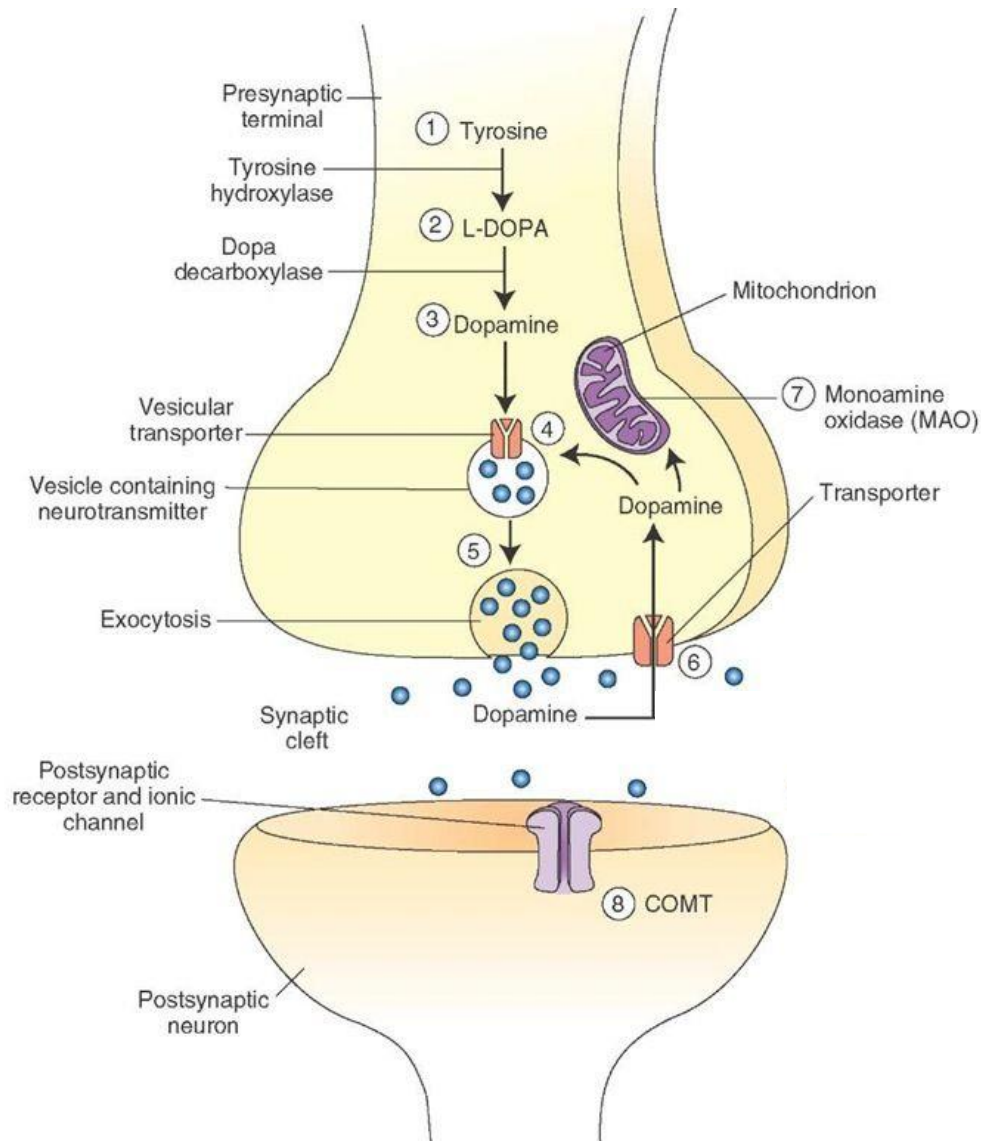
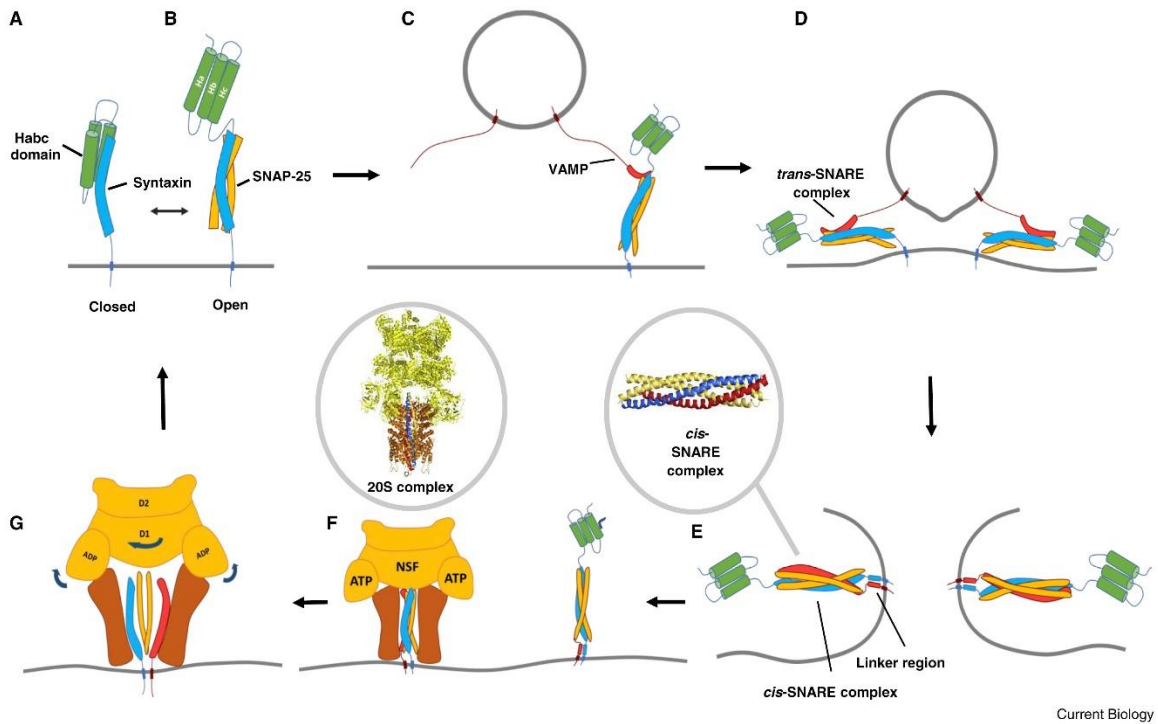


Figure 5. Synthesis and release of DA. DA is enzymatically generated from L-tyrosine by sequential tyrosine hydroxylase and aromatic L-amino acid decarboxylase activities. DA is translocated into vesicles through vesicular monoamine transporter. DA is released into the synapse after vesicular fusion with the axon terminal membrane. Excess cytosolic DA is catabolized by monoamine oxidase in neurons and catechol-o-methyltransferase in surrounding cells. Image reproduced from <https://i.pinimg.com/originals/6d/6b/60/6d6b60d62d807a077c7327bd177b216e.jpg>, with permission.



Current Biology

Figure 6. Protein mechanisms in vesicular-plasma membrane fusion and pore formation. A-B) Syntaxin conformation change recruits SNAP interaction. C-E) VAMP proteins (synaptotagmin, synaptobrevin) interact with the q-SNARE system which, with the aid of Ca^{2+} forms a cis-SNARE complex which fuses the plasma and vesicle membranes. F-G) SNAP and NSF proteins sequentially bind to the SNARE structure. ATP hydrolysis mediated by NSF induces conformational changes to the NSF structure which produces spring-loaded disassembly of all involved protein complexes. Imaged adapted from ref # 93, with permission.

causes its HaHbHc domain to move away from its glutamine rich region which recruits assembly of other t-SNARE α -helical proteins, such as SNAP-25. This t-SNARE complex interacts with the likewise α -helical v-SNARE proteins, synaptobrevin and synaptotagmin (Syt), forming a cis-SNARE complex. After action potential-stimulated Ca^{2+} influx and Ca^{2+} -Syt binding, this cis-SNARE structure acts like a zipper to draw the vesicular and plasma membranes together and provide the energy necessary for membrane fusion and pore formation^{93,96,97}. Additional SNAP proteins and the N-ethylmaleimide sensitive factor (NSF)-ATPase congeal to form a SNAP/SNARE/NSF 20s complex⁹⁸. NSF-catalyzed ATP hydrolysis disassembles the 20s and cis-SNARE structures^{99,100}.

DA exocytosis occurs through this pore. Only 25-40%^{101,102} of the estimated 33,000¹⁰³ vesicular DA molecules are released upon fusion events which allows the neuron to more finely control transmitter release and avoid arduous vesicle recycling tasks¹⁰¹. Once released into the synapse, DA interacts with its endogenous cognate receptors to produce DA's physiological outcomes. These DA receptors are of 5 separate classes, all of which are members of the GPCR superfamily and therefore have an extracellular amino-terminus, cytosolic carboxyl-terminus, and seven α -helical transmembrane (TM) domains¹⁰⁴. Conventionally, the DA receptor subclasses are divided according to their modulation of cAMP production: D₁ and D₅ receptors are coupled to the adenylate cyclase (AC)-stimulating G-protein, G $\alpha_{s/olf}$, while D₂, D₃, and D₄ receptor subtypes signal through G $\alpha_{i/o}$ to inhibit AC activity; D₁-type receptors stimulate protein kinase A (PKA) while D₂-type receptors blunt PKA (Figure 7). An important assimilation

point for dopamine receptor signaling is dopamine and cAMP regulated phosphoprotein, Mr 32 kDa (DARPP-32). PKA phosphorylates DARPP-32 at Thr34, turning DARPP-32 into a potent inhibitor of protein phosphatase 1 which, in turn, influences a plethora of cellular systems^{105,106}. DARPP-32 mediates the activity of several drugs of abuse that affect DAergic neurotransmission^{107,108}. It is now known that in addition to these canonical cAMP-PKA pathways, DA receptors signal through several cAMP-independent mechanisms including but not limited to: transactivation of multiple receptor tyrosine kinases^{109–111}; interaction with and modulation of N-type calcium channel^{112,113} and Na⁺/K⁺ ATPase^{114,115} operations; stimulation of phospholipase C^{116,117} through G_{βγ}¹¹⁸ and Gα_q^{119,120} mechanisms; coupling to β-arrestin, classically associated with receptor desensitization¹²¹, to form scaffolds¹²² for kinase and phosphatase signaling processes¹²³; and signaling through protein kinase B to prompt glycogen synthase kinase activity^{124–126}. DA receptors are functionally regulated through post-translational phosphorylation^{127–131} and palmitoylation^{132–138}. After DA is released into the synapse to signal through its target receptors, its concentration and duration in the synaptic schism is terminated through reuptake into the presynaptic neuron *via* the dopamine transporter.

The Dopamine Transporter

Structure and Mechanism of DA Transport

The dopamine transporter (DAT)¹³⁹ is the an integral membrane protein found predominantly in the perisynaptic membranes of presynaptic DA nerve

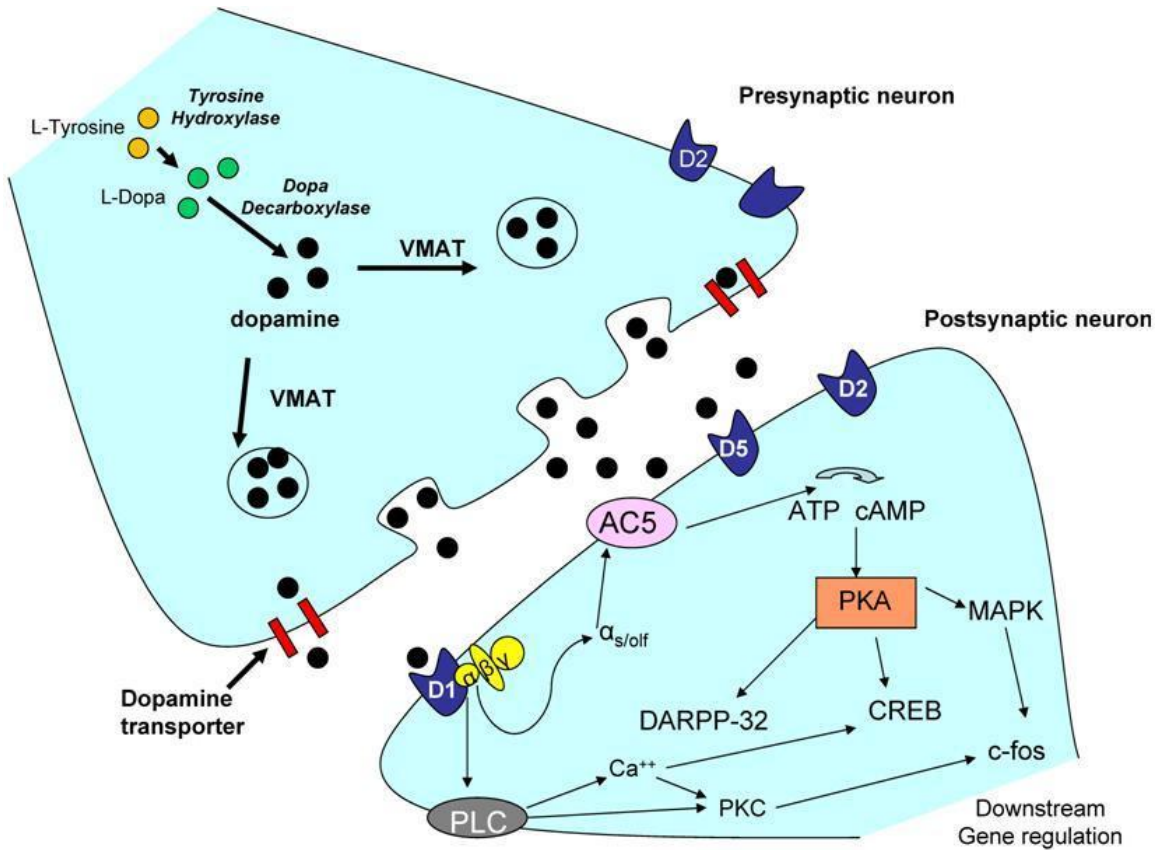


Figure 7. Dopamine receptor effector proteins and signaling cascades. Schematic representation of DA signaling through its cognate receptors. D₁ and D₅ receptors excite AC function through G $\alpha_{s/olf}$; D₂, D₃, and D₄ subtypes attenuate AC production of cAMP by G α_i . cAMP stimulates PKA which phosphorylates numerous downstream targets, like DARPP-32, and influences several signaling pathways and transcription factors. DA receptors have also been shown to activate PLC through G α_q and G $\beta\gamma$ proteins. Image adapted from <https://medicine1journal.wordpress.com/2013/08/15/congestive-heart-failure-pharmacological-approach-iii/> with permission.

terminals and is so named for its function: transport of DA from the synaptic space to the cytosol of the presynaptic neuron. After regulated control of vesicular DA egress, DAT is the primary means of controlling DA homeostasis in the synapse; thus, it regulates DA's influence on target pre- and post-synaptic neurons. DAT belongs to the solute carrier family 6 (SLC6)¹⁴⁰ gene family which also includes neurotransmitter and amino acid transporters for serotonin (5-HT), Norepinephrine (NE), γ -aminobutyric acid (GABA), and glycine, proline, taurine, and the osmolytes betaine and creatine with whom DAT shares high amino acid sequence homology and structural topology^{139,141–143}. Advancement in understanding the secondary structure of the neurotransmitter sodium symporters (NSSs; transporters DAT, SERT, NET) coincided with their molecular cloning^{144–147} and subsequent hydrophathy^{146,147} and topology^{148–150} assessments which deduced 12 α -helical transmembrane (TM) domains, cytosolic N- and C- termini, a large, glycosylated extracellular loop (EL) structure between α -helices III and IV, and a disulfide bond¹⁵¹ within this EL (Figure 8)¹⁵². The NSSs possess approximately 600 amino acids; the rat DAT (rDAT) isoform contains 619 residues, and the human (hDAT) consists of 620. It wasn't until the resolved X-ray crystal structure of the NSS bacterial homologue leucine transporter (LeuT) that the tertiary structure of the SLC6 family came into view¹⁴². LeuT, like the predicted NSS secondary structure, comprises 12 α -helical TM domains and intracellular N- and C- termini. The LeuT crystal also revealed unwound regions in TMs 1 and 6 which coordinate substrate binding^{142,153}, and a pseudo-symmetric inverted repeat structure wherein TMs 1-5 form a V-shape motif which is mirrored by similar, but inverted architecture of TMs

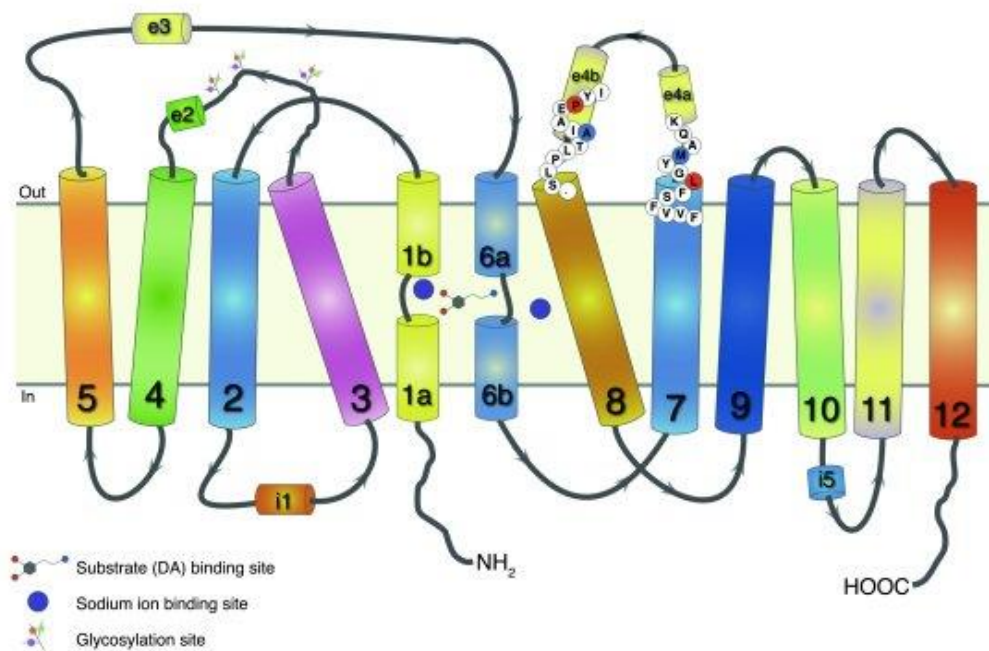


Figure 8. Secondary structure of DAT based on the LeuT crystal structure. Schematic representation of DAT topology. Relative position of DAT's 12 TM domains are shown with unwound regions as the putative site of substrate and Na^+ ion binding. Also shown are the intracellular amino and carboxyl termini and glycosylation events on EL 2. Image adapted from ref # 152, with permission.

6-10¹⁴². This '5 + 5 inverted repeat' motif has since been discovered in transporters unrelated to members of the SLC6 family or LeuT¹⁵⁴.

The *drosophila melanogaster* (d)DAT crystal structure was resolved in 2013 and provided further insight into DAT architecture (Figure 9)¹⁵⁵. DAT core tertiary structure is similar to LeuT in that TMs 1-5 and 6-10 form a 5 + 5 inverted repeat fold inside of which TMs 1, 3, 6, 8, and 10 form a substrate permeation pathway. This DAT crystal does, however, have several unique features. TM 12 has a kink induced by a proline residue halfway along its α -helix which causes the portion in the cytoplasmic plasma membrane leaflet to jut-out from the transporter. A cholesterol molecule is wedged between TMs 1a, 5, and 7 which likely helps maintain DAT in an outward-open structural conformation¹⁵⁶ as it inhibits free motion of TM 1a as DAT progresses through substrate bound and unbound conformations¹⁵⁷, though this cholesterol might be an artifact of the crystallization process. The intracellular C-terminus is composed of a 2.5 turn helix and acts as a latch through interaction with intracellular loop (IL) 1 which may play a role in substrate transport¹⁵⁵.

DAT-mediated DA translocation is conducted in an alternating access mechanism (Figure 10)¹⁵⁸. This process involves movement of the transporter through multiple conformations initiated by substrate binding to an outward-open conformation^{159,160}. This outward-open conformation exposes the substrate binding site to the extracellular solvent. After DA enters its binding pocket, Asp79 being crucial for coordination of DA's amine group^{161,162}, the transporter transitions

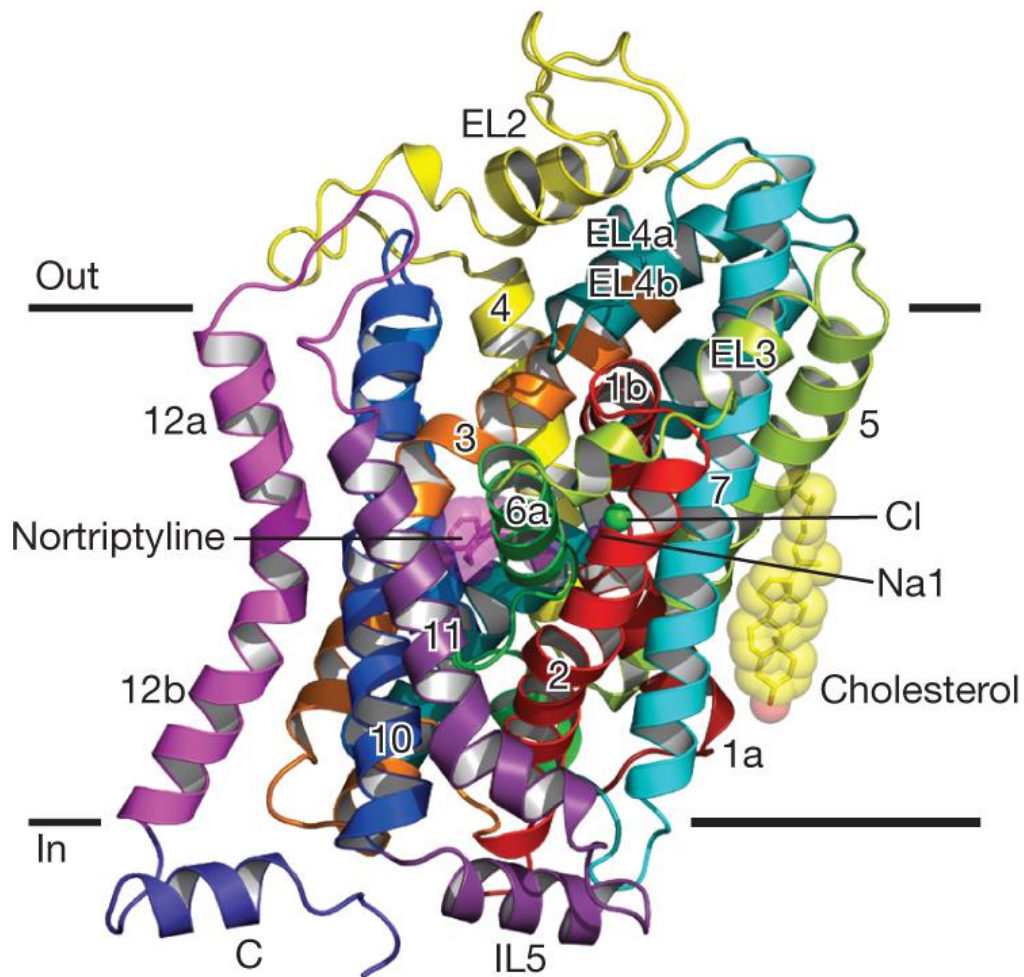


Figure 9. X-ray crystal structure of dDAT. Tertiary structure of dDAT locked in the outward-open conformation by the tricyclic antidepressant nortriptyline. Displayed are the locations of the 12 TM α -helical barrels, the cytoplasmic cap produced by the C-terminal peptide which contains a short helical segment (blue), the bend to TM 12 produced by Pro572 tilting TM 12b away from the permeation core (purple), and a cholesterol molecule (yellow) bound between TMs 1a, 5 and 7 where it reduces the ability of TM 1a to isomerize between its conformational states necessary for substrate translocation. Image adapted from ref # 155, with permission.

into an occluded position in which neither extracellular nor intracellular substrate-solvent exposure occurs *via* movement of TMs 1b, 6a, and EL4 into the substrate binding vestibule, forming an extracellular ‘gate’ which seals the substrate pocket from the extracellular milieu^{142,157,163}. The final transition from this occluded state to the inward-open, substrate-releasing conformation is induced by movement of TM 1a away from DAT’s core¹⁶⁴ and breaking of the intracellular gating network which is comprised of a salt bridge between Arg60 and Asp436 stabilized by cation- π stacking of Arg60 and Tyr335^{165,166}, and latching mechanisms formed by TM1a-IL1-C-terminus interactions¹⁵⁵. After DA is released into the cytosol, DAT isomerizes back into the outward-open conformation for further DA translocation events.

DAT is a secondary active transporter and as such the motive power for ‘uphill’ DA transport is supplied by movement of sodium ions down its Na⁺/K⁺-ATPase-maintained concentration gradient, like other members of the NSS family¹⁶⁷. DAT’s substrate transport process involves simultaneous transport of DA, two Na⁺ ions and one Cl⁻ ion; DAT is, therefore, a symporter. The first Na⁺ ion (Na1) stabilizes the outward-open conformation until substrate binding, and accommodates DA binding and DAT conformational transitions during transport rearrangements; it is coordinated by the side-chains of dDAT residues Asn49, Ser320, and Asn352 and backbone carbonyls of Ala44 and Ser320 from TMs 1 and 6^{155,168–170}. The second Na⁺ ion’s (Na2) location is accommodated by residues from TMs 1 and 8 by peptide carbonyls from Gly42, Val45, and Leu417 and side-chain oxygens of Ser421 and Asp420; this Na⁺ ion also stabilizes the outward-

open pre-substrate DAT structure, controls cation permeation of DAT, and its release into the cytosol triggers conformational isomerization to the inward-open pose^{155,169–172}. The Cl⁻ ion resides 5 Å away from the Na1 location and is coordinated by Tyr69, Gln316, Ser320, and Ser356 from TMs 2, 6, and 7; the Cl⁻ molecule increases affinity for Na⁺ at the Na2 site and thus regulates inward-open conformation probability^{155,172,173}. The alternating access conformational pivots occur only after the DA substrate binds to an outward-open conformation primed by two Na⁺ and one Cl⁻ co-substrates. Once DA binds, TMs 1b and 6a, with EL4, form a 'lid' which seals off access to extracellular solvent. The intracellular segment of TM 5 unwinds, granting cytosolic solvent access to the Na2 site. This event sparks the ultimate transition of DAT to its inward-open conformation which sees TM1a swing away from the substrate binding pocket producing solvation thereof and the concomitant entry of DA and the Na2 sodium into the neuronal cytosol (Figure 11)^{171,174,175}.

Regulation

DAT function is subject to extensive control through posttranslational modification and binding partner interactions. Rat and human DATs are glycosylated on Asn residues of EL2¹⁷⁶. This modification supports DA uptake V_{\max} , trafficking of the transporter to the plasma membrane and its retention there, and decreases potency of cocaine^{177–179}. Increased DAT glycosylation has been proposed as a mechanism which increases susceptibility to DA neuron loss

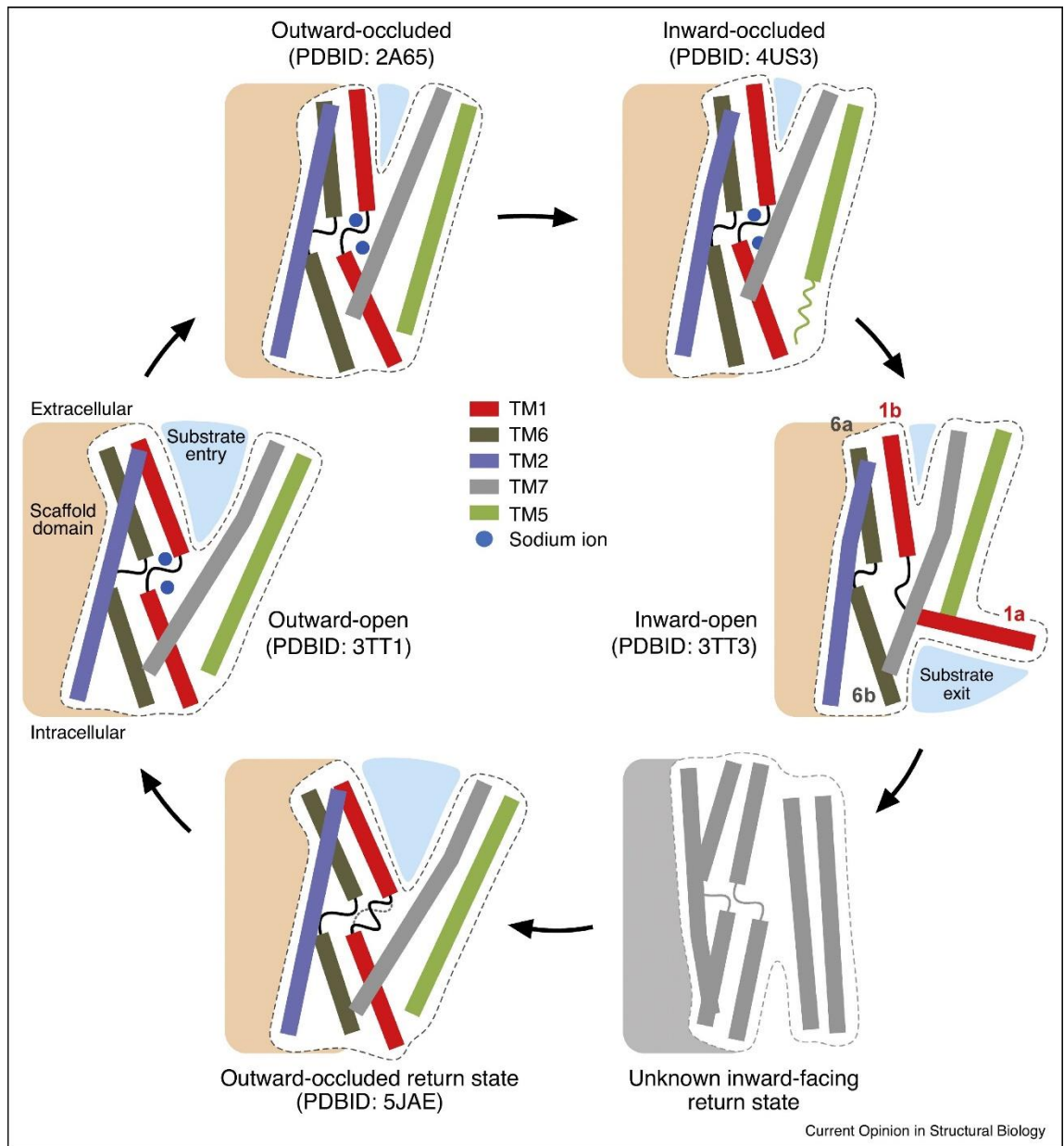


Figure 10. Alternating access mechanism of substrate transport. The substrate binding vestibule is exposed to extracellular solvent in the outward-open pose (left). After substrate binds in the permeation core, the transport protein undergoes structural rearrangements to restrict extracellular solvent access (top). This involves TMs 1b, 6a, and EL4 in the LeuT transport process. This occluded conformation is relieved by rearrangement of intracellular gating and loop networks and involves ‘swinging out’ of TM 1a which exposes the substrate binding locus to intracellular solvent into which substrate is released – this is the inward-open conformation (right). The transporter then moves back through the occluded pose to return to the outward-open conformation. Adapted from ref # 158, with permission.

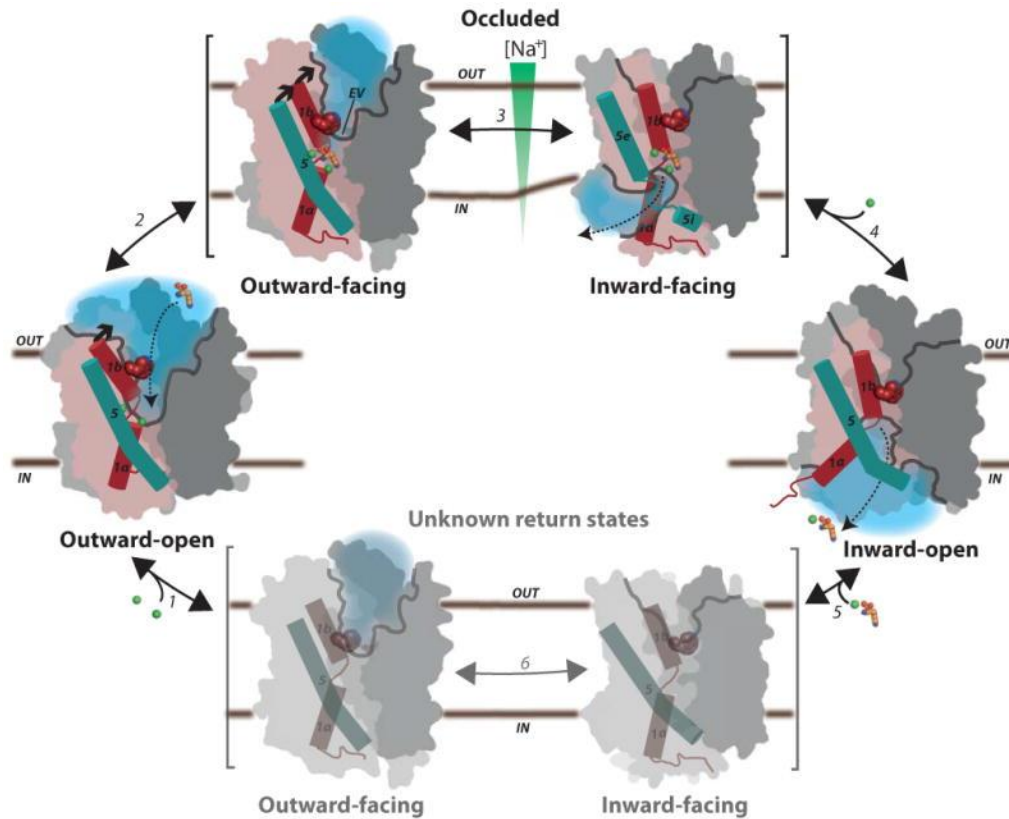


Figure 11. Na⁺ Involvement in the neurotransmitter transport process. Na⁺ ions (green spheres) enter into their Na1 and Na2 sites and stabilize the outward-open transporter conformation (1) which allows substrate to bind and induce isomerization to the occluded formation (2). This induces closer of the extracellular vestibule, causing TM 5i to unwind (3) and provide intracellular access to Na2, releasing this Na⁺ (4). TM 1a shifts away from the protein allowing substrate and Na⁺ from Na1 to enter the cytosol (5) after which the transporter returns to the outward-open conformation (6). Image adapted from ref # 175, with permission.

characteristic of Parkinson's disease by increasing DAT plasma membrane expression¹⁸⁰. The E3 ubiquitin ligases Nedd 4-2 and Parkin catalyze ubiquitylation of DAT on N-terminal Lys residues 19, 27 (hDAT), and 35 which contributes to PKC-stimulated DAT endocytosis and degradation^{181–183}. Parkin function has been demonstrated to support DAT function as mutant Parkin proteins, which result in PD, fail to properly ubiquitylate improperly folded transporters¹⁸⁴. Cholesterol likewise aids in DAT activity as removal of this molecule results in reduced DA transport V_{max} , increased K_m , loss of outward-open conformational stabilization, Amphetamine (AMPH)-stimulated DA reverse transport (efflux), and leads to aberrant PKC-induced downregulation^{156,185–187}. This cholesterol-DAT interplay contributes to DAT association with cholesterol-rich lipid raft membrane microdomains where scaffolding of DAT-involved signaling complexes is accomplished¹⁸⁶.

Membrane raft and non-raft DAT networks with multiple protein partners. The Ras-like GTPase in neurons, Rin, interacts with DAT's C-terminus to control endocytic processes after PKC activation¹⁸⁸. Similarly, Flotillin-1-DAT interplay contributes to transporter internalization as well as raft recruitment and AMPH-induced DA efflux¹⁸⁹. The SNARE protein Syntaxin 1a (Syn1a), along with the receptor for activated C kinase (RACK), complex with DAT to induce its internalization through phosphorylation by PKC¹⁹⁰. Syn1a interacts with the N-terminus of DAT by which it also blunts DA uptake, reduces transporter plasma membrane expression, and supports AMPH-stimulated DA reverse transport^{191–193}. The Lewy body aggregate protein, α -Synuclein, binds to DAT's distal C-

terminus where it enhances DA efflux, blunts DA uptake, and increases DAT-membrane raft localization^{194–196}. The G-protein $\beta\gamma$ subunits physically interact with the cytosolic carboxyl-peptide of DAT to promote DA efflux and blunt uptake^{197–199}. The D₂ DA autoreceptor partners with the DAT at its distal N-terminus to promote DAT recycling to the surface and acutely increase DA reuptake through PKC and extracellular signal regulated kinase (ERK)-related mechanisms, an operation that may be perturbed in Schizophrenia^{200–203} (Figure 12).

Perhaps the most studied of DAT's regulatory processes is phosphorylation²⁰⁴. Kinase-potentiated phosphorylation events have been demonstrated to exert functional control over DAT. Activation of PKC induces reduced DA transport V_{max} , enhances DA efflux parameters, and plays a role in DAT internalization²⁰⁵. PKC activators like phorbol 12-myristate, 13-acetate (PMA) and agonists for receptors coupled to $G\alpha_q$ stimulate transporter ³²P incorporation^{206,207}. Opposite of the PKC effect, ERK activity increases DAT plasma membrane expression and DA uptake capacity^{201,208}. Calcium-calmodulin dependent kinase II (CAMKII) interacts with DAT C-terminally and contributes to *in vivo* and heterologously expressed AMPH-induced, DAT-mediated DA efflux, but has only been shown to phosphorylate a DAT N-terminal peptide *in vitro*^{209–211}. PKA upregulates DAT function²¹². DAT surface expression and function is increased by tyrosine kinase activity²¹³, and insulin receptor-coupled Akt²¹⁴ and PI3K²¹⁵ activities maintain DAT surface levels. Okadaic acid inhibition of their function revealed the protein phosphatases 1 and 2a (PP1 and PP2a) act upon

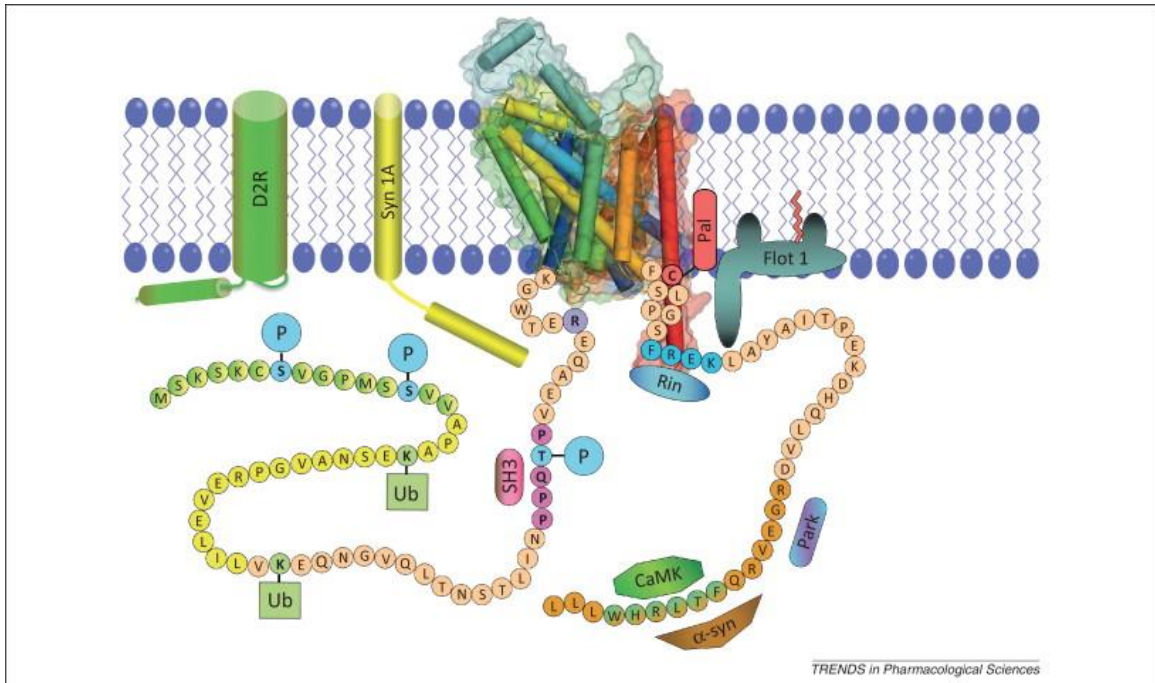


Figure 12. DAT binding partner interactions. Schematic representation of the relative locations of DAT protein interactors and posttranslational modifications. Pictured are the known ubiquitination, phosphorylation, and palmitoylation sites (discussed later) as well as the interacting proteins Flotillin-1, α -synuclein, Rin, Parkin, D₂ DA receptor, and Syn1a. Image adapted from ref # 227, with permission.

DAT to control basal transporter phosphorylation levels²⁰⁷, and of these, PP1 predominates^{216,217}, though a direct protein-protein interaction has been established between DAT and PP2A²¹⁸.

Phosphoamino acid analysis of DAT-³²PO₄ radiolabeling demonstrated around 90% of the tracer's incorporation occurred on Ser residues while the residual incorporation occurred on Thr residues, with the majority of this labeling happening on the distal N-terminus of DAT²¹⁹. Ser2, Ser4, Ser7, Ser12, and Ser13 reside in a PKC consensus domain, and truncation of this peptide eliminates the bulk of basal and stimulated ³²PO₄ radiolabeling^{206,220}. Individual Ser to Ala mutations fail to eliminate transporter ³²PO₄ incorporation, indicating multiple phosphorylation events occur at DAT's N-terminus. *In vitro* phosphorylation of the recombinant rDAT N-terminus (NDAT) was induced by PKC at Ser4, Ser7, and Ser13, and CAMKII phosphorylated Ser13 and PKA catalyzed phosphorylation of Ser7²¹⁶. Ser7 phosphorylation has been identified on the hDAT isoform by mass spectrometry and this event contributes to conformational equilibrium²²¹. ERK-catalyzed, proline-directed phosphorylation of rDAT Thr53 has likewise been demonstrated by mass spectrometry and requires peptide backbone isomerization by the prolyl isomerase PIN1 for dephosphorylation^{216,222,223}. This residue supports both DA uptake and AMPH-stimulated reverse transport, and its phosphorylation is stimulated by amphetamines^{216,223,224}. DAT phosphorylation site information is summarized in Figure 13.

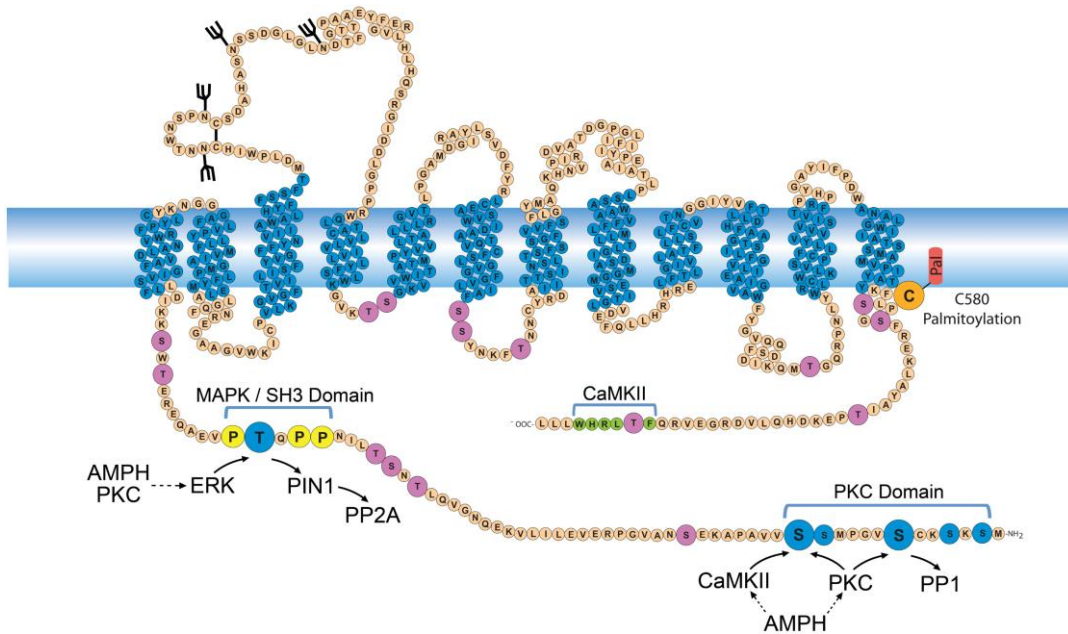


Figure 13. Phosphorylation of the dopamine transporter. Schematic diagram of rDAT phosphorylation sites. The majority of DAT phosphorylation occurs on the cytoplasmic rDAT N-terminus. Known phosphorylation sites, Ser7, Ser13, and Thr53 are represented by larger blue circles. Potential Thr and Ser phosphorylation sites are shown in purple. Other PKC Domain residues are blue, residues of the CAMKII binding domain are green, and Pro residues surrounding the proline-directed phosphorylation site, Thr53, are yellow. Enzymes involved in each phosphorylation event are indicated by solid arrows, and dashed arrows represent AMPH and PKC contribution to each event. The orange Cys residue is the known rDAT palmitoylation (red) site. Adapted from ref #204, with permission.

DAT-Mediated DA Efflux

In addition to synaptic clearance of DA, an important physiological event likewise mediated by DAT is non-vesicular release of DA, commonly known as DA efflux. This effect is reliably induced by amphetamines and is, along with competitive inhibition of DAT-coordinated reuptake of DA^{169,225}, responsible for the pharmacological and rewarding properties of AMPH and amphetamine-like compounds²²⁶. Multiple hDAT single nucleotide polymorphisms are unstimulated hyper-releasers of DA, a phenotype termed anomalous DA efflux (ADE), and this characteristic is thought to contribute to disease etiology²²⁷. Several cellular and DAT-centered mechanisms have been identified to produce DA efflux. N-terminal phosphorylation of DAT is necessary for AMPH-induced DA efflux²²⁸, a process which involves PKC and CAMKII activity^{204,229–231}. This amino-terminus forms electrostatic interactions with PIP₂-enriched membranes through distal Lys residues to propitiate DA efflux²³². AMPH generates a channel-like conformation of DAT through which quantal-like DA efflux occurs²³³; additionally, this channel conformation is able to depolarize the neuron²³⁴ which draws Na⁺ and Ca²⁺ into the cell²³⁵ further exciting DA release phenomena^{236,237}. DA redistribution from vesicles by AMPH action at VMAT2 increases the cytosolic efflux-ready DA concentration^{238–240}. Methamphetamine (METH) produces efflux in many of the same ways as AMPH but an additional sigma receptor functionality has been demonstrated to contribute to METH-induction of DA reverse transport^{241,242}.

DAT Disease Association

Because DA signaling is vital to many important neurological processes, maintenance of its normal transmission, a process to which proper DAT function is necessary, is paramount for sound mental health. As such aberrant DAT processes have been implicated in addiction, ADHD, and PD²⁴³. The DAT-targeting psychostimulants cocaine, AMPH, and ecstasy (MDMA) increase DA neurotransmission through inhibition of DA reuptake by DAT blockade (cocaine) or substrate properties characteristic of competition for the DAT substrate binding pocket and induction of reverse DA transport (AMPH, MDMA)^{244,245}; thus, as they greatly increase DA signaling in the mesocorticolimbic areas of the brain, they are highly addictive substances²⁴⁶. Chronic use of these compounds begets altered DA neuron synaptic connections and DAT surface expression^{247–250} which implies drug taking (or drug taking-like behaviors) can induce neurobiological changes that hamper the addict's reward computation, incentive salience attribution, and behavioral habits^{53,63,72}.

PD results from loss of substantia nigra DA neurons which precipitates dysfunction of coordinated movement. The DAT substrates 6-hydroxydopamine and 1-methyl-4-phenylpyridinium are extensively used in laboratory settings to reproduce loss of the nigrostriatal fiber to recapitulate characteristics of this disease; thus, DAT has long been hypothesized to play a role in PD pathology^{251,252}. While the majority of PD cases are of unknown origin, genetic mutations to α -synuclein and the E3 ubiquitin ligase Parkin, both DAT-interacting proteins, are causative of two familial types of PD²⁵³. DAT mutations which severely reduce levels of mature transporter and significantly reduce DA uptake

capacity have been found in patients with infantile parkinsonism-dystonia^{152,254,255}, and an individual with comorbid early-onset PD and ADHD was discovered to have multiple DAT amino acid polymorphisms which significantly blunt DA reuptake and induce an ADE phenotype²⁵⁶. These findings suggest a role for aberrant DAT forward and reverse transport characteristics in PD etiology.

Because attention and cognition are DA signaling-moderated processes²⁵⁷, malfunctioning DAT has been hypothesized to contribute to ADHD etiology^{258,259}. Indeed, the primary pharmacotherapies for ADHD are DAT-modulating compounds; AMPH and methylphenidate, which operates akin to cocaine, act to relieve the DAergic imbalance attributed to ADHD^{260–262}. Multiple hDAT missense mutations have been discovered in diagnosed individuals^{263,264}. These rare polymorphisms produce the amino acid substitutions Val55Ala, Arg237Gln, Ile312Phe, Val382Ala, Asp421Asn, Ala559Val, and Arg615Cys (Figure 14)^{227,265}. Val55Ala, Ile312Phe, Val382Ala, and Asp421Asn display reduced DA uptake capacity^{265,266}, and the Arg615Cys substitution generates AMPH-insensitivity, reduced membrane micro domain targeting, and is constitutively recycled²⁶⁷. The best-studied of these is Ala559Val. This hDAT polymorphism displays altered trafficking and lateral membrane mobility, elevated tonic phosphorylation of its N-terminus, and an ADE phenotype which is blocked by AMPH and dependent upon D₂ DA receptors and CAMKII activity^{268–271}. In addition, our lab has demonstrated Ala559Val hDAT to be palmitoylation deficient (Shetty et al. unpublished study).

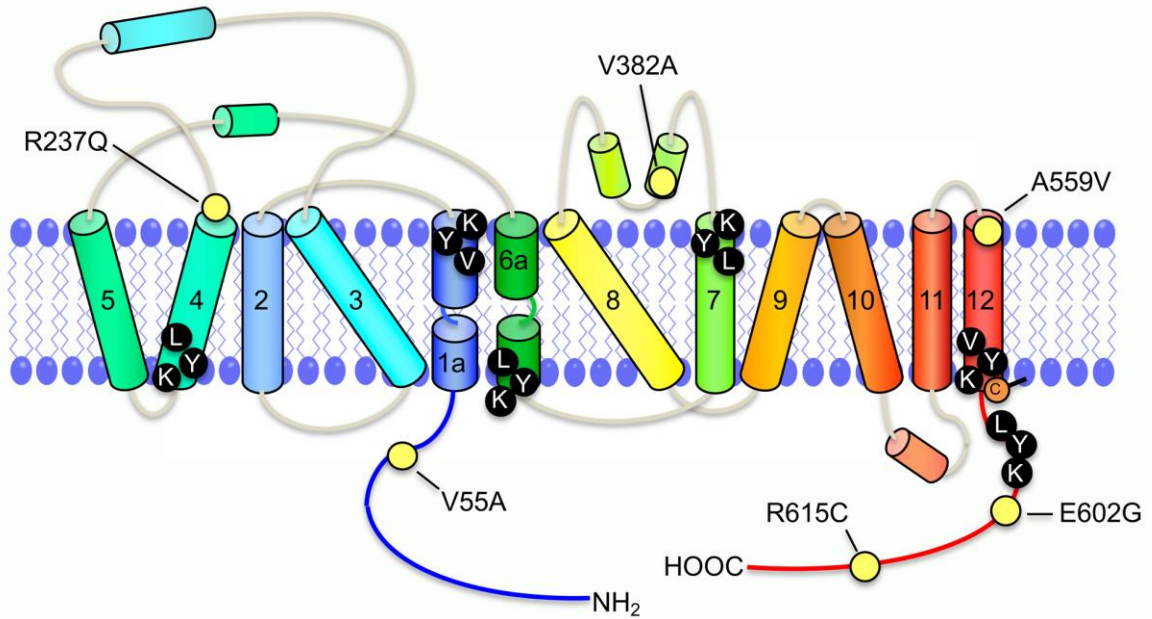


Figure 14. 2D topological diagram of location of hDAT coding variants. Yellow circles represent the relative locations of genetically produced transporter amino acid substitutions. Ala559 resides in the exofacial barrel of TM12 in a hydrophobic pocket generated by two Trp residues. This pocket is likely disrupted by the bulkier Val side chain which may alter TM12, and as a result, overall DAT conformation. Adapted from ref #227, with permission.

S-Palmitoylation

Overview

S-acylation (also known as S-palmitoylation) is the chemical reaction of a fatty acid (predominantly palmitate) to a target protein via enzymatic attachment of the acid locus to the objective protein's available cysteine sulfhydryl side chain, producing a thioester bond (Figure 15)²⁷². This attachment is unlike other protein lipidating events (N-myristoylation, o-acylation, prenylation), which produce stable covalent bonds, in that it is reversible²⁷³. This provides opportunity for the cell to control a protein's palmitoylation state in response to dynamic cell signaling²⁷⁴. The cell generates entire enzyme systems to catalyze protein S-acylation and deacylation: protein S-acyltransferases (PATs), also known as DHHC enzymes (DHHCs) for the presence of a conserved Asp-His-His-Cys motif at their catalytic domains, produces the sulfhydryl-lipid bond on the target protein, and acyl protein thioesterases (APT) and protein palmitoyl thioesterases (PPT) are the primary palmitate-removing enzymes²⁷⁵⁻²⁷⁷. In humans, the DHHC family of enzymes is comprised of 23 different genes of the name *zDHHC* for their conserved zinc finger Cys rich domain and DHHC tetrapeptide regions²⁷⁸. Structurally, these enzymes possess four to six TM domains and, based on the recent crystal structure of human *zDHHC20*, adopt a teepee-like conformation with the top just protruding into the luminal/extracellular space and the catalytic DHHC active site residing at the cytosol-membrane interface (Figure 16)²⁷⁹. An important feature of this structure is the hydrophobic cavity that spans the active site well into the plasma membrane; this cavity is crucial for housing the acyl group and confers acyl chain

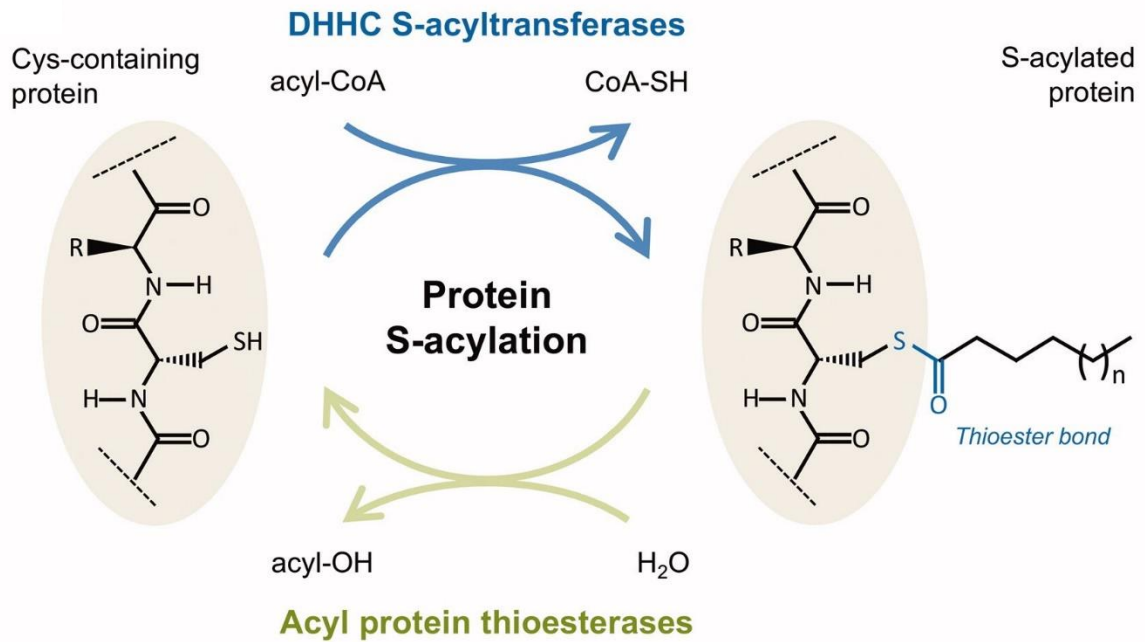


Figure 15. Mechanism of protein S-palmitoylation. Schematic diagram of the S-palmitoylation reaction. The fatty acid from an acyl-CoA molecule is covalently bound to an acceptor protein sulfhydryl to form a thioester bond. This reaction is catalyzed by DHHC enzymes. The opposite reaction is catalyzed by APTs or PPTs to produce both a free fatty acid and sulfhydryl group. Image adapted from ref # 272, with permission.

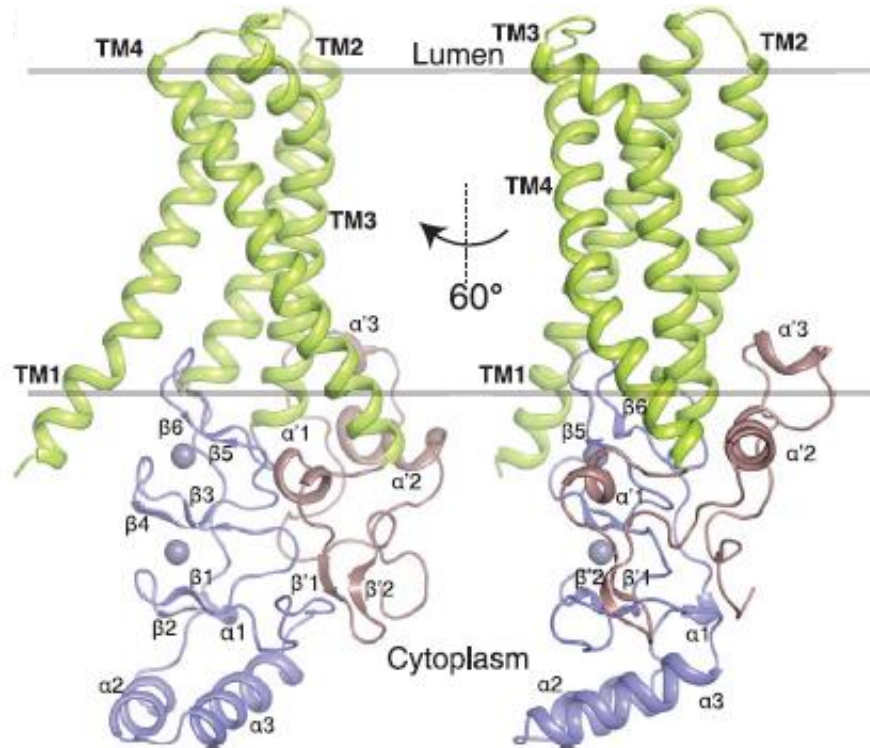


Figure 16. Structure of human DHHC20. hDHHC20 has four TM domains (green), a cytosolic Cys-rich domain (blue) which contains the catalytic DHHC motif and coordinates two Zn²⁺ ions and is comprised of multiple β-sheets and α-helices, and a C-terminal domain which provides additional contacts with the membrane through its hydrophobic residues. Adapted from ref #279, with permission.

length acceptance specificity of each DHHC^{279,280}. DHHC PATs operate by a ping-pong mechanism where the first step is an auto-acylation event followed by transfer of the acyl group to the substrate protein²⁸¹, and are themselves regulated by palmitoylation of Cys residues outside their catalytic domains²⁸². There are two APT and one active PPT enzymes which belong to the metabolic serine hydrolase superfamily, APT1, APT2, and PPT1^{277,283}. The APT enzymes catalyze the depalmitoylation of cytosolic palmitoyl-proteins and themselves undergo palmitoylation to shuttle between golgi, mitochondrial, and plasma membranes^{284–286}. PPT1 depalmitoylates degrading proteins in the lysosome and experiences dynamic palmitoylation cycling to reach the lysosomal membrane^{287–290}. More recently the α/β -hydrolase domain containing protein 17 (ABHD17) family was likewise demonstrated to catalyze depalmitoylating episodes, specifically of N-ras, PSD-95, and microtubule-associated protein 6^{291–293}. Though the depalmitoylases demonstrate some substrate specificity, the relative dearth of enzymes which perform this function indicates these enzymes have high substrate promiscuity or the existence of as of yet undiscovered deacylating proteins^{272,277}.

Once attached, the fatty acid confers local hydrophobicity to its substrate peptide to produce diverse, protein-specific, functional outcomes (Figure 17)²⁹⁴: targeting of cytosolic proteins to plasma or organelle membranes^{295–298}; myristylated or farnesylated proteins can undergo palmitoylation to reinforce membrane binding properties in a process known as kinetic trapping^{299–301}; S-acylation contributes to protein assembly and exit from endoplasmic reticulum or

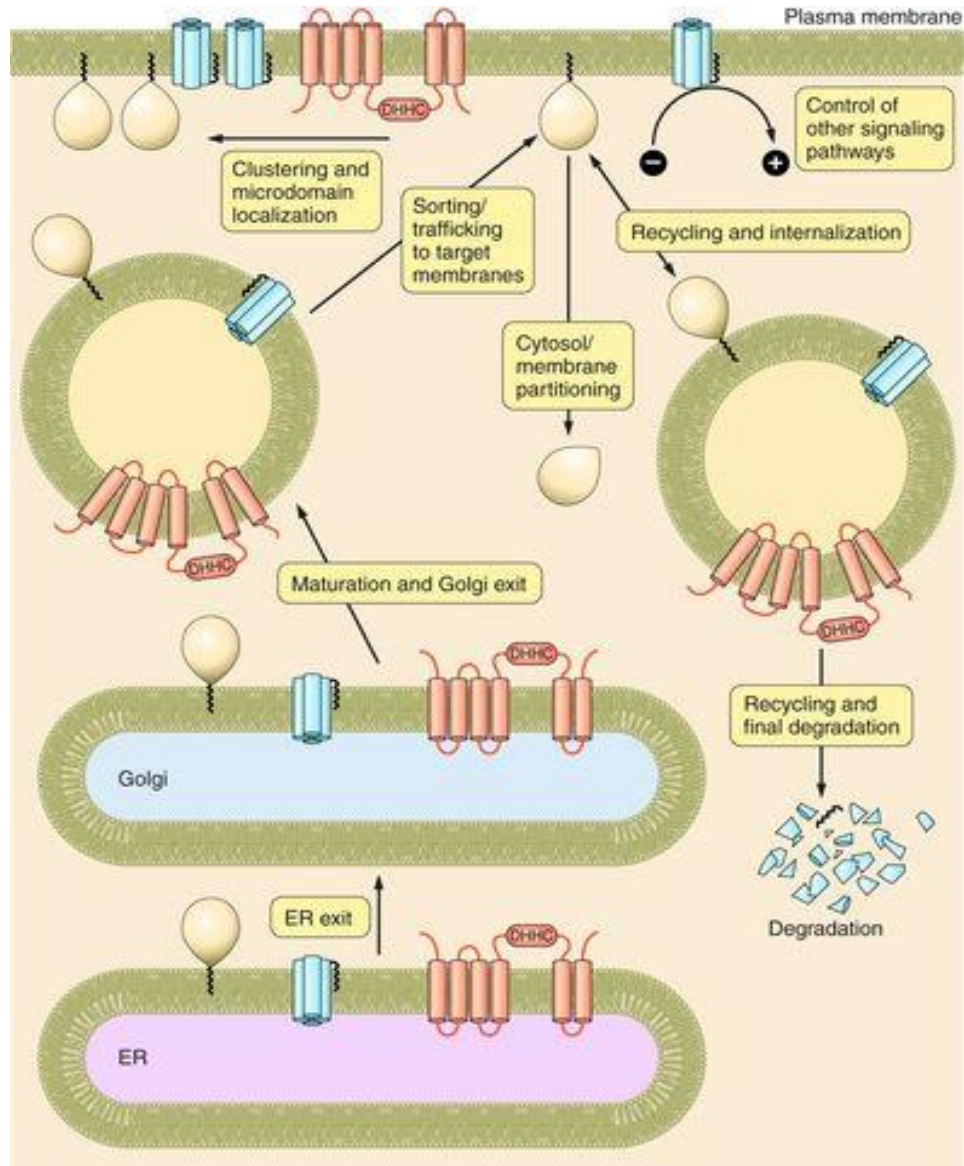


Figure 17. Functional consequences of protein palmitoylation. Schematic diagram of some protein-specific palmitoylation outcomes. Protein S-acylation can exert control over protein trafficking, aggregation, degradation, assembly, and/or oligomerization. Adapted from ref #294, with permission.

Golgi apparatus³⁰²; it can produce protein aggregation and oligomerization^{303,304}; it increases its target protein's stability^{305–307}; endosomal and lysosomal trafficking which controls protein recycling or degradation²⁹⁰; protein membrane microdomain affinity changes with S-acylation occurrence^{308,309}; and S-acylation is able to relieve TM domains of hydrophobic mismatch³¹⁰. From this it follows that the concert of S-acylation events in a cell at any given time regulate a wide variety of cellular processes, and, extrapolating further, organ function. The biological functions palmitoylation influences includes cell signaling³¹¹, exocytosis³¹², endocytosis^{313,314}, metabolism^{315,316}, immune system signaling^{317,318}, ion conductance^{319–323}, and a deluge of host-pathogen interactions^{324–329}. One can see further evidence for this in the ever-expanding array of diseases linked to aberrant S-acylation of important proteins³³⁰. Neuronal ceroid lipofuscinosis^{290,304,331}, multiple cancers³³², Huntington's disease^{303,333,334}, schizophrenia^{335,336}, inflammation³³⁷, and more^{278,338}. This hitherto underappreciated post-translational modification has been calculated to be the fifth most abundant human post-translational modification with approximately 1000 proteins demonstrated to be palmitoylated to date^{339,340}.

The Acyl-Biotinyl Exchange Assay

Acyl-biotinyl exchange (ABE) (Figure 18)³⁴¹ is the primary method used in these studies to investigate palmitoylation aspects of DAT's nature. This technique involves three basic steps: (1) blocking of non-acylated Cys thiol groups with N-ethylmaleimide or methyl methanethiosulfonate; (2) specific chemical cleavage of thioester bonds at neutral pH with hydroxylamine; (3) biotinylation of post-

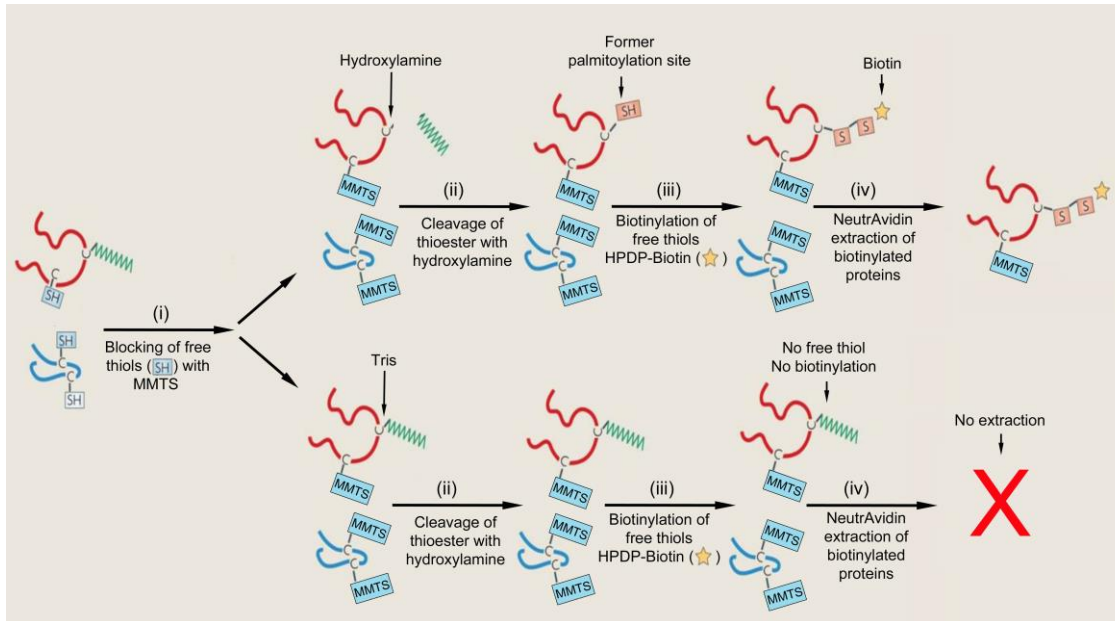


Figure 18. The ABE method. Outline of the major steps of the ABE technique. Free thiols are blocked by the MMTS reagent after which the sample is split into two. One half undergoes hydroxylamine cleavage of the thioester bond freeing a Cys sulfhydryl group while the other half is treated with Tris buffer which does not chemically remove palmitate from Cys thiols. A sulfhydryl-specific biotinylation reagent accesses the once-palmitoylated thiol, and biotinylated proteins are captured *via* avidin affinity chromatography. This capture does not occur in the Tris-treated sample. Peptides are eluted and are free for detection by SDS-PAGE and Western blotting or mass spectrometry.

palmitoylated sulfhydryl groups with thiol-reactive biotinylation reagents and subsequent NeutrAvidin affinity chromatography isolation. The strength of this assay is that it is Cys-centered. This allows for perhaps greater sensitivity than radiolabel procedures as protein-palmitate bonds are chemically severed, free palmitate is removed, and the label is applied whereas radiolabeling requires endogenous removal of unlabeled fatty acid and incorporation of the radiotracer³⁴². This technique labels the entire cellular volume of palmitoylated proteins and, consequently, is easily adapted to mass spectrometry proteomic techniques^{330,343}.

DAT Palmitoylation

rDAT and hDAT isoforms have been demonstrated to be palmitoylated in rat brain tissue and heterologous expression systems by both metabolic incorporation of [³H]palmitic acid and ABE techniques³⁴⁴. Incorporation of the [³H]fatty acid occurs rapidly with its detection at 1 hour, indicative of rapid tonic cycling of this modification of DAT. The irreversible PAT inhibitor, 2-bromopalmitate (2BP), significantly attenuates DAT palmitoylation indicating DAT palmitoylation is catalyzed by DHHCs. Acute 2BP treatment of rat striatal synaptosomes produced significant reduction in DA uptake V_{max} , while extended 2BP treatment times of DAT-expressing cells produces loss of full length DAT protein and low M_r DAT fragments³⁴⁴. These two findings indicate palmitoylation sustains acute DA uptake capacity and chronic control over DAT degradation. DAT is acylated by DHHCs 2, 3, 8, 15, and 17³⁴⁵. Co-expression of these PATs and rDAT produce significantly increased DA uptake and total DAT expression. Rat DAT possesses five cytoplasmic Cys residues predicted to be exposed to the

aqueous environment and available for S-palmitoylation. Cys6, Cys135, Cys341, Cys522, and Cys580 were mutated to Ala and assayed for any palmitoylation loss by [³H]palmitic acid metabolic incorporation. Cys580Ala radiolabeling was reduced by ~50% relative to WT while the others induced no change. This result indicates Cys580 is a primary site of DAT palmitoylation (Figure 19, top)^{344,346}. Cys580 resides at the cytoplasmic interface of TM12 and likely contributes to the proper architecture of that α -helix, perhaps aiding its kink¹⁵⁵. Cys580Ala rDAT displays attenuated DA uptake kinetics and an increased turnover rate, indicating Cys580 modification is crucial for DA uptake capacity and DAT stability^{345,347}. Our work has also demonstrated DAT phosphorylation and palmitoylation mechanisms reciprocally control each other³⁴⁷. Pharmacological positive or negative manipulation, or mutational ablation of known sites, of each modification produced the opposite effect on the corresponding modification. Thus, mutation of the known DAT PKC phosphorylation site, Ser7, induced increased transporter palmitoylation, and the Cys580Ala substitution increased DAT phosphorylation. Likewise, PKC activation decreased DAT palmitoylation, PKC inhibition increased DAT palmitoylation, 2BP treatment increased DAT phosphorylation, and DHHC2 overexpression decreased DAT phosphorylation (Figure 19, bottom)^{346,347}. That ~50% of the [³H]palmitate remains on Cys580Ala rDAT likely means incorporation is occurring at other site(s) (probably Cys6, Cys135, Cys 341, and/or Cys 522) undetectable by this technique which have yet to be elucidated. Mutagenesis of other sites may induce higher tonic palmitoylation of transporter populations still

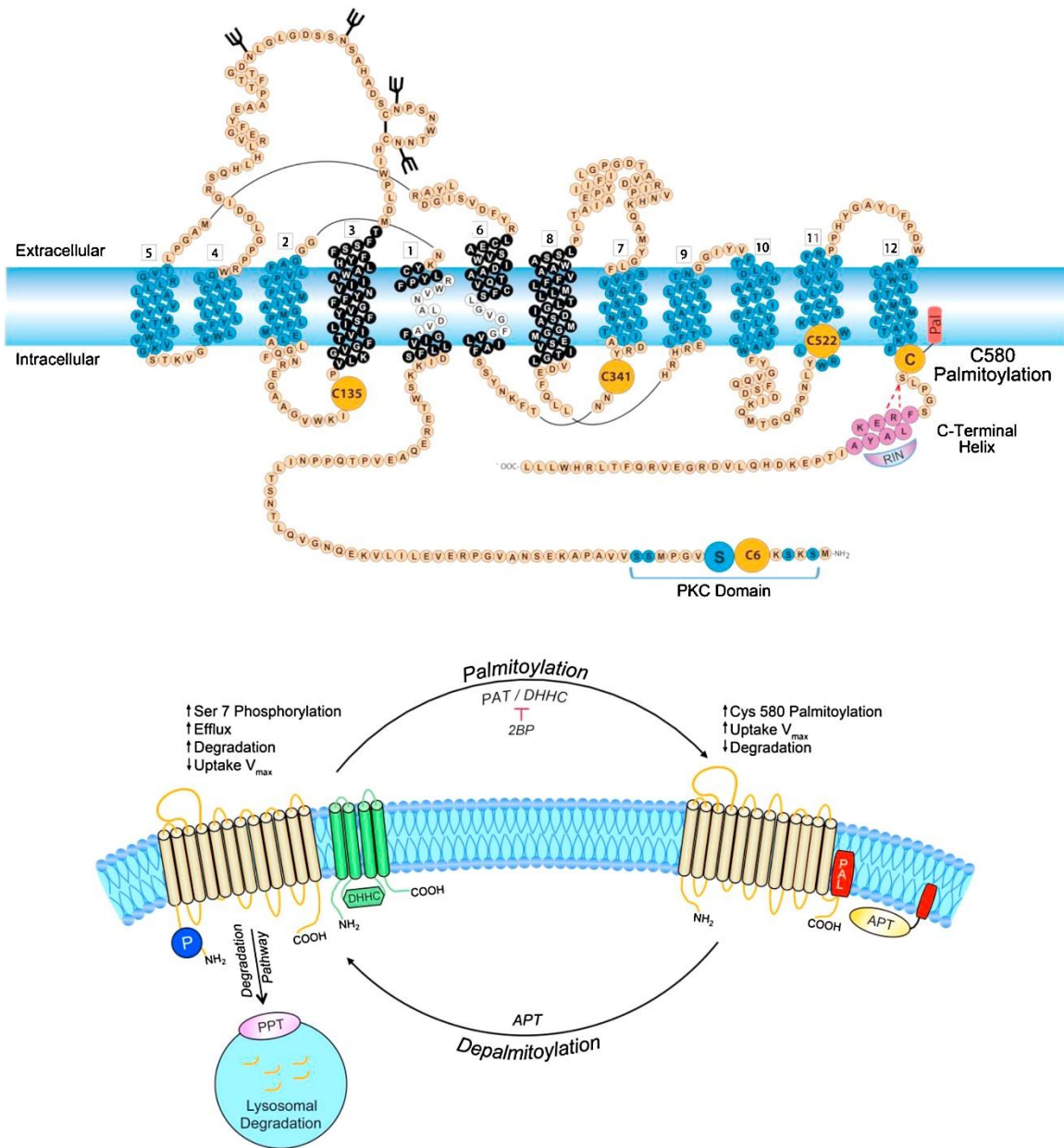


Figure 19. Dopamine transporter palmitoylation mechanisms. *Top* Schematic topological diagram of relative locations of potential DAT palmitoylation sites (orange circles) and known palmitoylation site, Cys580 (orange circle with attached red cylinder). *Bottom* DAT functional characteristics altered by its palmitoylation cycle. DAT palmitoylation increases DA uptake V_{max} and DAT stability while opposing DAT phosphorylation. Adapted from ref #346, with permission.

possessing Cys580. We therefore implemented alternate strategies, beginning with ABE analysis of intracellular Cys to Ala mutations, to resolve other DAT palmitoylation sites from background that cannot be detected by the radiolabeling technique.

CHAPTER 2

DAT N-TERMINAL PALMITOYLATION AND THIS MODIFICATION'S EFFECT ON DOPAMINE EFFLUX

Abstract

The dopamine transporter (DAT) is the dopaminergic neuron plasma membrane transport protein responsible for recollection of synaptic dopamine (DA) into the neuron after stimuli-induced transmitter release. DA signaling is responsible for a panoply of physiological consequences, and, as the primary conduit for DA entry into eponymous neurons, DAT is one of the most popular targets of legal and illegal chemical agents aiming to modulate DA signaling. Malfunctioning DATs are thought to contribute to a host of neurological maladies including bi-polar disorder, attention deficit/hyperactivity disorder (ADHD), addiction, and Parkinson disease. DAT operation is precisely controlled through protein interactors and post-translational modifications including phosphorylation, glycosylation, ubiquitination, and, of importance here, S-palmitoylation – the labile, enzymatic union of cysteine sulfhydryl moieties with the fatty acid palmitate *via* a thioester linkage. S-palmitoylation conveys protein-specific functions which can include protein oligomerization, membrane micro domain localization, protein maturation, and alleviating transmembrane domain hydrophobic mismatch. DAT palmitoylation was previously discovered at rat (r)DAT Cys580 and modification of this residue acutely increases DA uptake V_{max} without altering DAT surface

expression and opposes long-term DAT degradation. As the enzymatic processes of S-palmitoylation is primarily thought to occur on intracellularly accessible cysteines, Cys to Ala mutants of each intracellular rDAT cysteine residue (6, 135, 341, 522, and 580) were assessed for its S-palmitoylation phenotype by the acyl-biotinyl exchange (ABE) method. This process revealed an ~50% loss of palmitoylation detection in the Cys580Ala mutant alone, a result almost identical to the previous study utilizing incorporation of radiolabeled fatty acid. The remaining radiolabel and ABE signals imply the presence of one or more palmitoylation sites undetectable by these protocols. Subsequently, the alternate sites of rDAT S-palmitoylation were probed by utilizing a combination of multiple-site Cys to Ala mutagenesis, Asp-N and CNBr proteolytic peptide mapping of endogenous and heterologously expressed rDATs in conjunction with ABE analyses. These methodologies revealed Cys6 and, surprisingly, the exoplasmic Cys90 as the likely secondarily acylated rDAT sites. These residues were then assessed for functional relevance by surface biotinylation, DA transport saturation analyses, and reverse DA transport (efflux) assays. Palmitoylation of Cys6 residue may invoke tethering of the cytosolic NH₂-terminus of rDAT to the plasma membrane and this Cys residue was shown to support DAT-mediated DA efflux. Cys90 acylation may aid DAT endosomal retention and substrate reuptake as the Ala90 mutant displays increased surface populations and decreased apparent DA affinity. As DAT S-palmitoylation supports forward and reverse transport processes, therapeutic alteration of this DAT modification may alleviate DAT-involved disease burden.

Introduction

Cognition, movement, fear generalization, reinforcement learning, and, as a result, behavior are mammalian functions mediated in the central nervous system by the neurotransmitter dopamine (DA)^{42,65,244,348–350}. As DA contributes to these vital processes, its maintenance at a proper equilibrium is essential for individual health, and divergence from healthy DA homeostasis is hypothesized to contribute to the mental disorders attention-deficit/hyperactivity disorder (ADHD)³⁵¹, Parkinson disease³⁵², and schizophrenia³⁵³. Licit therapeutic strategies target the properties of DA flux²⁶², and abuse of these properties by illicit drug use, and even excess video game play^{22,26}, greatly increase the likelihood of addiction disorders¹⁰. It follows, then, that fine-tuned regulation of synaptic DA concentration is essential to well-being. After exocytotic transmitter release, DA signaling is primarily controlled through its removal from the perisynaptic space *via* the presynaptic plasmalemmal dopamine transporter (DAT) into the cytoplasm of the expressing neuron¹³⁹. DAT is a member of the sodium and chloride dependent solute carrier 6 family of neurotransmitter transporters¹⁴⁰ and is the molecular target of several therapeutic agents and drugs of abuse which manipulate DAT properties to alter synaptic DA concentration^{354,355}.

A large body of work has demonstrated DAT function to be precisely regulated by trafficking, post translational modification, and binding partner mechanisms²²⁷, and much of this regulation occurs at DAT's cytosolic N-terminus. Control over DAT endocytosis and lysosomal degradation is exerted by ubiquitination of three lysines on DAT's N-terminus¹⁸³, a process stimulated by

PKC activation¹⁸². The human DAT (hDAT) associates with the anionic phospholipid phosphatidylinositol (4,5)-bisphosphate (PIP₂) through distal N-terminal lysine residues, which alters hDAT stimulant interaction²³². Several proteins bind to N-terminal regions of DAT to modulate DAT function: the DA D2 autoreceptor binds N-terminally on DAT leading to the recruitment of additional DATs to the plasma membrane, increasing DA uptake²⁰⁰; the soluble N-ethylmaleimide-sensitive factor attachment receptor (SNARE) protein syntaxin 1A networks with the first 33 residues of DAT which reduces forward DA transport and promotes DA transport (efflux)^{191,193}; and multiple kinases phosphorylate DAT on its N-terminus³⁵⁶.

Striatal rDAT was demonstrated to be phosphorylated on N-terminal residues by aminopeptidase instigated loss of [³²P]radiolabel²¹⁹. At the distal N-terminus resides a protein kinase C (PKC) binding domain. Activation of this kinase significantly elevates transporter phosphorylation^{207,206}, blunts DA uptake velocity³⁵⁷, redistributes DATs away from the plasma membrane³⁵⁸, and phosphorylates an N-terminal DAT peptide (NDAT) at Ser4, Ser7, and Ser13 *in vitro*²²¹. Proline-guided phosphorylation occurs on rNDAT²¹⁶ through extracellular signal-related kinase (ERK) action at rDAT Thr53²²³; a process which is sensitive to psychostimulant activity and supports DA uptake and efflux³⁵⁹. Additionally, the human (h)DAT N-terminus undergoes phosphorylation at Ser and Thr residues²²¹ including Thr48^{360,361}. This N-terminal DAT phosphorylation pattern is essential for induction of DA efflux^{228,362}, and pharmacologic activation of DAT-mediated reverse transport coincides with phosphorylation of this DAT locus²⁰⁴.

Our lab has demonstrated DAT to be lipid-modified through the S-palmitoylation process³⁴⁴. S-palmitoylation is the enzymatic addition of one of a species of long chain saturated fatty acids, predominately palmitate, to sulfhydryl functional groups of cysteine residues creating a chemically labile thioester bond²⁹⁴. This process is catalyzed by the zDHHC gene family of palmitoyl acyltransferases (PATs)²⁷⁸ and reversed by two separate thioesterase families: palmitoyl protein thioesterases (PPTs) are lysosomal-resident enzymes which hydrolyze fatty acid-protein thioester linkages during protein degradation²⁸⁷; and acyl protein thioesterases (APT) are cytoplasmic thioesterase enzymes³⁶³. Palmitoylation increases the affinity of lipidated protein micro domains for the hydrophobic interior of an intracellular membrane, inducing substrate-subjective functional outcomes which can include: localizing the modified protein to a target membrane micro domain; trafficking the protein to recycling endosomes or to lysosomes; maturation of protein in the endoplasmic reticulum; alleviating hydrophobic mismatch of transmembrane α -helical structures; changing the profile of protein interactome interactors; and, ultimately, modulation of the function of the acylated protein²⁹⁴. The initial study on rDAT palmitoylation identified Cys580, which resides at the cytoplasmic interface of transmembrane domain (TM) 12, as the primary DAT palmitoylation site³⁴⁴. Mutation of this Cys residue induced fragmentation of the protein, demonstrating acylation of this residue antagonizes transporter degradation; additionally, loss of Cys580 palmitoylation suppressed DA transport V_{max} ³⁴⁷.

The first report on DAT palmitoylation did not exclude the occurrence of this modification on residues other than Cys580³⁴⁴, perhaps due to the limitations of the methodology used. More recently, a reciprocal coordination between DAT phosphorylation and palmitoylation was discovered to modulate DAT operation³⁴⁷. Through mutagenesis and pharmacological means, it was shown that when DAT phosphorylation increases palmitoylation decreases; alternatively, when phosphorylation decreases palmitoylation increases. The aim of this study was to probe for the existence of rDAT palmitoylation sites separate from Cys580 in native tissue and heterologous expression systems. We then analyze Ala mutations of the novel DAT palmitoylation sites for DA uptake kinetic parameters and assess the influence general cellular palmitoylation, and DAT-specific palmitoylation, exert over DAT-mediated DA efflux.

Results

Acyl-Biotinyl Exchange Analysis of Cys to Ala Point Mutant Palmitoylation

Our previous study identified Cys580 as a major DAT palmitoylation site using metabolic radiolabeling with [³H]palmitate. Our results suggested this method may have been inadequate to delineate a second, lower-stoichiometric, site if the incorporation of the radiolabeled fatty acid is indistinguishable from background labeling. To overcome this potential limitation, we employed the acyl-biotin exchange (ABE) protocol³⁴¹ which, due to increased availability of once-palmitoylated Cys residues *via* hydroxylamine (NH₂OH)-induced liberation of the fatty acid from the sulfhydryl functional group of Cys residues, produces higher sensitivity^{342,364}. This technique was used to delineate from background the effect

of mutational alteration of the five DAT intracellular Cys residues to determine the presence of DAT palmitoylation sites in addition to Cys580.

However, the ABE technique yielded results akin to our previous study (Figure 1): Cys580 is the major rDAT palmitoylation site, and removal of this site reduces DAT palmitoylation to ~50% (* $p < 0.05$ Cys580 *versus* WT, $n=8$), with no discernable S-palmitoylation loss associated with Cys to Ala ablation of the other potential sites ($p > 0.05$ for $\Delta 21$, Cys135Ala, Cys341Ala, and Cys522Ala *versus* WT, $n=3$ or more independent experiments). These results were nearly identical to the radiolabeling study; the incomplete loss of Cys580Ala ABE readout again indicates additional palmitoylation events on DAT, but the mutational loss of these additional sites may induce over-palmitoylation of Cys580 in these transporter populations.

Palmitoylation of Single Intracellular Cys rDATs

To resolve palmitoylation events which may occur at lower stoichiometry than Cys580 on WT rDATs, all intracellular Cys residues were mutated to Ala save one which was studied for the occurrence of DAT palmitoylation events at that particular cysteine *via* ABE (Figure 2). This methodology revealed Cys6 as a PAT substrate as rDAT populations possessing only Cys6 produced significantly greater ABE signal above rDATs possessing only intracellular Cys135, Cys341, or Cys522 ($^{##}p < 0.01$ Cys6 *versus* Cys135, Cys341, and Cys522). The Cys6 readout was similar to that of rDATs with only Cys580; therefore, this approach confirmed Cys580 as a DAT palmitoylation site. Here Cys6, like Cys580, was significantly less palmitoylated than WT ($^{***}p < 0.001$ Cys6 *versus* WT $n=8$; $^{***}p < 0.001$

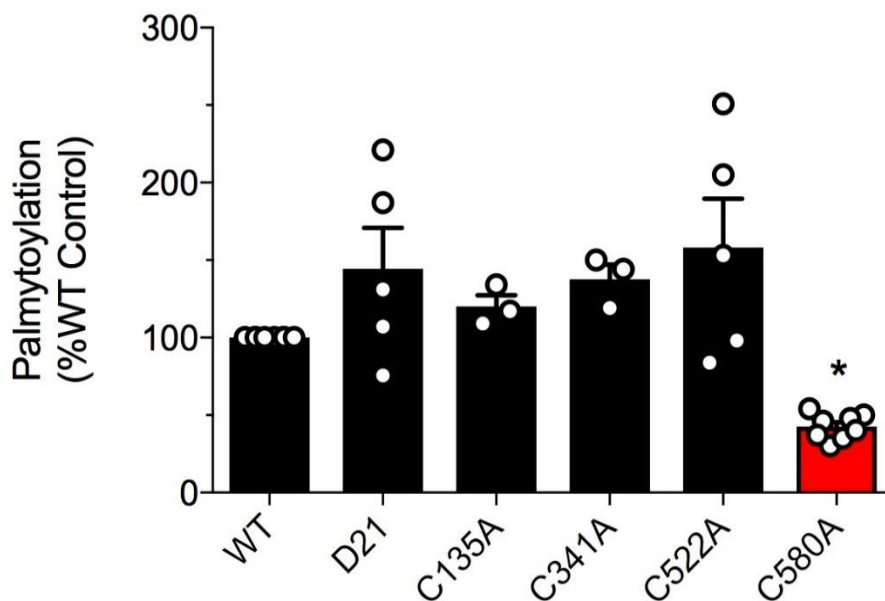
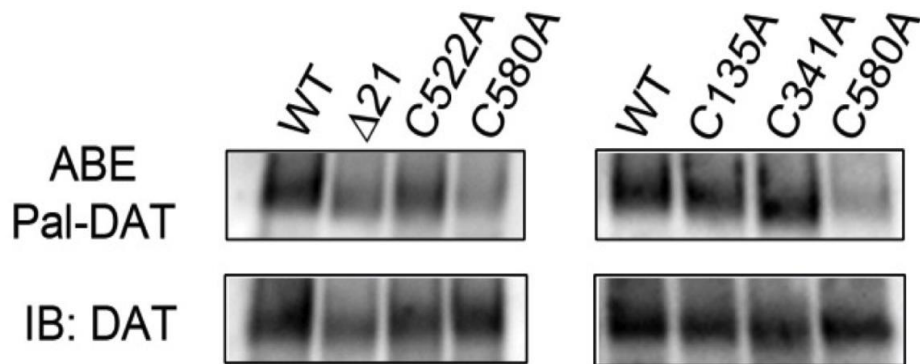


Figure 1. Palmitoylation levels of WT and mutant rDATs measured by ABE. Membranes isolated from LLCPK₁ cells expressing WT or Cys mutant DATs were subjected to ABE to determine palmitoylation levels. *Upper Panels:* ABE DAT levels normalized to Total DAT levels (*middle panels*). Samples were subjected to SDS-PAGE and immunoblotting using MAb 16. *Bottom Panel:* Quantification of palmitoylation intensity normalized to total DAT levels (means \pm SE of 3 or more independent experiments). C580A * $p < 0.05$ relative to WT, ANOVA with Dunnett's post hoc test. These experiments confirm Cys580 as an rDAT palmitoylation site but were unable to distinguish any other palmitoylation sites of perhaps lesser abundance.

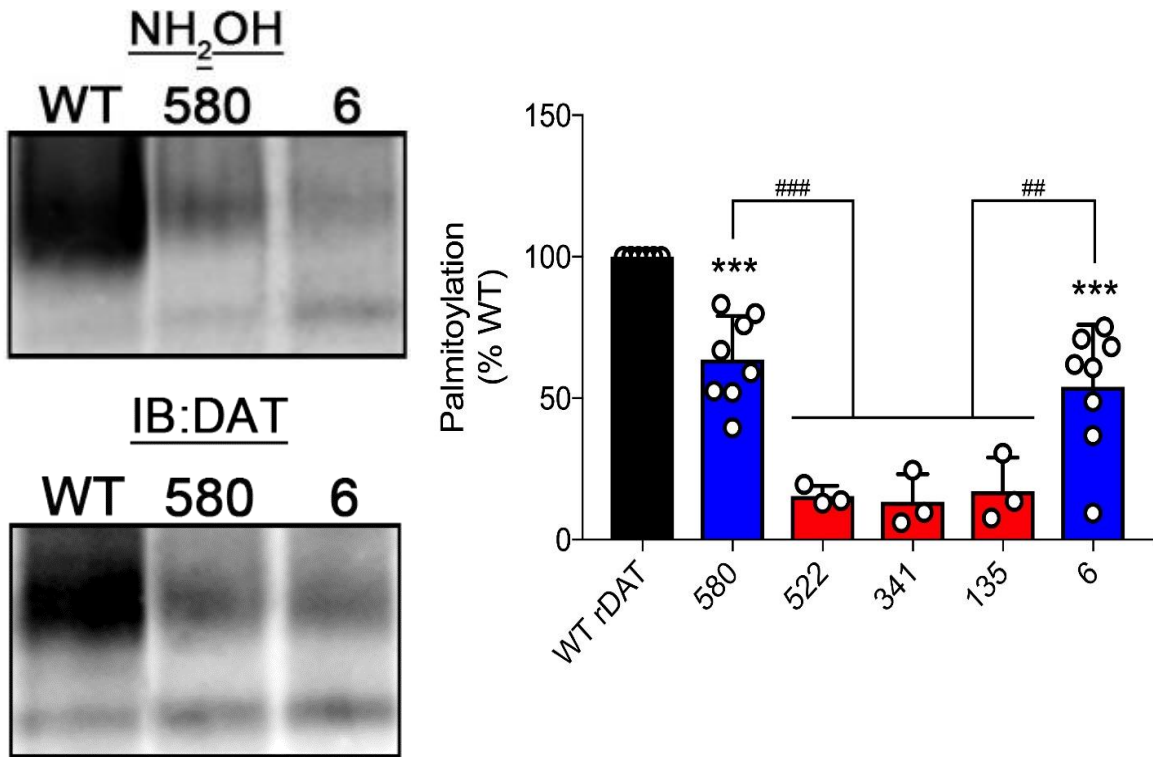


Figure 2. ABE analysis of WT and multiple Cys to Ala mutants of rDAT.

Mutants are named such that the number represents the only cysteine remaining on the cytosolic portion of rDAT, e.g. '580' is Cys522/341/135/6Ala, leaving only Cys580 available to intracellular S-palmitoylation. Membranes isolated from LLCPK₁ cells expressing the indicated DAT were subjected to ABE. These experiments confirm Cys580 as an rDAT palmitoylation site and support Cys 6 as an additional site of the fatty acid incorporation. n=3 for 522, 341, 135; n=8 for WT, 580, and 6. *** p<0.001 for 580 and 6 vs WT, ### p<0.001 for 580 vs 522, 341, 135, and ##p<0.01 for 6 vs 522, 341, 135 (means ± S.E.). Statistical analyses performed by ANOVA with Tukey's post hoc test.

Cys580 versus WT, n=8). That the Cys580 mutant did not possess palmitoylation signatures like WT is further evidence supporting the existence of extra-580 palmitoylation sites; this set of experiments impugns Cys6 as that site.

Palmitoylation of DATs with or without the Putative Palmitoylation Sites

To strengthen this finding, we compared palmitoylation signals of rDAT mutants possessing only the two putative palmitoylation sites (Cys135/341/522Ala) with an rDAT mutant population possessing the three intracellular Cys residues and without the two that are palmitoylated (Cys6/580Ala) (Figure 3). The results show palmitoylation of Cys135/341/522Ala to be at WT levels ($p>0.05$ Cys135/341/522Ala versus WT, n=3) while Cys6/580Ala ABE signals are at background levels ($**p<0.01$ Cys6/580Ala versus WT, n=3). This further supports Cys 6 as a second rat DAT palmitoylation site.

In Vivo Palmitoylation of the rDAT N-terminal Peptide

To determine if rDAT is palmitoylated on its N-terminus *in vivo*, an approach similar to previous photoaffinity labeling with subsequent proteolytic peptide mapping of the transporter was implemented^{365–368}. However, in these experiments the photoaffinity tagging was replaced with the ABE process. Enzymatic and chemical proteolysis of DATs isolated from rat striatum were subjected to the ABE process. The first approach utilized Asp-N; this enzyme selectively cleaves peptide bonds on the N-terminal side of aspartic acid residues and has been shown to generate a DAT peptide of approximately 19 kDa by

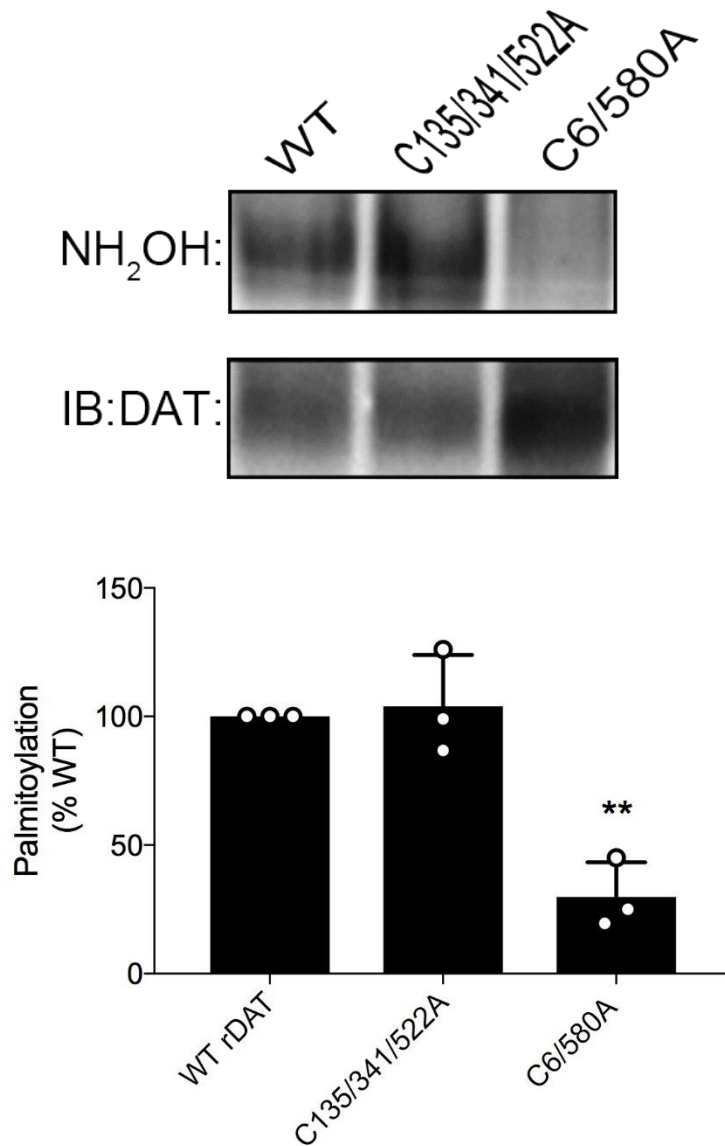


Figure 3. Palmitoylation analysis of mutant DATs containing only the Cys residues suspected of being palmitoylated or containing all Cys residues except the suspected palmitoylation sites. Indicated mutants were subjected to ABE as described previously. Data are presented as % WT control. $n=3$, 103.90 ± 7.80 $p>0.05$ for C135/314/522A *versus* rDATs (mean \pm S.E.), and ** $p<0.05$ for C6/580A *versus* WT (mean \pm S.E.). Statistical analyses were performed by ANOVA with Tukey's post hoc test. These results further support both Cys580 and Cys6 as palmitoylation sites as DATs possessing only these two intracellular Cys residues have WT level palmitoylation signatures.

[FJ1]

ASP-N proteolysis at Asp174, a peptide which is detected by a monoclonal DAT antibody against an N-terminal epitope (MAb16)³⁶⁹(Figure 4). Synaptosomal preparations from excised rat striatal tissue were treated with 1µg/mL Asp-N in SP buffer for 45 minutes at 25°C (control samples were incubated in SP alone) after which the samples underwent the ABE protocol. After isolation, digestion, ABE purification, and immunoblot detection with MAb16, a Western blotting signal of ~19 kDa emerged (Figure 5). This peptide is the N-terminus of rDAT (residues 1-174) and, because it was isolated by ABE, is modified by S-palmitoylation. This is the first demonstration of N-terminal rDAT palmitoylation *in vivo*. This portion of rDAT's N-terminus contains both Cys135 and Cys6, and the Asp-N-ABE protocol is unable to distinguish between S-palmitoylation at Cys6 and Cys135.

Cyanogen Bromide (CNBr) Digestion and ABE Analysis of the rDAT N-terminus

To further delineate if this *in vivo* N-terminal rDAT palmitoylation event occurs at Cys6 or Cys135, CNBr chemical proteolysis with subsequent ABE was utilized. CNBr cleaves peptide bonds C-terminally to methionine residues. CNBr selectively hydrolyzes DAT proximal to methionine residues (106, 111, 116) in the second transmembrane α -helix, generating a DAT N-terminal peptide of an approximate 11 kDa molecular weight³⁶⁶(Figure 6) detectable by MAb16 Western blotting. Importantly, this peptide does not include Cys135. Synaptosomes were prepared from extracted rat striatum and treated with 100 µL of 70% formic acid with or without 1M CNBr for 1 hour at 25°C in the dark followed by ABE analysis

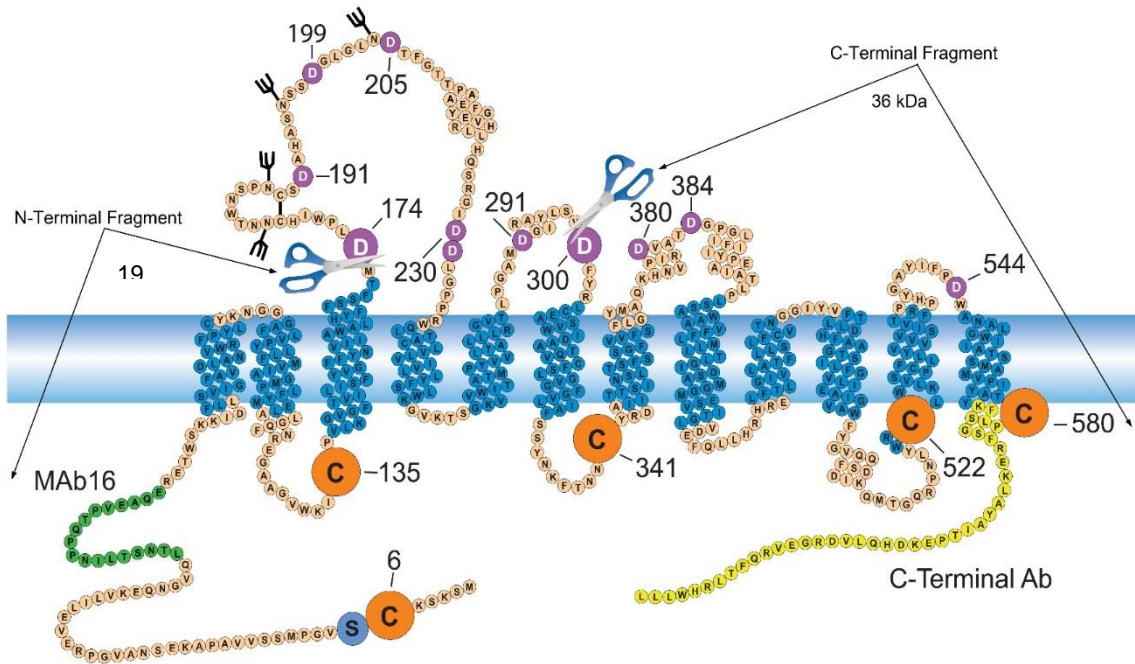


Figure 4. Asp-N schematic proteolytic profile of rDAT. Schematic diagram of the expanded membrane topology of DAT with 12 TMDs and intracellularly facing N- and C-termini. Vertical stacks of amino acids (blue) represent the 12 α -helical membrane spanning domains. The extracellularly available Asp residues are highlighted in mauve. The known sites of glycosylation (black branched sticks), phosphorylation within the PKC-domain containing Ser7 (blue circle) and relative sites of potential S-palmitoylation (orange circles) are shown. The C-terminal helix (yellow, FREKLAYA) is also shown, and is the epitope for the C-20 antibody. Asp-N proteolysis of rDAT will generate a 19 kDa peptide which can be visualized after immunoblotting with MAb16 and a 36 kDa peptide visible after immunoblotting with C-20.

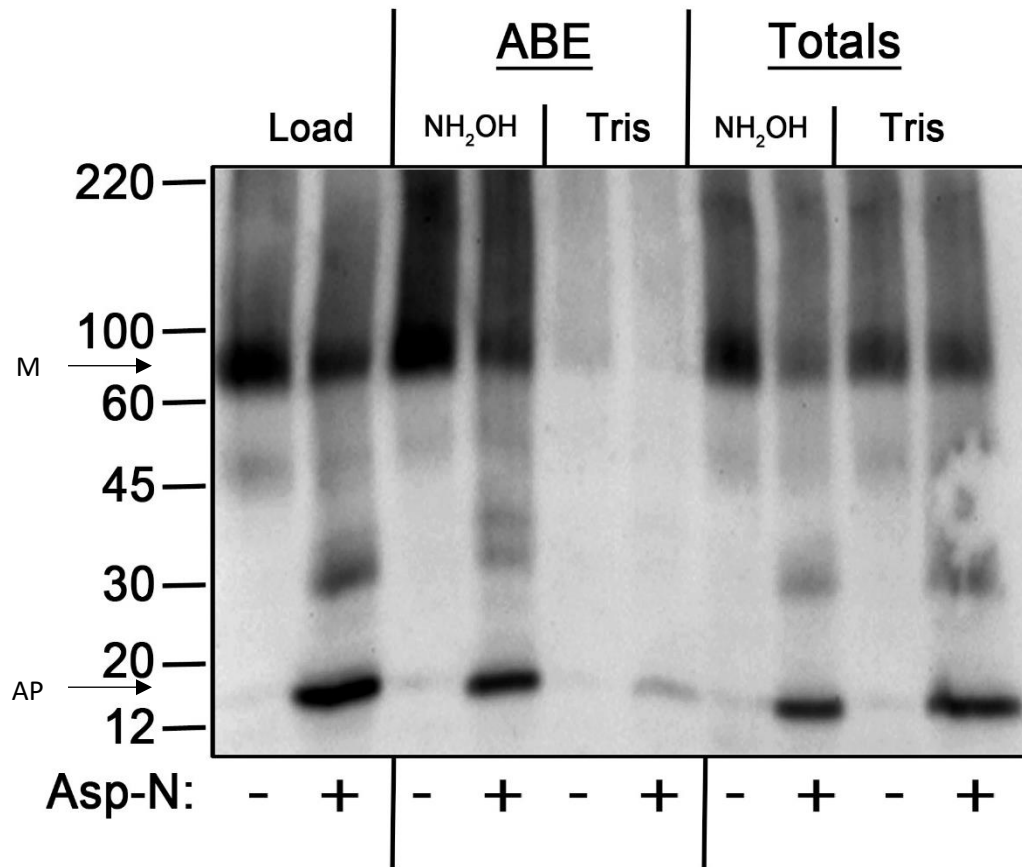


Figure 5. Asp-N proteolysis of rat striatal synaptosomes and subsequent detection of palmitoylated rDAT N-terminus by ABE. Synaptosomes were isolated from rat striatal brain tissue. Synaptosomes were digested with 1 $\mu\text{g}/\text{mL}$ Asp-N in SP buffer for 45 minutes at 25°C while control samples were incubated in SP alone under otherwise identical conditions. Digested synaptosomes were subjected to ABE. SDS-PAGE, and immunoblotting with MAb 16 revealed the presence of an ~19 kDa N-terminal palmitoylated fragment. 'M' arrow indicates mature DAT, and 'AP' arrow indicates Asp-N-generated DAT peptide whose presence in the NH₂OH ABE lane indicates N-terminal DAT palmitoylation. This acylation event likely occurs at Cys6 and/or Cys135. This procedure is unable to distinguish between these two sites.

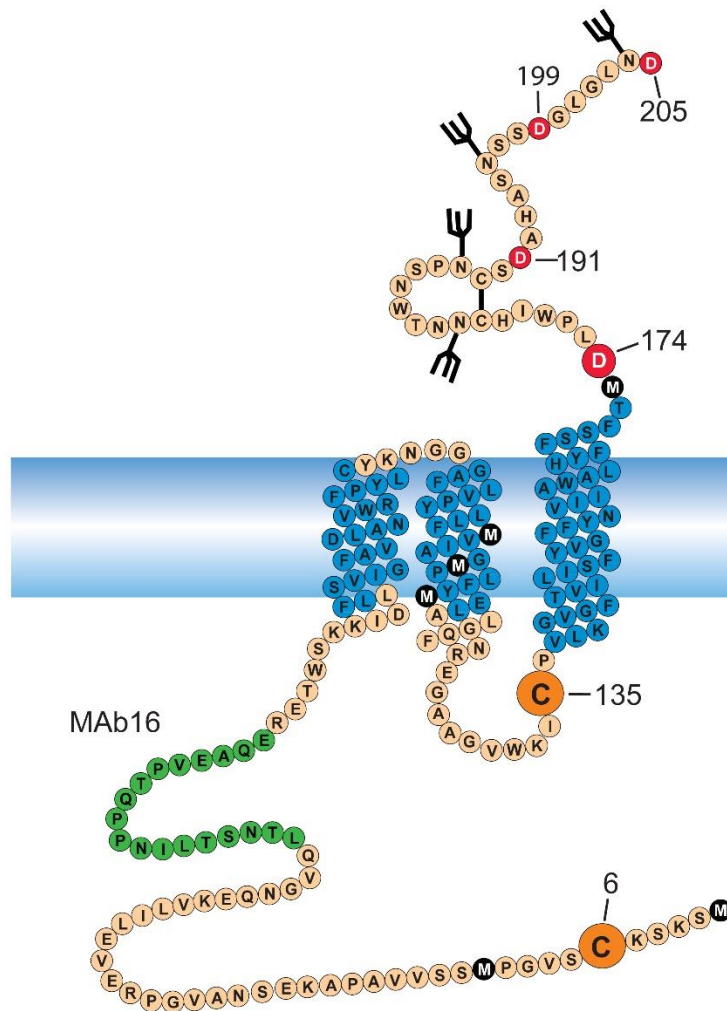


Figure 6. Depiction of N-terminal rDAT displaying N-terminal methionine residues, the primary aspartic acid cleavage site by Asp-N, and relative locations of intracellular cysteines potentially accessible for S-palmitoylation. Methionine residues are in black. The green residues on the N-terminus represent the epitope for anti-rDAT primary antibody MAb16. Cleavage with Asp-N at Asp174 (large red residue) produces an ~ 19-kDa N-terminal peptide containing the epitope for MAb 16, Cys6 and Cys135 as seen in Figure 6. CNBr digestion at Mets 106, 111, or 116 in transmembrane domain 2 would generate the ~11-kDa N-terminal DAT fragment seen in Figure 7.

(Figure 7). This experiment demonstrates the N-terminus of DAT remains palmitoylated in the absence of Cys135 – implicating Cys6 as the likely site of this modification. This, in combination with the preceding findings (Figures 1-3), supports Cys6 as an rDAT S-palmitoylation site and likely rules out this event occurring at Cys135.

CNBr Proteolytic Mapping of Cys to Ala rDATs Expressed in LLCPK₁ Cells

To confirm the *in vivo* proteolytic peptide mapping-ABE results, the same set of experiments performed on striatal rDAT were implemented on WT, Cys6Ala, and Cys135Ala rDATs. Plasma membrane fractions of LLCPK₁ cells stably expressing each of the aforementioned DATs were isolated and treated with 1M CNBr in 70% formic acid. Control samples were treated with formic acid alone to control for fragmentation induced by acid hydrolysis. After 1 hour incubation in the dark, the samples were subjected to the ABE process and palmitoylated DAT peptides were detected by MAb16 immunoblotting (Figure 8). The ~11 kDa palmitoylated DAT peptide presented in both the WT and Cys135Ala rDATs, which was expected, but also the Cys6Ala rDATs, which was not anticipated. This result suggests either the presence of additional N-terminal palmitoylation events, or non-sulfhydryl binding of the sulfhydryl-specific biotinylating reagent. The more likely answer is an additional lipidation event, though the only other Cys amino acid resident to the N-terminal peptide generated from CNBr chemical fragmentation is Cys90, which resides on the extracellular surface of transmembrane domain 1.

[FJ3]

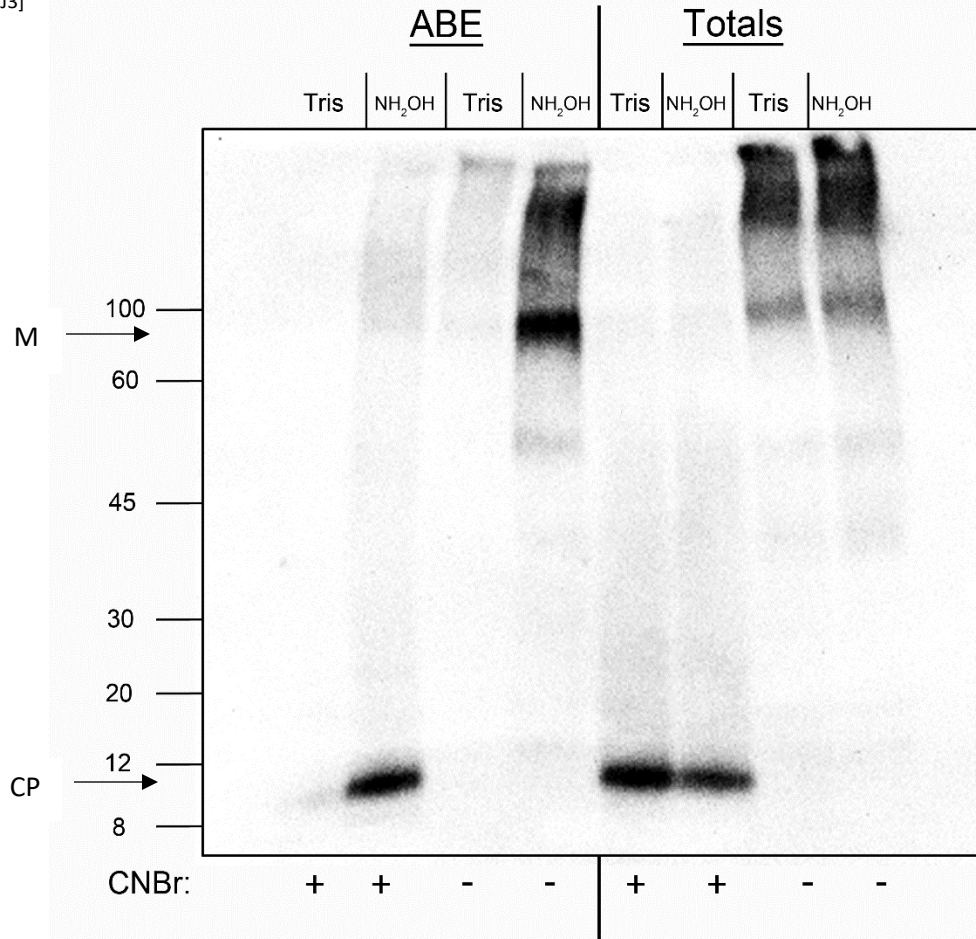


Figure 7. CNBr digestion of rat striatal synaptosomes and subsequent detection of palmitoylated rDAT N-terminus by ABE. Synaptosomes were prepared from extracted rat striatum and treated with 100 μ L of 70% formic acid with or without 1 M CNBr for 1 hour at 25°C in the dark. Digested synaptosomes were then subjected to ABE as described above and palmitoylated peptides were detected by SDS-PAGE and immunoblot analysis with Mab 16. 'M' arrow indicates mature DAT, and 'CP' arrow indicates CNBr-generated DAT peptide whose presence in the NH₂OH ABE lane indicates N-terminal DAT palmitoylation, most likely at Cys 6.

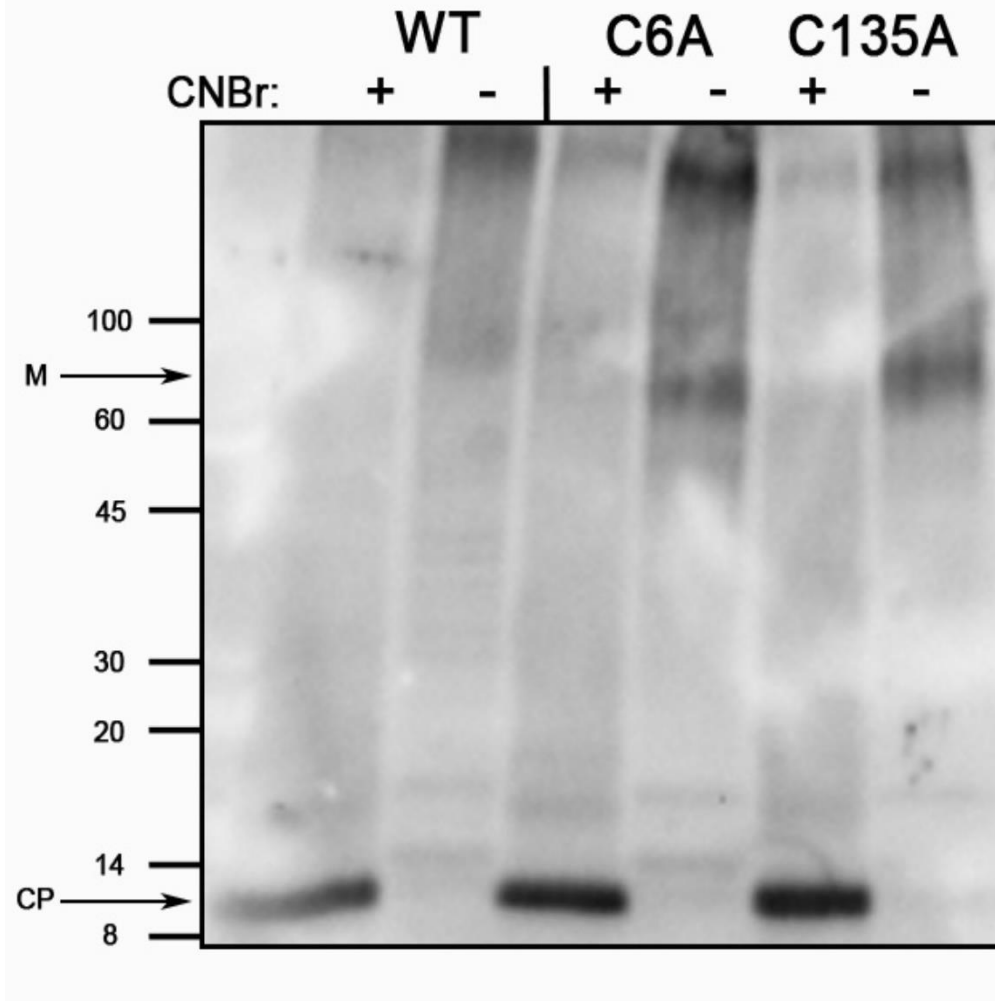


Figure 8. CNBr digestion of WT, Cys6Ala, Cys135Ala rDATs in LLC_{PK}₁ cells. LLC_{PK}₁ cells stably expressing the indicated rDAT were subjected to CNBr chemical fragmentation at a concentration of 1M CNBr in water and formic acid (CNBr '+' lanes) or water and formic acid alone (CNBr '-' lanes) for 1 h at ambient temperature in the dark. Reactions were terminated with 900 μ L of water and lyophilized. Final pellets were solubilized in 4SB buffer and subjected to ABE analysis and immunoblotting with MAb16. 'M' arrow indicates mature DAT, and 'CP' arrow indicates CNBr-generated DAT peptide. Presence of a CP in the C6A lane implies additional N-terminal DAT palmitoylation events on this peptide which may occur on the only other Cys residue, 90.

Analysis of Cys90 Palmitoylation

Cys90Ala rDAT cDNA was generated and the protein was transiently produced in LLCPK₁ cells for assay by ABE (Figure 9). These experiments demonstrate Cys90 to undergo S-acylation as the Cys90Ala rDAT ABE signature was significantly reduced *versus* WT (0.96 ± 0.05 *versus* 1.34 ± 0.13 ABE DAT to total DAT ratio, * $p < 0.05$). This is only a modest reduction in palmitoylation, which is expected as the palmitoylation substrates Cys580 and Cys6 are still present in this DAT population; however, Cys90 may be acylated at higher stoichiometric levels than Cys6 as the loss in Cys90Ala palmitoylation is detectable by ABE alone while the Cys6Ala loss of palmitoylation is not. This Cys residue is known to be highly reactive to MTS reagents^{370,371} and reactive oxygen species of DA *ortho*-quinone³⁷² which alter DA binding properties of DAT. Palmitoylation of Cys90 would be remarkable for multiple reasons. This result would represent, to our knowledge, the first known extracellular palmitoylation event. The application of the lipid to Cys90 would likely occur co-translationally in the ER while the majority of palmitoylating events occur post-translationally in the Golgi^{298,373}. Though it may be reversible, re-palmitoylation likely does not occur once DAT is presented at the plasma membrane as the acyltransferase machinery capable of re-applying palmitate resides within the cell³⁰¹.

Surface Expression Analysis of Palmitoylation-Deficient rDATs

The palmitoylation of Cys6 or Cys90 may serve different functions in DAT regulation than palmitoylation of Cys580, which, in stably expressing heterologous expression systems, supports DA uptake V_{\max} and opposes DAT

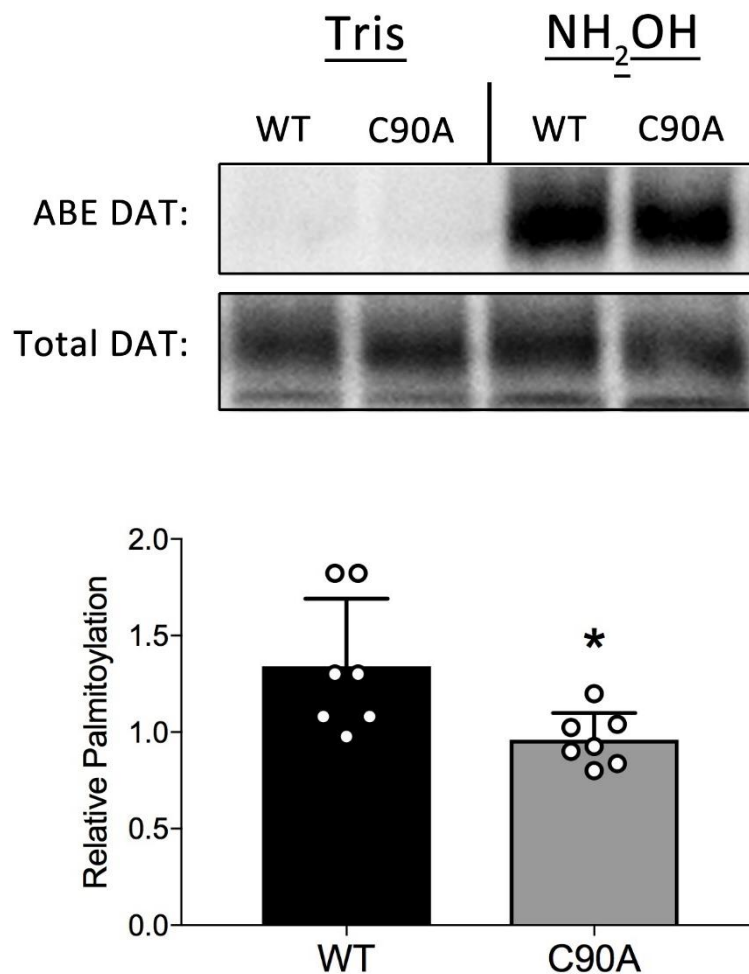


Figure 9. Palmitoylation characterization of Cys90Ala rDAT. WT or Cys90Ala rDATs were transiently transfected into LLC_{PK}₁ cells and ~36 h later were collected and plasma membrane isolation was performed. The samples were then subjected to the ABE protocol and palmitoylated DATs were detected by Western blotting with MAb 16. 0.96 ± 0.05 versus 1.34 ± 0.13 ABE DAT to total DAT ratio, * $p < 0.05$ $n = 7$ (mean \pm S.E.M.) Statistical analyses were performed by Student's *t* test. This result S-palmitoylation may occur on Cys90.

degradation³⁴⁴. To determine the functional outcomes of Cys6 and Cys90 palmitoylation, Cys6Ala, Cys6/580Ala, and Cys90Ala rDATs were analyzed for surface expression and DA uptake saturation kinetics.

The Cys580ala stably expressed in LLCPK₁ cells displayed acute functional alterations which were not precipitated by a loss of plasma membrane transporters. Here we tested all the palmitoylation-deficient mutants for differential surface expression patterns by cell surface biotinylation analysis after transient transfection in LLCPK₁ cells (Figure 10). The Cys580Ala rDAT has unaltered surface characteristics (Figure 10b) (n=3, 0.94 ± 0.06 versus 1.18 ± 0.14 surface to total DAT ratio, $p>0.05$) compared to WT rDAT. The same holds true for both Cys6Ala (Figure 10a) (n=3, 0.96 ± 0.06 versus 1.02 ± 0.04 surface to total DAT ratio, $p>0.05$) and Cys6/580Ala (Figure 10c) (n=7, 1.02 ± 0.03 versus 1.06 ± 0.07 surface to total DAT ratio, $p>0.05$); however, the Cys90Ala rDAT (Figure 10d) (n=5, 1.05 ± 0.03 versus 0.95 ± 0.02 surface to total DAT ratio, $*p<0.05$) displayed elevated surface transporter levels relative to WT rDAT. The increase in surface expression may not be due to loss of a lipidating event at Cys90, but rather the loss of a reactive Cys. An alternative is the lipidation of Cys90 keeps this population of DATs in an endosomal pool where they can be acted upon by PPTs in the event increased DA uptake capacity is required by the cell; e.g. post-action potential DA exocytosis - the result of the Ala90 rDAT would be less endosomal retention and increased plasma membrane transporters.

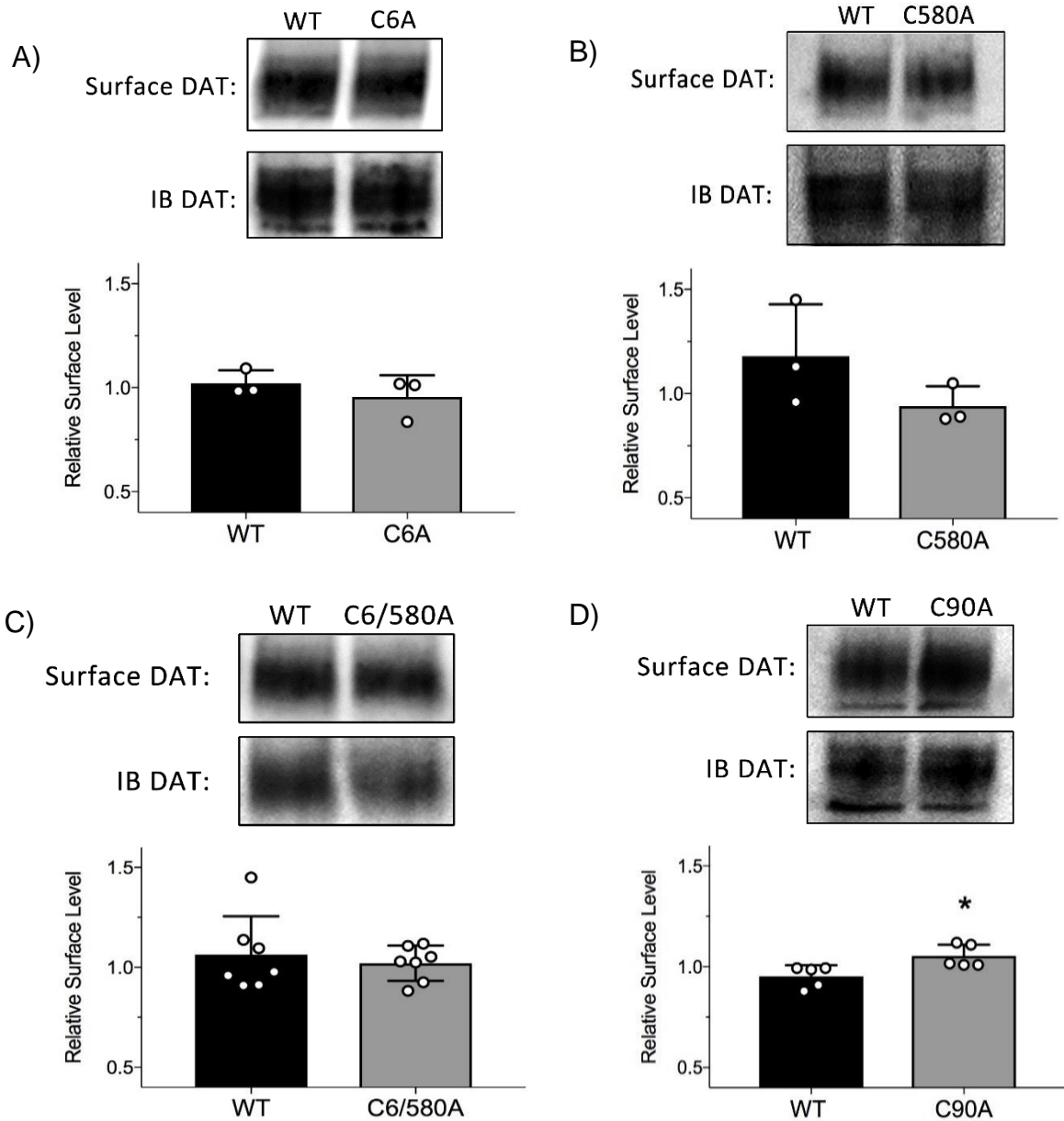


Figure 10. Surface biotinylation analysis of Cys to Ala rDATs' surface expression. WT, Cys6Ala, Cys580Ala, Cys6/580Ala, or Cys90Ala rDAT were transiently transfected in LLC_{PK}1 cells ~36 h prior to surface biotinylation analyses. A): Cys6Ala versus WT n=3, 0.96 ± 0.06 versus 1.02 ± 0.04 surface to total DAT ratio, $p > 0.05$; B): Cys580Ala versus WT, n=3, 0.94 ± 0.06 versus 1.18 ± 0.14 surface to total DAT ratio, $p > 0.05$. C): Cys6/580Ala versus WT, n=7, 1.02 ± 0.03 versus 1.06 ± 0.07 surface to total DAT ratio, $p > 0.05$. D): Cys90Ala versus WT, n=5, 1.05 ± 0.03 versus 0.95 ± 0.02 surface to total DAT ratio, * $p < 0.05$. (mean \pm S.E.M.). These results indicate unchanged plasma membrane populations in Cys6Ala, Cys580Ala, and Cys6/580Ala populations while mutational alteration of Cys90 to Ala induces increased DAT surface populations. This effect may be due to loss of Cys90 palmitoylation.

DA Uptake Saturation Kinetics of Palmitoylation Deficient rDATs

To further examine the functional outcomes that loss of palmitoylation confers upon DAT, [³H]DA saturation transport studies were performed on Cys6Ala, Cys580Ala, Cys6/580Ala, and Cys90Ala rDATs transiently expressed in LLCPK₁ cells. Figures 11-14 detail the surface normalized Michaelis-Menten saturation curves and kinetic parameters (K_m and V_{max}) reflecting the DA transport kinetics of these rDATs. Cys6Ala rDAT ($K_m = 1.63 \pm 0.24$ versus 2.09 ± 0.68 , $p > 0.05$ μM ; $V_{max} = 165.8 \pm 7.8$ versus 186.7 ± 27.6 pmol/min/mg, $p > 0.05$) (Figure 11), like Cys6/580Ala rDAT ($K_m = 2.19 \pm 0.14$ versus 1.80 ± 0.15 μM , $p > 0.05$; $V_{max} = 137.0 \pm 24.4$ versus 129.3 ± 19.0 pmol/min/mg, $p > 0.05$) (Figure 13), displays unaltered uptake kinetics relative to WT; transiently generated Cys580Ala (Figure 12) harbors different kinetics than our stable Cys580Ala LLCPK₁ line, exhibiting a significantly larger K_m for DA than WT (2.43 ± 0.19 versus 1.62 ± 0.16 μM , $*p < 0.05$) and no statistical change in its maximal uptake velocity (254.3 ± 61.9 versus 143.0 ± 27.8 pmol/min/mg, $p > 0.05$). Interestingly, Cys90Ala rDAT is also characterized by an increase K_m for DA compared to WT (Figure 14) (2.86 ± 0.40 versus 1.50 ± 0.24 μM , $*p < 0.05$) with no detectable change in uptake velocity (126.4 ± 20.43 versus 140.6 ± 9.29 pmol/min/mg, $p > 0.05$). These results are summarized in Table 1.

These studies further explored the role DAT palmitoylation sites contribute to the DA reuptake process. Though they did not reveal a significant contribution of these sites to maximal velocity of DA transport, which is contrary to our previous characterization of the stably expressed Cys580Ala transporter, they did

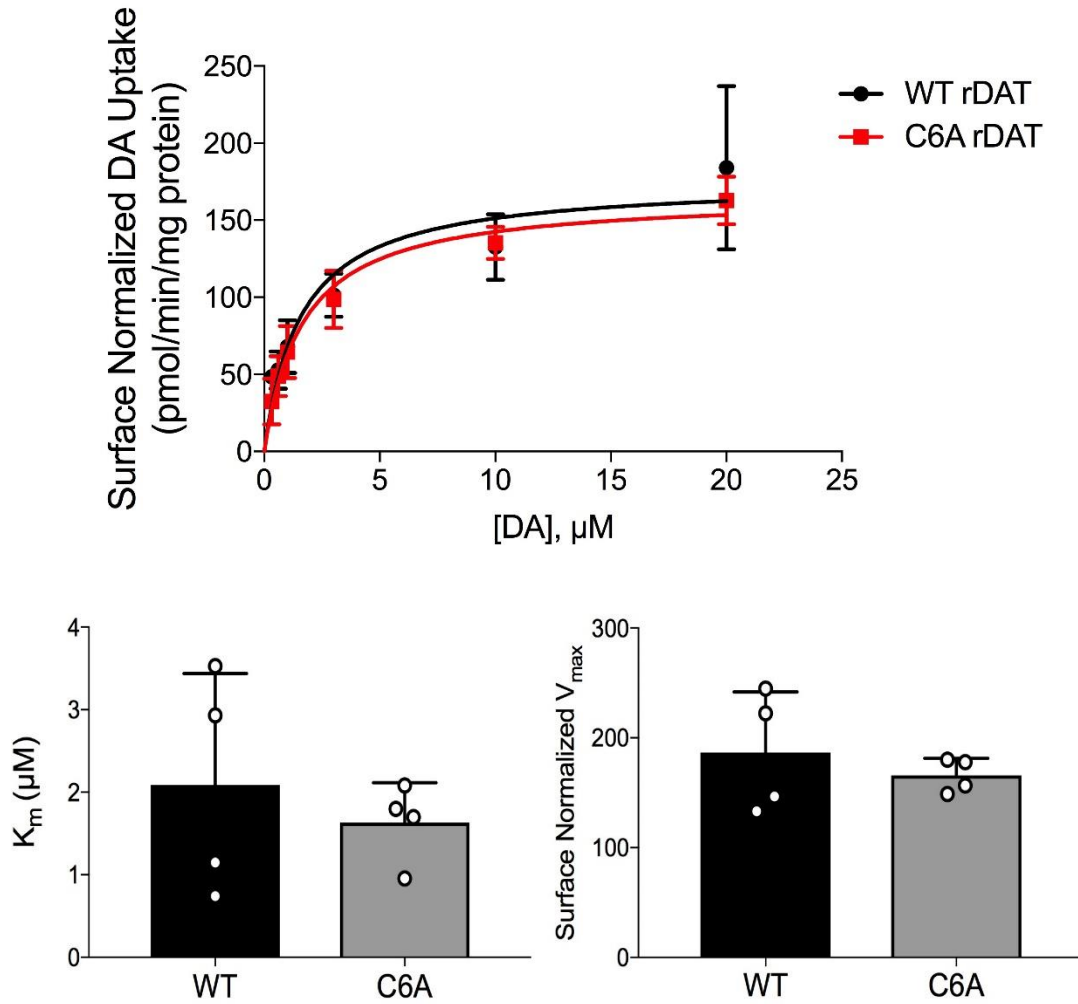


Figure 11. Saturation analyses of Cys6Ala rDAT. LLCPK₁ cells transiently transfected ~36 h with WT or Cys6Ala rDAT cDNA before analysis for their respective DA uptake kinetic characteristics. *Upper panel:* is a Michaelis-Menten graph displaying surface normalized [³H]DA saturation analyses with increasing DA concentrations (0.32-20 μM). The mean uptake values ± S.E. of four independent experiments are shown. *Bottom left:* histogram represents Michaelis-Menten constant for DA uptake saturation experiments n=4, $K_m = 1.63 \pm 0.24$ versus 2.09 ± 0.68 , $p > 0.05$ μM (mean ± S.E.M.). *Bottom right:* The histogram shows V_{max} values for surface normalized DA uptake saturation experiments n=4, $V_{max} = 165.8 \pm 7.8$ versus 186.7 ± 27.6 pmol/min/mg, $p > 0.05$ (mean ± S.E.M.). Statistical analyses were performed by Student's *t*-test.

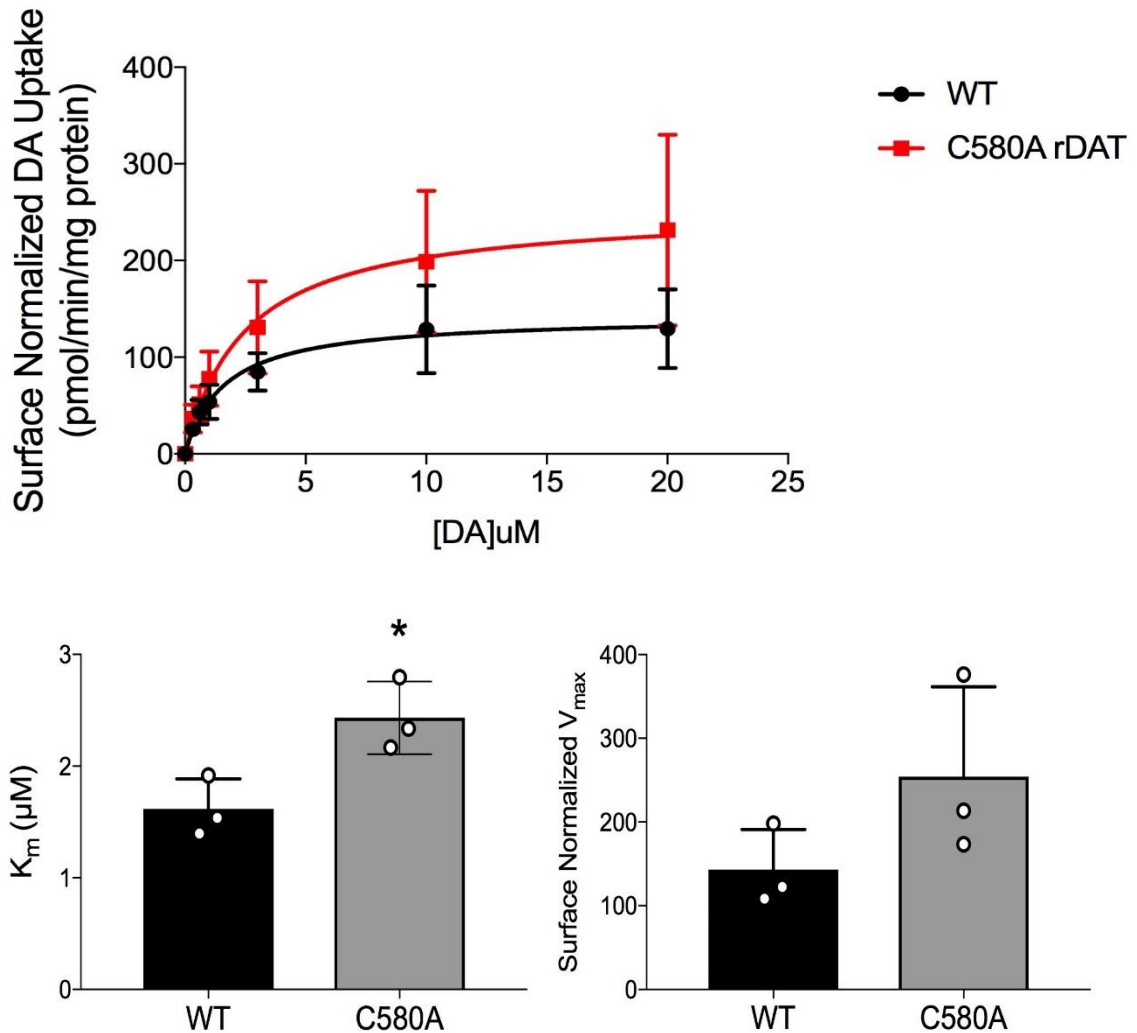


Figure 12. Saturation analyses of Cys580Ala rDAT. LLCPK₁ cells transiently transfected ~36 h with WT or Cys580Ala rDAT cDNA before analysis for their respective DA uptake kinetic characteristics. *Upper Panel:* Michaelis-Menten graph representing surface normalized [³H]DA saturation analyses with increasing DA concentrations (0.32-20 μM). The mean uptake values ± S.E. of three independent experiments are shown. *Bottom Left:* Histogram representing the Michaelis-Menten constant (K_m) for DA uptake saturation experiments $n=3$, 2.43 ± 0.19 versus 1.62 ± 0.16 μM, *, $p<0.05$ C580A versus WT (mean ± S.E.M.). *Bottom Right:* The right histogram displays V_{max} values for surface normalized DA uptake saturation experiments $n=3$, 254.3 ± 61.9 versus 143.0 ± 27.8 pmol/min/mg, $p>0.05$. (mean ± S.E.M.). Statistical analyses were performed by Student's *t*-test.

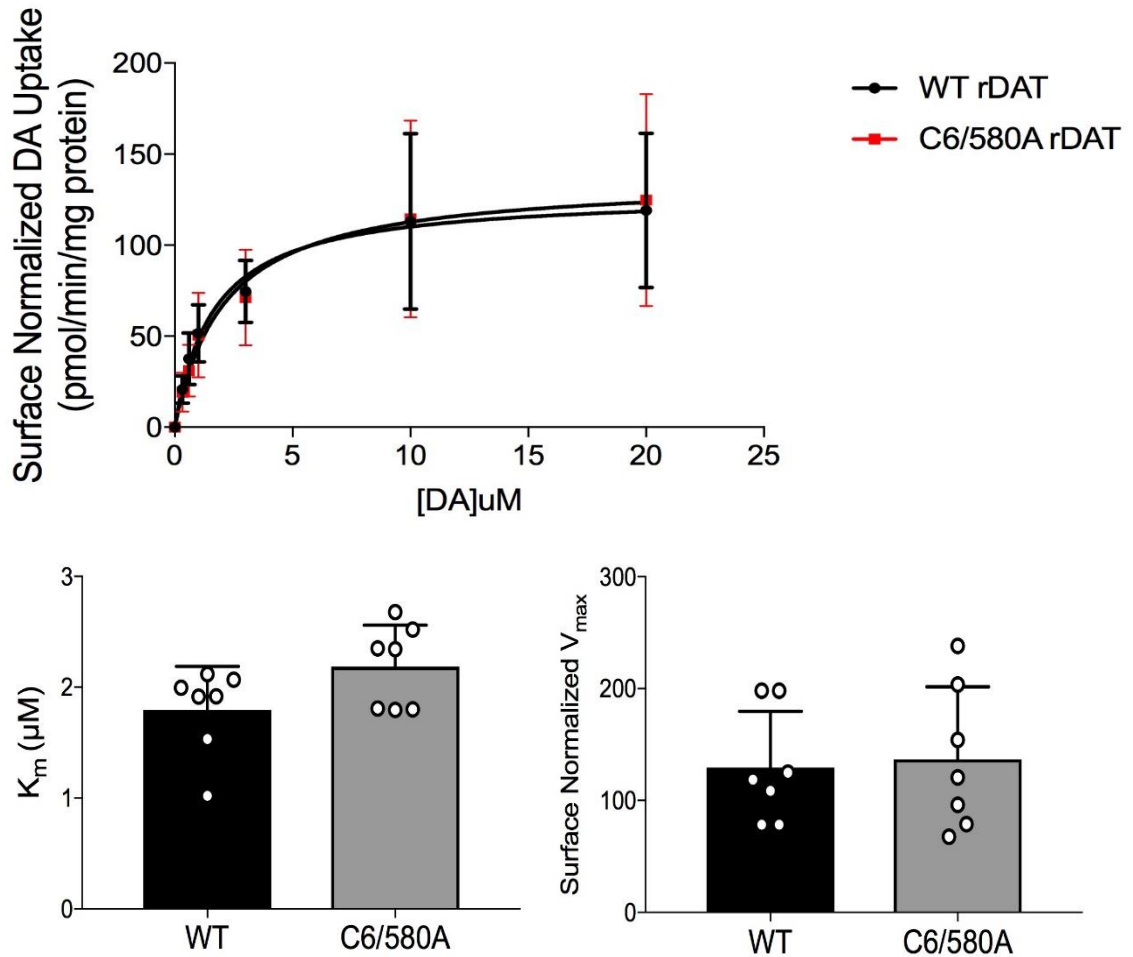


Figure 13. Saturation analyses of Cys6/580Ala rDAT. LLCPK₁ cells transiently transfected ~36 h with WT or Cys6/580Ala rDAT cDNA before analysis for their respective DA uptake kinetic characteristics. *Upper Panel:* Michaelis-Menten plots of surface normalized [³H]DA saturation analyses in increasing DA concentrations (0.32-20 μM). The mean uptake values ± S.E. of seven independent experiments are shown. *Bottom Left:* Histogram representing Michaelis-Menten constant (K_m) for DA uptake saturation experiments n=7, K_m = 2.19 ± 0.14 versus 1.80 ± 0.15 μM, p>0.05 (mean ± S.E.M.). *Bottom Right:* The histogram shows V_{max} values for surface normalized DA uptake saturation experiments n=7, 137.0 ± 24.4 versus 129.3 ± 19.0 pmol/min/mg, p>0.05 (mean ± S.E.M.). Statistical analyses were performed by Student's *t*-test.

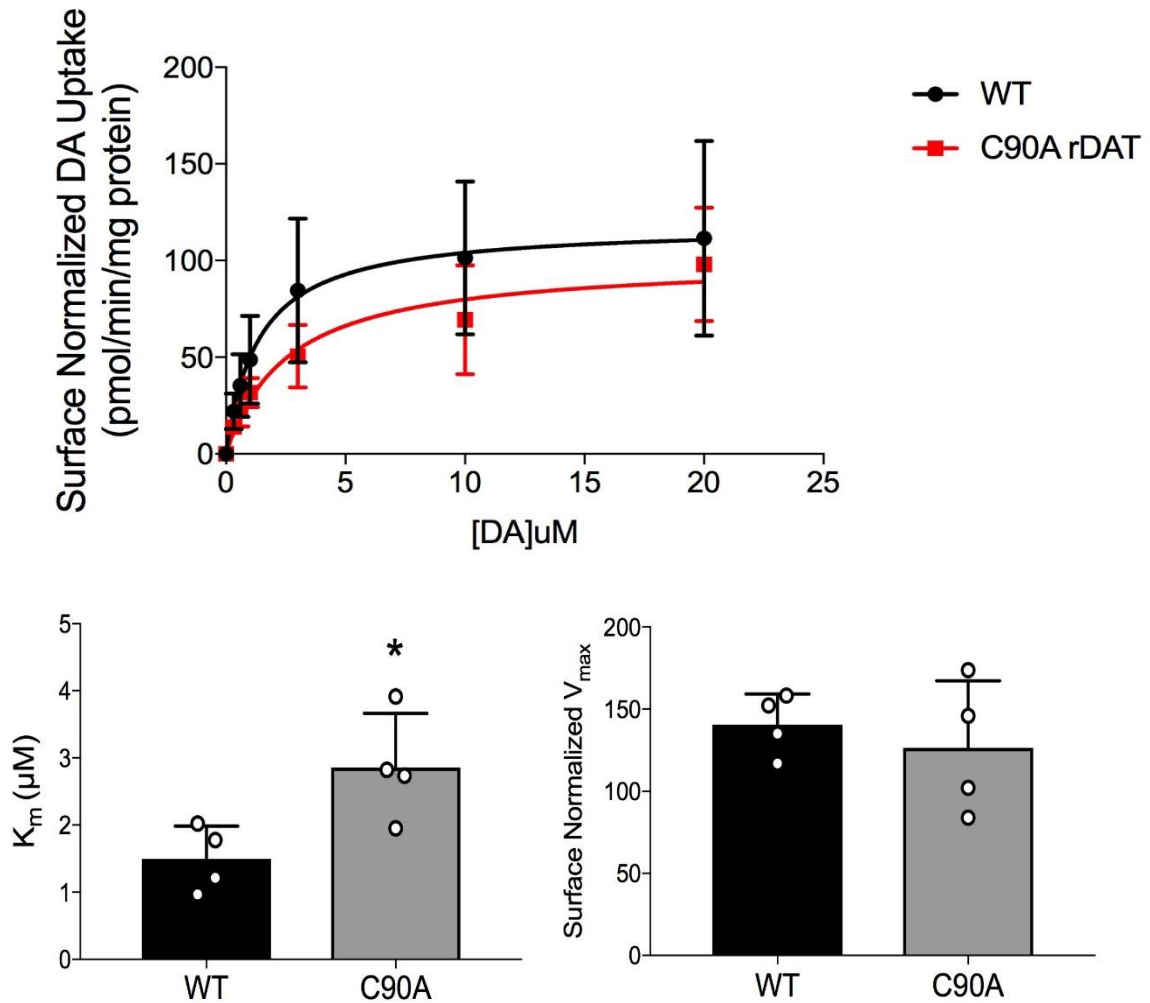


Figure 14. Saturation analyses of Cys90Ala rDAT. LLC_{PK}₁ cells transiently transfected ~36 hours with WT or Cys90Ala rDAT cDNA before analysis for their respective DA uptake kinetic characteristics. Upper panel is surface normalized [³H]DA saturation analysis with increasing DA concentrations (0.32-20 μM). The mean uptake values ± S.E. of four independent experiments are shown. Bottom left panel is a histogram representing the Michaelis-Menten constant (K_m) for DA uptake saturation experiments n=4 2.86 ± 0.40 versus 1.50 ± 0.24 μM, *p<0.05. The bottom right panel is a histogram showing V_{max} values for surface normalized DA uptake saturation experiments n=4, 126.4 ± 20.43 versus 140.6 ± 9.29 pmol/min/mg, p>0.05. Statistical analyses were performed by Student's *t*-test.

rDAT Line:	K_m (μM)	V_{max} (pmol/min/mg)
Cys6Ala	1.63 ± 0.24	165.8 ± 7.8
Cys580Ala	$2.43 \pm 0.19^*$	254.3 ± 61.9
Cys6/580Ala	2.19 ± 0.14	137.0 ± 24.4
Cys90Ala	$2.86 \pm 0.40^*$	126.4 ± 20.43

Table 1. Summary of palmitoylation deficient rDATs DA transport kinetics versus WT. Cys6Ala: $K_m = 1.63 \pm 0.24$ versus 2.09 ± 0.68 , $p > 0.05$ μM ; $V_{\text{max}} = 165.8 \pm 7.8$ versus 186.7 ± 27.6 pmol/min/mg, $p > 0.05$. Cys580Ala: 2.43 ± 0.19 versus 1.62 ± 0.16 μM , * $p < 0.05$; 254.3 ± 61.9 versus 143.0 ± 27.8 pmol/min/mg, $p > 0.05$. Cys6/580Ala: $K_m = 2.19 \pm 0.14$ versus 1.80 ± 0.15 μM , $p > 0.05$; $V_{\text{max}} = 137.0 \pm 24.4$ versus 129.3 ± 19.0 pmol/min/mg, $p > 0.05$. Cys90Ala: 2.86 ± 0.40 versus 1.50 ± 0.24 μM , * $p < 0.05$; 126.4 ± 20.43 versus 140.6 ± 9.29 pmol/min/mg, $p > 0.05$. Statistical analyses were performed by Student's *t*-test of means \pm S.E.

reveal that the apparent affinities for DA of two of the transporter types (Cys580Ala and Cys90Ala) were significantly increased – visualized by the significant increase in their respective Michaelis-Menten constants. To determine how the relative contribution of these DAT palmitoylation sites and the cellular palmitoylation micro environment contribute to DA transport, these DAT palmitoylation site mutants were treated with the irreversible acyltransferase inhibitor 2-bromopalmitate (2BP)^{374,375} and analyzed for DAT functional outcomes.

Global Palmitoylation Inhibition with 2BP Effect on DA Uptake

2BP was initially demonstrated to reduce synaptosomal DAT-mediated DA uptake *via* decreasing DAT palmitoylation³⁴⁴. Here, LLCPK₁ cells expressing each of the transiently produced Cys → Ala DAT mutants were pre-incubated with 7.5 μM 2BP for 90 minutes at 37°C and 5% CO₂ prior to DA uptake with 3 μM DA containing the 10 nM [³H]DA tracer for 30 minutes in a 37°C water bath. Subsequently, these cells were lysed with 1% Tx-100 for 20 min at RT and the contents were collected and analyzed for radioactivity by scintillation counting (Figure 15).

The results of these experiments suggest a synergistic relationship between DAT palmitoylation and global palmitoylation events. The WT transporter exhibited the largest DA uptake downregulation by 2BP which, as all its potential palmitoylation sites remain intact, stands to reason (Figure 15a) (52.33 ± 9.28 WT treated *versus* WT control, ***p*<0.01, *n*=3). The Cys6Ala (Figure 15b) and Cys580Ala DATs (Figure 15c) experienced similar downregulation patterns

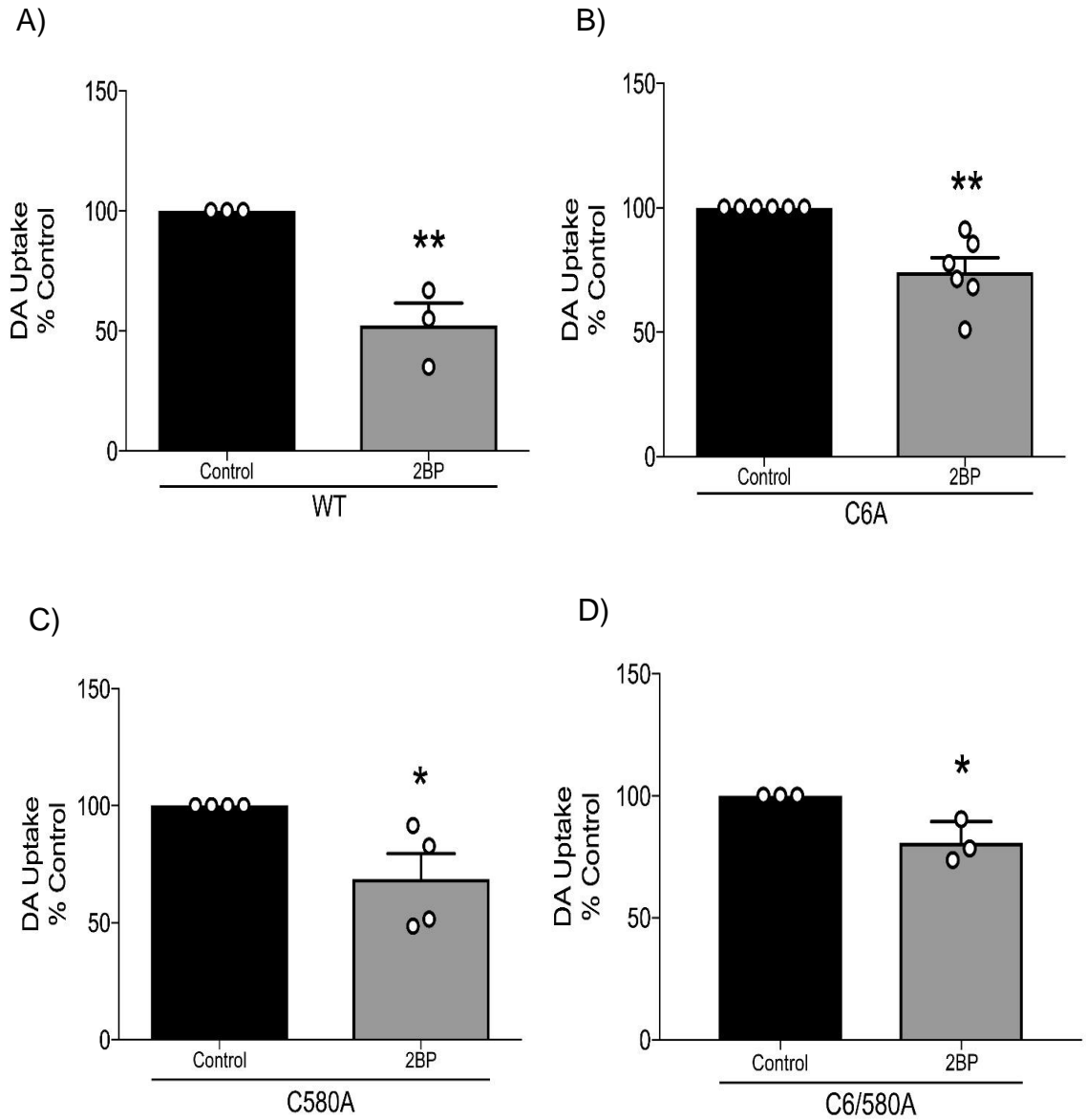


Figure 15. 2BP downregulation of DA uptake decreases with palmitoylation-deficient rDATs. Cells transiently producing WT, Cys6Ala, or Cys580Ala rDATs for ~36 hours were incubated with 7.5 μ M 2BP for 90 min at 37°C and 5% CO₂ prior to [³H]DA uptake analysis. DA uptake data are presented as %control 52.33 \pm 9.28 WT treated *versus* WT control, ** p <0.01, n =3. 74.05 \pm 5.82 Cys6Ala treated *versus* Cys6Ala control, ** p <0.01, n =6. 68.63 \pm 10.89 Cys580Ala treated *versus* Cys580Ala control, * p <0.05, n =4. 80.83 \pm 4.97 Cys6/580Ala treated *versus* Cys6/580Ala control, * p <0.05, n =3. Statistical analyses were performed by Student's t -test of mean \pm S.E. These results indicate mutational ablation of rDAT palmitoylation sites reduces 2BP efficiency in reducing DAT-mediated DA uptake.

(74.05 ± 5.82 Cys6Ala treated *versus* Cys6Ala control, ** $p < 0.01$, $n=6$; 68.63 ± 10.89 Cys580Ala treated *versus* Cys580Ala control, * $p < 0.05$, $n=4$). The loss of the single palmitoylation site reduced the 2BP-induced DAT down regulatory effect without completely abating it. The Cys6/580Ala DATs were even further resistant to 2BP induced DAT down-regulation (80.83 ± 4.97 Cys6/580Ala treated *versus* Cys6/580Ala control, * $p < 0.05$, $n=3$) (Figure 15d). The Cys90Ala rDATs have yet to be tested by this methodology. Eliminating the palmitate-accepting residues from DAT attenuated the 2BP precipitated loss of DA uptake in an almost stoichiometric manner, as individual loss-of-palmitoylation-site rDATs display less reuptake loss than WT but more than the double site mutant (Figure 16). The double palmitoylation site mutant, however, still undergoes significant 2BP-promoted reuptake loss, implicating S-palmitoylation events on Cys90 or within the DAT interactome playing a role in stabilizing DAT function; i.e. syntaxin 1a is an acyl-protein^{376,377} whose interaction with DAT modulates DA reuptake. Though the effect protein S-acylation has on this interaction has yet to be studied, syntaxin 1a palmitoylation could either induce or inhibit its DAT interaction, rendering it an iteration of a non-DAT palmitoylation event affecting DAT function.

Palmitoylation Deficient rDATs Display Altered DA efflux

Understanding the DA efflux phenomenon is of paramount importance to DAT-targeted pharmaceutical interventions for psychiatric disorders, particularly ADHD^{378,379}. Indeed, nonsynonymous hDAT single nucleotide polymorphisms exhibiting phenotypic aberrant DA release have been associated with ADHD³⁸⁰

	X vs. Column A
Pearson r	
r	0.9570
95% confidence interval	-0.05095 to 0.9991
R squared	0.9158
P value	
P (two-tailed)	0.0430
P value summary	*
Significant? (alpha = 0.05)	Yes

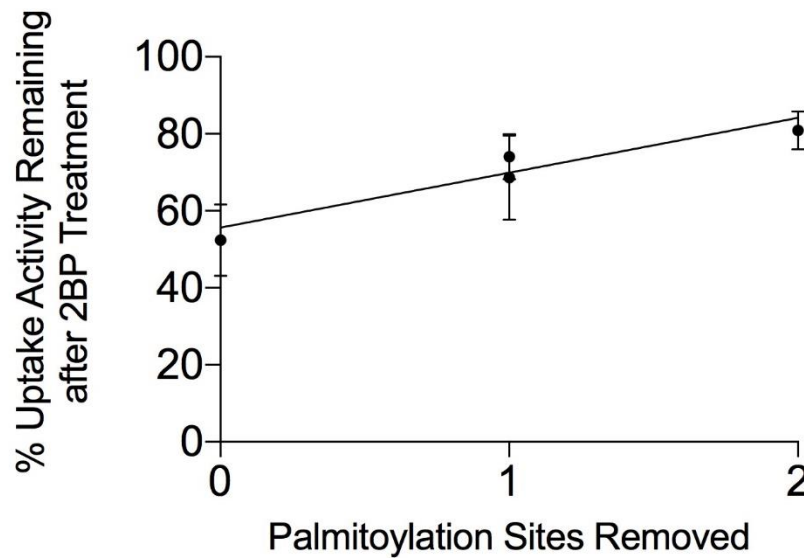


Figure 16. Significant correlation between 2BP-induced DAT downregulation and number of DAT palmitoylation sites. A Pearson correlation coefficient of 0.9570 indicates the efficiency of 2BP in limiting DAT-mediated DA uptake is strongly correlated to the number of palmitoylation sites present on DAT.

and Parkinsonism²⁵⁶. This DA export process is pharmacologically induced by DAT substrates like AMPH^{226,381} and other AMPH congeners³⁸². While many distinct molecular mechanisms integrate at DAT to contribute to DAT-mediated reverse DA transport^{233,237,240}, N-terminal phosphorylation of the transporter is perhaps the best-known²²⁹. As DAT phosphorylation contributes to efflux and has a reciprocal interplay with DAT palmitoylation, DAT palmitoylation may exert influence over DAT-mediated basal and AMPH-stimulated DA efflux mechanisms.

The palmitoylation site Cys to Ala rDATs were subjected to the biochemical efflux assay. This process entails: DAT forward transport to 'load' the cells with a DA mixture containing a [³H]DA radiotracer in KRH; washout of free radiolabel on ice with 4°C KRH; addition of efflux buffer (KRH alone for basal or KRH with 10 μM AMPH for stimulated efflux); collection of efflux buffer after 1 minute; lysis and collection of uptake control cells; analysis of all collected lysates and supernatants for radioactivity. Data are presented as % internal [³H]DA which is derived from basal or AMPH treated supernatant counts divided by corresponding uptake control counts then multiplied by 100. The palmitoylation deficient rDATs were transiently transfected into LLCPK₁ cells and compared to WT for differences in both basal and/or 10μM AMPH-induced DA efflux (Figure 17). The Cys6Ala rDAT mutation (Figure 17a) produced an inhibition of both basal and AMPH-generated efflux (** $p < 0.01$ C6A basal *versus* WT basal $n=5$; * $p < 0.05$, C6A AMPH *versus* WT AMPH $n=5$). The Cys580Ala rDAT (Figure 17b) displays no significant change in basal DA release ($p > 0.05$ Cys580Ala basal *versus* WT basal, $n=4$) but does

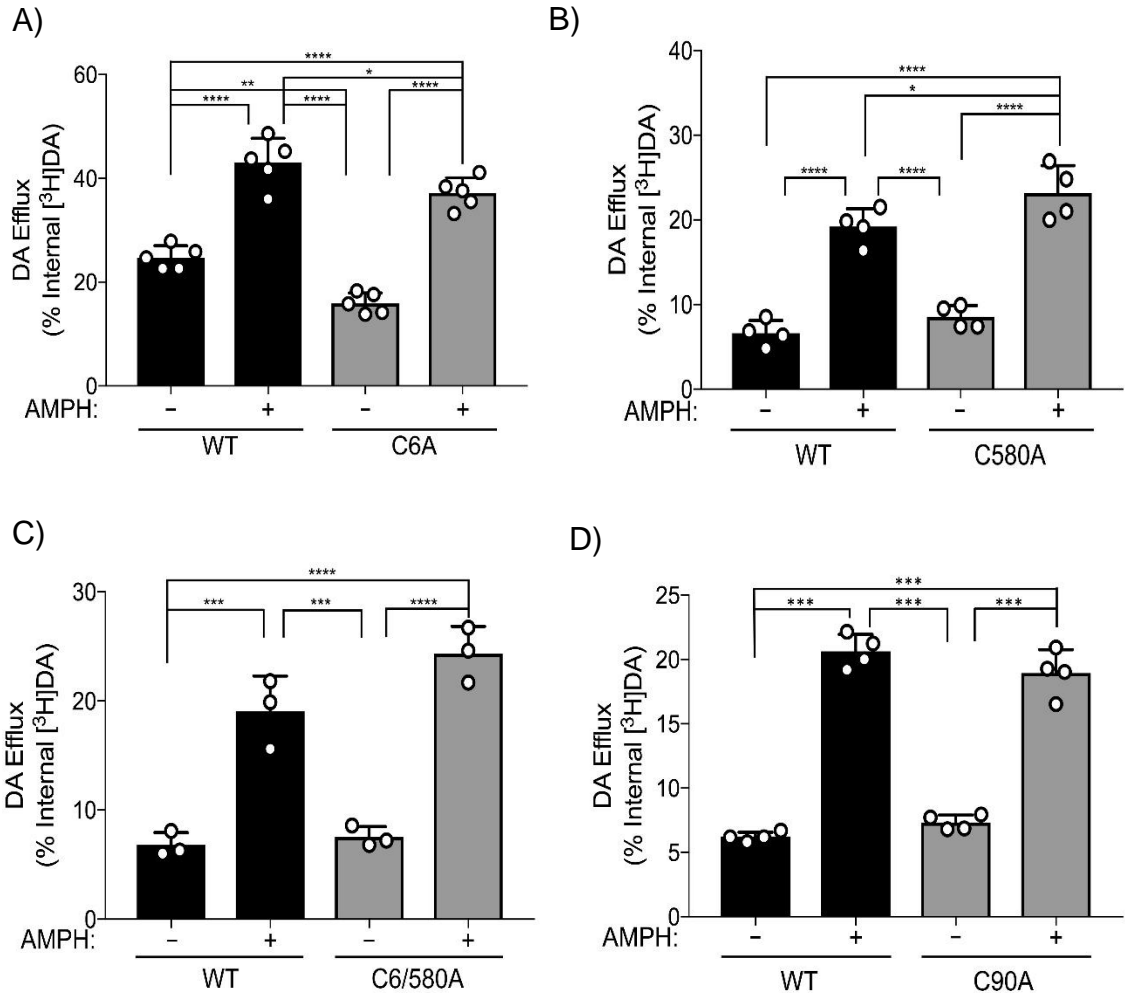


Figure 17. Cys6 and Cys580 impose opposite effects on DA reverse transport. [³H]DA efflux was analyzed by our biochemical reverse transport assay. Data are expressed as % internal [³H]DA. 100% internal DA was determined by scintillation counting of lysate from loaded cells which received no efflux buffer. C6A: ** $p < 0.01$ C6A Basal versus WT Basal $n = 5$; * $p < 0.05$, C6A AMPH versus WT AMPH $n = 5$. C580A: $p > 0.05$ Cys580Ala Basal versus WT Basal, $n = 4$; * $p < 0.05$ Cys580Ala AMPH versus WT AMPH, $n = 4$. C6/580A: $p > 0.05$ Cys6/580Ala Basal versus WT Basal; $p > 0.05$ Cys6/580Ala AMPH versus WT AMPH, $n = 3$. $p > 0.05$ Cys90Ala Basal versus WT Basal; $p > 0.05$ Cys90Ala AMPH versus WT AMPH, $n = 4$. Statistical analyses were performed by ANOVA with Tukey's post hoc test of mean \pm S. E. These results indicate Cys6 acylation events may support the DA efflux paradigm while Cys580 palmitoylation may oppose it.

potentiate AMPH-induced release ($*p < 0.05$ Cys580Ala AMPH *versus* WT AMPH, $n=4$), and both Cys90Ala ($p > 0.05$ Cys90Ala basal *versus* WT basal; $p > 0.05$ Cys90Ala AMPH *versus* WT AMPH, $n=4$) and Cys6/580Ala rDATs presented no alterations to either basal or AMPH-stimulated DA efflux. ($p > 0.05$ Cys6/580Ala basal *versus* WT basal; $p > 0.05$ Cys6/580Ala AMPH *versus* WT AMPH, $n=3$).

These data demonstrate that elimination of rDAT palmitoylation sites does indeed affect the DAT-mediated DA release mechanism; losing Cys6 results in ablated efflux patterns while mutation of Cys580 slightly, though not statistically significantly, induced increased basal DA efflux and statistically enlarged AMPH-induced release. Interestingly, the combination mutant, Cys6/580Ala rDAT, displayed neither altered basal nor altered AMPH DA efflux relative to WT, alleviating both Ala6 and Ala580 rDAT efflux phenotypes (Figure 17c). Cys90Ala rDAT also has unchanged basal and AMPH-triggered DA release, this, combined with its K_m and surface anomalies, suggest a palmitoylation event at Cys90 may contribute to DAT trafficking and stabilization of a TM domain vital for DA uptake.

Global Palmitoylation Inhibition by 2BP Effect on DA Efflux

Ala580 rDATs have elevated basal phosphorylation, and treating synaptosomes with 2BP generates increased whole protein phosphorylation of native rDAT³⁴⁷. This information, along with the data from the previous study (Figure 17), lend credence to the idea that both DAT palmitoylation and the cellular palmitoylome cooperate in coordinating the DAT-mediated DA efflux mechanism. To further explore this cooperativity, LLCPK₁ cells expressing WT or one of the

palmitoylation deficient rDATs were incubated with 7.5 μ M 2BP for 90 minutes in KRH prior to analysis for DA efflux (Figure 18).

Induction of DA efflux by 10 μ M AMPH from the WT transporter was potentiated by treatment with 2BP (Figure 18a) (** p <0.01 WT 2BP AMPH *versus* WT AMPH, n =5), and basal 2BP-stimulated efflux levels approach higher levels than control basal though not yet statistically significant (p >0.05 WT 2BP basal *versus* WT basal, n =5). However, 2BP basal levels are also not statistically different than control AMPH-stimulated efflux (p >0.05 WT 2BP basal *versus* WT AMPH, n =5) suggesting further experiments may demonstrate 2BP to generate AMPH-like DA efflux. Ala6 rDATs (Figure 18b) also display greater AMPH-induced efflux after 2BP treatment than its control AMPH counterpart (** p <0.01 C6A 2BP AMPH *versus* C6A AMPH, n =6) and this mutant exhibited no alteration to basal efflux levels (p >0.05 C6A 2BP basal *versus* C6A basal, n =6). The Cys580Ala (Figure 18c) mutation does not result in altered basal or AMPH-stimulated DA efflux after 2BP treatment (p >0.05 C580A 2BP Basal *versus* C580A basal, n =5; p >0.05 C580A 2BP AMPH *versus* C580A AMPH, n =5). Likewise, the Cys6/580Ala rDATs (Figure 18d) display DA efflux signatures which are unaffected by 2BP pretreatment (p >0.05 C6/580A 2BP Basal *versus* WT Basal, n =3; p >0.05 C6/580A 2BP AMPH *versus* C6/580A AMPH, n =3). Cys90Ala rDAT has yet to be analyzed by this methodology.

Discussion

These studies demonstrate DAT thioacylation may occur at multiple sites distinct from Cys580, which is the site previously identified in WT transporters.

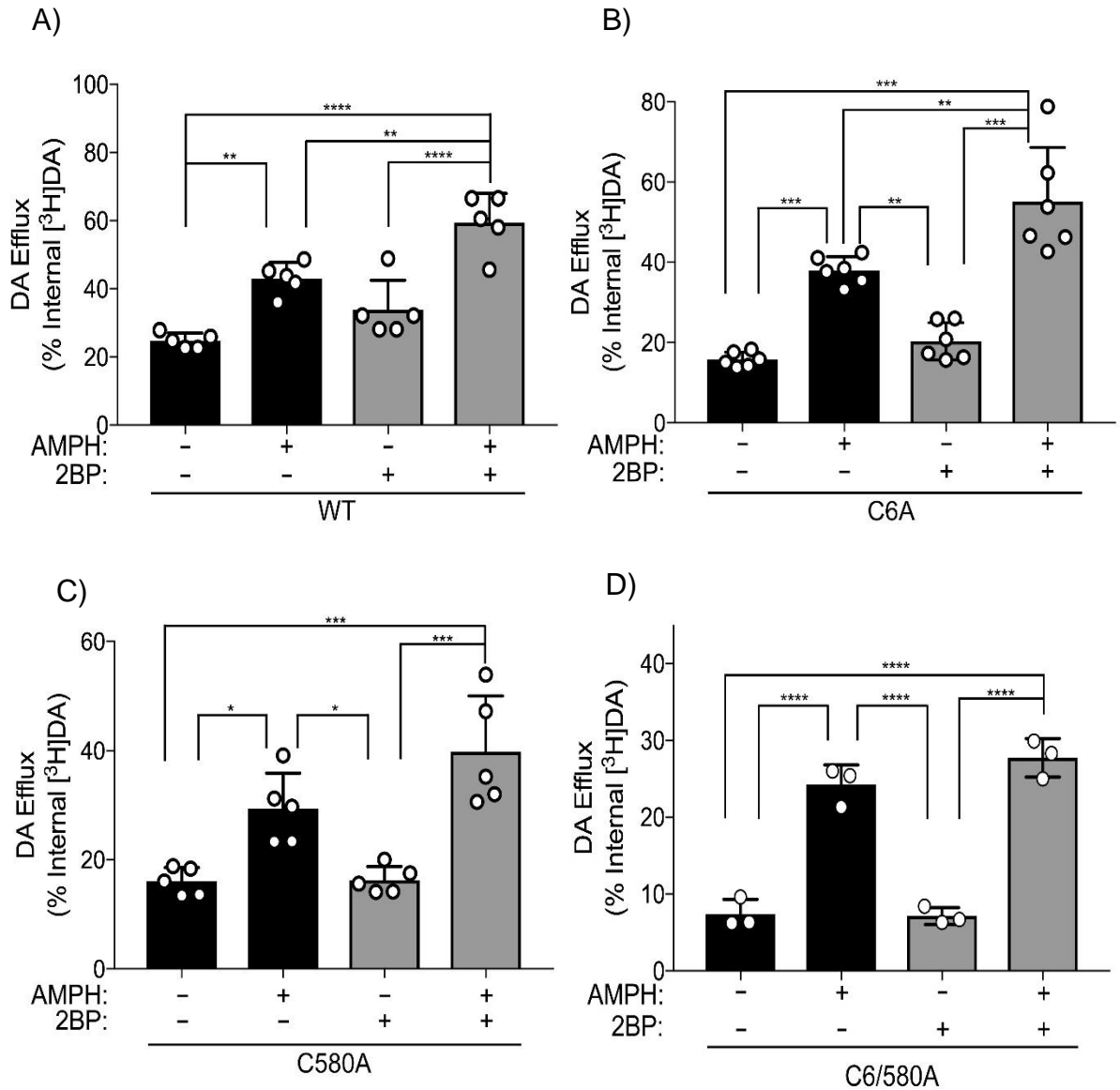


Figure 18. 2BP affects DA efflux. [³H]DA efflux was analyzed by our biochemical reverse transport assay. Cells transiently expressing either WT, Cys6Ala, or Cys580Ala rDATs were incubated with 7.5μM 2BP for 90 min at 37°C and 5% CO₂ after which DA reverse transport assays were conducted. WT: $p > 0.05$ WT 2BP Basal versus WT Basal, $n = 5$; $**p < 0.01$ WT 2BP AMPH versus WT AMPH, $n = 5$. C6A: $p > 0.05$ C6A 2BP basal versus C6A Basal, $n = 6$; $**p < 0.01$ C6A 2BP AMPH versus C6A AMPH, $n = 6$. C580A: $p > 0.05$ C580A 2BP Basal versus C580A basal, $n = 5$; $p > 0.05$ C580A 2BP AMPH versus C580A AMPH, $n = 5$. C6/580A: $p > 0.05$ C6/580A 2BP Basal versus WT Basal, $n = 3$; $p > 0.05$ C6/580A 2BP AMPH versus C6/580A AMPH, $n = 3$. Statistical analyses were performed by ANOVA with Tukey's post hoc test of means \pm S.E.

The evidence provided identifies Cys6, located on DAT's distal N-terminus, and Cys90, nestled amidst the head groups of the exofacial PM leaflet atop DAT TM1, as the likely additional sites of this modification. This report also details the DA transport kinetic impact resultant from ablation of these acylated residues, surface transporter population vicissitudes, and the regulation of DA efflux exerted by DAT palmitoylation in particular, as well as palmitoylation in general. These results echo and expand upon previous DAT palmitoylation reports^{344,347}: homeostasis of DAT and cellular palmitoylation events are crucial for synaptic DA homeostasis.

To understand the impact post translational modifications exert upon their modified protein, it is vital to understand where they occur. Initial DAT palmitoylation site exploration³⁴⁴ utilized bulk [³H]palmitate incorporation into Cys mutant DATs and elucidated Cys580 of rDAT as the major locus of radiolabel incorporation. This method was unable to eliminate the presence of other sites of DAT thioacylation as a significant amount of residual Cys580Ala radiolabeling remained. Unfortunately, the additional palmitoylation locations were also not readily discoverable by ABE (Figure 1), a procedure used for its more rapid repeatability (days *versus* weeks/months) and increased sensitivity³⁴², of single Cys residue point mutations (Cys90, due to its location, was not considered at this time). Several different biochemical approaches were then necessary. Initially, all Cys residues were changed to Ala save one to discern if the single remaining intracellular Cys is a PAT substrate. Palmitoylation analysis by ABE of these DAT mutants identified Cys6 as a palmitoylation site – at least when no other intracellular Cys residues are available for this modification (Figure 2). Importantly,

this methodology also demonstrated Cys580 as a palmitoylation site. Figure 3 demonstrates ABE of the combination Cys6/580 rDAT mutant displays ABE signatures near rDATs possessing only Cys135, Cys341, or Cys522 (Figure 2), while DATs with these two sites and lacking the other three intracellular Cys residues (Cys135/341/522Ala) presents WT-level palmitoylation. These results rule out Cys135, 341, and 522 as palmitoylation sites and implicate Cys6 in addition to Cys580 as a site for this modification. The loss of Cys6 not resulting in reduced palmitoylated DAT signatures is troubling, though a possible explanation is the transporters lacking this residue undergo increased acylation of Cys580 or other residues.

To strengthen the mutagenesis data, *in vivo* determination of N-terminal DAT palmitoylation occurring at distinct primary sequence loci was made. This was achieved through enzymatic and chemical DAT fragmentation and subsequent ABE purification of the palmitoylated peptides. The protocols for these experiments were derived from previous studies on site localization of binding of photoaffinity ligands to the DA permeation pathway of DAT^{366–368,383}. The result was an amalgam of proteolysis, ABE, and epitope-specific immunoblotting techniques. This protocol was first applied with Asp-N, use of which generates an approximately 19 kDa molecular weight rDAT peptide which is readily detected by immunoblotting with an antibody against an N-terminal DAT antigen³⁶⁹. This multi-step palmitoylated peptide isolation procedure demonstrated that *in vivo* DAT palmitoylation occurs at regions other than the C-terminus (Cys580) and the occurrence is likely Cys135, Cys6, or least likely, Cys90 (Figures 4 & 5). CNBr

chemical proteolysis of DAT occurs predominantly at the methionine cluster in TM2 and produces a peptide lacking Cys135 (Figure 6)^{366–368,383}. This procedure produced a palmitoylated DAT peptide of approximately 11 kDa representing Cys6 as the likely palmitoylated residue (Figure 7); the composite of this result and the mutagenesis results effectively eliminate Cys135 as a DAT palmitoylation site.

The CNBr fragmentation/ABE process was next applied to Cys6Ala and Cys135Ala rDATs expressed in LLCPK₁ cells (Figure 8), and the result was surprising: the Cys6Ala rDAT still harbored a palmitoylated N-terminus. This is most likely due to an additional palmitoylated residue, likely Cys90, in this peptide. ABE analysis of Cys90Ala rDATs displayed significantly reduced ABE readout than the WT transporter (Figure 9). The fractional values of Cys90Ala (0.96 ± 0.05) compared to WT (1.34 ± 0.13) imply this DAT mutant maintains around 70% WT palmitoylation. This is a lower stoichiometric level than Cys580 and, as the two experiments testing Cys580Ala acylation only removed ~50% of the signal, leaves room for the possibility of additional palmitoylated residues – like Cys6.

Surface biotinylation assays were used to probe for alterations to transporter PM population changes which would allude to altered trafficking patterns provoked by loss of a palmitoylation site (Figure 10). The initial DAT palmitoylation study described no surface alterations upon Cys580 mutation or 2BP treatment though chronic palmitoylation inhibition resulted in expedited DAT degradation³⁴⁴. Here, the Ala6, Ala580, and Ala6/580 rDATs exhibit steady-state PM levels akin to the WT form; surprisingly, Ala90 rDAT shows increased surface transporter levels. The uptake kinetic data demonstrate unaltered DA saturation

transport kinetics for Cys6Ala (Figure 11) and Cys6/580Ala (Figure 13). The mutation of the Cys90 (Figure 14) and Cys580 (Figure 12) both generated increased K_m relative to WT. No mutation generated significant alterations to maximal DA uptake velocity. These data demonstrate DA reuptake parameters are dependent upon lipidating events at certain residues, but not others. These experiments were conducted *via* transient induction of the full length DATs which may explain the Cys580 result differing from the data obtained from stably-expressing cell lines³⁴⁷. Acute translation and modification of the DAT protein may vary between tissue, cell line, and protein production procedure.

The magnitude of 2BP-induced down-regulation of DA transport decreased linearly with loss of palmitoylated Cys residues (Figures 15 & 16). WT>Cys580Ala>Cys6Ala>Cys6/580Ala. This stands to reason as 2BP would produce less DAT-subjective effects as less DAT-lipidation events are occurring. The remaining 2BP-induced down-regulation of the Cys6/580Ala potentially results from loss of Cys90 palmitoylation or reduced protein-protein interactions which are propitiated by palmitoylating events. These analyses should be performed on both Cys90Ala rDAT and the triple combination Cys6/90/580Ala rDAT.

The DAT substrate AMPH³⁸⁴ which stimulates N-terminal DAT phosphorylation²²⁹ and interacts with vesicular monoamine transporters³⁸⁵ is a powerful inducer of DA efflux. Palmitoylation deficient rDAT mutants exhibited different AMPH-induced efflux patterns. A Cys6 palmitoylation event seems to support efflux as loss of this residue incurs ablated basal and AMPH induced release, while Cys580 palmitoylation events oppose efflux as elimination of this

Cys potentiates AMPH responsiveness. Global and DAT-specific palmitoylation was examined further by 2BP inhibition of the global palmitoylation process. AMPH-stimulation of DA release was potentiated by 2BP in the WT and Cys6Ala transporters and no basal increase of DA efflux was seen in any of the transporter populations.

The rDAT palmitoylation site detection studies revealed Cys6 and Cys90 as potential additional loci of this modification. Palmitoylation of these residues would generate interesting structural and functional consequences. Fatty acid attachment to Cys6 of DAT's distal N-terminus would likely result in the tethering of this peptide to membranous structures in proximity to it. Multiple transmembrane proteins undergo acylation of their NH₂ termini: Phospholemman requires palmitoylation of N-terminal Cys residues 40 and 42 to blunt Na⁺-K⁺-ATPase activity³⁸⁶; The ATP-binding cassette transporters A1³⁸⁷ and G1³⁸⁸ require thioacylation of their NH₂ domains for PM localization and cholesterol efflux onto their target lipoproteins. Tethering of DAT's N-terminus was previously reported as being mediated by interactions with PIP₂^{389,390} potentiating AMPH-induced DA efflux²³², a characteristic shared with SERT³⁹¹, though SERT-PIP₂ interplay is not coordinated through its NH₂ domain. The palmitoylation of Cys6 may operate synergistically with PIP₂ to strengthen DAT's N-terminal interaction with the PM, similar to the 'kinetic trapping'³⁹² phenomenon in which one lipid modification (frequently N-myristoylation or prenylation) weakly increases the target protein's hydrophobicity enough to produce transient membrane interactions with DHHC populated membranes to further lipidate the protein, creating stronger membrane

affinity. This 'kinetic trapping' process has been documented to affect the function of several peripheral membrane proteins³⁹³⁻³⁹⁶. Indeed, Cys6Ala rDATs display reduced basal and AMPH-induced efflux (Figure 17a), a phenotype similar to DAT interaction with PIP₂ depleted membranes^{232,389} (summarized in Figure 19). Cys6 acylation would also likely impact NH₂-terminus interacting proteins; interactions between syntaxin 1a, dopamine D2 receptor, ubiquitin ligases, and protein kinases may be contingent upon or sterically inhibited by Cys6 palmitoylation. The neighboring amino acid, Ser7, is a phosphorylated residue, and one expects Cys6 acylation to have significant implications for the phosphorylation status of Ser7, a scenario brought into clearer focus by the recent insight of the reciprocal relationship between DAT phosphorylation and palmitoylation³⁴⁷. It is interesting to speculate that palmitoylation is an additional DAT N-terminal post-translational modification coordinating the protein's function in a 'barcoding' fashion analogous to diverse GPCR phosphorylation patterns activating different signaling, protein interaction, or endocytic outcomes³⁹⁷. Multiple proteins experience reciprocal palmitoylation and ubiquitination^{305,329}. A DAT post-translational modification interplay has been demonstrated between phosphorylation-palmitoylation crosstalk³⁴⁷, and alluded to between DAT phosphorylation-ubiquitination³⁹⁸ where PKC activators induce enhanced DAT ubiquitination and degradation^{183,182}, though these studies do not demonstrate concomitant PKC phosphorylation and ubiquitination of DAT. Cys6 palmitoylation may modulate both DAT ubiquitination and phosphorylation, creating another layer of detail in the picture of fine-tuned signaling assimilating at DAT's NH₂ peptide, marking it with phosphorylation,

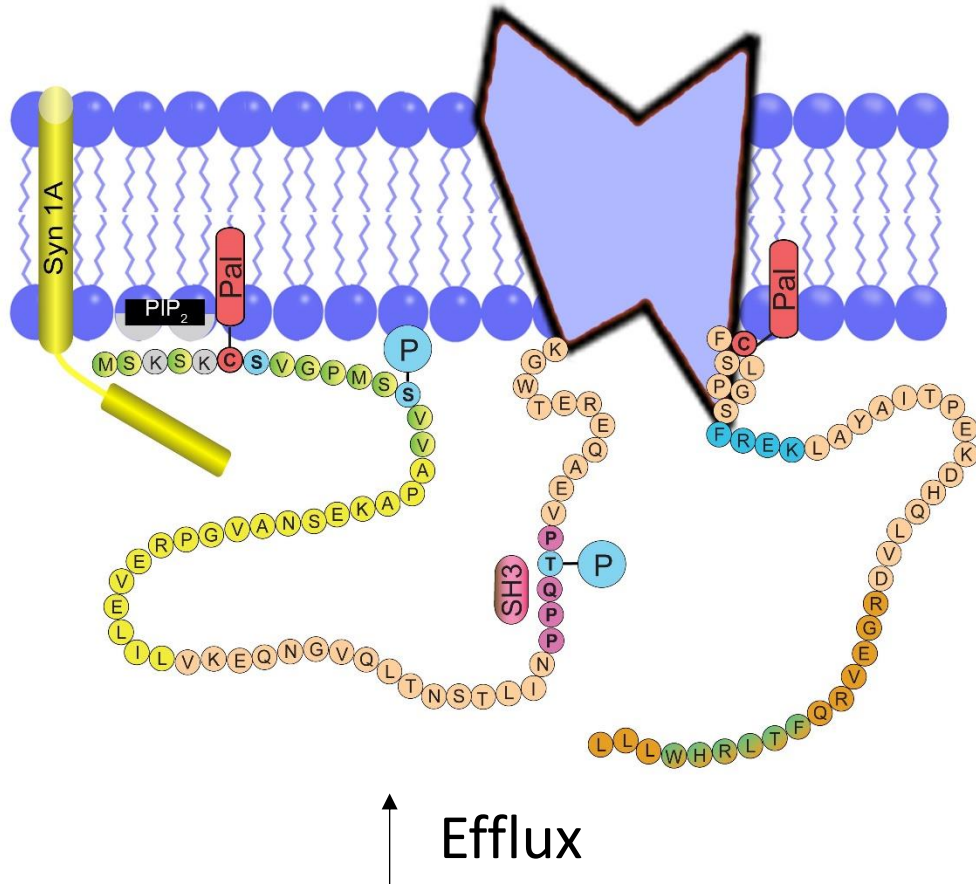


Figure 19. Schematic of Cys6 palmitoylation tethering DAT's N-terminus to the plasma membrane. Cys6 palmitoylation would likely tether DAT's N-terminal peptide to the plasma membrane. This tethering event may aid the DAT-mediated DA efflux process. Palmitoylation of this residue may also contribute to Lys3 and Lys5's interaction with PIP₂ phospholipids as well as increase the likelihood of Syn1a interaction with the DAT N-terminus – both events which likewise increase DAT-mediated DA efflux.

ubiquitination, and now palmitoylation; an image which is also likely affected by cellular machinery cycling the palmitoylation status of Cys90.

Cys90 thioesterification would likewise generate interesting outcomes. These suggest Cys90 to be an S-palmitoylation substrate (figure 9), Cys90Ala rDATs to have increased surface presence (Figure 10d), and increased K_m for DA (Figure 14). The location of this residue precluded its inclusion into the initial acylation site exploration experiments as it is located on the exoplasmic leaflet of the PM. This location renders the possibility of S-palmitoylation on plasma membrane Cys90 being reversible unlikely, though a portion of the PPT enzymes are secreted^{399,400} so removal of the synapse-side palmitate is possible, but its re-addition is unlikely. This, coupled with the findings that Cys90 is highly reactive to MTS reagents^{370,371}, imply very few surface DATs are acylated at Cys90, implicating it as an intracellular phenomenon. Because the DHHC domain of the PAT enzymes lies proximal to the cytoplasmic portion of the membrane⁴⁰¹, the intriguing palmitoylation/depalmitoylation cycle of Cys90 would occur with the co-translational attachment of the fatty acid within the ER^{373,402}; post-translational Cys90 will be oriented toward the organelle lumen or, while at the PM, extracellularly, without access to the PAT catalytic motif. The depalmitoylation of Cys90, therefore, is likewise a lumen event - indicating a PPT-catalyzed process rather than APT. PPT's have been classically associated with lysosomal protein degradation²⁸⁷⁻²⁸⁹; however, an increasing body of evidence implicates malfunctioning endosomal²⁹⁰ and synaptic vesicular^{400,403} PPT1 in infantile neuronal ceroid lipofuscinosis (INCL) etiology. The presence of this enzyme is

essential for accurate turnover of several key palmitoylated protein components of vesicular fusion machinery⁴⁰³ - syntaxin 1a^{376,377}, SNAP25^{404–407}, cysteine string protein^{408,409}, synaptobrevin⁴¹⁰, and synaptotagmin I^{404,411–413}. The significantly elevated PM population of the Cys90Ala mutant may be an effect of losing palmitoylation of Cys90 which may sequester the acylated DATs in endosomes; events which coordinate vesicular DA egress and require activated PPT1 for recycling of vesicular machinery may concomitantly draw endosomal DATs to the PM for reuptake of the released transmitter *via* depalmitoylation of Cys90. Thus the Ala90 rDAT would lose endosomal retention and display elevated PM expression (Figure 10d). It is interesting to note that the lack of loss of surface transporters upon treatment of rat striatal synaptosomes with 2BP may be an effect of losing Cys90 acylation, which would replenish plasma membrane DAT populations that traffic away from the plasma membrane in response to loss of Cys580 acylation, an event which is known to antagonize DAT degradation³⁴⁴. This implies palmitoylation at different locations of the same substrate protein (90 *versus* 580) yield opposite phenotypic results.

DAT-mediated substrate translocation requires transition through many physical permutations of the transporter in an alternating access fashion^{159,160}; synaptic DA, two Na⁺¹⁷² ions and one Cl⁻¹⁷³ ion cosubstrates bind to an outward-open conformation triggering conformational progression through an occluded structure and ultimately achieving an inward-open state whereupon substrate and cosubstrates are released into the cytoplasm¹⁵⁷. The substrate permeation pathway of DAT involves amino acid residues from TMs 1, 3, 6, and 8¹⁵⁵. The

analysis of the DA uptake saturation kinetics revealed Cys90Ala rDATs have significantly increased K_m for DA uptake than their WT counterparts (Figure 14). From the immediately preceding account of how palmitoylation of Cys90 may come about, it is unlikely the loss of Ala90's apparent DA affinity is due to loss of lipidation of this residue, but rather loss of the chemical interactions supported by the sulfhydryl side chain with polar head regions of the exofacial leaflet of the PM. This may produce an instability in TM1, which moves significantly during the DA transport process, precipitating overall reduction of the integrity of this portion of the substrate translocation route, hampering these DAT's ability to interact with DA. Additionally, a cholesterol molecule binds in a groove formed by TMs 1, 5, and 7¹⁵⁵, and an alanine at rDAT position 90 may alter conformational dynamics of this region. Cholesterol has been demonstrated to be an important influencer of DAT conformation¹⁵⁶ and, therefore, function, stabilizing both forward and reverse DA transport¹⁸⁷. Thus disruption of Cys90 producing a loss of cholesterol-DAT interaction could also explain the loss of apparent affinity for DA presented by the Ala90 DATs (Figure 15).

The report on Cys580Ala uptake saturation kinetics yielded surprising results (Figure 13). Though these experiments, like the previous study of Cys580Ala rDAT³⁴⁷, were performed in LLC PK₁ cells, these DATs were generated by transient transfection while the former were stably produced. Here the K_m was significantly higher than WT, and V_{max} , though apparently elevated, was not significantly higher. The past report found these transporters have an unchanged K_m for DA but a significantly reduced maximal DA transport velocity³⁴⁷. This may

be due to altered modification and binding partner interactions of the transiently *versus* stably translated proteins or the transfection reagent affecting plasma membrane characteristics, with trickle-down effect on plasma membrane protein (DAT) function. Further studies need to be done to determine whether stable or transient transfection better reflects the *in vivo* biological reality.

The experiments reporting the 2BP effect on palmitoylation-deficient DATs' DA uptake capabilities attempt to expand upon previous results demonstrating that 2BP treatment downregulates [³H]DA uptake in rat striatal synaptosome preparations³⁴⁴, and differentiate between the effects of global and DAT-specific palmitoylation events on DA uptake (Figure 15). 2BP stimulated loss of DA reuptake was positively correlated to the number of acylation sites present on the DATs (Figure 16); The WT transporter population succumbed to the greatest 2BP generated DA transport loss while the combination Cys6/580Ala transporters were affected the least. This result stands to reason as a reduction in the number of DAT acylation sites would indicate the residual loss of function (or gain in the case of other proteins⁴¹⁴) induced by 2BP to be a result of more global palmitoylation inhibition than DAT-subjective palmitoylation blockade. It is, therefore, unsurprising that the Cys6/580Ala rDATs display the least 2BP created loss of function. Additionally, it should be noted that the mutation of these sites may produce *a priori* effects which would otherwise be accounted for by 2BP treatment; i.e., DAT-interacting proteins may lose their binding interaction due to mutagenesis of the Cys residue(s) rather than a binding partner losing its palmitoylation moiety *via* 2BP rendering it incapable of interacting with DAT. The presence of both Cys6

and Cys580 may be vital to establish some binding partner interactions; though, mutagenesis-induced loss of these would-be-interactions produce no change in uptake kinetics of the Cys6/580Ala rDATs (Figure 13). The Cys90Ala and Cys6/90/580Ala transporters need to be assessed by this method as it would be interesting to see if the triple combination DAT-palmitoylation deficient mutant displays no DA transport loss upon 2BP treatment.

The efflux experiments (Figures 17 and 18) reveal that S-acylation significantly contributes to DAT-mediated reverse DA transport process. The hitherto discovered DAT structural and functional factors which support AMPH-stimulated DA release are: the NH₂-terminus in general³⁶²; the specific phosphorylation thereof²²⁸; its PIP₂-mediated tethering to the PM²³²; the induction of a channel-like mode of the transporter, enabling quantum-like transmitter release²³³; ion conductance promulgating PM depolarization²³⁴ producing Ca²⁺ influx^{235,236} and propagation of neuronal excitability⁴¹⁵; elevated accumulation of intracellular Na⁺ ions requisite for DA efflux²³⁷; and AMPH action at the cognate vesicular transporter^{239,240}. The mutation of Cys6 blunted both basal and AMPH stimulated efflux while Cys580 alteration potentiated AMPH's DA releasing action (Figure 17a). This Cys6Ala phenotype may be due to losing PIP₂-mediated DAT N-terminal-PM interplay whose structural outcomes and concomitant protein interactor differences confer dampened DA efflux characteristics to the transporter. Ala580 rDAT's increased capacity for AMPH stimulated release may be due to its susceptibility toward inherent elevated phosphorylation and is therefore more prone to AMPH effects. Likewise, palmitoylation of Cys580 stabilizes DA

reuptake³⁴⁷ and losing this modification may allow easier conformational isomerization of the transporter and greater substrate access to its inward-open form, easing substrate efflux. The contrary efflux patterns of Cys6Ala and Cys580Ala rDATs cancel out in the Cys6/580Ala transporters which behave like WT DATs upon AMPH treatment, and in like manner Cys90Ala does not deviate from the AMPH-WT phenotype.

General cellular palmitoylation was demonstrated to contribute significantly to the DAT-mediated efflux paradigm (Figure 18). WT transporters display 2BP-basal release like AMPH-stimulated release, and 2BP and AMPH induce additive DA release effects on WT DATs. This is partially due to the ability of 2BP to induce transporter phosphorylation³⁴⁷, but also loss of lipidation of other proteins which would propitiate DA efflux parameters: The Na⁺/K⁺-ATPase requires palmitoylation for its function³²¹ and loss thereof would induce efflux-favorable cytoplasmic accumulation of Na⁺ ions; DAT-interacting D2 receptors undergo S-acylation^{136,416} and loss of its palmitoylation may alter its interaction with the transporter, altering the nature of AMPH-stimulated DA release; 2BP-reduced syntaxin 1a acylation may support its interaction with DAT, especially if, like DAT, these modifications interact reciprocally at syntaxin 1a, as the SNARE protein's enhanced phosphorylation has been demonstrated to increase its DAT partnering and promotion of reverse DA transport⁴¹⁷. The 2BP treatment of Cys6Ala and Cys580Ala (Figures 18b and c) transporters generated results congruent with the AMPH treatment of these transporters alone (Figures 17a and b). Cys6Ala DATs have potentiated AMPH-induced DA release after incubation with 2BP (Figure

18b), consistent with losing acylation events at Cys580, and Cys580Ala DATs display unaltered AMPH-stimulated DA release patterns (Figure 18c), consistent with losing Cys6 acylation events as the Cys6Ala mutation attenuated DA efflux (Figure 17a). 2BP had no effect on the induction of either basal or AMPH-propelled efflux from Cys6/580Ala DATs (Figure 18d). As with the 2BP effect on DA uptake of these transporters (Figure 15d), this may be due to the structural or interactor characteristics which would otherwise be altered by 2BP.

This study relates the potential for two additional rDAT S-palmitoylated residues, Cys6 and Cys90, and the impact these residues have on both forward and reverse DA transport; Cys6 acylation significantly affects the dynamic of the NH₂-domain and supports DA efflux, and Cys90 acylation has significant implications for the trafficking of the transporter and the residue is important to the integrity of the substrate permeation pathway. Importantly, this study implicates palmitoylation in playing an important role in the complex DA efflux process. Our lab has demonstrated the hyper effluxing hDAT coding variant Ala559Val³⁸⁰ to be deficient in S-palmitoylation, and it is conceivable, in light of this study, that improper palmitoylation of DAT may contribute to this aberrant efflux phenotype. It may be possible, therefore, to achieve reversal of this anomalous DA efflux characteristic *via* therapeutic intervention at the level of DAT palmitoylation. The theory of targeting protein palmitoylation to alleviate disease states is not new⁴¹⁸, and with the emergence of multiple illnesses being associated with aberrant protein S-palmitoylation^{332,419}, psychiatric disorders involving DA homeostasis may be beneficially impacted through modulation of DAT S-acylation.

Methods

Cell Culture and Site Directed Mutagenesis

Lilly Laboratory Cell Porcine Kidney (LLCPK₁)⁴²⁰ parental cells or LLCPC₁ cells stably expressing WT or mutant rDATs were grown in Dulbecco's Modified Eagle Medium (DMEM) containing 5% fetal bovine serum, 100 µg/mL penicillin/streptomycin, and supplemented with 400 µg/mL of the selection reagent Geneticin (G418) for stably expressing cell lines. Cells were maintained in a humidified incubator with 5% CO₂ at 37°C. Cys to Ala rDAT mutant DNA constructs were generated using the Stratagene QuickChange® PCR kit from template WT rDAT pcDNA 3.0 vector cDNA, and nucleic acid substitution was confirmed by sequencing (Eurofins MWG). For generation of multiple Cys to Ala substitutions, sequential addition of mutations were performed such that Cys135Ala mutation was introduced into the Cys6Ala rDAT template and subsequently Cys341Ala mutation was introduced into the Cys6/135Ala rDAT template until all the rDAT cDNA constructs containing only one intracellular Cys residue were produced.

Transfection

For generation of cell lines stably expressing WT or mutant rDAT constructs⁴²¹, LLCPC₁ parental cells were seeded into 12-well plates and grown to ~50% confluence. At this point the cells were transfected. X-tremGENE transfection reagent was mixed with plasmid DNA (1.4 µg of DNA/well) at a reagent:DNA ratio of 3:2 in OptiMEM for 20 min at ambient temperature after which the transfection complex was added to each well dropwise. After ~36 hours, the

cells were then transferred to a culture flask to undergo selection of expressing cells *via* 800 µg/mL G418 treatment. After two subculture passages at this G418 concentration, the cells were collected, the plasma membranes were harvested, and expression of rDAT was analyzed by immunoblotting with the anti-DAT mouse monoclonal antibody MAb16. If the transfection was successful, the stably expressing rDAT cells were maintained in 400 µg/mL of G418 for all subsequent uses. For transient production of the desired rDATs, LLCPK₁ parent cells were seeded into 24-well (0.5 µg DNA/well) or 100 mM plates (5 µg DNA/plate) and grown to ~80% confluence. X-tremeGENE transfection reagent was mixed with plasmid DNA at an X-tremeGENE:DNA ratio of 3:2 in OptiMEM for 20 min at ambient temperature. After the incubation, the transfection construct was added to each well containing 0.5 mL of DMEM for 24-well plates or 5 mL of DMEM for 100 mM plates. Experiments were performed ~36 hours post-transfection.

SDS-PAGE and Western Blotting

DAT proteins and peptides were denatured in Laemmli sample buffer (SB: 125 mM Tris-HCl, 20% glycerol, 4% SDS, 200 mM DTT, 0.005% bromophenol blue) and were electrophoretically resolved using 4-20% polyacrylamide gels alongside a ColorBurst protein standard. Proteins were then transferred to a transfer buffer (25 mM Tris-HCl, 192 mM Glycine, 0.1% SDS, 10% methanol) - equilibrated polyvinylidene fluoride (PVDF) membrane after which blocking was performed with a 3% BSA/PBS buffer. Primary MAb16 antibody was diluted 1:1,000 in the blocking solution and the blocked PVDF membrane was incubated in this antibody solution for 1 hour at ambient temperature. After five washes the

membrane was incubated in alkaline phosphatase (AP)-linked anti-mouse IgG secondary antibody diluted to a 1:5,000 ratio in blocking buffer for 1 hour followed by 5 additional washes. 3 mL of Immun-Star™ AP substrate (Bio-Rad) was applied to the membrane and incubation proceeded for 5 min at ambient temperature. Generated chemiluminescent Western blot band intensities were quantified using Quantity One® software (Bio-Rad).

Plasma Membrane Preparation

rDAT-LLCPK₁ cells expressing the indicated DATs were grown in 150 mm plates to ~90% confluency. Cells were washed twice with Buffer B (0.25mM sucrose, 10 mM triethanolamine, and pH was adjusted to 7.8 with 100 mM acetic acid), scraped, and collected in Buffer B containing a protease inhibitor cocktail of 1 µM phenylmethylsulfonyl fluoride (PMSF) and 5 µM Ethylenediaminetetraacetic acid (EDTA) at 4°C. Cells were then pelleted *via* centrifugation at 3,000 x *g* for 5 min at 4°C, supernatants were removed, and the cell pellets were suspended in Buffer C (0.25 M sucrose, 10 mM triethanolamine, 1 mM EDTA, and the pH was adjusted to 7.8 with 100 mM acetic acid) and subsequently homogenized using 30 up and down strokes in a Dounce homogenizer. Cellular debris and nuclei were cleared from the homogenates by centrifugation at 800 x *g* for 10 min. The post-nuclear supernatant was collected and centrifuged at 18,000 x *g* for 12 min, and the resulting plasma membrane pellet was suspended in sucrose phosphate (SP) buffer (10 mM sodium phosphate, 0.32 M sucrose, pH 7.4 with 1 µM PMSF and 5 µM EDTA).

Synaptosome Preparation

Male Sprague-Dawley rats weighing between 200 and 300g were decapitated, and striatal hemispheres were excised, weighed, and stored in ice-cold SP buffer. The striata were homogenized in 2 mL ice-cold SP buffer with 30 up and down strokes in a glass-Teflon homogenizer, diluted with a further 8 mL SP buffer, and centrifuged at 3000 x g for 2 min at 4°C. The supernatant fraction was isolated and subjected to an additional centrifugation at 15,000 x g for 12 min. The resulting P2 pellet encompassing synaptosomes was suspended in SP buffer with protease inhibitors and the tissue was diluted to 20 mg/mL using the original wet weight of the striatal tissue.

Asp-N Endoproteinase Proteolysis

Striatal synaptosomes or membranes from rDAT expressing LLCPK₁ cell were prepared as described above and divided equally into two microfuge tubes. The preparations were acetone precipitated with an acetone to sample volume ratio of 4:1 for 1 hour at -20°C. The pellets were suspended in SP buffer and equal volumes were divided between one control and one Asp-N treated microfuge tube. The same volume of SP was added to the negative control test tube and SP buffer containing 2 µg/mL endoproteinase Asp-N was added to the treatment test tube creating a final endoproteinase concentration of 1 µg/mL. For membrane preparations, 0.1% SDS (v/v) was added to the digestion and control samples. Enzymatic digestions were carried out for 45 minutes at ambient temperature with nutation. Both samples were then centrifuged at 18,000 x g for 12 min at and the resultant pellet was used for further experimentation.

CNBr Chemical Proteolysis

Equal volumes of striatal synaptosomes or membrane preparations of the indicated rDAT-expressing LLCPK₁ cells were divided into CNBr treated or control microfuge tubes and acetone precipitated with 4x sample volume for 1 hour at -20°C. The samples were centrifuged at 18,000xg for 10 minutes and supernatants were removed. Precipitated experimental pellets were then suspended in 70 µL formic acid, 10 µL water, and 20 µL 5M CNBr (1M final concentration) or 70 µL formic acid and 30 uL water for untreated samples. Digestion was performed for 1 hour at 25°C in the dark. CNBr was removed *via* 3 repetitions of dilution with 900uL water and lyophilization. Final pellets were then used in subsequent experimentation.

Acyl-Biotinyl Exchange

Our ABE method was adapted from Wan et al³⁴¹ where detection of palmitoylated proteins are described in three steps: Free cysteine thiols are blocked; thioester linked palmitoyl groups are specifically removed by hydroxylamine (NH₂OH); and the previously palmitoylated and now free sulfhydryl groups are biotinylated. Membranes isolated from WT rDAT or rDAT mutant LLCPK₁ cells or rat striatal synaptosome preparations were solubilized in 250 µL of ABE lysis buffer (50 mM HEPES pH 7.0, 2% SDS (w/v), 1 mM EDTA) containing protease inhibitor and 20mM methyl methanethiosulfonate (MMTS) to react with unbound Cys sulfhydryl moieties and incubated for one hour at ambient temperature. MMTS was removed by a 1 mL acetone precipitation and centrifugation at 18,000 x g for 10 min. The pellet was dissolved in 250 µL 4SB ABE buffer (50 mM Tris, 5 mM EDTA, 4% SDS, pH 7.4) and remnant MMTS was

removed by an additional 1 mL acetone precipitation and centrifugation. The pellet was then subjected to a further acetone wash. The pellet was suspended in 200 μ L 4SB buffer and thioesterified palmitate molecules were specifically removed by hydroxylamine (NH_2OH); The sample was split equally (100 μ L) into negative control (800 μ L, 50 mM Tris-treated) and NH_2OH -treated (1.4 mM) halves and incubated at ambient temperature for 30 min with end-over-end mixing. The free sulfhydryl groups were reacted with 100 μ L (0.4 mM final concentration) of a sulfhydryl-specific biotinylating reagent, HPDP-biotin in the Tris or NH_2OH mixtures. The now HPDP-biotin-containing samples were incubated for 3 min in a 37°C water bath then at ambient temperature for 1 hour. Excess NH_2OH and biotin reagents were removed by the 4:1 acetone to sample volume precipitation, centrifugation at 18,000 $\times g$, supernatant aspiration, 250 μ L 4SB pellet suspension, 1 mL acetone precipitation, centrifugation at 18,000 $\times g$, supernatant aspiration, 1 mL acetone wash, centrifugation at 18,000 $\times g$, and supernatant aspiration workflow. The final pellet was suspended in 75 μ L ABE lysis buffer and 10 μ L of this was set aside for total DAT immunoblotting while 65 μ L was added to 50 μ L of a 50% slurry of Neutravidin resin in 1500 μ L Tris buffer to affinity purify the biotinylated proteins or peptides overnight at 4°C with nutation. Unbound peptides were washed away by three cycles of 8,000 $\times g$ centrifugation and 900 μ L radio immunoprecipitation assay buffer (RIPA: 1% Tx-100, 1% sodium deoxycholate, 0.1% SDS, 125 mM sodium phosphate, 150 mM NaCl, 2 mM EDTA, 50 mM NaF). Proteins and peptides were eluted from the final pellet by incubation in 2x Laemmli

SB for 20 min at ambient temperature. Samples were then subjected to SDS-PAGE, and immunoblotted with mouse anti-rDAT primary antibody (MAb16).

2BP DA Uptake Assay

LLCPK₁ parent cells were grown in 24-well plates until ~80% confluent then were transiently transfected with the indicated rDAT DNA. 36 hours prior to the assay, the cells were washed with 0.5 mL 37°C KRH buffer and resupplied with KRH buffer with or without 7.5 μ M 2BP for 90 min at 37°C and 5% CO₂. After the 2BP incubation, DA uptake was conducted for 30 min at 37°C with 3 μ M total DA containing 10 nM [³H]DA. Excess DA was rapidly washed out with KRH buffer and the cells were lysed with 1% Tx-100 for 20 min at ambient temperature. Lysates were collected and analyzed for [³H] content by liquid scintillation counting. 2BP uptake data are presented as % uptake control.

DA Efflux Assay

LLCPK₁ parent cells were seeded onto 24-well assay plates at 50,000 cells/well and allowed to grow to ~80% confluence (~24 h). Cellular production of WT or mutant DATs was induced by transient transfection for ~36 hours prior to assay. DAT-expressing LLCPK₁ cells were loaded *via* DA DAT-mediated uptake of 3 μ M DA containing 10 nM [³H]DA for 30 minutes in 37°C Krebs Ringer/HEPES buffer (KRH, 25 mM HEPES, 125 mM NaCl, 2.8 mM KCl, 1.2 mM KH₂PO₄, 1.2 mM MgSO₄, 5.6 mM glucose, 1.3 mM CaCl₂, 1.1 mM ascorbic acid). Extracellular DA was washed out 3 times with 4°C KRH on ice, and the assay plate was transferred back to the water bath and 37°C KRH efflux buffer with or without 10 μ M AMPH

was rapidly added to avoid cell drying and displacement upon buffer addition. The efflux buffer was collected after one minute and analyzed for radioactive content; one column of cells received no efflux buffer and was lysed with 1% Triton X-100 for 20 min at ambient temperature and served as the total internal [³H]DA control and was analyzed in parallel for [³H] content by liquid scintillation counting. The efflux values are expressed as a percent of the total intracellular [³H]DA. Where indicated cells were incubated with 7.5 μM 2BP in KRH for 90 min prior to the 30 min load portion of the experiment.

DA Uptake Saturation Analysis

Saturation analyses were performed on LLC_{PK}₁ cells transiently producing WT or mutant DATs in 24-well assay plates 36 h post-transfection. The cells were rinsed once and then resupplied with 0.5 ml of 37°C KRH buffer. The DA concentrations used were varied from 0.32 μM to 20 μM containing 10 nM [³H]DA and uptake was performed in triplicate for 8 min; nonspecific uptake was determined by DA uptake in the presence of 100 μM (-)-cocaine. After 8 min, cells were rapidly washed 2 times with ice-cold KRH buffer and solubilized in 1% Tx-100 for 20 min at ambient temperature with rocking. Radioactive DA present in the collected lysates was assessed by liquid scintillation counting. Kinetic values were analyzed using Prism software, and V_{max} values for each DAT line were normalized to transporter surface levels determined by surface biotinylation assays performed in parallel for each experiment.

Surface Biotinylation

LLCPK₁ parent cells were seeded onto 24-well assay plates and grown to ~80% confluence at which point 12 wells of each plate were transiently transfected with the indicated rDAT plasmid 36 hours prior to the biotinylation assay. After transfection the cells were washed three times with ice cold Hank's balanced salt solution containing Mg⁺ and Ca²⁺ ions (HBSS Mg-Ca: 1mM MgSO₄, 0.1 mM CaCl₂, pH 7.4), and subsequently incubated twice with 0.5 mg/mL of membrane-impermeable sulfo-NHS-SS-biotin for 25 min on ice with rocking. The biotinylation reagent was removed and the reaction was quenched by two sequential incubations with 100 mM glycine in HBSS Mg-Ca for 20 min on ice with rocking. Cells were washed with HBSS Mg-Ca and lysed with 125 μL RIPA buffer containing protease inhibitor in each well after which the lysates from 12 wells (one full DAT line) were collected in a 2 mL microcentrifuge tube. 100 μg of protein from each lysate were incubated with NeutrAvidin beads overnight at 4°C with nutation. The beads were washed three times with RIPA buffer and the bound protein was eluted with 32 μl of SB followed by SDS-PAGE and immunoblotting for DAT with MAb16.

CHAPTER 3

EFFECTS OF THE PARKINSON-INDUCING NEUROTOXINS MPP⁺ AND 6-OHDA ON DOPAMINE TRANSPORTER FUNCTION AND MODIFICATION

Abstract

Synaptic action of the neurotransmitter dopamine (DA) is primarily terminated by reuptake into presynaptic dopaminergic neurons via dopamine transporters (DATs). DATs are integral plasmalemmal proteins whose reuptake function is tightly coordinated by interplay between the post translational modifications phosphorylation and palmitoylation. The psychostimulant amphetamine (AMPH) is a DAT substrate known to empty sequestered DA from vesicles and induce protein kinase C (PKC)-dependent DAT phosphorylation, resulting in reverse transport of DA (efflux) and greatly increased DA signaling. Elevated DA concentrations similar to those produced by AMPH create neurotoxic conditions as DA oxidation produces free radicals and hinders mitochondrial respiration, thus strict spatial and temporal control of cytosolic and synaptic DA is essential for neuronal health. DA induced oxidative stress is an important pathogenic mediator in Parkinson disease (PD), and animal models of PD are generated by the neurotoxins 1-methyl-4-phenylpyridinium ion (MPP⁺) and 6-hydroxydopamine (6-OHDA) which selectively target DAT-expressing neurons, are translocated to the cytosol by DAT, and perturb the oxidative balance within the cell to produce the nigrostriatal DA neuron death observed in PD. It is therefore

intriguing to investigate DAT-involved mechanisms in terms of PD etiology as atypical DAT function could contribute to DA oxidative stress and is hypothesized to play a role in other neurological disorders including attention deficit/hyperactivity disorder (ADHD) and addiction. DAT expression occurs around synaptic terminals, along axons, and on dendritic spines, and efflux via DATs located on dendrites in the substantia nigra has been shown to diminish dopaminergic signaling. It is possible, therefore, for aberrant regulation and localization of DA clearance and DAT-mediated DA efflux to profoundly influence the excitability of neurons and play a significant role in neurodegeneration in the progression of PD. This is even more interesting in the light of recent studies revealing DAT polymorphisms in patients diagnosed with a psychiatric disorder or early onset PD that display an elevated basal DA efflux phenotype. In this study, we are investigating the effect of DAT substrates and PD-inducing neurotoxins on DAT phosphorylation, palmitoylation, down-regulation, and reverse transport to better understand aberrant DAT mechanisms which may contribute the onset of PD. Our findings indicate MPP⁺ and 6-OHDA differentially alter DAT function. 6-OHDA inhibits basal and attenuates PMA-induced DAT phosphorylation, does not significantly reduce DA uptake, and decreases DA efflux. MPP⁺ does not change basal or PMA stimulated DAT phosphorylation yet it induces significant DA efflux which may be an additional means by which MPP⁺ produces neurodegeneration. This MPP⁺ induced efflux was not abolished by pretreatment with the PKC inhibitor bisindolylmaleimide (BIM). Although AMPH-induced efflux was blunted after BIM treatment, significant efflux remained, supporting evidence of mechanisms

independent of PKC mediated DAT phosphorylation for the stimulation of DA efflux.

Introduction

Parkinson Disease (PD) is the second most common neurodegenerative illness and its prevalence is expected to increase proportionately with the size of aging populations⁴²². PD pathology⁴²³ is characterized by progressive, selective⁴²⁴ loss of substantia nigra (SN) pars compacta dopamine (DA) neurons and aggregation of proteinaceous fibril superstructures, comprised primarily of α -synuclein, known as Lewy bodies⁴²⁵. The clinical presentation of this illness, though phenotypically heterogeneous, is manifest through aberrant locomotor output in the form of bradykinesia, resting tremor, postural instability, and/or rigidity⁴²⁶; however, onset of these symptomatic traits generally does not appear until 66%-80%³⁵² of SN DAergic neurons are lost, generating further striatal DA deficiency⁴²⁷ and causing the resultant motor dissonance to occur. These data spurred interest in finding prodromal manifestations of PD, and associations between disease onset and manifold pre-motor symptoms were established^{428,429}: olfactory malfunction⁴³⁰; rapid eye movement sleep behavior disorder^{431,432}; constipation^{433,434}; and depression^{435,436} with antidepressant use have been identified as potential pre-motor symptoms in PD development. PD treatment methodologies⁴³⁷ target motor symptoms of the disorder and primarily entail replenishing DA function *via* increasing striatal DA concentration through elevating DA synthesis with the product of its rate-limiting enzymatic step, levodopa, mimicking synaptic DA action by DA receptor agonists, or attenuating enzymatic

DA degradation with monoamine oxidase and/or catechol-o-methyl transferase inhibitors⁴³⁸. While these pharmacotherapies improve quality of life, their long-term use, coupled with the progression of the disease, result in increasing severity of symptoms including dementia, dyskinesia, and psychosis^{439,440}.

At a biochemical level, PD etiology has been linked to several protein and organellar malfunctions. Inherited PD stems from polymorphisms of genes coding for α -synuclein, E3 ubiquitin ligase, leucine-rich repeat kinase 2, and other proteins^{253,441}, while idiopathic PD derives from numerous risk factors like exposure to pesticides and use of beta blockers⁴⁴². The resultant synuclein aggregation induces cellular damage through endoplasmic reticulum stress, mitochondrial impairment⁴⁴³, neuroinflammation⁴⁴⁴, and reactive oxygen species production⁴⁴⁵, all of which induce cell death. As previously mentioned, the locus and cell type of these apoptotic events is a common link between inherited and idiopathic PD and that is consistent loss of substantia nigra DA neurons. A peculiarity of this subset of neurons is their high expression of the DA transporter (DAT), the high-affinity DA reuptake protein^{139,446}. Indeed, the extent of PD-induced loss of DAergic neurons from the brain's primary DA pathways is greatest in the nigrostriatal tract³⁵², followed by ventral tegmental area-originating mesocortical and mesolimbic structures^{447,448}, while the tuberoinfundibular tract remains largely unaffected⁴²⁴. These losses positively correlate with both DAT mRNA⁴⁴⁹⁻⁴⁵¹ and protein expression^{452,453} in these regions. It is for this reason DAT has been hypothesized as a molecular gateway through which PD pathogenicity occurs^{251,454}.

Two neurotoxic compounds used extensively in laboratories to create facsimiles of PD for study in multiple model systems operate as DAT substrates; their experimental efficacy is due to their transport selectivity by DAT and therefore poison neurons specifically expressing DATs. These compounds, 6-hydroxydopamine (6-OHDA) and 1-methyl-4-phenyl-1,2,3,6-tetrahydropyridine (MPTP) (Figures 1 & 2), induce the DAergic neuron losses characteristic of PD, and do so through overlapping biochemical mechanisms⁴⁵⁵. Under physiologic conditions 6-OHDA induces cell death after rapid auto-oxidation⁴⁵⁶ and generation of oxygen-derived free radical species^{457,458}, perhaps through iron-catalyzed ROS activity^{459,460}. Additionally, 6-OHDA inhibits complex I of the mitochondrial electron transport chain^{461,462} and induces neuronal death primarily through apoptotic pathways⁴⁶³. MPTP neurotoxicity occurs after its monoamine oxidase conversion to 1-methyl-4-phenylpyridinium (MPP⁺) in astrocytes^{464,465}, flux from these cells through organic cation transporter 3⁴⁶⁶ or extraneuronal monoamine transporter⁴⁶⁷, and neuronal entry *via* DAT. Once in the cytosol, MPP⁺ is sequestered into vesicles through VMAT2^{468,469} which empties vesicular DA into the cytosol, producing its oxidation by-products and their concomitant oxidative damage^{470,471}. MPP⁺ likewise inhibits mitochondrial ATP production^{443,472}, but unlike 6-OHDA, has been shown to destabilize cytoskeletal structures^{473,474}, and cause acute increased striatal DA release^{475,476}. The toxic functional outcomes of these compounds are

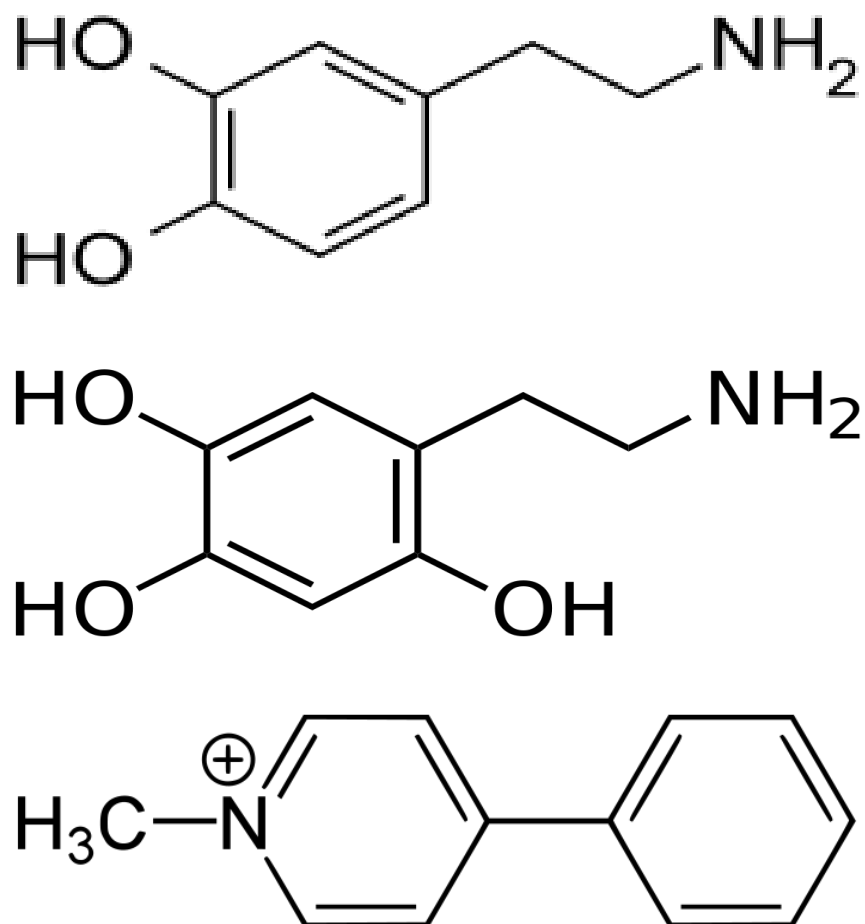


Figure 1. Chemical structures of 6-OHDA and MPP⁺. Chemical structures of Dopamine (top), 6-hydroxydopamine (middle), and 1-methyl-4-phenylpyridinium (bottom).

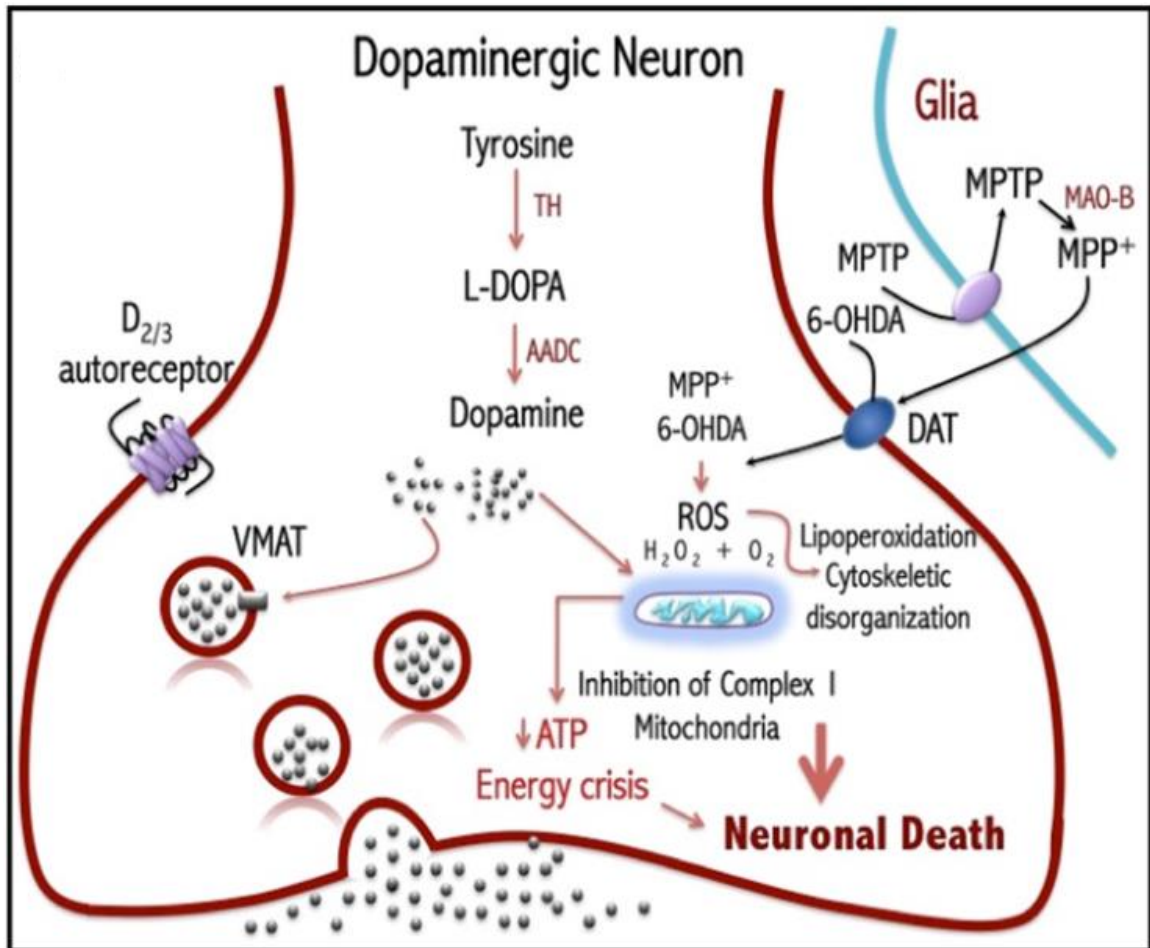


Figure 2. Known neurotoxic mechanisms of 6-OHDA and MPP⁺. Schematic diagram of DA, 6-OHDA, and MPP⁺ Neurotoxic mechanisms. After synthesis, DA is packaged into vesicles via the vesicular monoamine transporter where it is trafficked to the plasma membrane for exocytotic release into the synapse. Cytosolic DA metabolism is known to generate ROS. DA can be oxidized to form reactive quinones that react further on to form neurotoxic compounds and protein adducts. MPP⁺ is enzymatically generated in glial cells via MAO. 6-OHDA and MPP⁺ enter neurons through DAT and induce their toxic effects by inhibition of complex I of oxidative phosphorylation, formation of ROS by lipid peroxidation, or disruption of cytoskeletal integrity.

dependent upon their DAT-mediated entry into neurons^{477–479}, and many of their DAT-specific effects have hitherto been unexplored.

This study investigates the biochemical effects exerted by the PD-generating neurotoxins upon heterologously expressed DATs; DA reuptake, DA reverse transport, DAT phosphorylation, and DAT palmitoylation changes induced by 6-OHDA and MPP⁺ were assessed. Our findings reveal that, despite sharing multiple cytotoxic mechanisms, 6-OHDA and MPP⁺ have striking dissimilarities in regards to DAT phosphorylation, DA uptake downregulation, and DAT-mediated DA efflux. Significantly, this study further investigates the DA efflux phenomenon associated with early onset PD and ADHD, an event recapitulated by MPP⁺, and highlights the extreme caution needed in prescribing or using pharmaceuticals inducing carrier-mediated DA efflux.

Results

6-OHDA and MPP⁺ Competitively Inhibit DAT-mediated DA Uptake

To investigate the concentrations at which DA uptake by WT rDATs in LLC_{PK1} expression systems were inhibited by 6-OHDA and MPP⁺, competition uptake assays were utilized. The half maximal inhibitory concentration (IC₅₀) was determined for the LLC_{PK1} – WT rDAT model by [³H]DA uptake assays with unchanged 0.5 μM DA in the presence of increasing concentrations (10⁻⁷ to 10⁻¹ M) of 6-OHDA or MPP⁺ (Figure 3). The IC₅₀ for 6-OHDA was approximately 1mM (1025 ± 185 uM, n=2 independent experiments performed in triplicate), and the

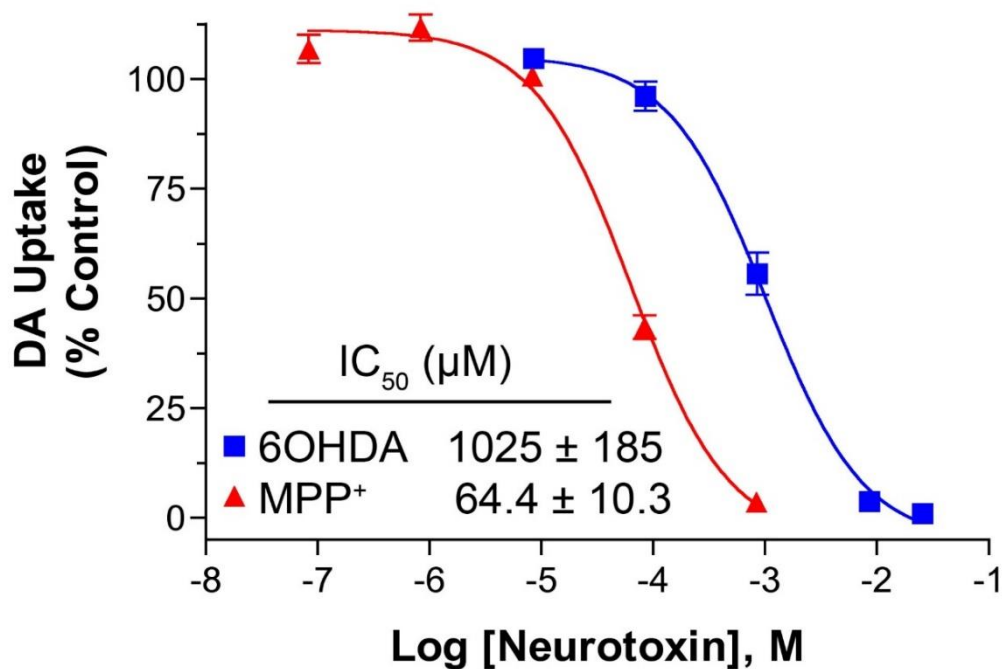


Figure 3. MPP⁺ has a 16-fold greater potency than 6-OHDA for the inhibition of DA uptake. LLCPK₁-rDAT cells were assayed for [³H]DA uptake activity in the presence of 10⁻⁷- 10⁻¹ M 6-OHDA or MPP⁺. Reactions contained 0.5 μM DA with the indicated inhibitor concentration and were conducted at 37°C for 8 min after which cells were washed, lysed, collected, and analyzed for radioactivity by scintillation counting. IC₅₀ values for 6-OHDA and MPP⁺ were determined by non-linear regression analysis and data are presented as mean ± S.E. of two experiments carried out in triplicate. Foster and Vaughan, unpublished data.

MPP⁺ IC₅₀ was 64.4 ± 10.3 μM (n=2 independent experiments performed in triplicate). While these compounds do not have particularly high affinity for the DA translocation site on DAT (for reference, see DA saturation analysis studies in chapter II), they do exhibit competitive inhibition of DA uptake, indicating competition for the primary substrate permeation pathway of DAT in LLCPK₁ cells. This, of course, corresponds with what has been known about these compounds for some time – they require DAT to enter DAergic neurons to exert their neurotoxic effects. Also, as DA uptake was competitively inhibited by 6-OHDA and MPP⁺, these experiments indicate the LLCPK₁ – DAT model system is valid to utilize for further experimentation with these compounds.

6-OHDA and MPP⁺ Induce Downregulation of DAT Activity

The extent to which the neurotoxic DAT substrates are able to downregulate DAT uptake capacity was next interrogated. 20 μM of 6-OHDA, MPP⁺, and DA in parallel with 400 nM phorbol-12-myristate-13-acetate (PMA), a PKC-activator known to down-regulate DAT function yet not requiring DAT activity to enter the cell's cytoplasm, were applied to LLCPK₁ cells expressing WT rDAT 30 minutes prior to washout with 4°C KRH and [³H]DA uptake testing (Figure 4). In these experiments, MPP⁺ (*p*<0.01 *versus* 6-OHDA) and DA (*p*<0.05 *versus* 6-OHDA) induced significantly greater downregulation of DAT function than did 6-OHDA, though no substrate attenuated DAT activity to the extent of PMA. These results indicate these DAT substrates produce down regulatory effects on DAT-mediated DA uptake, but do so, perhaps, by varying means. That 6-OHDA induces significantly less uptake attenuation may indicate it affects DAT internalization or

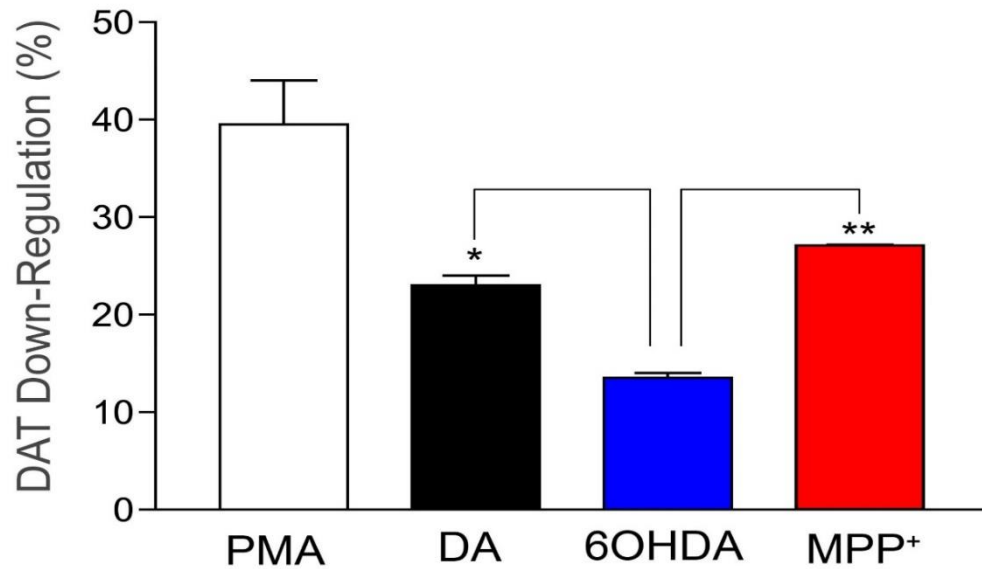


Figure 4. 6-OHDA induces DAT downregulation to a significantly lesser extent than DA or MPP⁺. LLCPK₁-rDAT cells were pretreated with vehicle, 400 nM PMA, 20 μM DA, 20 μM 6-OHDA, or 20 μM MPP⁺ at 37°C for 30 min followed by rapid washout at 4°C prior to assay for DA uptake. Down-regulation is reported as the percent difference in transport activity between the vehicle and substrate or PMA pretreatments. Data are presented as mean ± S.E. of two experiments carried out in triplicate. ***p*<0.01 MPP⁺ versus 6-OHDA, **p*<0.05 DA versus 6-OHDA. Foster and Vaughan, unpublished data.

regulatory pathways differently than MPP⁺ or DAT's cognate substrate, DA; though MPP⁺ induced effects similar to DA on DAT activity, this by no means indicates they operate through similar mechanisms to blunt DAT function.

Incubation of 6-OHDA and MPP⁺ on DAT-Expressing Cells Affects DA Uptake and Requires Functional DATs

To delineate whether the functional downregulation generated from the activity of 6-OHDA and MPP⁺ results from the active DAT-mediated translocation of these compounds into the cell or allosteric, extracellular binding events, DA uptake activity was assessed after incubation of these substances in the absence or presence of the high affinity DAT inhibitor, cocaine. This was assessed *via* incubating LLCPK₁ cells expressing WT rDAT with 20 μM of each neurotoxin in parallel with 20 μM DA and 400 nM PMA for 30 minutes prior to drug washout and [³H]DA uptake analysis (Figure 5). As a control to demonstrate that any effect 6-OHDA or MPP⁺ produces on DA uptake results from their DAT-mediated entry into the cell, the indicated incubations were simultaneously performed in the presence of 100 μM of cocaine. The results of these experiments show incubation with MPP⁺ ($p < 0.01$), like PMA ($p < 0.05$) but unlike 6-OHDA ($p > 0.05$) significantly reduces subsequent DAT mediated DA uptake vs. control. The concomitant incubation of the tested compounds with cocaine successfully blocked the MPP⁺-induced DA uptake losses observed in the absence of cocaine ($p > 0.05$). The short incubation period utilized (30min) hints at acute effects on intrinsic DAT properties such as conformational alterations, binding partner interactions, post-translational

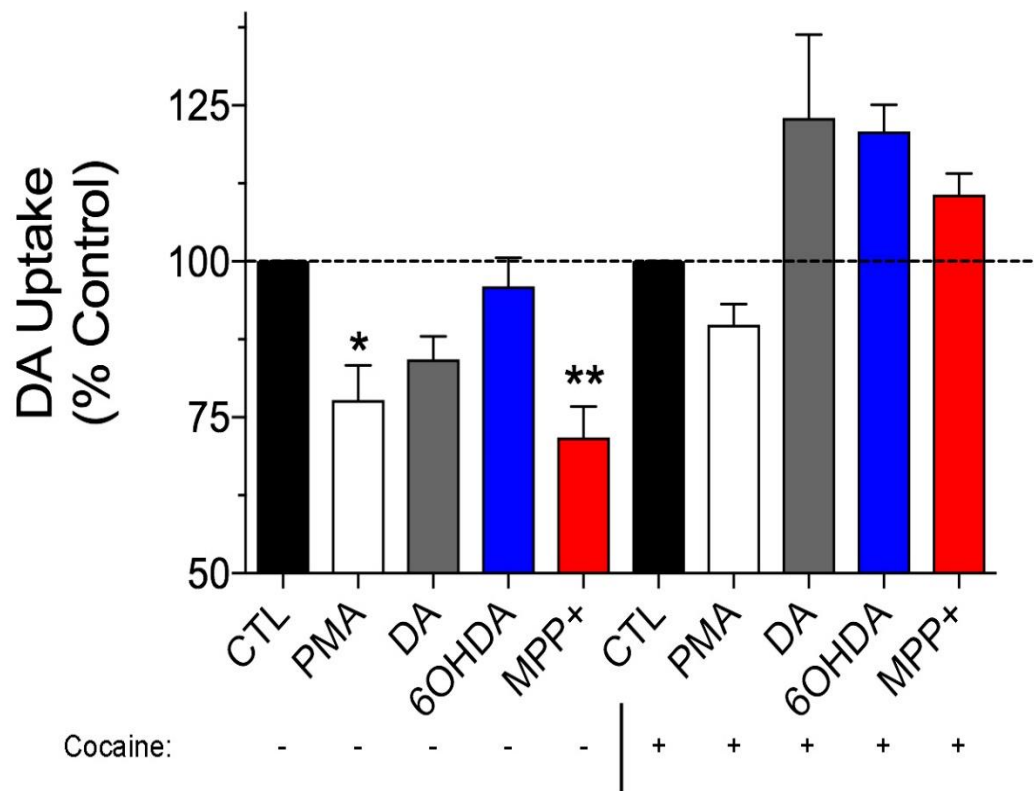


Figure 5. Neurotoxin downregulation of DAT requires their DAT-mediated transport. LLC-PK₁-rDAT cells were pretreated with vehicle, 400 nM PMA, 20 μM DA, 20 μM 6-OHDA, or 20 μM MPP⁺ at 37°C for 30 min with or without 100 μM cocaine followed by rapid washout at 4°C prior to assay for DA uptake with 3 μM DA containing 10 nM [³H]DA for 8 min at 37°C. Cells were rapidly washed and lysates were collected and analyzed for radioactive DA content by scintillation counting. Uptake is reported as the percent vehicle control. ***p*<0.01 MPP⁺ versus Control, **p*<0.05 PMA versus Control. These results indicate MPP⁺ induces significant DAT activity downregulation and requires DAT-mediated cell entry to achieve this effect.

modifications, or transporter internalization, rather than the generation of cell-toxifying reactive oxygen species, which take more time to be produced and built up to an extent at which they can induce significant cell damage. These compounds require DAT-mediated cell entry.

Neurotoxin Effects on DAT-Mediated Reverse DA Transport

Reverse transport (efflux) of DA *via* DAT has been implicated in the neuropathology of ADHD and Parkinson's disease. It follows, then, that an additional mechanism by which 6-OHDA or MPP⁺ may be able to induce its neurotoxic effects is the generation of DAT-mediated DA efflux. To test this we performed a biochemical efflux assay which involves 'loading' DAT-expressing cell system with [³H]DA through DAT-mediated uptake for 30 min, followed by 3 washouts of extracellular radiolabeled DA with 4°C KRH on ice. Efflux is subsequently induced by the addition of the 37°C KRH efflux buffer containing vehicle (to determine the basal efflux level), AMPH (strong DAT-mediated DA efflux inducer, positive control), or the indicated neurotoxin for 5 minutes. This buffer is then collected and assayed for radioactivity by scintillation counting. These efflux experiments were conducted at the sub IC₅₀ concentrations used in the previous experiments (Figure 6) as well as the determined IC₅₀ values (1 mM for 6-OHDA and 60 μM for MPP⁺) (Figure 7) determined from the experiments described in figure 1. Interestingly, the results of the efflux studies strongly implicate MPP⁺ as an efflux inducing compound at both 20 μM ($p < 0.05$ *versus* Basal) and its IC₅₀, 60 μM ($p < 0.01$ *versus* Basal). Additionally, though not

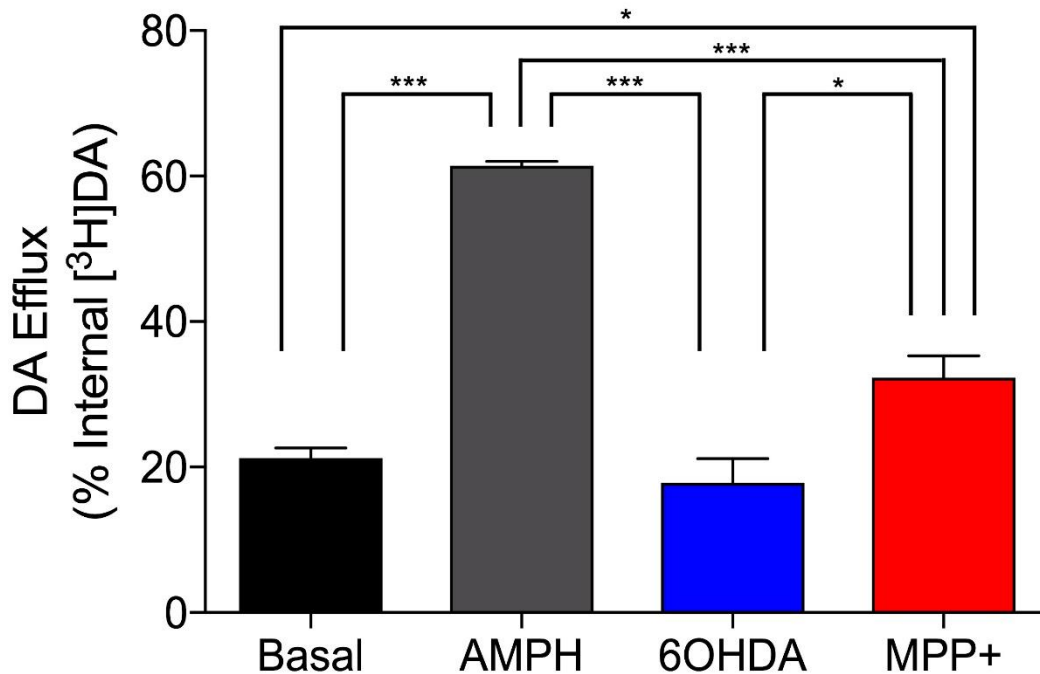


Figure 6. 20 μ M MPP⁺ induces DA efflux. LLCPK₁ cells expressing wild type rat DAT were grown in 24-well plates and subjected to the DA efflux assay. Efflux was induced by the addition of 37° KRH buffer alone to determine basal efflux or KRH containing 10 μ M AMPH, 20 μ M 6-OHDA, 20 μ M AMPH, 20 μ M MPP⁺ to determine compound-induced DA efflux (n=3). The efflux buffer was collected after 5 minutes and analyzed for radioactivity by scintillation counting. * p <0.05 MPP⁺ versus Basal and 6-OHDA, *** p <0.001 MPP⁺ versus AMPH, *** p <0.001 AMPH versus Basal and 6-OHDA. Data are presented as % internal [³H]DA. Statistical analyses were performed by ANOVA with Tukey's post hoc test of mean \pm S.E. These results indicate MPP⁺ induces DAT-mediated DA efflux.

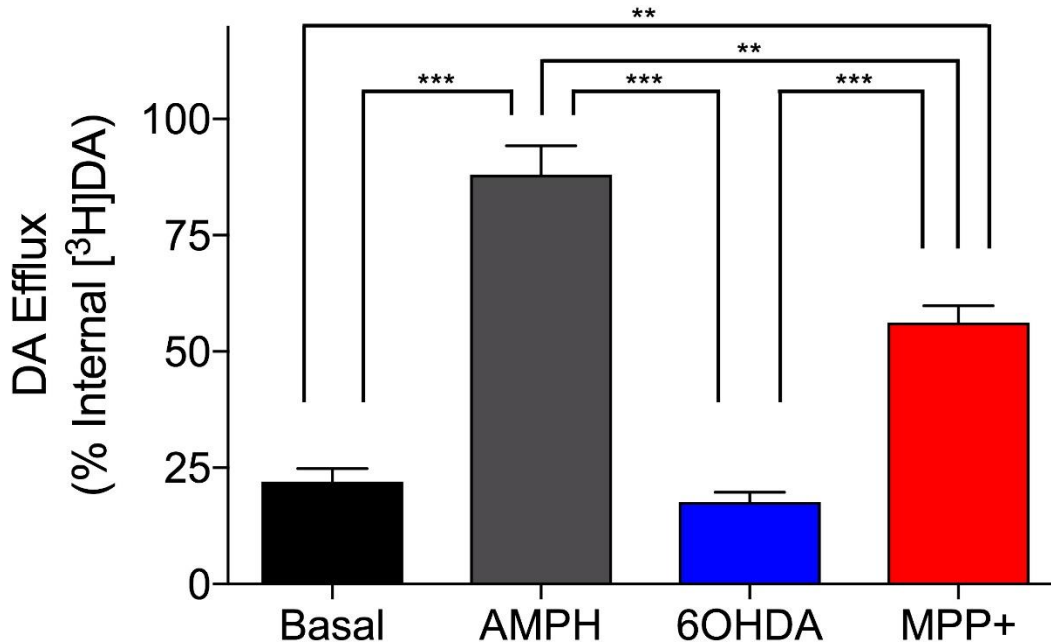


Figure 7. IC₅₀ concentration of neurotoxin effect on DA efflux. LLCPK₁ cells expressing wild type rat DAT were grown in 24-well plates and subjected to the biochemical DA efflux assay. Efflux was induced by the addition of 37° KRH buffer alone to determine basal efflux or KRH containing 10 μM AMPH, 1 mM 6-OHDA, 60 μM MPP⁺ to determine drug-induced efflux (n=3). The efflux buffer was extracted after 5 minutes and assayed for radioactivity by scintillation counting. ***p*<0.01 MPP⁺ versus Basal and AMPH, ****p*<0.001 MPP⁺ versus 6-OHDA, ****p*<0.001 AMPH versus Basal and 6-OHDA. Statistical analyses were performed by ANOVA with Tukey's post hoc test of mean ± S.E. These experiments confirm MPP⁺ is a strong inducer of DA efflux as the IC₅₀ concentration produced marked increase in DA efflux.

statistically significant, 6-OHDA tended to lower DA efflux in rDAT LLCPK₁ systems at both 20 μ M ($p>0.05$ versus Basal) and 1 mM ($p>0.05$ versus Basal).

This same experiment paradigm was applied to human DAT (hDAT) expressing LLCPK₁ cells to determine whether the same efflux event is produced by MPP⁺ interaction with the human DAT isoform (Figure 8). MPP⁺ did induce significantly increased levels of DA release relative to basal control from hDAT LLCPK₁ cells ($p<0.001$ versus Basal). Additionally, 6-OHDA significantly reduced DA efflux from WT hDAT cells ($p<0.01$ versus Basal) supporting the trend seen with WT rDAT cells (Figures 6 & 7). These experiments reveal two distinct mechanisms by which neurotoxicity may occur: the AMPH-like rapid release and increase of extracellular DA concentration produced by MPP⁺, and the blunting of DAT-mediated DA release seen after 6-OHDA treatment, resulting in elevated cytosolic DA tone and increased potential for generation of DA oxidation species. To our knowledge, 6-OHDA attenuation of DA efflux represents the first finding of a DAT substrate blunting the DA efflux effect.

Inhibiting PKC Reduces Neurotoxin-Induced DA Efflux

An important molecular mechanism involved in DAT-mediated DA efflux is phosphorylation of the transporter by PKC. To determine if this kinase's activity contributes to the elevated DA efflux induced by MPP⁺ treatment or the reduced DA release event initiated by 6-OHDA exposure, the previously utilized biochemical DA efflux assay was conducted after inhibition of PKC with 10 μ M of the PKC inhibitor bisindolemaleimide (BIM) during the 30 minute DA uptake load phase. 20 μ M and IC₅₀ concentrations of each neurotoxin were used on both BIM

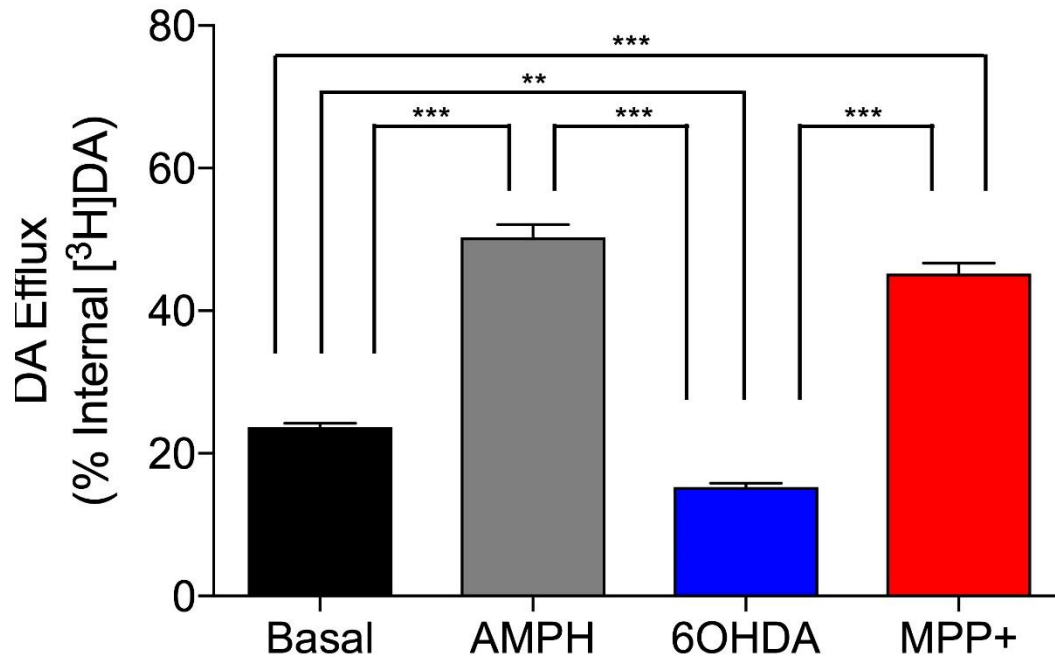


Figure 8. 6-OHDA blunts DA efflux from WT hDATs. LLCPK₁ cells expressing wild type human DAT were grown in 24-well plates and subjected to the biochemical DA efflux assay. Efflux was induced by the addition of 37° KRH buffer alone to determine basal efflux or KRH containing 10 μM AMPH, 1 mM 6-OHDA, 60 μM MPP⁺ to determine drug-induced efflux (n=3). The efflux buffer was extracted after 5 minutes and assayed for radioactivity by scintillation counting. ****p*<0.001 MPP⁺ versus 6-OHDA and Basal, ***p*<0.01 6-OHDA versus Basal, ****p*<0.001 AMPH versus 6-OHDA and Basal. Statistical analyses were performed by ANOVA with Tukey's post hoc test of mean ± S.E. This set of experiments further support MPP⁺ as an efflux inducer and demonstrate 6-OHDA as an inhibitor of the DAT-mediated DA efflux process.

treated and untreated LLCPK₁-rDAT cells (Figures 9 & 10). Additionally, BIM inhibition of PKC was tested in regards to the AMPH-stimulated DA efflux mechanism as well (Figure 11). Both basal ($p < 0.01$ versus Basal) and 20 μ M 6-OHDA treatment ($p < 0.01$ versus Basal) saw reduced DA efflux upon BIM treatment relative to untreated basal release (Figure 9). These data demonstrate that steady-state PKC activity, and likely phosphorylation of DAT itself, significantly contributes to a homeostatic DA leak through DAT. The extent of this basal release is no doubt exacerbated by 30 minutes of DA intake; nonetheless, unstimulated DAT-mediated DA release activity is significantly lessened by PKC inhibition. That 20 μ M 6-OHDA release characteristics were further blunted by BIM treatment is unsurprising as both molecules likely function through different mechanisms to modulate DAT-mediated efflux. While at 1 mM, 6-OHDA may interfere with BIM-induced mechanisms other than DAT phosphorylation through PKC, as the 5 minute 6-OHDA exposure is likely insufficient to alter this DAT PTM, yet does relieve the BIM-induced DA efflux attenuation. Once again MPP⁺ induced significantly elevated DA efflux (Figure 10) at both 20 ($p < 0.05$ versus Basal) and 60 μ M ($p < 0.001$ versus Basal) concentrations relative to basal control values and the 60 μ M event was reduced upon PKC inhibition ($p < 0.001$ versus MPP⁺ 60 μ M). BIM treatment preceding 20 μ M MPP⁺-stimulated efflux did not significantly reduce the release pattern relative to the untreated 20 μ M MPP⁺ paradigm ($p > 0.05$ versus Basal) though this same BIM exposure did not eliminate the significant increase relative to the basal control release ($p > 0.05$ 20 μ M MPP⁺ + BIM versus Basal). And though BIM treatment did not completely ablate 60 μ M MPP⁺ activation of efflux

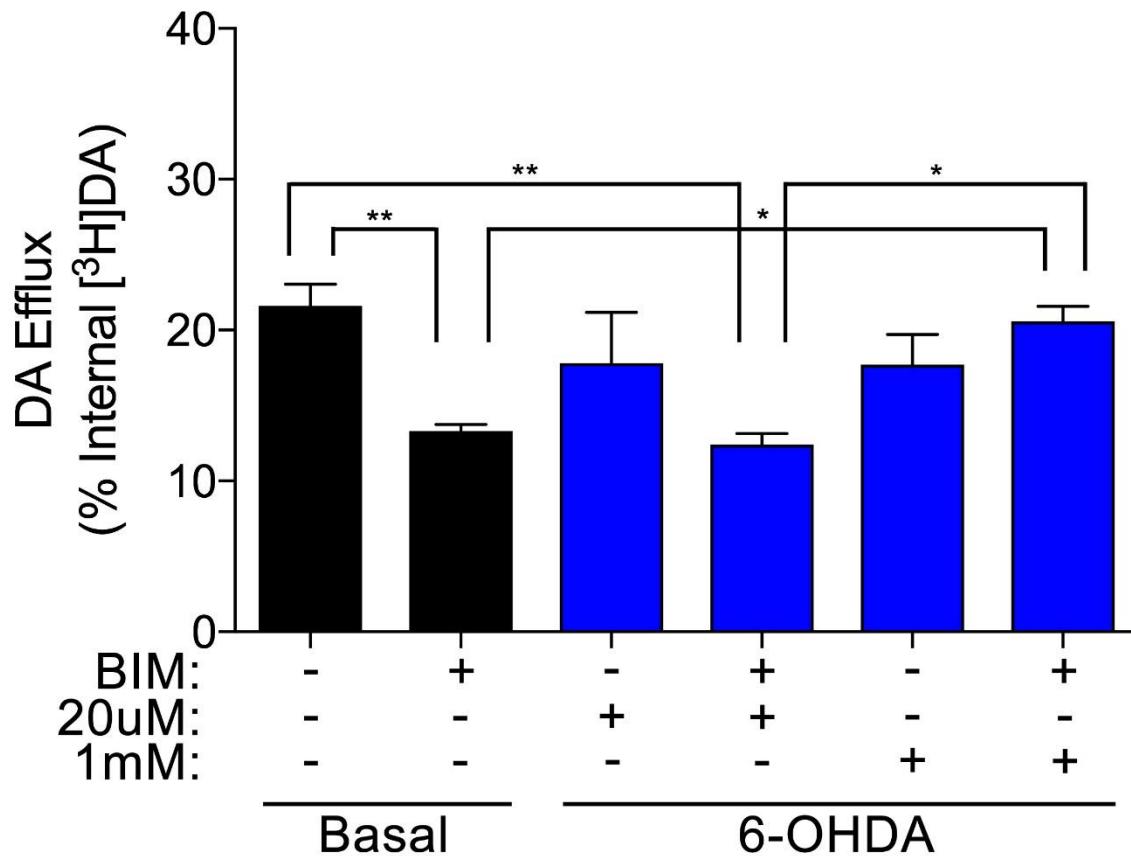


Figure 9. PKC inhibition effect on 6-OHDA DA efflux signature. LLCPK₁ cells expressing wild type rat DAT were grown in 24-well plates and subjected to the DA efflux assay after BIM treatment. Efflux was induced by the addition of 37° KRH buffer alone to determine basal or KRH containing 20 μM or 1 mM 6-OHDA (n=3) and collected 5 minutes subsequently and assessed for radioactivity by scintillation counting. Data are presented as % internal [³H]DA. 100% internal [³H]DA was determined by lysing and assessing radioactive content of cells receiving no efflux buffer. ***p*<0.01 Basal versus Basal + BIM and 6-OHDA 20 μM + BIM, **p*<0.05 6-OHDA 1 mM versus Basal + BIM and 6-OHDA 20 μM + BIM. Statistical analyses were performed by ANOVA with Tukey's post hoc test of mean ± S.E.

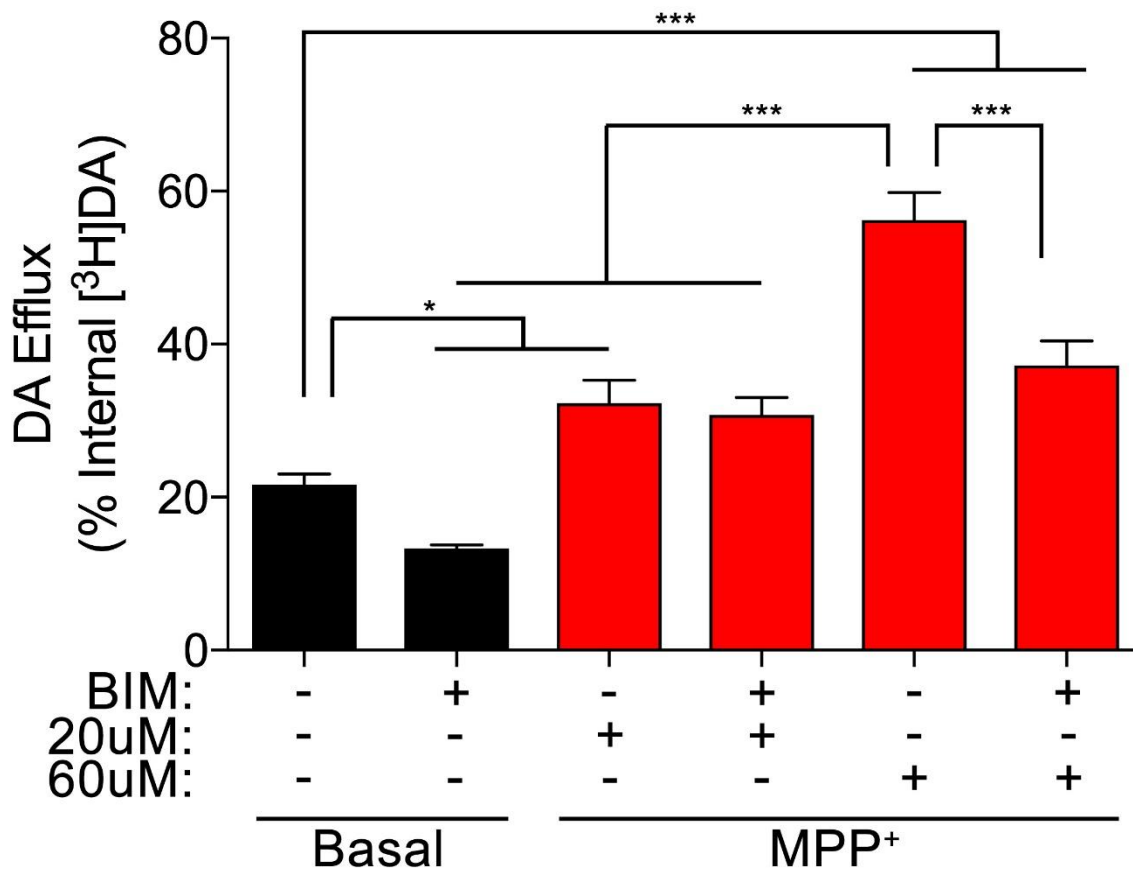


Figure 10. PKC inhibition reduces MPP⁺-induced DA efflux. LLCPK₁ cells expressing wild type rat DAT were grown in 24-well plates and subjected to the biochemical DA efflux protocol after BIM treatment. Efflux was induced by the addition of 37° KRH buffer alone to determine basal or KRH containing 20 μM or 60 μM MPP⁺ (n=3) and collected 5 min subsequently and assessed for radioactivity by scintillation counting. Data are presented as % internal [³H]DA. 100% internal [³H]DA was determined by lysing and assessing radioactive content of cells receiving no efflux buffer. **p*<0.05 Basal + BIM versus Basal, **p*<0.05 MPP⁺ 20 μM versus Basal, ****p*<0.001 MPP⁺ 60 μM and MPP⁺ 60 μM + BIM versus Basal, ****p*<0.001 MPP⁺ 60 μM versus Basal + BIM, MPP⁺ 20 μM, MPP⁺ 20 μM + BIM, and MPP⁺ 60 μM + BIM. Statistical analyses were performed by ANOVA with Tukey's post hoc test of mean ± S.E. These results indicate PKC activity contributes to the MPP⁺-stimulated DA efflux paradigm, but may not be the sole contributor to this process.

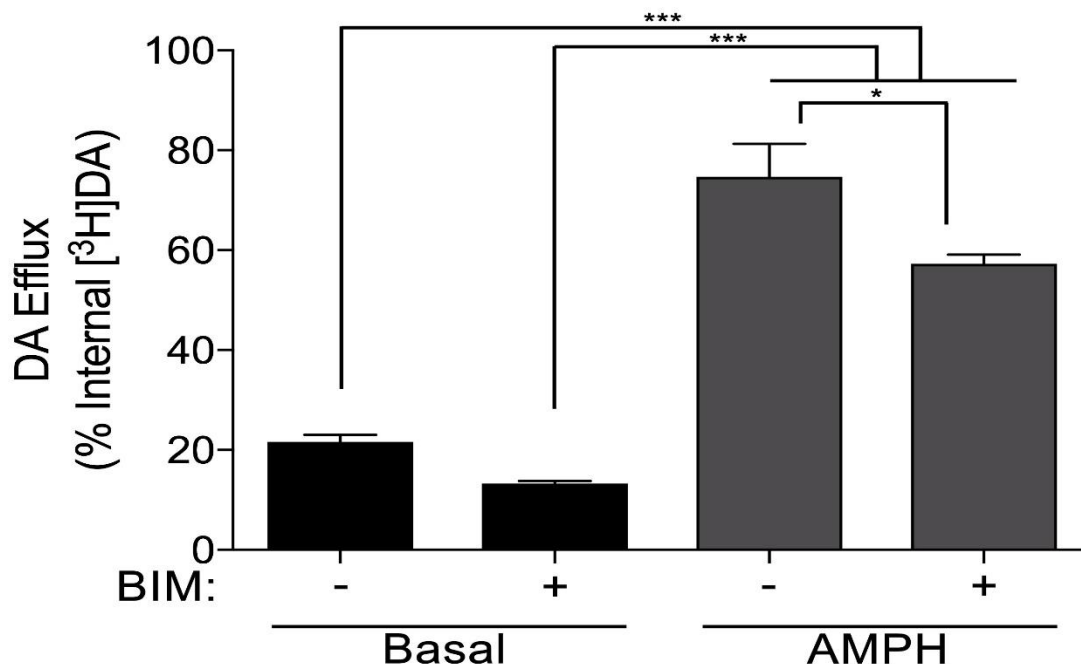


Figure 11. PKC inhibition reduces AMPH-stimulated DA efflux. LLCPK₁ cells expressing wild type rat DAT were grown in 24-well plates and subjected to the DA efflux assay. Efflux was induced by the addition of 37° KRH buffer alone to determine basal or KRH containing 10 μM AMPH (n=6) and collected 5 minutes subsequently and assessed for radioactivity by scintillation counting. Data are presented as % internal [³H]DA. 100% internal [³H]DA was determined by lysing and assessing radioactive content of cells receiving no efflux buffer. ****p*<0.001 Basal versus AMPH and AMPH + BIM, ****p*<0.01 Basal + BIM versus AMPH and AMPH + BIM, **p*<0.05 AMPH + BIM versus AMPH. Statistical analyses were performed by ANOVA with Tukey's post hoc test of mean ± S.E. These studies confirm PKC contributes to, but is not the only mechanism by which AMPH-induced DA efflux occurs.

($p < 0.001$ versus Basal), it did greatly reduce 60 μM MPP⁺-induced efflux ($p < 0.001$ MPP⁺ 60 μM + BIM versus MPP⁺ 60 μM). This same pattern was achieved by AMPH-induced DA efflux (Figure 11). AMPH stimulation was significantly curtailed by PKC inhibition ($p < 0.001$ AMPH + BIM versus AMPH). These experiments reveal that MPP⁺ stimulation of DA efflux utilizes at least one mechanism in common with AMPH, PKC activity, and perhaps, like AMPH, operates through additional mechanisms to induce DA efflux.

Neurotoxin Effect on DAT Phosphorylation

To further understand the forward and reverse DA transport effects induced upon neurotoxin-exposed DATs, we assessed the effect of MPP⁺ and 6-OHDA on two prominent DAT post-translational modifications – phosphorylation and palmitoylation. Neurotoxin-induced DAT phosphorylation was assessed by radiolabeling with [³²P] metabolically incorporated by kinase activity into rDATs expressed in LLCPK₁ cells (Figure 12). These cells were treated with neurotoxins for 30 minutes with or without 200 nM PMA during which [³²P] incorporation was conducted. Equal amounts of radiolabeled DATs were immunoprecipitated with a poly16 crosslinked protein A sepharose column, subjected to SDS-PAGE and autoradiography. This signal was then normalized to equal amounts of rDAT immunoblotted with MAb16 (Figure 13). Intriguingly, 6-OHDA significantly reduced both basal ($p < 0.01$ 6-OHDA versus Control) and PMA-stimulated ($p < 0.01$ 6-OHDA + PMA versus Control + PMA) [³²P]phosphorylation of rDAT relative to control in each condition in this expression system. This suggests the attenuated DA efflux

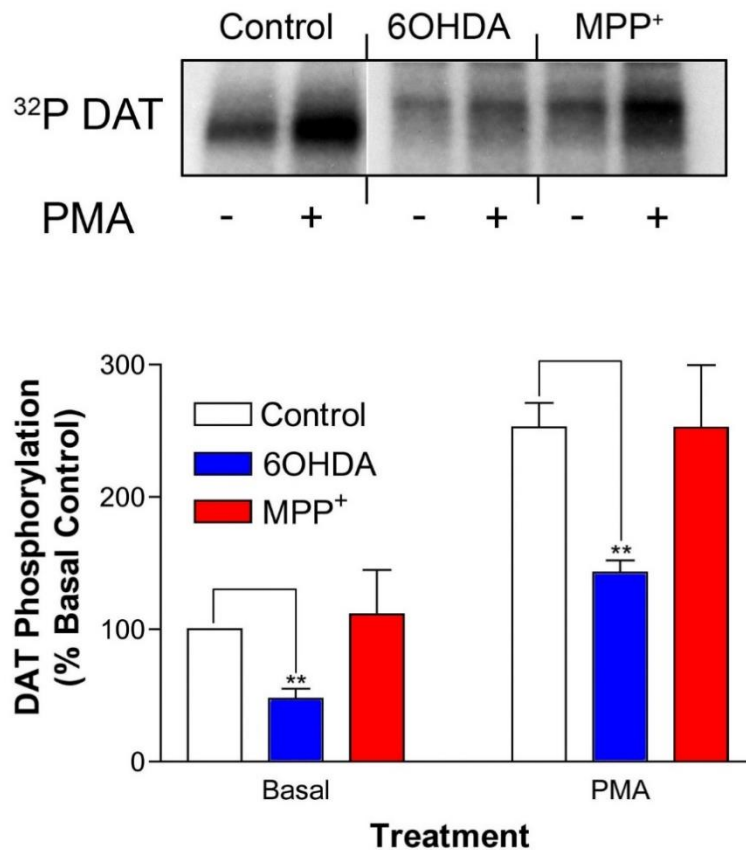


Figure 12. 6-OHDA inhibits basal and attenuates PMA-induced DAT phosphorylation. rDAT-LLCPK₁ cells labeled with ³²PO₄ were treated with vehicle, 1 mM 6-OHDA or 1 mM MPP⁺ for 30 min at 37°C. Vehicle or PMA treatment was conducted in parallel wells during the same incubation period. (*Upper Panel*) Representative autoradiogram of poly 16 immunoprecipitated ³²PO₄-labeled DATs. (*Lower Panel*) Quantification of ³²PO₄-labeled DAT band intensities from three independent experiments, ***p* < 0.01 (student's t-test). Foster and Vaughan, unpublished observation. These results indicate one means by which 6-OHDA induces attenuation of DA efflux may be by inhibiting transporter phosphorylation. Also, MPP⁺ generates DA efflux without altering DAT phosphorylation.

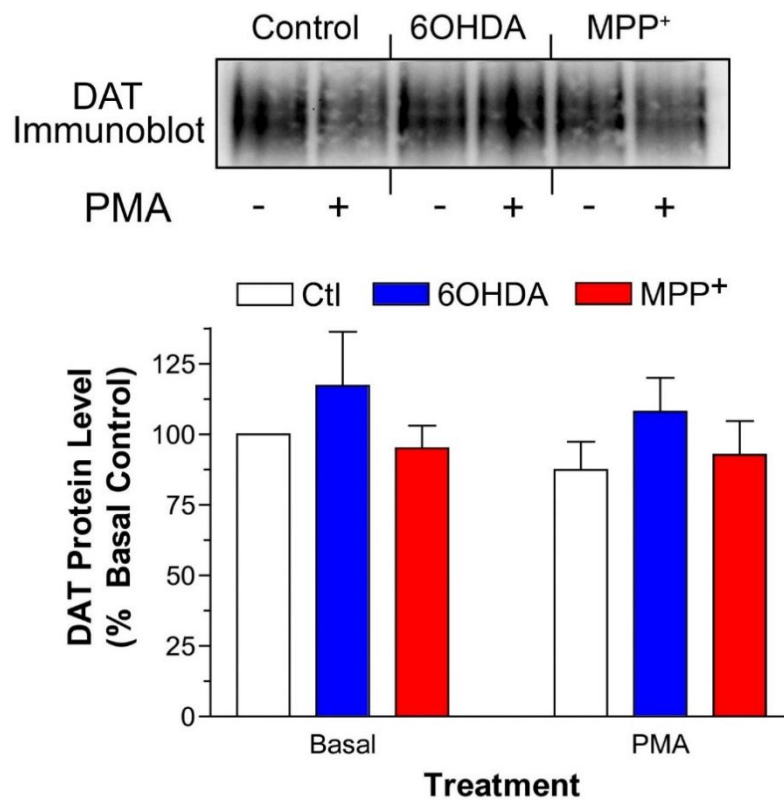


Figure 13. Total DAT protein expression is unchanged after neurotoxin treatment. (*Upper Panel*) Representative immunoblot showing DAT protein levels in sample lysates from [³²P] labeling experiments. (*Lower Panel*) Quantification of DAT content in rDAT-LLCPK₁ cell lysates labeled with ³²PO₄; three independent experiments. These results demonstrate neurotoxin treatment does not induce loss of total transporter expression. Foster and Vaughan, unpublished finding.

effect generated by 6-OHDA upon DATs may involve blunting of DAT phosphorylation mechanisms. Also surprising was the discovery that MPP⁺ application does not affect basal ($p > 0.05$ MPP⁺ versus Basal) or PMA-stimulated ($p > 0.05$ MPP⁺ + PMA versus Basal + PMA) transporter phosphorylation, which is crucial for AMPH-stimulated DA efflux. This implies the drug induces carrier-mediated DA efflux through mechanisms other than direct transporter phosphorylation, and the BIM-attenuated DA release occurs through inhibiting PKC phosphorylation of DAT-interacting proteins. The neurotoxin treatments were shown to alter DAT phosphorylation characteristics without altering total DAT protein levels (Figure 13).

Neurotoxin Effect on DAT Palmitoylation

As DAT palmitoylation plays a role in the protein's DA uptake stability^{344,347} and is an additional mechanism involved in DAT-mediated DA efflux (Chapter 1), DAT palmitoylation was analyzed after neurotoxin treatment to discern if these compounds generate changes in this modification of DAT (Figure 14). To assess transporter palmitoylation alterations resultant from 6-OHDA or MPP⁺ treatment, rDAT-LLCPK₁ cells were pretreated for one hour with IC₅₀ concentrations of both neurotoxins after which membrane preparations were performed and acyl-biotinyl exchange (ABE) analysis was conducted. The ABE inquiry demonstrated these neurotoxins have no effect on rDAT palmitoylation at the concentration and time used. Perhaps longer treatment times will produce DAT palmitoylation changes, but their acute effects generated on DAT forward and reverse DA transport is independent of DAT palmitoylation modulation. At a 1 hour and 400 nM treatment

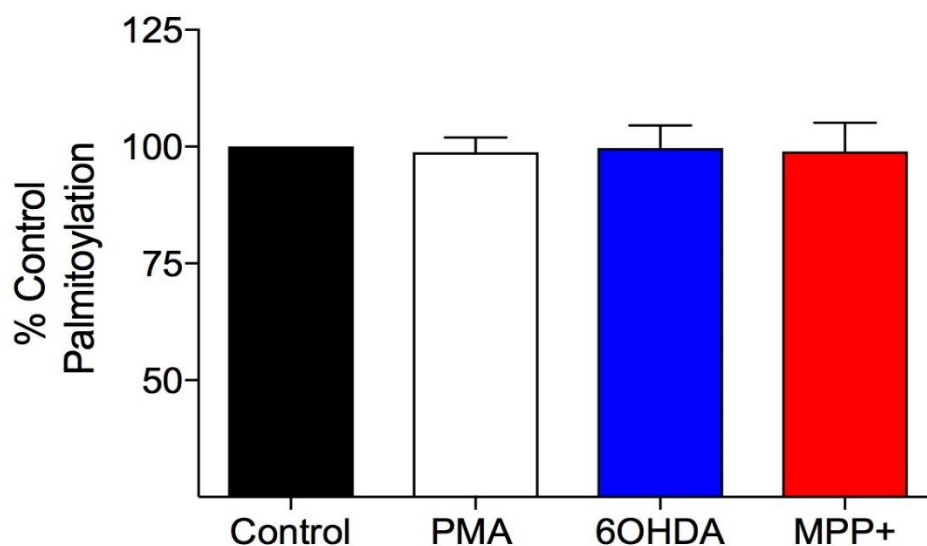
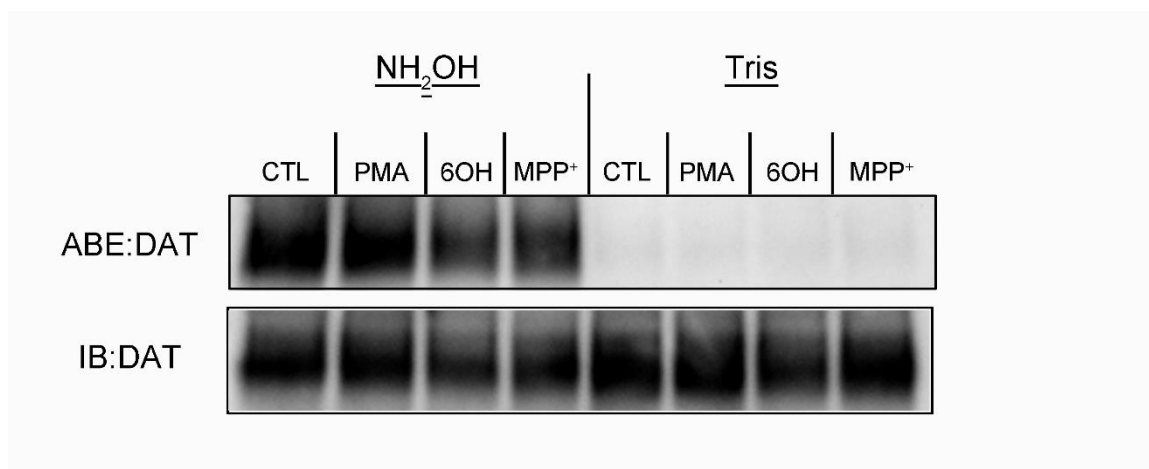


Figure 14. Neurotoxin effect on DAT palmitoylation. Membranes isolated from rDAT-LLCPK₁ cells treated with vehicle, 400 nM PMA, 1 mM 6-OHDA, or 60 μM MPP⁺ for 1 hr at 37° C were subjected to ABE. Hydroxylamine (NH_2OH) removes palmitate and enables the subsequent binding of the sulfhydryl-specific HPDP-biotin thereby allowing for detection of palmitoylated protein via NeutrAvidin chromatography and western blotting (*upper left panel*). Band intensities from these blots are quantified and normalized to their corresponding total immunoblotted DAT signals shown in the lower panel. Statistical analysis was performed by ANOVA with Tukey's post hoc test $p > 0.05$, $n = 3$.

paradigm, PMA also failed to reduce DAT palmitoylation. The concentration was chosen as it was used in the preceding experiments despite 1 μ M being previously demonstrated to significantly reduce DAT palmitoylation³⁴⁷.

Discussion

The neuronal expression of DAT is strongly positively correlated with susceptibility of the neuron to death in the etiology and progression of PD^{449–453}; as such, the aim of this study was to discern any DAT-specific effects produced by the PD-inducing neurotoxins, 6-OHDA and MPP⁺, widely used in the medical science research of this disease. The experiments were conducted in the LLCPC₁ cell system stably expressing DATs. Competitive uptake assays (Figure 3) determined that 6-OHDA and MPP⁺ do compete for the transporter DA translocation site in this system and that their IC₅₀ concentrations for it are 1 mM and 60 μ M respectively. Figures 4 and 5 represent experiments performed which demonstrate these compounds downregulate DAT function and that their down regulatory effects are DAT-mediated transport dependent. The next set of results decisively confirm that MPP⁺ is an inducer of DA efflux at both 20 (Figure 6) and 60 μ M (Figure 7) concentrations from rDAT, an effect which is contributed to by functional PKC (Figure 10), and at 60 μ M with hDAT (Figure 8). MPP⁺ was previously discovered to dramatically increase extracellular DA levels when perfused into the striatum⁴⁸⁰ and this release was DAT-dependent⁴⁷⁶, so the finding that 6-OHDA reduces DA efflux, though not significantly, from rDAT-LLCPC₁ cells (Figures 6 & 7), and significantly from hDAT-LLCPC₁ cells (Figure 8) is rather interesting and reveals a striking difference between the mechanisms by which

these two compounds operate. This 6-OHDA-reduced DA efflux effect was further blunted by BIM inhibition of PKC (Figure 9), though this may be due to unstimulated release being reduced by the same inhibitor (Figure 9). Though these compounds produced no change in transporter expression (Figure 13) or palmitoylation levels (Figure 14), 6-OHDA, interestingly, blunted basal and PMA-stimulated transporter phosphorylation (Figure 12). This may explain the attenuation of reverse DA transport by 6-OHDA, though the 5 minute exposure to the drug during the efflux protocol may not allow enough time for the reversal of transporter phosphorylation to occur as the phosphorylation (Figure 12) was assessed after a 30 min drug exposure. To our knowledge, this is the first time a DAT substrate has been demonstrated to blunt both DA efflux and DAT phosphorylation. MPP⁺ altered neither DAT phosphorylation (Figure 12), DAT expression (Figure 13), nor DAT palmitoylation (Figure 14).

As seen in Figures 2 and 3, pretreatment of DAT-expressing cells with the PD-inducing neurotoxic DAT substrates downregulated DAT-mediated DA uptake activity – MPP⁺ to a greater extent than 6-OHDA (Figures 4 & 5). These results are consistent with the general behavior of DAT function after exposure to its substrates for the time used in these experiments (30 min); that is to say, DAT-conducted transport of substrate (DA, AMPH, or methamphetamine) across the plasma membrane reduces the capacity of the same DAT population to translocate subsequent substrate^{220,481–486}. This effect, however, occurs after substrate exposure times greater than 1 min, before this point substrates rapidly recruit transporter copies from endosomal pools to the plasma membrane⁴⁸⁷, acutely

increasing DA uptake capacity. Depending on the study, the substrate-induced downregulation of DAT activity has been shown to be one^{484,488} or a combination^{483,486} of transporter internalization and PKC activity, and depends on substrate species^{482,485,489}. Interestingly, substrate exposure induces this DAT uptake attenuation upon dorsal striatal DATs and not nucleus accumbens DATs^{481,483,485}, suggesting a cellular environment sensitive to DAT substrates in dorsal striatal neurons and absent in accumbens neurons which responds to transporter activity or cytosolic substrate to shut down DAT function. These could be an outcome of divergent post-translational modification, endocytic, or antioxidant mechanisms. It may be one of these systems which responds differently to DAT or cytosolic chemistries instigated by 6-OHDA or MPP⁺ to produce their contrasting effects on DAT activity. Transporter surface population alterations need to be assessed to determine whether the observed toxin-induced DA uptake downregulation results from a loss of plasma membrane protein or other DAT-intrinsic or cellular environment factors.

Perhaps the most intriguing results from this study surround the DA efflux investigations and reveal further differences between the actions of 6-OHDA and MPP⁺ (Figures 6-11). MPP⁺ acts as a DA efflux enhancer while 6-OHDA is a DA efflux reducer. The efflux response to MPP⁺, like AMPH, was blunted after PKC inhibition though not abolished. This suggests that MPP⁺ and AMPH utilize PKC activity to prompt DAT-mediated DA efflux in a similar manner. That MPP⁺^{476,490,491} and AMPH^{492,493} also act as substrates for the vesicular monoamine transporter 2 (VMAT2)^{239,240} further supports these molecules sharing similar DA-efflux inducing

identities. These VMAT2 substrates empty vesicles of sequestered transmitter to elevate cytosolic DA concentration, a process associated with degeneration of the nigrostriatal DA tract⁴⁹⁴, perhaps by increasing the likelihood of DA-derivative reactive oxygen species toxicity and/or enhancing DAT-facilitated DA efflux causing a perturbed synaptic DA homeostasis. 6-OHDA reduction of carrier-mediated reverse DA transport renders this compound unique amongst DAT substrates. The mechanism by which this occurs may involve oxidation damage to important protein actors to the efflux schema, or its direct modification of DAT which biases the transporter in an efflux-unfavorable conformation. PKC may be a target of 6-OHDA activity which may be the mechanism by which 6-OHDA attenuates basal and PKC-stimulated transporter phosphorylation, which, in turn, would ablate DA efflux.

The neurotoxic effects on the DAT phosphorylation (Figure 12) and palmitoylation (Figure 13) post-translational processes illuminated a potential mechanism by which one of the studied compounds may alter DA efflux. Increased transporter phosphorylation is classically identified with increased DA efflux capacity²²⁹, and, therefore, compounds which can reduce transporter phosphorylation, like 6-OHDA, can conceivably reduce transporter-mediated efflux. That MPP⁺ did not increase basal or PMA-stimulated DAT phosphorylation may be due to low stoichiometric abundance of the induced phosphorylation event which cannot be distinguished by the methodology used, especially in the PMA background. The BIM-induced reduction of MPP⁺-stimulated DA efflux may be a result of losing off target PKC and DAT interactors whose interplay is supported by

MPP⁺ action rather than a loss of direct MPP⁺-triggered DAT phosphorylation. Neither 6-OHDA nor MPP⁺ attenuated DAT palmitoylation which may be a result of insufficient toxin exposure time or DAT palmitoylation being insensitive to these compounds. As there is a reciprocal relationship between DAT phosphorylation and palmitoylation³⁴⁷, 6-OHDA may generate increased transporter acylation after longer drug incubation periods.

As stated previously, an anomalous DA efflux phenotype has been linked to patients diagnosed with ADHD³⁸⁰ and early onset PD²⁵⁶. This DA efflux event is now linked to disease etiology, drug rewarding and abuse properties^{226,495}, and an additional potential mechanism by which PD can be induced after MPP⁺ exposure. DAT-mediated DA efflux does not only occur at perisynaptic DATs; indeed, dopaminergic neuronal dendrites form dendro-dendritic synapses in the substantia nigra^{496,497}, and DA release at these synapses was proposed as a mechanism by which these neurons can self-inhibit^{498,499}. A seminal study⁵⁰⁰ elucidated the mechanism by which this auto-inhibitory process occurs: DAT-mediated DA efflux at dendro-dendritic synapses. MPP⁺-produced DA efflux at this locus would likely induce the same auto-inhibitory effect on the nigro-striatal dopaminergic nerve cluster; perhaps stimulation of DA release by MPP⁺ contributes to this drug's neurotoxic profile. This substantia nigra dendritic DA release is likewise elicited by AMPH treatment^{498,501}. Taken further, both METH and AMPH use is associated with PD⁵⁰²⁻⁵⁰⁴, and a similar study observed an increased risk for PD amongst users of AMPH and METH but not cocaine⁵⁰⁵. These studies, along with the MPP⁺ DA efflux data presented herein, suggest induction of DA efflux at dendro-dendritic

synapses of the substantia nigra as a mechanism by which loss of the nigrostriatal DAergic tract, witnessed in PD, can be exacerbated. An antidote to this flux problem may be derived from uncovering the mechanisms by which 6-OHDA blunts DAT-mediated DA release, as one of them may reveal a novel therapeutic input point at which aberrant DA efflux-associated diseases can be alleviated. Perhaps this input point can remain DAT if a high-affinity DAT substrate can be synthesized which mimics the properties of 6-OHDA which enable it to dampen DAT-mediated DA efflux (conceivably, one such property is reducing DAT phosphorylation) without the properties which cause massive oxidative damage.

Methods

Cell Culture

LLCPK₁⁴²⁰ cells stably expressing WT or mutant rDATs were grown in Dulbecco's Modified Eagle Medium (DMEM) containing 5% fetal bovine serum, 100 µg/mL penicillin/streptomycin, and supplemented with 400 µg/mL of the selection reagent Geneticin (G418) for stably expressing cell lines. Cells were maintained in a humidified incubator with 5% CO₂ at 37°C.

Generation of DAT-Expressing LLCPC₁ Cells

For generation of cell lines stably expressing WT hDAT or rDAT cDNA constructs⁴²¹, LLCPC₁ parental cells were seeded into 12-well plates and grown to ~50% confluence. At this point the cells were transfected. X-tremGENE transfection reagent was mixed with plasmid DNA (1.4 µg of DNA/well of a 12-well plate) at a reagent:DNA ratio of 3:2 in OptiMEM for 20 min at ambient temperature

after which the transfection complex was added to each well and transfection proceeded for ~36 hours. The cells were then transferred to a culture flask to undergo selection of expressing cells *via* 800 µg/mL G418 treatment. After two subculture passages at this G418 concentration, the cells were collected, the plasma membranes were harvested, and expression of r or hDAT was analyzed by immunoblotting with the anti-DAT mouse monoclonal antibody MAb16. If the transfection was successful, the stably expressing rDAT cells were maintained in 400 µg/mL of G418 for all subsequent uses.

SDS-PAGE and Western Blotting

DAT proteins and peptides were denatured in Laemmli sample buffer (SB: 125 mM Tris-HCl, 20% glycerol, 4% SDS, 200 mM DTT, 0.005% bromophenol blue) and were electrophoretically resolved using 4-20% polyacrylamide gels alongside a ColorBurst protein standard. Proteins were then transferred to a transfer buffer (25 mM Tris-HCl, 192 mM Glycine, 0.1% SDS, 10% methanol) - equilibrated polyvinylidene fluoride (PVDF) membrane after which blocking was performed with a 3% BSA/PBS buffer. Primary MAb16 antibody was diluted 1:1,000 in the blocking solution and the blocked PVDF membrane was incubated in this antibody solution for 1 hour at ambient temperature. After five washes the membrane was incubated in alkaline phosphatase (AP)-linked anti-mouse IgG secondary antibody diluted to a 1:5,000 ratio in blocking buffer for 1 hour followed by 5 additional washes. 3 mL of Immun-Star™ AP substrate (Bio-Rad) was applied to the membrane and incubation proceeded for 5 min at ambient temperature.

Generated chemiluminescent Western blot band intensities were quantified using Quantity One® software (Bio-Rad).

Neurotoxin Dose-Response Assay on Inhibition of DA Uptake

WT rDAT LLC_{PK1} cells were seeded in 24-well assay plates and grown to ~80% confluence. Immediately preceding the assay, serial dilutions of 6-OHDA (final reaction concentrations of 1×10^{-5} , 1×10^{-4} , 1×10^{-3} , 1×10^{-2} , and 3×10^{-2}) and MPP⁺ (final reaction concentrations of 1×10^{-7} , 1×10^{-6} , 1×10^{-5} , 1×10^{-4} , and 1×10^{-3}) in 150 μ L of Krebs Ringer/HEPES buffer (KRH, 25 mM HEPES, 125 mM NaCl, 2.8 mM KCl, 1.2 mM KH₂PO₄, 1.2 mM MgSO₄, 5.6 mM glucose, 1.3 mM CaCl₂) containing 25 μ M DA. The cells were washed with 37°C KRH after which 500 μ L of 37°C KRH was added to each well. Assay plates were placed in a rocking water bath at 37°C. DA uptake was initiated by addition of 10 μ L of the appropriate neurotoxin/DA mixture to each well at timed intervals. The uptake reaction proceeded for 8 minutes and was terminated by aspiration of the reaction mixture and 2 washes of each well with ice-cold KRH. The cells were solubilized with 250 μ L of Triton X-100 at ambient temperature for 30 minutes with gentle shaking. The solubilized cells were collected in scintillation vials to which 3 mL of scintillation fluid was added. Radioactivity was assayed by scintillation counting. The extent of DA uptake inhibition was relative to uptake control wells which received no neurotoxin inhibitor, and IC₅₀ concentrations of each neurotoxin were determined by nonlinear regression analysis (one site competitive binding).

DA Uptake Downregulation Assay

WT rDAT-LLCPK₁ cells were seeded in 24-well assay plates and grown to ~80% confluence. These cells were washed with 37°C KRH and subsequently pretreated with vehicle, 400 nM PMA, 20 μM DA, 20 μM 6-OHDA, or 20 μM MPP⁺ in 500 μL KRH at 37°C and 5% CO₂ for 30 min. The cells were then rapidly washed with 4°C KRH three times prior to assay for DA uptake. DA uptake was induced by addition of 10 μL of the DA reaction mixture (Final concentration of DA was 3 μM) at timed intervals. DA uptake continued for 8 minutes and was terminated by removal of reaction buffer and well washout with 1 mL of ice-cold KRH. The cells were solubilized with 250 μL Triton X-100 for 30 minutes at ambient temperature and gentle rocking. Cell lysate was collected into scintillation vials and radioactive content was determined by scintillation counting. DA uptake downregulation is expressed as the percentage of DA uptake loss compared to untreated control cells.

Neurotoxin Pre-Incubation DA Uptake Assay

24-well plates grown to ~80%-90% confluence with LLCPC₁ rDAT or hDAT cells were washed with 0.5 mL 37°C KRH buffer and resupplied with KRH buffer with or without 400 nM PMA, 20 μM DA, 20 μM 6-OHDA, or 20 μM MPP⁺ for 30 min at 37°C and 5% CO₂. These same concentrations were incubated in the presence of 100 μM cocaine for the DAT uptake control conditions, also for 30 min at 37°C and 5% CO₂. After the substrate incubation, DA uptake was conducted for 8 min at 37°C with 3 μM total DA containing 10 nM [³H]DA. Excess DA was rapidly washed out with KRH buffer and the cells were lysed by incubation with 250 μL 1% Tx-100 for 20 min at ambient temperature. The lysates were collected and

analyzed for [³H] content by liquid scintillation counting. Neurotoxin uptake data are presented as % uptake control. The cocaine-treated conditions were compared to the cocaine control conditions.

Neurotoxin DA Efflux Assay

Stably expressing WT hDAT or rDAT-expressing LLCPK₁ cells were grown in 24-well assay plates to ~80% confluence. Cells were loaded *via* DA DAT-mediated uptake of 3 μM DA containing 10 nM [³H]DA for 30 minutes in 37°C KRH. Extracellular DA was rapidly washed out 3 times with 4°C KRH on ice, and the assay plate was transferred back to the water bath and 37°C KRH efflux buffer with KRH alone, 10 μM AMPH, or the indicated neurotoxin concentration was rapidly added to avoid cell drying and rupture upon buffer addition. The efflux buffer was collected after five minutes and analyzed for radioactive content; one column of cell wells received no efflux buffer and was lysed by incubation with 1% Triton X-100 for 20 min at ambient temperature and served as the total internal [³H]DA control and was analyzed in parallel for [³H] content by liquid scintillation counting. The efflux values are expressed as a percent of the total intracellular [³H]DA. For the PKC inhibition DA efflux experiments, cells were incubated with 10 μM Bisindolylmaleimide (BIM) in KRH during the 30 min load portion of the experiment.

Dopamine Transporter Phosphorylation Assay

WT rDAT LLCPK₁ cells were grown to 80% confluence in 6-well assay plates. Once desired confluence was achieved, cell medium was replaced with PO₄-free medium and incubated for 1 hour at 37°C and 5% CO₂. 10 μL of ³²PO₄-containing medium was then added to each well (final radioactivity concentration: 0.5

mCi/mL). This incubation proceeded for 2 hours after which 1mM of each neurotoxic compound was added for 30 minutes with or without the transporter phosphorylation-stimulating 200 nM PMA positive control. Cells were washed three times with ice-cold Buffer B (0.25 mM Sucrose, 10 mM triethanolamine, and pH was adjusted to 7.8 with 100 mM acetic acid), scraped, and collected in separate microfuge tubes. The collected cells were centrifuged at 2,000 xg for 5 min at 4°C and supernatants were discarded. Cell lysis was produced by resuspension and nutation of pellet in 750 µL lysis buffer (10 mM triethanolamine pH 7.8, 2 mM ethylenediaminetetraacetic acid [EDTA], 150 mM NaCl, and 0.1% Triton X-100 containing 100 mM DTT and protease inhibitor cocktail) for 10 minutes at 4°C. This was followed by centrifugation of samples at 4,000 x g for 5 minutes. The supernatants were transferred to fresh microfuge tubes and 200 µL of 2% SDS (0.5% final concentration) was added and vortexed well. These samples were subjected to a final centrifugation at 20,000 x g for 30 minutes at 4°C. 900 µL of the supernatant fraction was collected from which 25 µL was analyzed by Western blotting to ascertain DAT levels. Equal DAT protein from each sample (200 µL, or adjusted to 200 µL with lysis buffer) was isolated by immunoprecipitation with protein A cross-linked to the rDAT-reactive poly-16 antibody in immunoprecipitation buffer (IPB, 50 mM Tris, 0.1% Triton X-100, pH 8.0) for 2 hours at 4°C with nutation. The column was washed 4 times with IPB containing 0.1% SDS at ambient temperature and DAT was eluted with 35 µL of 1x sample buffer. Samples were subjected to SDS-PAGE for 1 hour 45 minutes at 150 V and 35 mA in a 4-20% polyacrylamide gradient gel. The gels were dried and

radioactive content was assessed by autoradiography. Autoradiography signatures were normalized to equal, immunoblotted DATs from each sample and data are presented as % basal DAT phosphorylation.

Plasma Membrane Preparation

WT rDAT-LLCPK₁ cells were grown in 150 mm plates to ~80% confluence. 400 nM PMA, 1 mM 6-OHDA, or 60 μ M MPP⁺ in KRH or KRH alone was applied to two plates each for 1 hour at 37°C and 5% CO₂. After treatment, cells were washed twice with Buffer B, scraped, and collected in Buffer B containing a protease inhibitor cocktail of 1 μ M phenylmethylsulfonyl fluoride (PMSF) and 5 μ M EDTA at 4°C. Cells were then pelleted *via* centrifugation at 3,000 x g for 5 min at 4°C, supernatants were removed, and the cell pellets were suspended in Buffer C (0.25 M sucrose, 10 mM triethanolamine, 1 mM EDTA, and the pH was adjusted to 7.8 with 100 mM acetic acid) and subsequently homogenized using a Dounce homogenizer. Cellular debris and nuclei were cleared from the homogenates by centrifugation at 800 x g for 10 min. The post-nuclear supernatant was collected and centrifuged at 18,000 x g for 12 min, and the resulting plasma membrane pellet was suspended in sucrose phosphate (SP) buffer (10 mM dibasic sodium phosphate, 0.32 M sucrose, pH 7.4 with 1 μ M PMSF and 5 μ M EDTA).

Acyl-Biotinyl Exchange

This ABE method was adapted from Wan et al³⁴¹ where detection of palmitoylated proteins are described in three steps: Free cysteine thiols are blocked; thioester linked palmitoyl groups are specifically removed by hydroxylamine (NH₂OH); and the previously palmitoylated and now free sulfhydryl

groups are biotinylated. Plasma membranes isolated from control, PMA, or neurotoxin-treated WT rDAT LLC_{PK1} cells were solubilized in 250 μ L of ABE lysis buffer (50 mM HEPES pH 7.0, 2% SDS (w/v), 1 mM EDTA) containing protease inhibitor and 20 mM methyl methanethiosulfonate (MMTS) to react with unbound Cys sulfhydryl moieties and incubated for one hour at ambient temperature. MMTS was removed by a 1 mL acetone precipitation and centrifugation at 18,000 \times g for 10 min. The pellet was dissolved in 250 μ L 4SB ABE buffer (50 mM Tris, 5 mM EDTA, 4% SDS, pH 7.4) and remnant MMTS was removed by an additional 1 mL acetone precipitation and centrifugation. The pellet was then subjected to a further acetone wash. The pellet was suspended in 200 μ L 4SB buffer and thioesterified palmitate molecules were specifically removed by hydroxylamine (NH₂OH); The sample was split equally (100 μ L) into negative control (800 μ L, 50 mM Tris-treated) and NH₂OH-treated (1.4 mM) halves and incubated at ambient temperature for 30 min with end-over-end mixing. The free sulfhydryl groups were reacted with 100 μ L (0.4 mM final concentration) of a sulfhydryl-specific biotinylating reagent, HPDP-biotin in the Tris or NH₂OH mixtures. The now HPDP-biotin-containing samples were incubated for 3 min in a 37°C water bath then at ambient temperature for 1 hour. Excess NH₂OH and biotin reagents were removed by the 4:1 acetone to sample volume precipitation, centrifugation at 18,000 \times g, supernatant aspiration, 250 μ L 4SB pellet suspension, 1 mL acetone precipitation, centrifugation at 18,000 \times g, supernatant aspiration, 1 mL acetone wash, centrifugation at 18,000 \times g, and supernatant aspiration workflow. The final pellet was suspended in 75 μ L ABE lysis buffer and 10 μ L of this was set aside for total

DAT immunoblotting while 65 μ L was added to 50 μ L of a 50% slurry of Neutraavidin resin in 1500 μ L Tris buffer to affinity purify the biotinylated proteins or peptides overnight at 4°C with nutation. Unbound peptides were washed away by three cycles of 8,000 \times *g* centrifugation and 900 μ L radioactive immunoprecipitation assay buffer (RIPA: 1% Tx-100, 1% sodium deoxycholate, 0.1% SDS, 125 mM sodium phosphate, 150 mM NaCl, 2 mM EDTA, 50 mM NaF). Proteins and peptides were eluted from the final pellet by incubation in 2x Laemmli SB for 20 min at ambient temperature. Samples were then subjected to SDS-PAGE, and immunoblotted with mouse anti-rDAT primary antibody (MAb16).

CHAPTER 4

DISCUSSION

Limitations of the Work Presented in this Dissertation

Many of the data presented are from analysis of mutation of the putative palmitoylation sites. As such, the presented data may be a result of the amino acid substitution rather than loss of palmitoylation of that residue.

The main drawback of the ABE method is that the assay is susceptible to capture of proteins which are modified through thioester bonds between Cys residues and modifying groups other than a fatty acid. If the protein of interest forms non S-palmitoylation thioester bonds it will be picked up as a false positive for S-palmitoylation by ABE. Examples of other post-translational modifications that form thioester bonds include S-acetylation, which is supported by surrounding basic residues like the situation with DAT Cys6, the phosphopantetheine prosthetic group's sulfhydryl modifying an interacting protein's Ser hydroxyl, and acyl-CoA substrates⁵⁰⁶⁻⁵⁰⁸. The ABE method is unable to detect multiple modification events on poly-palmitoylated proteins which the acyl-PEG exchange (APE) method is able to do by incorporation of maleimides of known M_r into the protein which can be visualized by multiple upward band shifts in a Western blot corresponding to the number of the protein's acylation sites⁵⁰⁹.

The biochemical efflux assay used throughout this dissertation relies on expressed DAT to transport extracellularly-applied [³H]DA into the cell to supply the efflux-ready substrate pool. The act of transporting DA induces transporter downregulation^{481–485} which likely affects DA efflux capacity as well as AMPH interaction with DAT. Scintillation counting of the radiolabeled DA, though quantitative, does not represent a 1:1 ratio of counted DA to effluxed DA. This assay can only be performed on heterologous expression systems or immediately after tissue excision.

The majority of experiments in this dissertation were performed on DAT-expressing cells and ought to be confirmed in endogenous tissue.

Future Studies

The APE method should be optimized for endogenous rDAT to confirm the number of S-palmitoylation sites. This will be difficult as one needs a large Mr maleimide linker to produce distinguishable DAT bands as it produces a thick, ~80 kDa Western blot signature. [³H]palmitic acid labeling of WT NDAT, Cys6Ala NDAT, and Cys90Ala rDAT could be performed to confirm that modification of Cys6 and Cys90 is actually a palmitoylation event as opposed to an alternative thioester-based modification. To assess the 2BP-induced and Cys mutant DAT conformational alterations, binding assays of the high affinity cocaine analog [³H]-2β-carbomethoxy-3β-(4-fluorophenyl)tropane) can be implemented. The contribution of global palmitoylation (using 2BP) and the novel DAT palmitoylation sites to DAT downregulation can be analyzed by PMA treatment and DA uptake assays. The test if PIP₂ and cholesterol-DAT interactions are supported by

palmitoylation events, PIP₂ inhibition³⁹¹ and cholesterol depletion¹⁵⁶ can be used to see if forward or reverse transport process are affected by these conditions. Cys90Ala rDAT should be assessed by microscopy to determine if palmitoylation of this residue suppresses surface transporter levels and increases endosomal DAT content. All the experiments described in chapter 2 that can be applied to Cys6/90/580Ala rDAT should be carried out. Time course neurotoxin treatment should be implemented to assess whether 6-OHDA or MPP⁺ have any effect on DAT palmitoylation and surface transporter expression. DAT palmitoylation characteristic can be influenced to attempt to alleviate the anomalous DA efflux phenotype of Ala559Val and other DAT single nucleotide polymorphisms associated with disease.

Summary Conclusions

The first study strongly supports the existence of amino-terminal palmitoylation. It indicates the residues Cys6 and Cys90 as the potential palmitoylation sites in addition to Cys580. This study further concludes a Cys90 acylation event may suppress surface transporter expression and this residue is important for maintaining DAT uptake K_m for DA. Mutation of Cys6 to Ala decreases basal and AMPH-stimulated DA efflux, and global palmitoylation contributes to DA uptake stabilization and dampens DA efflux. Manipulation of DAT palmitoylation status may be an avenue of approach to finer pharmaceutical control over DAT activity.

The second study concluded 6-OHDA is a DAT substrate which blunts both DA efflux and transporter phosphorylation, and MPP⁺ downregulates DA uptake

and strongly induces DA efflux. This study further implicates the DA efflux phenomenon as contributing to PD pathology²⁵⁶, and warns against the use of efflux-inducing DAT pharmacotherapies which predispose one to PD.

CHAPTER 5

REFERENCES

1. Witzel, M. The Development of the Vedic Canon and its Schools: The Social and Political Milieu. *Insid. Texts, Beyond Texts*. 257–348 (1997).
2. Mahdihassan, S. Evolution of ephedra as the soma of rigveda. *Ancient science of life* **2**, 93–937 (1982).
3. Mahdihassan, S. & Mehdi, F. S. Soma of the Rigveda and an Attempt to Identify It. *Am. J. Chin. Med.* **17**, 1–8 (1989).
4. Padhy, S. & Dash, S. K. The Soma Drinker of Ancient India: An Ethno-Botanical Retrospection . *J. Hum. Ecol.* **15**, 19–26 (2004).
5. McDonald, A. A botanical perspective on the identity of soma (*Nelumbo nucifera gaertn.*) based on scriptural and iconographic records. *Econ. Bot.* **58**, 5147–5173 (2004).
6. Leonti, M. & Casu, L. Soma, food of the immortals according to the Bower Manuscript (Kashmir, 6th century A.D.). *J. Ethnopharmacol.* **155**, 373–386 (2014).
7. Huxley, A. *Brave New World*. Chatto & Windus (1932).
8. Yager, L. M., Garcia, A. F., Wunsch, A. M. & Ferguson, S. M. The ins and outs of the striatum: Role in drug addiction. *Neuroscience* **301**, 529–541 (2015).
9. Volkow, N. D. & Morales, M. The Brain on Drugs: From Reward to Addiction. *Cell* **162**, 712–725 (2015).
10. Sulzer, D. How Addictive Drugs Disrupt Presynaptic Dopamine Neurotransmission. *Neuron* **69**, 628–649 (2011).
11. Hernandez, L., Lee, F. & Hoebel, B. G. Simultaneous microdialysis and amphetamine infusion in the nucleus accumbens and striatum of freely moving rats: Increase in extracellular dopamine and serotonin. *Brain Res. Bull.* **19**, 623–628 (1987).
12. Kalivas, P. W. & Duffy, P. Effect of acute and daily cocaine treatment on extracellular dopamine in the nucleus accumbens. *Synapse* **5**, 48–58 (1990).

13. Hull, E. M. *et al.* Dopaminergic control of male sex behavior in rats: Effects of an intracerebrally-infused agonist. *Brain Res.* **370**, 73–81 (1986).
14. Arnow, B. A. *et al.* Brain Activation and Sexual Arousal in Healthy, Heterosexual Males. *Brain* **125**, 1014–1023 (2002).
15. Melis, M. R. *et al.* Oxytocin injected into the ventral tegmental area induces penile erection and increases extracellular dopamine in the nucleus accumbens and paraventricular nucleus of the hypothalamus of male rats. *Eur. J. Neurosci.* **26**, 1026–1035 (2007).
16. Eaton, R. C. *et al.* D2 receptors in the paraventricular nucleus regulate genital responses and copulation in male rats. *Pharmacol. Biochem. Behav.* **39**, 177–181 (1991).
17. Guadarrama-Bazante, I. L. & Rodríguez-Manzo, G. Nucleus accumbens dopamine increases sexual motivation in sexually satiated male rats. *Psychopharmacology (Berl)*. **236**, 1303–1312 (2019).
18. Volkow, N. D., Wang, G. J. & Baler, R. D. Reward, dopamine and the control of food intake: Implications for obesity. *Trends Cogn. Sci.* **15**, 37–46 (2011).
19. Frank, S. *et al.* Dopamine depletion reduces food-related reward activity independent of BMI. *Neuropsychopharmacology* **41**, 1551–1559 (2016).
20. Hsiao, S. & Smith, G. P. Raclopride reduces sucrose preference in rats. *Pharmacol. Biochem. Behav.* **50**, 121–125 (1995).
21. Yokum, S., Gearhardt, A. N., Harris, J. L., Brownell, K. D. & Stice, E. Individual differences in striatum activity to food commercials predict weight gain in adolescents. *Obesity* **22**, 2544–2551 (2014).
22. Koeppe, M. J. *et al.* Evidence for striatal dopamine release during a video game. *Nature* **393**, 266–268 (1998).
23. Sussman, S. & Moran, M. B. Hidden addiction: Television. *J. Behav. Addict.* **2**, 125–132 (2013).
24. Tamir, D. I. & Mitchell, J. P. Disclosing information about the self is intrinsically rewarding. *Proc. Natl. Acad. Sci. U. S. A.* **109**, 8038–8043 (2012).
25. Kubey, B. R. & Csikszentmihalyi, M. Television Addiction Is No Mere Metaphor. *Sci. Am.* **286**, 74–81 (2002).
26. Kuss, D. J. & Griffiths, M. D. Internet and gaming addiction: A systematic literature review of neuroimaging studies. *Brain Sci.* **2**, 347–374 (2012).
27. Mathews, C. L., Morrell, H. E. R. & Molle, J. E. Video game addiction, ADHD symptomatology, and video game reinforcement. *Am. J. Drug Alcohol Abuse* **45**, 67–76 (2019).

28. Pontes, H. M., Taylor, M. & Stavropoulos, V. Beyond 'facebook Addiction': The Role of Cognitive-Related Factors and Psychiatric Distress in Social Networking Site Addiction. *Cyberpsychology, Behav. Soc. Netw.* **21**, 240–247 (2018).
29. Kuss, D. J. & Griffiths, M. D. Social networking sites and addiction: Ten lessons learned. *Int. J. Environ. Res. Public Health* **14**, (2017).
30. Everitt, B. J. & Robbins, T. W. Neural systems of reinforcement for drug addiction: from actions to habits to compulsion. *Nat. Neurosci.* **8**, 1481–9 (2005).
31. Freimuth, M. *et al.* Expanding the scope of dual diagnosis and Co-addictions: Behavioral addictions. *J. Groups Addict. Recover.* **3**, 137–160 (2008).
32. Volkow, N. D., Wang, G. J., Tomasi, D. & Baler, R. D. The addictive dimensionality of obesity. *Biol. Psychiatry* **73**, 811–818 (2013).
33. Berridge, K. C. & Kringelbach, M. L. Pleasure Systems in the Brain. *Neuron* **86**, 646–664 (2015).
34. Berridge, K. C. & Robinson, T. E. What is the role of dopamine in reward: hedonic impact, reward learning, or incentive salience? *Brain Res. Rev.* **28**, 309–369 (1998).
35. Wise, R. A. Dopamine and reward: The anhedonia hypothesis 30 years on. *Neurotox. Res.* **14**, 169–183 (2008).
36. Skinner, B. F. *Science and Human Behavior*. (Macmillan, 1953).
37. Pavlov. *Conditioned Reflexes: An Investigation of the Physiological Activity of the Cerebral Cortex*. (1927).
38. Daw, N. D. & Tobler, P. N. Value Learning through Reinforcement: The Basics of Dopamine and Reinforcement Learning. *Neuroeconomics Decis. Mak. Brain Second Ed.* 283–298 (2013). doi:10.1016/B978-0-12-416008-8.00015-2
39. Glimcher, P. W. Understanding Dopamine and Reinforcement Learning: The Dopamine Reward Prediction Error Hypothesis. *Proc. Natl. Acad. Sci. U. S. A.* **108**, 1–8 (2011).
40. Segovia, K. N., Correa, M. & Salamone, J. D. Slow phasic changes in nucleus accumbens dopamine release during fixed ratio acquisition: A microdialysis study. *Neuroscience* **196**, 178–188 (2011).
41. Salamone, J. D., Correa, M., Nunes, E. J., Randall, P. A. & Pardo, M. The Behavioral Pharmacology of Effort-related Choice Behavior: Dopamine, Adenosine and Beyond. *J. Exp. Anal. Behav.* **97**, 125–146 (2012).
42. Schultz, W., Dayan, P. & Montague, P. R. A neural substrate of prediction

- and reward. *Science (80-.)*. **275**, 1593–1599 (1997).
43. Ilango, A., Shumake, J., Wetzell, W., Scheich, H. & Ohl, F. W. The role of dopamine in the context of aversive stimuli with particular reference to acoustically signaled avoidance learning. *Front. Neurosci.* **6**, 1–9 (2012).
 44. Fiorillo, C. D., Song, M. R. & Yun, S. R. Multiphasic temporal dynamics in responses of midbrain dopamine neurons to appetitive and aversive stimuli. *J. Neurosci.* **33**, 4710–4725 (2013).
 45. Day, J. J., Roitman, M. F., Wightman, R. M. & Carelli, R. M. Associative learning mediates dynamic shifts in dopamine signaling in the nucleus accumbens. *Nat. Neurosci.* **10**, 1020–1028 (2007).
 46. Schultz, W. Dopamine Reward Prediction Error Coding. *Dialogues Clin. Neurosci.* **18**, 23–32 (2016).
 47. Takahashi, Y. K. *et al.* Dopamine Neurons Respond to Errors in the Prediction of Sensory Features of Expected Rewards. *Neuron* **95**, 1395–1405.e3 (2017).
 48. Bayer, H. M. & Glimcher, P. W. Midbrain dopamine neurons encode a quantitative reward prediction error signal. *Neuron* **47**, 129–141 (2005).
 49. Tobler, P. N., Fiorillo, C. D. & Schultz, W. Adaptive coding of reward value by dopamine neurons. *Science (80-.)*. **307**, 1642–1645 (2005).
 50. Fiorillo, C. D., Tobler, P. N. & Schultz, W. Discrete Coding of Reward Probability and Uncertainty by Dopamine Neurons. *Science (80-.)*. **299**, 1898–1902 (2003).
 51. Roesch, M. R., Calu, D. J. & Schoenbaum, G. Dopamine neurons encode the better option in rats deciding between differently delayed or sized rewards. *Nat. Neurosci.* **10**, 1615–1624 (2007).
 52. Flagel, S. B. *et al.* A selective role for dopamine in stimulus-reward learning. *Nature* **469**, 53–59 (2011).
 53. Berridge, K. C. From prediction error to incentive salience: Mesolimbic computation of reward motivation. *Eur. J. Neurosci.* **35**, 1124–1143 (2012).
 54. Pecina, S., Cagniard, B., Berridge, K. C., Aldridge, J. W. & Zhuang, X. Hyperdopaminergic Mutant Mice Have Higher ‘Wanting’ But Not ‘Liking’ for Sweet Rewards. *J. Neurosci.* **23**, 9395–9402 (2004).
 55. Berridge, K. C. The debate over dopamine’s role in reward: The case for incentive salience. *Psychopharmacology (Berl)*. **191**, 391–431 (2007).
 56. Peciña, S., Smith, K. S. & Berridge, K. C. Hedonic hot spots in the brain. *Neuroscientist* **12**, 500–511 (2006).
 57. Smith, K. S., Berridge, K. C. & Aldridge, J. W. Disentangling pleasure from incentive salience and learning signals in brain reward circuitry. *Proc. Natl.*

- Acad. Sci.* **108**, E255–E264 (2011).
58. Mahler, S. V., Smith, K. S. & Berridge, K. C. Endocannabinoid hedonic hotspot for sensory pleasure: Anandamide in nucleus accumbens shell enhances ‘liking’ of a sweet reward. *Neuropsychopharmacology* **32**, 2267–2278 (2007).
 59. Steinberg, E. E. *et al.* A causal link between prediction errors, dopamine neurons and learning. *Nat. Neurosci.* **16**, 966–973 (2013).
 60. Whitton, A. E., Treadway, M. T. & Pizzagalli, D. A. Reward processing dysfunction in major depression, bipolar disorder and schizophrenia. *Curr. Opin. Psychiatry* **28**, 7–12 (2015).
 61. McFarland, B. R. & Klein, D. N. Emotional reactivity in depression: Diminished responsiveness to anticipated reward but not to anticipated punishment or to nonreward or avoidance. *Depress. Anxiety* **26**, 117–122 (2009).
 62. Olney, J. J., Warlow, S. M., Naffziger, E. E. & Berridge, K. C. Current perspectives on incentive salience and applications to clinical disorders. *Curr. Opin. Behav. Sci.* **22**, 59–69 (2018).
 63. Berridge, K. C. & Robinson, T. (University of M. Liking, wanting and the incentive salience theory of addiction. *Am. Psychol.* **71**, 670–679 (2016).
 64. Robinson, M. J. F., Anselme, P., Suchomel, K. & Berridge, K. C. Amphetamine-induced sensitization and reward uncertainty similarly enhance incentive salience for conditioned cues. *Behav. Neurosci.* **129**, 502–511 (2015).
 65. Huys, Q. J. M., Tobler, P. N., Hasler, G. & Flagel, S. B. *The role of learning-related dopamine signals in addiction vulnerability. Progress in Brain Research* **211**, (2014).
 66. Bartholow, B. D. *et al.* University-Affiliated Alcohol Marketing Enhances the Incentive Salience of Alcohol Cues. *Psychol. Sci.* **29**, 83–94 (2018).
 67. Pieters, R. & Wedel, M. Attention Capture and Transfer in Advertising: Brand, Pictorial, and Text-Size Effects. *J. Mark.* **68**, 36–50 (2004).
 68. Kelly, B., Hattersley, L., King, L. & Flood, V. Persuasive food marketing to children: Use of cartoons and competitions in Australian commercial television advertisements. *Health Promot. Int.* **23**, 337–344 (2008).
 69. Lombardot, É. Nudity in Advertising: What Influence on Attention-Getting and Brand Recall? *Rech. Appl. en Mark. (English Ed.)* **22**, 23–41 (2007).
 70. Dudley, S. C. Consumer Attitudes Toward Nudity in Advertising. *J. Mark.* **7**, 89–96 (1999).
 71. Allen, C. T. & Janiszewski, C. A. Assessing the Role of Contingency

- Awareness in Attitudinal Conditioning with Implications for Advertising Research. *J. Mark. Res.* **26**, 30 (1989).
72. John, L. K., Milkman, K. L. & John, L. K. The Role of Incentive Saliency in Habit Formation. *Harvard Bus. Sch. Work. Pap.* (2016).
 73. Atkin, C. K., Neuendorf, K. & McDermott, S. The Role of Alcohol Advertising in Excessive and Hazardous Drinking. *J. Drug Educ.* **13**, 313–325 (1983).
 74. Mikołajczak-Degrauwe, K. & Brengman, M. The influence of advertising on compulsive buying - The role of persuasion knowledge. *J. Behav. Addict.* **3**, 65–73 (2014).
 75. Hoek, J. & Gendall, P. Advertising and obesity: A behavioral perspective. *J. Health Commun.* **11**, 409–423 (2006).
 76. Lobstein, T. & Dobb, S. Evidence of a possible link between obesogenic food advertising and child overweight. *Obes. Rev.* **6**, 203–208 (2005).
 77. Veerman, J. L., Van Beeck, E. F., Barendregt, J. J. & MacKenbach, J. P. By how much would limiting TV food advertising reduce childhood obesity. *Eur. J. Public Health* **19**, 365–369 (2009).
 78. Simpson, N. *et al.* Dopamine-Mediated Autocrine Inhibitory Circuit Regulating Human Insulin Secretion in Vitro. *Mol. Endocrinol.* **26**, 1757–1772 (2012).
 79. Ustione, A. & Piston, D. W. Dopamine Synthesis and D3 Receptor Activation in Pancreatic β -Cells Regulates Insulin Secretion and Intracellular $[Ca^{2+}]$ Oscillations. *Mol. Endocrinol.* **26**, 1928–1940 (2012).
 80. Farino, Z. J. *et al.* New roles for dopamine D2 and D3 receptors in pancreatic beta cell insulin secretion. *Mol. Psychiatry* (2019). doi:10.1038/s41380-018-0344-6
 81. Levite, M. Dopamine and T cells: Dopamine receptors and potent effects on T cells, dopamine production in T cells, and abnormalities in the dopaminergic system in T cells in autoimmune, neurological and psychiatric diseases. *Acta Physiol.* **216**, 42–89 (2016).
 82. Pinoli, M., Marino, F. & Cosentino, M. Dopaminergic Regulation of Innate Immunity: a Review. *J. Neuroimmune Pharmacol.* **12**, 602–623 (2017).
 83. Torres-Rosas, R. *et al.* Dopamine mediates vagal modulation of the immune system by electroacupuncture. *Nat. Med.* **20**, 291–295 (2014).
 84. Geier, E. G. *et al.* Structure-based ligand discovery for the Large-neutral Amino Acid Transporter 1, LAT-1. *Proc. Natl. Acad. Sci. U. S. A.* **110**, 5480–5485 (2013).
 85. Lewitt, P. A. Levodopa therapy for Parkinson's disease: Pharmacokinetics

- and pharmacodynamics. *Mov. Disord.* **30**, 64–72 (2015).
86. Salvatore, M. F., Waymire, J. C. & Haycock, J. W. Depolarization-stimulated catecholamine biosynthesis: Involvement of protein kinases and tyrosine hydroxylase phosphorylation sites in situ. *J. Neurochem.* **79**, 349–360 (2001).
 87. Lindgren, N. *et al.* Activation of extracellular signal-regulated kinases 1 and 2 by depolarization stimulates tyrosine hydroxylase phosphorylation and dopamine synthesis in rat brain. *Eur. J. Neurosci.* **15**, 769–773 (2002).
 88. Kitahama, K. *et al.* Adrenergic neurons in human brain demonstrated by immunohistochemistry with antibodies to phenylethanolamine-N-methyltransferase (PNMT): Discovery of a new group in the nucleus tractus solitarius. *Neurosci. Lett.* **53**, 303–308 (1985).
 89. Meiser, J., Weindl, D. & Hiller, K. Complexity of dopamine metabolism. *Cell Commun. Signal.* **11**, 34 (2013).
 90. Wimalasena, K. Vesicular Monoamine Transporters: Structure-Function, Pharmacology, and Medicinal Chemistry. *Med. Res. Revis.* **4**, 483–519 (2011).
 91. Vale, R. D. The molecular motor toolbox for intracellular transport. *Cell* **112**, 467–480 (2003).
 92. Appert-Rolland, C., Ebbinghaus, M. & Santen, L. Intracellular transport driven by cytoskeletal motors: General mechanisms and defects. *Phys. Rep.* **593**, 1–59 (2015).
 93. Yoon, T. Y. & Munson, M. SNARE complex assembly and disassembly. *Curr. Biol.* **28**, R397–R401 (2018).
 94. Szule, J. A. *et al.* Regulation of synaptic vesicle docking by different classes of macromolecules in active zone material. *PLoS One* **7**, (2012).
 95. Jung, J. H., Szule, J. A., Marshall, R. M. & McMahan, U. J. Variable priming of a docked synaptic vesicle. *Proc. Natl. Acad. Sci. U. S. A.* **113**, E1098–E1107 (2016).
 96. Vardjan, N., Jorgačevski, J. & Zorec, R. Fusion pores, SNAREs, and exocytosis. *Neuroscientist* **19**, 160–174 (2013).
 97. Zorec, R. SNARE-mediated vesicle navigation, vesicle anatomy and exocytotic fusion pore. *Cell Calcium* **73**, 53–54 (2018).
 98. Zhao, M. *et al.* Mechanistic insights into the recycling machine of the SNARE complex. *Nature* **518**, 61–67 (2015).
 99. Vivona, S. *et al.* Disassembly of all snare complexes by N-ethylmaleimide-sensitive factor (NSF) is initiated by a conserved 1:1 interaction between α -soluble NSF attachment protein (SNAP) and SNARE complex. *J. Biol.*

- Chem.* **288**, 24984–24991 (2013).
100. Ryu, J.-K. *et al.* Spring-loaded unraveling of a single SNARE complex by NSF in one round of ATP turnover. *Science* (80-.). **347**, 1485–1489 (2015).
 101. Staal, R. G. W., Mosharov, E. V. & Sulzer, D. Dopamine neurons release transmitter via a flickering fusion pore. *Nat. Neurosci.* **7**, 341–346 (2004).
 102. Omiatek, D. M., Dong, Y., Heien, M. L. & Ewing, A. G. Only a fraction of quantal content is released during exocytosis as revealed by electrochemical cytometry of secretory vesicles. *ACS Chem. Neurosci.* **1**, 234–245 (2010).
 103. Omiatek, D. M. *et al.* The real catecholamine content of secretory vesicles in the CNS revealed by electrochemical cytometry. *Sci. Rep.* **3**, 1–6 (2013).
 104. Beaulieu, J.-M. & Gainetdinov, R. R. The Physiology, Signaling, and Pharmacology of Dopamine Receptors. *Pharmacol. Rev.* **63**, 182–217 (2011).
 105. Svenningsson, P. *et al.* DARPP-32: An Integrator of Neurotransmission. *Annu. Rev. Pharmacol. Toxicol.* **44**, 269–296 (2004).
 106. Nishi, A., Snyder, G. L. & Greengard, P. Bidirectional regulation of DARPP-32 phosphorylation by dopamine. *J. Neurosci.* **17**, 8147–8155 (1997).
 107. Nairn, A. C. *et al.* The role of DARPP-32 in the actions of drugs of abuse. *Neuropharmacology* **47**, 14–23 (2004).
 108. Svenningsson, P., Nairn, A. C. & Greengard, P. DARPP-32 mediates the actions of multiple drugs of abuse. *Drug Addict. From Basic Res. to Ther.* **7**, 3–16 (2005).
 109. Swift, J. L. *et al.* Quantification of receptor tyrosine kinase transactivation through direct dimerization and surface density measurements in single cells. *Proc. Natl. Acad. Sci.* **108**, 7016–7021 (2011).
 110. Chi, S. S. *et al.* Transactivation of PDGFR by dopamine D4 receptor does not require PDGFR dimerization. *Mol. Brain* **3**, 1–12 (2010).
 111. Iwakura, Y., Nawa, H., Sora, I. & Chao, M. V. Dopamine D1 receptor-induced signaling through TrkB receptors in striatal neurons. *J. Biol. Chem.* **283**, 15799–15806 (2008).
 112. Kisilevsky, A. E. & Zamponi, G. W. D2 dopamine receptors interact directly with N-type calcium channels and regulate channel surface expression levels. *Channels* **2**, 269–277 (2008).
 113. Kisilevsky, A. E. *et al.* D1 Receptors Physically Interact with N-Type Calcium Channels to Regulate Channel Distribution and Dendritic Calcium Entry. *Neuron* **58**, 557–570 (2008).

114. Blom, H. *et al.* Nearest neighbor analysis of dopamine D1 receptors and Na⁺-K⁺-ATPases in dendritic spines dissected by STED microscopy. *Microsc. Res. Tech.* **75**, 220–228 (2012).
115. Hazelwood, L. A., Free, R. B., Cabrera, D. M., Skinbjerg, M. & Sibley, D. R. Reciprocal modulation of function between the D1 and D2 dopamine receptors and the Na⁺,K⁺-ATPase. *J. Biol. Chem.* **283**, 36441–36453 (2008).
116. Medvedev, I. O. *et al.* D1 Dopamine Receptor Coupling to PLC Regulates Forward Locomotion in Mice. *J. Neurosci.* **33**, 18125–18133 (2013).
117. Lee, S. P. *et al.* Dopamine D1 and D2 receptor co-activation generates a novel phospholipase C-mediated calcium signal. *J. Biol. Chem.* **279**, 35671–35678 (2004).
118. Hernández-López, S. *et al.* D2 dopamine receptors in striatal medium spiny neurons reduce L-type Ca²⁺ currents and excitability via a novel PLCβ1-IP3-Calcineurin-signaling cascade. *J. Neurosci.* **20**, 8987–8995 (2000).
119. Rashid, A. J., O'Dowd, B. F., Verma, V. & George, S. R. Neuronal Gq/11-coupled dopamine receptors: an uncharted role for dopamine. *Trends Pharmacol. Sci.* **28**, 551–555 (2007).
120. Rashid, A. J. *et al.* D1-D2 dopamine receptor heterooligomers with unique pharmacology are coupled to rapid activation of Gq/11 in the striatum. *Proc. Natl. Acad. Sci. U. S. A.* **104**, 654–659 (2007).
121. Ferguson, S. S. G., Barak, L. S., Zhang, J. & Caron, M. G. G-protein-coupled receptor regulation: Role of G-protein-coupled receptor kinases and arrestins. *Can. J. Physiol. Pharmacol.* **74**, 1095–1110 (1996).
122. Luttrell, L. M. *et al.* Activation and targeting of extracellular signal-regulated kinases by β-arrestin scaffolds. *Proc. Natl. Acad. Sci. U. S. A.* **98**, 2449–2454 (2001).
123. Beaulieu, J. M. *et al.* An Akt/β-arrestin 2/PP2A signaling complex mediates dopaminergic neurotransmission and behavior. *Cell* **122**, 261–273 (2005).
124. Beaulieu, J.-M. *et al.* Lithium antagonizes dopamine-dependent behaviors mediated by an AKT/glycogen synthase kinase 3 signaling cascade. *Proc. Natl. Acad. Sci. U. S. A.* **101**, 5099–104 (2004).
125. Beaulieu, J.-M. *et al.* Regulation of Akt signaling by D2 and D3 dopamine receptors in vivo. *J. Neurosci.* **27**, 881–885 (2007).
126. Beaulieu, J. M., Gainetdinov, R. R. & Caron, M. G. The Akt-GSK-3 signaling cascade in the actions of dopamine. *Trends Pharmacol. Sci.* **28**, 166–172 (2007).
127. Gurevich, E. V., Gainetdinov, R. R. & Gurevich, V. V. G protein-coupled receptor kinases as regulators of dopamine receptor functions. *Pharmacol.*

- Res. **111**, 1–16 (2016).
128. Villar, V. A. M. *et al.* G protein-coupled receptor kinase 4 (GRK4) regulates the phosphorylation and function of the dopamine D3 receptor. *J. Biol. Chem.* **284**, 21425–21434 (2009).
 129. Rex, E. B. *et al.* Identification of RanBP 9/10 as interacting partners for protein kinase C (PKC) γ/δ and the D1 dopamine receptor: Regulation of PKC-mediated receptor phosphorylation. *Mol. Pharmacol.* **78**, 69–80 (2010).
 130. Morris, S. J. *et al.* Differential desensitization of dopamine D2 receptor isoforms by protein kinase C: The importance of receptor phosphorylation and pseudosubstrate sites. *Eur. J. Pharmacol.* **577**, 44–53 (2007).
 131. Namkung, Y. & Sibley, D. R. Protein kinase C mediates phosphorylation, desensitization, and trafficking of the D2 dopamine receptor. *J. Biol. Chem.* **279**, 49533–49541 (2004).
 132. Jin, H., Xie, Z., George, S. R. & O’Dowd, B. F. Palmitoylation occurs at cysteine 347 and cysteine 351 of the dopamine D1 receptor. *Eur. J. Pharmacol.* **386**, 305–312 (1999).
 133. Zhang, X. & Kim, K. M. Palmitoylation of the carboxyl-terminal tail of dopamine D4 receptor is required for surface expression, endocytosis, and signaling. *Biochem. Biophys. Res. Commun.* **479**, 398–403 (2016).
 134. Kong, M. M. C., Verma, V., O’Dowd, B. F. & George, S. R. The role of palmitoylation in directing dopamine D1 receptor internalization through selective endocytic routes. *Biochem. Biophys. Res. Commun.* **405**, 445–449 (2011).
 135. Ng, G. Y. K. *et al.* Phosphorylation and Palmitoylation of the Human D2 L Dopamine Receptor in Sf9 Cells. *J. Neurochem.* **63**, 1589–1595 (1994).
 136. Grünewald, S., Haase, W., Reiländer, H. & Michel, H. Glycosylation, palmitoylation, and localization of the human D(2S) receptor in baculovirus-infected insect cells. *Biochemistry* **35**, 15149–15161 (1996).
 137. Zhang, X. *et al.* Palmitoylation on the carboxyl terminus tail is required for the selective regulation of dopamine D2 versus D3 receptors. *Biochim. Biophys. Acta - Biomembr.* **1858**, 2152–2162 (2016).
 138. Arango-Lievano, M. *et al.* A GIPC1-Palmitate Switch Modulates Dopamine Drd3 Receptor Trafficking and Signaling. *Mol. Cell. Biol.* **36**, 1019–1031 (2016).
 139. Giros, B. & Caron, M. G. Molecular characterization of the dopamine transporter. *Trends Pharmacol. Sci.* **14**, 43–49 (1993).
 140. Chen, N. H., Reith, M. E. A. & Quick, M. W. Synaptic uptake and beyond: The sodium- and chloride-dependent neurotransmitter transporter family

- SLC6. *Pflugers Arch. Eur. J. Physiol.* **447**, 519–531 (2004).
141. Masson, J., Sagné, C., Hamon, M. & El Mestikawy, S. Neurotransmitter transporters in the central nervous system. *Pharmacol. Rev.* **51**, 439–464 (1999).
 142. Yamashita, A., Singh, S. K., Kawate, T., Jin, Y. & Gouaux, E. Crystal structure of a bacterial homologue of Na⁺/Cl⁻-dependent neurotransmitter transporters. *Nature* **437**, 215–23 (2005).
 143. Gether, U., Andersen, P. H., Larsson, O. M. & Schousboe, A. Neurotransmitter transporters: molecular function of important drug targets. *Trends Pharmacol. Sci.* **27**, 375–383 (2006).
 144. Kilty, J. E., Lorang, D. & Amara, S. G. Cloning and Expression of a Cocaine-Sensitive Rat Dopamine Transporter. **254**, 578–579 (1991).
 145. Blakely, R. D. *et al.* Cloning and expression of a functional serotonin transporter from rat brain. *Nature* **354**, 66–70 (1991).
 146. Pacholczyk T, Blakely RD, A. S. Expression cloning of an antidepressant-sensitive noradrenaline transporter. *Lett. To Nat.* **350**, 350 (1991).
 147. Shimada, S. *et al.* Cloning and Expression of a Cocaine-Sensitive Dopamine Transporter Complementary DNA. *Science (80-)*. **254**, 576–578 (1991).
 148. Chen, J. G., Liu-Chen, S. & Rudnick, G. Determination of external loop topology in the serotonin transporter by site-directed chemical labeling. *J. Biol. Chem.* **273**, 12675–12681 (1998).
 149. Melikian, H. E. *et al.* Human Norepinephrine Transporter. *J. Biol. Chem.* **269**, 12290–12297 (1994).
 150. Brüss, M., Hammermann, S. B. & Bönisch, H. Antipeptide Antibodies Confirm the Topology of the Human Norepinephrine Transporter. *J. Biol. Chem.* **270**, 9197–9201 (1995).
 151. Chen, R. *et al.* Direct evidence that two cysteines in the dopamine transporter form a disulfide bond. *Mol. Cell. Biochem.* **298**, 41–48 (2007).
 152. Kurian, M. *et al.* Homozygous loss-of-function mutations in the gene encoding the dopamine transporter are associated with infantile parkinsonism-dystonia. *J. Clin. Invest.* **119**, 1595–1603 (2009).
 153. Singh, S. K., Piscitelli, C. L., Yamashita, A. & Gouaux, E. A competitive inhibitor traps LeuT in an open-to-out conformation. *Science* **322**, 1655–1661 (2008).
 154. Abramson, J. & Wright, E. M. Structure and function of Na⁺-symporters with inverted repeats. *Curr. Opin. Struct. Biol.* **19**, 425–432 (2009).
 155. Penmatsa, A., Wang, K. H. & Gouaux, E. X-ray structure of dopamine

- transporter elucidates antidepressant mechanism. *Nature* **503**, 85–91 (2013).
156. Hong, W. C. & Amara, S. G. Membrane cholesterol modulates the outward facing conformation of the dopamine transporter and alters cocaine binding. *J. Biol. Chem.* **285**, 32616–32626 (2010).
 157. Krishnamurthy, H. & Gouaux, E. X-ray structures of LeuT in substrate-free outward-open and apo inward-open states. *Nature* **481**, 469–74 (2012).
 158. Navratna, V. & Gouaux, E. Insights into the mechanism and pharmacology of neurotransmitter sodium symporters. *Curr. Opin. Struct. Biol.* **54**, 161–170 (2019).
 159. Forrest, L. R. *et al.* Mechanism for alternating access in neurotransmitter transporters. *Proc. Natl. Acad. Sci.* **105**, 10338–10343 (2008).
 160. Forrest, L. R. & Rudnick, G. The Rocking Bundle: A Mechanism for Ion-Coupled Solute Flux by Symmetrical Transporters. *Physiology* **24**, 377–386 (2009).
 161. Beuming, T. *et al.* The binding sites for cocaine and dopamine in the dopamine transporter overlap. *Nat. Neurosci.* **7**, 780–789 (2008).
 162. Koldsø, H., Christiansen, A. B., Sinning, S. & Schiøtt, B. Comparative modeling of the human monoamine transporters: Similarities in substrate binding. *ACS Chem. Neurosci.* **4**, 295–309 (2012).
 163. Kazmier, K. *et al.* Conformational dynamics of ligand-dependent alternating access in LeuT. *Nat. Struct. Mol. Biol.* **21**, 472–479 (2014).
 164. Dehnes, Y. *et al.* Conformational changes in dopamine transporter intracellular regions upon cocaine binding and dopamine translocation. *Neurochem. Int.* **73**, 4–15 (2014).
 165. Kniazeff, J. *et al.* An intracellular interaction network regulates conformational transitions in the dopamine transporter. *J. Biol. Chem.* **283**, 17691–17701 (2008).
 166. Billesbølle, C. B. *et al.* Substrate-induced unlocking of the inner gate determines the catalytic efficiency of a neurotransmitter: Sodium symporter. *J. Biol. Chem.* **290**, 26725–26738 (2015).
 167. Kristensen, A. S. *et al.* SLC6 Neurotransmitter Transporters : Structure, Function, and Regulation. *Pharmacol. Rev.* **63**, 585–640 (2011).
 168. Penmatsa, A., Wang, K. H. & Gouaux, E. X-ray structures of *Drosophila* with nisoxetine and reboxetine. *Nat. Struct. Mol. Biol.* **22**, 506–509 (2015).
 169. Wang, K. H., Penmatsa, A. & Gouaux, E. Neurotransmitter and psychostimulant recognition by the dopamine transporter. *Nature* **521**, 322–327 (2015).

170. Tavoulari, S. *et al.* Two Na⁺ sites control conformational change in a neurotransmitter transporter homolog. *J. Biol. Chem.* **291**, 1456–1471 (2016).
171. Razavi, A. M., Khelashvili, G. & Weinstein, H. A Markov State-based Quantitative Kinetic Model of Sodium Release from the Dopamine Transporter. *Sci. Rep.* **6**, 1–14 (2017).
172. Borre, L., Andreassen, T. F., Shi, L., Weinstein, H. & Gether, U. The second sodium site in the dopamine transporter controls cation permeation and is regulated by chloride. *J. Biol. Chem.* **289**, 25764–25773 (2014).
173. Kantcheva, A. K., Quick, M., Shi, L., Winther, A. L. & Stolzenberg, S. Chloride binding site of neurotransmitter sodium symporters. *Proc. Natl. Acad. Sci.* **110**, 8489–8494 (2013).
174. Stolzenberg, S. *et al.* Mechanism of the association between Na⁺ binding and conformations at the intracellular gate in neurotransmitter:sodium symporters. *J. Biol. Chem.* **290**, 13992–14003 (2015).
175. Malinauskaitė, L. *et al.* A mechanism for intracellular release of Na⁺ by neurotransmitter/sodium symporters. *Nat. Struct. Mol. Biol.* **21**, 1006–12 (2014).
176. Vaughan, R. A., Brown, V. L., McCoy, M. T. & Kuhar, M. J. Species- and brain region-specific dopamine transporters: immunological and glycosylation characteristics. *J. Neurochem.* **66**, 2146–52 (1996).
177. Torres, G. E. *et al.* Oligomerization and Trafficking of the Human Dopamine Transporter. *J. Biol. Chem.* **278**, 2731–2739 (2003).
178. Daniels, G. M. & Amara, S. G. Regulated trafficking of the human dopamine transporter. Clathrin-mediated internalization and lysosomal degradation in response to phorbol esters. *J. Biol. Chem.* **274**, 35794–35801 (1999).
179. Li, L. Bin *et al.* The role of N-glycosylation in function and surface trafficking of the human dopamine transporter. *J. Biol. Chem.* **279**, 21012–21020 (2004).
180. Afonso-Oramas, D. *et al.* Dopamine transporter glycosylation correlates with the vulnerability of midbrain dopaminergic cells in Parkinson's disease. *Neurobiol. Dis.* **36**, 494–508 (2009).
181. Vina-Vilaseca, A. & Sorkin, A. Lysine 63-linked polyubiquitination of the dopamine transporter requires WW3 and WW4 domains of Nedd4-2 and UBE2D ubiquitin-conjugating enzymes. *J. Biol. Chem.* **285**, 7645–7656 (2010).
182. Miranda, M., Wu, C. C., Sorkina, T., Korstjens, D. R. & Sorkin, A. Enhanced ubiquitylation and accelerated degradation of the dopamine transporter mediated by protein kinase C. *J. Biol. Chem.* **280**, 35617–

35624 (2005).

183. Manuel Miranda, Kalen R. Dionne, Tatiana Sorkina, and A. S. Three Ubiquitin Conjugation Sites in the Amino Terminus of the Dopamine Transporter Mediate Protein Kinase C-dependent Endocytosis of the Transporter. *Mol. Biol. Cell* **18**, 313–323 (2007).
184. Jiang, H., Jiang, Q. & Feng, J. Parkin increases dopamine uptake by enhancing the cell surface expression of dopamine transporter. *J. Biol. Chem.* **279**, 54380–54386 (2004).
185. Adkins, E. M. *et al.* Membrane mobility and microdomain association of the dopamine transporter studied with fluorescence correlation spectroscopy and fluorescence recovery after photobleaching. *Biochemistry* **46**, 10484–10497 (2007).
186. Foster, J. D., Adkins, S. D., Lever, J. R. & Vaughan, R. A. Phorbol ester induced trafficking-independent regulation and enhanced phosphorylation of the dopamine transporter associated with membrane rafts and cholesterol. *J. Neurochem.* **105**, 1683–1699 (2008).
187. Jones, K. T., Zhen, J. & Reith, M. E. A. Importance of cholesterol in dopamine transporter function. *J. Neurochem.* **123**, 700–715 (2012).
188. Navaroli, D. M. *et al.* The plasma membrane-associated gtpase rin interacts with the dopamine transporter and is required for protein kinase c-regulated dopamine transporter trafficking. *J. Neurosci.* **31**, 13758–13770 (2011).
189. Cremona, M. L. *et al.* Flotillin-1 is essential for PKC-triggered endocytosis and membrane microdomain localization of DAT. *Nat. Neurosci.* **14**, 469–477 (2011).
190. Lee, K. H., Kim, M. Y., Kim, D. H. & Lee, Y. S. Syntaxin 1A and receptor for activated C kinase interact with the N-terminal region of human dopamine transporter. *Neurochem. Res.* **29**, 1405–1409 (2004).
191. Binda, F. *et al.* Syntaxin 1A interaction with the dopamine transporter promotes amphetamine-induced dopamine efflux. *Mol. Pharmacol.* **74**, 1101–1108 (2008).
192. Carvelli, L., Blakely, R. D. & DeFelice, L. J. Dopamine transporter/syntaxin 1A interactions regulate transporter channel activity and dopaminergic synaptic transmission. *Proc. Natl. Acad. Sci. U. S. A.* **105**, 14192–14197 (2008).
193. Cervinski, M. A., Foster, J. D. & Vaughan, R. A. Syntaxin 1A regulates dopamine transporter activity, phosphorylation and surface expression. *Neuroscience* **170**, 408–416 (2010).
194. Lee, F. J. S., Liu, F., Pristupa, Z. B. & Niznik, H. B. Direct binding and functional coupling of α -synuclein to the dopamine transporters accelerate

- dopamine-induced apoptosis. *FASEB J.* **15**, 916–926 (2001).
195. Butler, B. *et al.* Dopamine transporter activity is modulated by α -synuclein. *J. Biol. Chem.* **290**, 29542–29554 (2015).
 196. Swant, J. *et al.* A-Synuclein Stimulates a Dopamine Transporter-Dependent Chloride Current and Modulates the Activity of the Transporter. *J. Biol. Chem.* **286**, 43933–43943 (2011).
 197. Garcia-Olivares, J. *et al.* Inhibition of Dopamine Transporter Activity by G Protein $\beta\gamma$ Subunits. *PLoS One* **8**, 1–9 (2013).
 198. Garcia-Olivares, J. *et al.* G $\beta\gamma$ subunit activation promotes dopamine efflux through the dopamine transporter. *Mol. Psychiatry* **22**, 1673–1679 (2017).
 199. Mauna, J. C. *et al.* G protein $\beta\gamma$ subunits play a critical role in the actions of amphetamine. *Transl. Psychiatry* **9**, (2019).
 200. Lee, F. J. S. *et al.* Dopamine transporter cell surface localization facilitated by a direct interaction with the dopamine D2 receptor. *EMBO J.* **26**, 2127–2136 (2007).
 201. Bolan, E. a *et al.* D2 receptors regulate dopamine transporter function via an extracellular signal-regulated kinases 1 and 2-dependent and phosphoinositide 3 kinase-independent mechanism. *Mol. Pharmacol.* **71**, 1222–1232 (2007).
 202. Lee, F. J. S., Pei, L. & Liu, F. Disruption of the dopamine transporter-dopamine D2 receptor interaction in schizophrenia. *Synapse* **63**, 710–712 (2009).
 203. Chen, R. *et al.* Protein kinase C β is a modulator of the dopamine D2 autoreceptor-activated trafficking of the dopamine transporter. *J. Neurochem.* **125**, 663–672 (2013).
 204. Foster, J. D. & Vaughan, R. A. Phosphorylation mechanisms in dopamine transporter regulation. *J. Chem. Neuroanat.* 1–9 (2016). doi:10.1016/j.jchemneu.2016.10.004
 205. German, C. L., Baladi, M. G., McFadden, L. M., Hanson, G. R. & Fleckenstein, A. E. Regulation of the Dopamine and Vesicular Monoamine Transporters: Pharmacological Targets and Implications for Disease. *Pharmacol. Rev.* **67**, 1005–1024 (2015).
 206. Grånäs, C., Ferrer, J., Loland, C. J., Javitch, J. A. & Gether, U. N-terminal truncation of the dopamine transporter abolishes phorbol ester- and substance P receptor-stimulated phosphorylation without impairing transporter internalization. *J. Biol. Chem.* **278**, 4990–5000 (2003).
 207. Vaughan R. A.; Uhl, G. R.; Kuhar, M. J., R. A. . H. Protein kinase C-mediated phosphorylation and functional regulation of dopamine transporters in striatal synaptosomes. *J Biol Chem* **272**, 15541–6. (1997).

208. Morón, J. a *et al.* Mitogen-activated protein kinase regulates dopamine transporter surface expression and dopamine transport capacity. *J. Neurosci.* **23**, 8480–8488 (2003).
209. Steinkellner, T. *et al.* In vivo amphetamine action is contingent on α CaMKII. *Neuropsychopharmacology* **39**, 2681–2693 (2014).
210. Steinkellner, T. *et al.* Ca²⁺/calmodulin-dependent protein kinase II α (α CaMKII) controls the activity of the dopamine transporter: Implications for angelman syndrome. *J. Biol. Chem.* **287**, 29627–29635 (2012).
211. Fog, J. U. *et al.* Calmodulin Kinase II Interacts with the Dopamine Transporter C Terminus to Regulate Amphetamine-Induced Reverse Transport. *Neuron* **51**, 417–429 (2006).
212. Batchelor, M. & Schenk, J. O. Protein kinase A activity may kinetically upregulate the striatal transporter for dopamine. *J. Neurosci.* **18**, 10304–10309 (1998).
213. Hoover, B. R., Everett, C. V., Sorkin, A. & Zahniser, N. R. Rapid regulation of dopamine transporters by tyrosine kinases in rat neuronal preparations. *J. Neurochem.* **101**, 1258–1271 (2007).
214. Speed, N. K. *et al.* Akt-Dependent and Isoform-Specific Regulation of Dopamine Transporter Cell Surface Expression. *ACS Chem. Neurosci.* **1**, 476–481 (2010).
215. Carvelli, L. *et al.* PI 3-kinase regulation of dopamine uptake. *J Neurochem* **81**, 859–869 (2002).
216. Gorentla, B. K., Moritz, A. E., Foster, J. D. & Vaughan, R. A. Proline-directed phosphorylation of the dopamine transporter N-terminal domain. *Biochemistry* **48**, 1067–1076 (2009).
217. Foster, J. D., Pananusorn, B., Cervinski, M. A., Holden, H. E. & Vaughan, R. A. Dopamine transporters are dephosphorylated in striatal homogenates and in vitro by protein phosphatase 1. *Mol. Brain Res.* **110**, 100–108 (2003).
218. Bauman, A. L. *et al.* Cocaine and antidepressant-sensitive biogenic amine transporters exist in regulated complexes with protein phosphatase 2A. *J. Neurosci.* **20**, 7571–8 (2000).
219. Foster, J. D., Pananusorn, B. & Vaughan, R. A. Dopamine transporters are phosphorylated on N-terminal serines in rat striatum. *J. Biol. Chem.* **277**, 25178–25186 (2002).
220. Cervinski, M. A., Foster, J. D. & Vaughan, R. A. Psychoactive substrates stimulate dopamine transporter phosphorylation and down-regulation by cocaine-sensitive and protein kinase C-dependent mechanisms. *J. Biol. Chem.* **280**, 40442–40449 (2005).

221. Moritz, A. E. *et al.* Phosphorylation of dopamine transporter serine 7 modulates cocaine analog binding. *J. Biol. Chem.* **288**, 20–32 (2013).
222. Lu, K. P. & Zhou, X. Z. The prolyl isomerase PIN1: A pivotal new twist in phosphorylation signalling and disease. *Nat. Rev. Mol. Cell Biol.* **8**, 904–916 (2007).
223. Foster, J. D. *et al.* Dopamine transporter phosphorylation site threonine 53 regulates substrate reuptake and amphetamine-stimulated efflux. *J. Biol. Chem.* **287**, 29702–29712 (2012).
224. Challasivakanaka, S. *et al.* Dopamine transporter phosphorylation site threonine 53 is stimulated by amphetamines and regulates dopamine transport, efflux, and cocaine analog binding. *J. Biol. Chem.* **292**, 19066–19075 (2017).
225. Schmitz, Y., Lee, C. J., Schmauss, C., Gonon, F. & Sulzer, D. Amphetamine distorts stimulation-dependent dopamine overflow: effects on D2 autoreceptors, transporters, and synaptic vesicle stores. *J. Neurosci.* **21**, 5916–24 (2001).
226. Sulzer, D., Sonders, M. S., Poulsen, N. W. & Galli, A. Mechanisms of neurotransmitter release by amphetamines: A review. *Prog. Neurobiol.* **75**, 406–433 (2005).
227. Vaughan, R. A. & Foster, J. D. Mechanisms of dopamine transporter regulation in normal and disease states. *Trends Pharmacol. Sci.* **34**, 489–496 (2013).
228. Khoshbouei, H. *et al.* N-terminal phosphorylation of the dopamine transporter is required for amphetamine-induced efflux. *PLoS Biol.* **2**, 387–393 (2004).
229. Karam, C. S. & Javitch, J. A. Phosphorylation of the Amino Terminus of the Dopamine Transporter: Regulatory Mechanisms and Implications for Amphetamine Action. in *Advances in Pharmacology* **82**, 205–234 (2018).
230. Johnson, L. A., Guptaroy, B., Lund, D., Shamban, S. & Gnegy, M. E. Regulation of amphetamine-stimulated dopamine efflux by protein kinase C β . *J. Biol. Chem.* **280**, 10914–10919 (2005).
231. Chen, R. *et al.* Protein Kinase C Is a Critical Regulator of Dopamine Transporter Trafficking and Regulates the Behavioral Response to Amphetamine in Mice. *J. Pharmacol. Exp. Ther.* **328**, 912–920 (2009).
232. Hamilton, P. J. *et al.* PIP 2 regulates psychostimulant behaviors through its interaction with a membrane protein. *Nat. Chem. Bio.* **10**, 582–589 (2015).
233. Kahlig, K. M. *et al.* Amphetamine induces dopamine efflux through a dopamine transporter channel. *Proc. Natl. Acad. Sci. U. S. A.* **102**, 3495–500 (2005).

234. Carvelli, L., McDonald, P. W., Blakely, R. D. & DeFelice, L. J. Dopamine transporters depolarize neurons by a channel mechanism. *Proc. Natl. Acad. Sci. U. S. A.* **101**, 16046–51 (2004).
235. Cameron, K. N., Solis, E., Ruchala, I., De Felice, L. J. & Eltit, J. M. Amphetamine activates calcium channels through dopamine transporter-mediated depolarization. *Cell Calcium* **58**, 457–466 (2015).
236. Gnegy, M. E. *et al.* Intracellular Ca²⁺ regulates amphetamine-induced dopamine efflux and currents mediated by the human dopamine transporter. *Mol. Pharmacol.* **66**, 137–143 (2004).
237. Khoshbouei, H., Wang, H., Lechleiter, J. D., Javitch, J. A. & Galli, A. Amphetamine-induced dopamine efflux: A voltage-sensitive and intracellular Na⁺-dependent mechanism. *J. Biol. Chem.* **278**, 12070–12077 (2003).
238. Sulzer, D. *et al.* Amphetamine redistributes dopamine from synaptic vesicles to the cytosol and promotes reverse transport. *J. Neurosci.* **15**, 4102–8 (1995).
239. Piffl, C., Drobny, H., Reither, H., Hornykiewicz, O. & Singer, E. Mechanism of the dopamine-releasing actions of amphetamine and cocaine: plasmalemmal dopamine transporter versus vesicular monoamine transporter. *Mol. Pharmacol.* **47**, 368–373 (1995).
240. Freyberg, Z. *et al.* Mechanisms of amphetamine action illuminated through optical monitoring of dopamine synaptic vesicles in *Drosophila* brain. *Nat. Commun.* **7**, 1–15 (2016).
241. Sambo, D. O. *et al.* The sigma-1 receptor modulates methamphetamine dysregulation of dopamine neurotransmission. *Nat. Commun.* **8**, (2017).
242. Hedges, D. M. *et al.* Methamphetamine Induces Dopamine Release in the Nucleus Accumbens Through a Sigma Receptor-Mediated Pathway. *Neuropsychopharmacology* **43**, 1405–1414 (2018).
243. Hahn, M. K. & Blakely, R. D. The functional impact of SLC6 transporter genetic variation. *Ann. Rev. Pharma. Tox.* **47**, 401–441 (2007).
244. Giros, B., Jaber, M., Jones, S. R., Wightman, R. M. & Caron, M. G. Hyperlocomotion and indifference to cocaine and amphetamine in mice lacking the dopamine transporter. *Nature* **379**, 606–612 (1996).
245. Verrico, C. D., Miller, G. M. & Madras, B. K. MDMA (Ecstasy) and human dopamine, norepinephrine, and serotonin transporters: Implications for MDMA-induced neurotoxicity and treatment. *Psychopharmacology (Berl)*. **189**, 489–503 (2007).
246. Urban, N. B. L. & Martinez, D. Neurobiology of Addiction. Insight from Neurochemical Imaging. *Psychiatr. Clin. North Am.* **35**, 521–541 (2012).

247. Mash, D. C., Pablo, J., Ouyang, Q., Hearn, W. L. & Izenwasse, S. Dopamine transport function is elevated in cocaine users. *J. Neurochem.* **81**, 292–300 (2002).
248. Dos Santos, M. *et al.* Cocaine increases dopaminergic connectivity in the nucleus accumbens. *Brain Struct. Funct.* (2017). doi:10.1007/s00429-017-1532-x
249. Lohr, K. M., Masoud, S. T., Salahpour, A. & Miller, G. W. Membrane transporters as mediators of synaptic dopamine dynamics: implications for disease. *Eur. J. Neurosci.* **45**, 20–33 (2017).
250. Koob, G. F. & Volkow, N. D. Neurobiology of addiction: a neurocircuitry analysis. *The Lancet Psychiatry* **3**, 760–773 (2016).
251. Miller, G. W., Gainetdinov, R. R., Levey, a I. & Caron, M. G. Dopamine transporters and neuronal injury. *Trends Pharmacol. Sci.* **20**, 424–9 (1999).
252. Piffl, C., Giros, B. & Caron, M. G. Dopamine Transporter Expression Confers Cytotoxicity to Low Doses of the Parkinsonism-inducing Neurotoxin 1-Methyl-4-phenylpyridinium. *J. Neurosci.* **13**, 4246–4253 (1993).
253. Cookson, M. R. The Biochemistry of Parkinson's Disease. *Annu. Rev. Biochem.* **74**, 29–52 (2005).
254. Kurian, M. A. *et al.* Clinical and molecular characterisation of hereditary dopamine transporter deficiency syndrome: An observational cohort and experimental study. *Lancet Neurol.* **10**, 54–62 (2011).
255. Ng, J. *et al.* Dopamine transporter deficiency syndrome : phenotypic spectrum from infancy to adulthood. *Brain* **137**, 1107–1119 (2014).
256. Hansen, F. H. *et al.* Missense mutations in the dopamine transporter gene associate with adult parkinsonism and ADHD. *J. Clin. Invest.* **124**, 3107–3120 (2014).
257. Nieoullon, A. Dopamine and the regulation of cognition and attention. *Prog. Neurobiol.* **67**, 53–83 (2002).
258. Madras, B. K., Miller, G. M. & Fischman, A. J. The dopamine transporter and attention-deficit/hyperactivity disorder. *Biol. Psychiatry* **57**, 1397–1409 (2005).
259. Madras, B. K., Miller, G. M. & Fischman, A. J. The dopamine transporter: relevance to attention deficit hyperactivity disorder (ADHD). *Behav Brain Res* **130**, 57–63 (2002).
260. Gomez-Sanchez, C. I. *et al.* Pharmacogenetics of methylphenidate in childhood attention-deficit/hyperactivity disorder: Long-Term effects. *Sci. Rep.* **7**, 1–8 (2017).

261. Mergy, M. A. *et al.* Genetic targeting of the amphetamine and methylphenidate-sensitive dopamine transporter: On the path to an animal model of attention-deficit hyperactivity disorder. *Neurochem. Int.* **73**, 56–70 (2014).
262. Seeman, P. & Madras, B. K. Anti-hyperactivity medication: methylphenidate and amphetamine. *Mol. Psychiatry* **3**, 386–396 (1998).
263. Grunhage, F. *et al.* Systematic screening for DNA sequence variation in the coding region of the human dopamine transporter gene. *Mol. Psychiatry* **5**, 275–282 (2000).
264. Mazei-Robison, M. S., Couch, R. S., Shelton, R. C., Stein, M. A. & Blakely, R. D. Sequence variation in the human dopamine transporter gene in children with attention deficit hyperactivity disorder. *Neuropharmacology* **49**, 724–736 (2005).
265. Herborg, F., Andreassen, T. F., Berlin, F., Loland, C. J. & Gether, U. Neuropsychiatric disease-associated genetic variants of the dopamine transporter display heterogeneous molecular phenotypes. *J. Biol. Chem.* **293**, 7250–7262 (2018).
266. Lin, Z. & Uhl, G. R. Human dopamine transporter gene variation: Effects of protein coding variants V55A and V382A on expression and uptake activities. *Pharmacogenomics J.* **3**, 159–168 (2003).
267. Sakrikar, D. *et al.* Attention Deficit/Hyperactivity Disorder-Derived Coding Variation in the Dopamine Transporter Disrupts Microdomain Targeting and Trafficking Regulation. *J. Neurosci.* **32**, 5385–5397 (2012).
268. Bowton, E. *et al.* SLC6A3 coding variant Ala559Val found in two autism probands alters dopamine transporter function and trafficking. *Transl. Psychiatry* **4**, e464 (2014).
269. Bowton, E. *et al.* Dysregulation of Dopamine Transporters via Dopamine D2 Autoreceptors Triggers Anomalous Dopamine Efflux Associated with Attention-Deficit Hyperactivity Disorder. *J. Neurosci.* **30**, 6048–6057 (2010).
270. Mergy, M. A. *et al.* The rare DAT coding variant Val559 perturbs DA neuron function, changes behavior, and alters in vivo responses to psychostimulants. *Proc. Natl. Acad. Sci. U. S. A.* **111**, E4779–88 (2014).
271. Thal, L. B. *et al.* Single quantum dot imaging reveals PKC β -dependent alterations in membrane diffusion and clustering of an ADHD/autism/bipolar disorder-associated dopamine transporter variant. *ACS Chem. Neurosci.* acschemneuro.8b00350 (2018). doi:10.1021/acschemneuro.8b00350
272. Zaballa, M. E. & van der Goot, F. G. The molecular era of protein S-acylation: spotlight on structure, mechanisms, and dynamics. *Crit. Rev.*

- Biochem. Mol. Biol.* **53**, 420–451 (2018).
273. Jiang, H. *et al.* Protein Lipidation: Occurrence, Mechanisms, Biological Functions, and Enabling Technologies. *Chem. Rev.* **118**, 919–988 (2018).
274. Iwanaga, T., Tsutsumi, R., Noritake, J., Fukata, Y. & Fukata, M. Dynamic protein palmitoylation in cellular signaling. *Prog. Lipid Res.* **48**, 117–127 (2009).
275. Tsutsumi, R., Fukata, Y. & Fukata, M. Discovery of protein-palmitoylating enzymes. *Pflugers Arch. Eur. J. Physiol.* **456**, 1199–1206 (2008).
276. Tabaczar, S., Czogalla, A., Podkalicka, J., Biernatowska, A. & Sikorski, A. F. Protein palmitoylation: Palmitoyltransferases and their specificity. *Exp. Biol. Med.* **242**, 1150–1157 (2017).
277. Won, S. J., Cheung See Kit, M. & Martin, B. R. Protein depalmitoylases. *Crit. Rev. Biochem. Mol. Biol.* **53**, 83–98 (2018).
278. Greaves, J. & Chamberlain, L. H. DHHC palmitoyl transferases: Substrate interactions and (patho)physiology. *Trends Biochem. Sci.* **36**, 245–253 (2011).
279. Rana, M. S. *et al.* Fatty acyl recognition and transfer by an integral membrane S-acyltransferase. *Science (80-.)*. **359**, (2018).
280. Greaves, J. *et al.* Molecular basis of fatty acid selectivity in the zDHHC family of S-acyltransferases revealed by click chemistry. *Proc. Natl. Acad. Sci.* **114**, E1365–E1374 (2017).
281. Jennings, B. C. & Linder, M. E. DHHC protein S-acyltransferases use similar ping-pong kinetic mechanisms but display different Acyl-CoA specificities. *J. Biol. Chem.* **287**, 7236–7245 (2012).
282. Abrami, L. *et al.* Identification and dynamics of the human ZDHHC16-ZDHHC6 palmitoylation cascade. *Elife* **6**, 1–24 (2017).
283. Long, J. Z. & Cravatt, B. F. The metabolic serine hydrolases and their functions in mammalian physiology and disease. *Chem. Rev.* **111**, 6022–6063 (2011).
284. Kong, E. *et al.* Dynamic palmitoylation links cytosol-membrane shuttling of acyl-protein thioesterase-1 and acyl-protein thioesterase-2 with that of proto-oncogene H-Ras product and growth-associated protein-43. *J. Biol. Chem.* **288**, 9112–9125 (2013).
285. Vartak, N. *et al.* The autodepalmitoylating activity of APT maintains the spatial organization of palmitoylated membrane proteins. *Biophys. J.* **106**, 93–105 (2014).
286. Kathayat, R. S. *et al.* Active and dynamic mitochondrial S-depalmitoylation revealed by targeted fluorescent probes. *Nat. Commun.* **9**, (2018).

287. Camp, L. a & Hofmann L, S. Purification and Properties of a Palmitoyl-Protein Thioesterase That Cleaves Palmitate From H-Ras*. *J. Biol. Chem.* **268**, 22566–22574 (1993).
288. Camp, L. a, Verkruyse, L. A., Afendis, S. J., Slaughter, C. A. & Hofmann, S. L. Molecular Cloning and Expression of Palmitoyl-protein Thioesterase. *J. Biol. Chem.* **269**, 23212–23219 (1994).
289. Verkruyse, L. A. & Hofmann, S. L. Lysosomal Targeting of Palmitoyl-protein Thioesterase. *J. Biol. Chem.* **271**, 15831–15836 (1996).
290. Bagh, M. B. *et al.* Misrouting of v-ATPase subunit V0a1 Dysregulates Lysosomal Acidification in a Neurodegenerative Lysosomal Storage Disease Model. *Nat. Commun.* **8**, 1–16 (2017).
291. Lin, D. T. S. & Conibear, E. ABHD17 proteins are novel protein depalmitoylases that regulate N-Ras palmitate turnover and subcellular localization. *Elife* **4**, 1–14 (2015).
292. Yokoi, N. *et al.* Identification of PSD-95 depalmitoylating enzymes. *J. Neurosci.* **36**, 6431–6444 (2016).
293. Tortosa, E. *et al.* Dynamic Palmitoylation Targets MAP6 to the Axon to Promote Microtubule Stabilization during Neuronal Polarization. *Neuron* **94**, 809-825.e7 (2017).
294. Chamberlain, L. H. & Shipston, M. J. The Physiology of Protein S-Acylation. *Physiol. Rev.* **95**, 341–376 (2015).
295. Craven, S. E., El-Husseini, A. E. & Bredt, D. S. Synaptic targeting of the postsynaptic density protein PSD-95 mediated by lipid and protein motifs. *Neuron* **22**, 497–509 (1999).
296. El-Husseini, A. E. *et al.* Dual Palmitoylation of Psd-95 Mediates Its Vesiculotubular Sorting, Postsynaptic Targeting, and Ion Channel Clustering. *J. Cell Biol.* **148**, 159–172 (2000).
297. Michaelson, D., Ahearn, I., Bergo, M., Young, S. & Philips, M. Membrane Trafficking of Heterotrimeric G Proteins via the Endoplasmic Reticulum and Golgi. *Mol. Biol. Cell* **13**, 3294–3302 (2002).
298. Rocks, O. *et al.* An acylation cycle regulates localization and activity of palmitoylated ras isoforms. *Science (80-.)*. **307**, 1746–1752 (2005).
299. Aicart-Ramos, C., Valero, R. A. & Rodriguez-Crespo, I. Protein palmitoylation and subcellular trafficking. *Biochim. Biophys. Acta - Biomembr.* **1808**, 2981–2994 (2011).
300. Resh, M. D. Fatty acylation of proteins: The long and the short of it. *Prog. Lipid Res.* **63**, 120–131 (2016).
301. Salaun, C., Greaves, J. & Chamberlain, L. H. The intracellular dynamic of

- protein palmitoylation. *J. Cell Biol.* **191**, 1229–1238 (2010).
302. Drisdell, R. C., Manzana, E. & Green, W. N. The role of palmitoylation in functional expression of nicotinic $\alpha 7$ receptors. *J. Neurosci.* **24**, 10502–10510 (2004).
 303. Huang, K. *et al.* Huntingtin-interacting protein HIP14 is a palmitoyl transferase involved in palmitoylation and trafficking of multiple neuronal proteins. *Neuron* **44**, 977–986 (2004).
 304. Greaves, J. *et al.* Palmitoylation-induced aggregation of cysteine-string protein mutants that cause neuronal ceroid lipofuscinosis. *J. Biol. Chem.* **287**, 37330–37339 (2012).
 305. Valdez-Taubas, J. & Pelham, H. Swf1-dependent palmitoylation of the SNARE Tlg1 prevents its ubiquitination and degradation. *EMBO J.* **24**, 2524–2532 (2005).
 306. Rossin, A. *et al.* Fas palmitoylation by the palmitoyl acyltransferase DHHC7 regulates Fas stability. *Cell Death Differ.* **22**, 643–653 (2015).
 307. Murphy, J. & Kolandaivelu, S. Palmitoylation of Progressive Rod-Cone Degeneration (PRCD) Regulates protein stability and localization. *J. Biol. Chem.* **291**, 23036–23046 (2016).
 308. Melkonian, K. A., Ostermeyer, A. G., Chen, J. Z., Roth, M. G. & Brown, D. A. Role of lipid modifications in targeting proteins to detergent-resistant membrane rafts. *J. Biol. Chem.* **274**, 3910–3917 (1999).
 309. Levental, I., Grzybek, M. & Simons, K. Greasing their way: Lipid modifications determine protein association with membrane rafts. *Biochemistry* **49**, 6305–6316 (2010).
 310. Abrami, L., Kunz, B., Iacovache, I. & Van Der Goot, F. G. Palmitoylation and ubiquitination regulate exit of the Wnt signaling protein LRP6 from the endoplasmic reticulum. *Proc. Natl. Acad. Sci. U. S. A.* **105**, 5384–5389 (2008).
 311. Holland, S. M. *et al.* Palmitoylation controls DLK localization, interactions and activity to ensure effective axonal injury signaling. *Proc. Natl. Acad. Sci.* **113**, 763–768 (2016).
 312. Woolfrey, K. M., Sanderson, J. L. & Dell'Acqua, M. L. The Palmitoyl Acyltransferase DHHC2 Regulates Recycling Endosome Exocytosis and Synaptic Potentiation through Palmitoylation of AKAP79/150. *J. Neurosci.* **35**, 442–456 (2015).
 313. Hilgmann, D. W., Fine, M., Linder, M. E., Jennings, B. C. & Lin, M. J. Massive endocytosis triggered by surface membrane palmitoylation under mitochondrial control in BHK fibroblasts. *Elife* **2013**, 1–16 (2013).
 314. Lin, M. J. *et al.* Massive palmitoylation-dependent endocytosis during

- reoxygenation of anoxic cardiac muscle. *Elife* **2013**, 1–16 (2013).
315. Shen, L. F. *et al.* Role of S-Palmitoylation by ZDHHC13 in Mitochondrial function and Metabolism in Liver. *Sci. Rep.* **7**, 1–14 (2017).
 316. Zhao, L. *et al.* CD36 palmitoylation disrupts free fatty acid metabolism and promotes tissue inflammation in non-alcoholic steatohepatitis. *J. Hepatol.* **69**, 705–717 (2018).
 317. Zingler, P. *et al.* Palmitoylation is required for TNF-R1 signaling. *Cell Commun. Signal.* **17**, 1–16 (2019).
 318. Hansen, A. L. *et al.* Nitro-fatty acids are formed in response to virus infection and are potent inhibitors of STING palmitoylation and signaling. *Proc. Natl. Acad. Sci.* **115**, 201806239 (2018).
 319. Jindal, H. K., Folco, E. J., Liu, G. X. & Koren, G. Posttranslational modification of voltage-dependent potassium channel Kv1.5: COOH-terminal palmitoylation modulates its biological properties. *Am. J. Physiol. Circ. Physiol.* **294**, H2012–H2021 (2008).
 320. Jeffries, O., Tian, L., McClafferty, H. & Shipston, M. J. An electrostatic switch controls palmitoylation of the large conductance voltage- and calcium-activated potassium (BK) channel. *J. Biol. Chem.* **287**, 1468–1477 (2012).
 321. Howie, J., Tulloch, L. B., Shattock, M. J. & Fuller, W. Regulation of the cardiac Na⁺ pump by palmitoylation of its catalytic and regulatory subunits. *Biochem. Soc. Trans.* **41**, 95–100 (2013).
 322. Zheng, W. *et al.* Regulation of TRPP3 channel function by N-terminal domain palmitoylation and phosphorylation. *J. Biol. Chem.* **291**, 25678–25691 (2016).
 323. Shipston, M. J. S-acylation dependent post-translational cross-talk regulates large conductance calcium- and voltage- activated potassium (BK) channels. *Front. Physiol.* **5 JUL**, 1–9 (2014).
 324. Russo, I., Oksman, A. & Goldberg, D. E. Fatty acid acylation regulates trafficking of the unusual Plasmodium falciparum calpain to the nucleolus. *Mol. Microbiol.* **72**, 229–245 (2009).
 325. Hicks, S. W., Charron, G., Hang, H. C. & Galán, J. E. Subcellular targeting of salmonella virulence proteins by host-mediated S-palmitoylation. *Cell Host Microbe* **10**, 9–20 (2011).
 326. Lin, Y. H. *et al.* Host cell-catalyzed S-palmitoylation mediates Golgi targeting of the legionella ubiquitin ligase GobX. *J. Biol. Chem.* **290**, 25766–25781 (2015).
 327. Jones, M. L., Collins, M. O., Goulding, D., Choudhary, J. S. & Rayner, J. C. Analysis of protein palmitoylation reveals a pervasive role in Plasmodium

- development and pathogenesis. *Cell Host Microbe* **12**, 246–258 (2012).
328. Frénal, K. *et al.* Global analysis of apicomplexan protein S-acyl transferases reveals an enzyme essential for invasion. *Traffic* **14**, 895–911 (2013).
 329. Abrami, L., Leppla, S. H. & Gisou Van Der Goot, F. Receptor palmitoylation and ubiquitination regulate anthrax toxin endocytosis. *J. Cell Biol.* **172**, 309–320 (2006).
 330. Sanders, S. S. *et al.* Curation of the Mammalian Palmitoylome Indicates a Pivotal Role for Palmitoylation in Diseases and Disorders of the Nervous System and Cancers. *PLoS Comput. Biol.* **11**, 1–20 (2015).
 331. Henderson, M. X. *et al.* Neuronal ceroid lipofuscinosis with DNAJC5/CSP α mutation has PPT1 pathology and exhibit aberrant protein palmitoylation. *Acta Neuropathol.* **131**, 621–637 (2016).
 332. Yeste-Velasco, M., Linder, M. E. & Lu, Y. J. Protein S-palmitoylation and cancer. *Biochim. Biophys. Acta - Rev. Cancer* **1856**, 107–120 (2015).
 333. Sanders, S. S. & Hayden, M. R. Aberrant palmitoylation in Huntington disease. *Biochem. Soc. Trans.* **43**, 205–210 (2015).
 334. Goytain, A., Hines, R. M. & Quamme, G. A. Huntingtin-interacting proteins, HIP14 and HIP14L, mediate dual functions, palmitoyl acyltransferase and Mg²⁺ transport. *J. Biol. Chem.* **283**, 33365–33374 (2008).
 335. Mukai, J. *et al.* Evidence that the gene encoding ZDHHC8 contributes to the risk of schizophrenia. *Nat. Genet.* **36**, 725–731 (2004).
 336. Chen, W. Y. *et al.* Case-control study and transmission disequilibrium test provide consistent evidence for association between schizophrenia and genetic variation in the 22q11 gene ZDHHC8. *Hum. Mol. Genet.* **13**, 2991–2995 (2004).
 337. Beard, R. S. *et al.* Palmitoyl acyltransferase DHHC21 mediates endothelial dysfunction in systemic inflammatory response syndrome. *Nat. Commun.* **7**, (2016).
 338. Chen, B., Sun, Y., Niu, J., Jarugumilli, G. K. & Wu, X. Protein Lipidation in Cell Signaling and Diseases: Function, Regulation, and Therapeutic Opportunities. *Cell Chem. Biol.* **25**, 817–831 (2018).
 339. Khoury, G. A., Baliban, R. C. & Floudas, C. A. Proteome-wide post-translational modification statistics: Frequency analysis and curation of the swiss-prot database. *Sci. Rep.* **1**, 1–5 (2011).
 340. Blanc, M. *et al.* SwissPalm: Protein Palmitoylation database. *F1000Research* **4**, 261 (2015).
 341. Wan, J., Roth, A. F., Bailey, A. O. & Davis, N. G. Palmitoylated proteins:

- Purification and identification. *Nat. Protoc.* **2**, 1573–1584 (2007).
342. Drisdell, R. C. & Green, W. N. Labeling and quantifying sites of protein palmitoylation. *Biotechniques* **36**, 276–285 (2004).
343. Zhou, B. *et al.* Low-background acyl-biotinyl exchange largely eliminates the co-isolation of non-S-acylated proteins and enables deep S-acylproteomic analysis. *Anal. Chem.* 588988 (2019). doi:10.1101/588988
344. Foster, J. D. & Vaughan, R. A. Palmitoylation Controls Dopamine Transporter Kinetics, Degradation, and Protein Kinase C-dependent Regulation *. *J. Biol. Chem.* **286**, 5175–5186 (2011).
345. Bolland, D. E., Moritz, A. E., Stanislawski, D. J., Vaughan, R. A. & Foster, J. D. Palmitoylation by Multiple DHHC Enzymes Enhances Dopamine Transporter Function and Stability. *ACS Chem. Neurosci.* (2019). doi:10.1021/acscchemneuro.8b00558
346. Rastedt, D. E., Vaughan, R. A. & Foster, J. D. Palmitoylation mechanisms in dopamine transporter regulation. *J. Chem. Neuroanat.* **83–84**, 3–9 (2017).
347. Moritz, A. E. *et al.* Reciprocal Phosphorylation and Palmitoylation Control Dopamine Transporter Kinetics *. *J. Biol. Chem.* **290**, 29095–29105 (2015).
348. Asok, A., Kandel, E. R. & Rayman, J. B. The Neurobiology of Fear Generalization. *Front. Behav. Neurosci.* **12**, 1–15 (2019).
349. Schultz, W. Responses of midbrain dopamine neurons to behavioral trigger stimuli in the monkey. *J. Neurophysiol.* **56**, 1439–1461 (1986).
350. Jo, Y. S., Heymann, G. & Zweifel, L. S. Dopamine Neurons Reflect the Uncertainty in Fear Generalization. *Neuron* **100**, 916–925.e3 (2018).
351. T., S., E.B., J., H., A. & V.A., R. A dynamic developmental theory of attention-deficit/hyperactivity disorder (ADHD) predominantly hyperactive/impulsive and combined subtypes. *Behav. Brain Sci.* **28**, 397–419 (2005).
352. B Pakkenberg, A Møller, H. J. & G Gundersen, A Mouritzen Dam, H. P. The absolute number of nerve cells in substantia nigra in normal subjects and in patients with Parkinson's disease estimated with an unbiased stereological method. *J. Neurol. Neurosurg. Psychiatry* **54**, 30–33 (1991).
353. Trossbach, S. V. *et al.* Misassembly of full-length Disrupted-in-Schizophrenia 1 protein is linked to altered dopamine homeostasis and behavioral deficits. *Mol. Psychiatry* **21**, 1561–1572 (2016).
354. Pramod, A. B., Foster, J., Carvelli, L. & Henry, L. K. SLC6 transporters: Structure, function, regulation, disease association and therapeutics. *Mol. Aspects Med.* **34**, 197–219 (2013).

355. Ashok, A. H., Mizuno, Y., Volkow, N. D. & Howes, O. D. Association of Stimulant Use With Dopaminergic Alterations in Users of Cocaine, Amphetamine, or Methamphetamine A Systematic Review and Meta-analysis. *JAMA psychiatry* 1–9 (2017). doi:10.1001/jamapsychiatry.2017.0135
356. Bermingham, D. P. & Blakely, R. D. Kinase-dependent Regulation of Monoamine Neurotransmitter Transporters. *Pharmacol. Rev.* **68**, 888–953 (2016).
357. Huff, R. A., Vaughan, R. A., Kuhar, M. J. & Uhl, G. R. Phorbol Esters Increase Dopamine Transporter Phosphorylation and Decrease Transport Vmax. *J. Neurochem.* **68**, 225–232 (2002).
358. Melikian, H. E. & Buckley, K. M. Membrane Trafficking Regulates the Activity of the Human Dopamine Transporter. *J. Neurosci.* **19**, 7699–7710 (1999).
359. Challasivakanaka, S. *et al.* Dopamine transporter phosphorylation site threonine 53 is stimulated by amphetamines and regulates dopamine transport, efflux, and cocaine analog binding. *J. Biol. Chem.* **292**, 19066–19075 (2017).
360. Yang, J. W. *et al.* Dephosphorylation of human dopamine transporter at threonine 48 by protein phosphatase PP1/2A up-regulates transport velocity. *J. Biol. Chem.* **294**, 3419–3431 (2019).
361. Fraser, R. *et al.* An N-Terminal Threonine Mutation Produces an Efflux-Favorable , Sodium-Primed Conformation of the Human Dopamine Transporter. *Mol. Pharmacol.* **86**, 76–85 (2014).
362. Sucic, S. *et al.* The N terminus of monoamine transporters is a lever required for the action of amphetamines. *J. Biol. Chem.* **285**, 10924–10938 (2010).
363. Duncan, J. a & Gilman, A. G. A Cytoplasmic Acyl-Protein Thioesterase A Cytoplasmic Acyl-Protein Thioesterase That Removes Palmitate from G Protein alpha Subunits and p21 RAS *. *J. Biol. Chem.* **273**, 15830–15837 (1998).
364. Gao, X. & Hannoush, R. N. A Decade of Click Chemistry in Protein Palmitoylation: Impact on Discovery and New Biology. *Cell Chem. Biol.* **25**, 236–246 (2018).
365. Vaughan, R. A., Agoston, G. E., Lever, J. R. & Newman, A. H. Differential Binding of Tropane-Based Photoaffinity Ligands on the Dopamine Transporter. *J. Neurosci.* **19**, 630–636 (2018).
366. Parnas, M. L. *et al.* Labeling of Dopamine Transporter Transmembrane Domain 1 Proximity of Cocaine and Substrate Active Sites. *Mol. Pharmacol.* **73**, 1141–1150 (2008).

367. Dahal, R. A. *et al.* Computational and biochemical docking of the irreversible cocaine analog RTI 82 directly demonstrates ligand positioning in the dopamine transporter central substrate-binding site. *J. Biol. Chem.* **289**, 29712–29727 (2014).
368. Tomlinson, M. J. *et al.* Identification of the benztropine analog [125 I]GA II 34 binding site on the human dopamine transporter. *Neurochem. Int.* **123**, 34–45 (2019).
369. Gaffaney, J. D. *et al.* Antagonist-induced conformational changes in dopamine transporter extracellular loop two involve residues in a potential salt bridge. *Neurochem. Int.* **73**, 16–26 (2014).
370. Ferrer, J. V. & Javitch, J. A. Cocaine alters the accessibility of endogenous cysteines in putative extracellular and intracellular loops of the human dopamine transporter. *Proc. Natl. Acad. Sci.* **95**, 9238–9243 (2002).
371. Reith, M. E. A., Berfield, J. L., Wang, L. C., Ferrer, J. V. & Javitch, J. A. The Uptake Inhibitors Cocaine and Benztropine Differentially Alter the Conformation of the Human Dopamine Transporter. *J. Biol. Chem.* **276**, 29012–29018 (2001).
372. Whitehead, R. E., Ferrer, J. V., Javitch, J. A. & Justice, J. B. Reaction of oxidized dopamine with endogenous cysteine residues in the human dopamine transporter. *J. Neurochem.* **76**, 1242–1251 (2001).
373. Gorleku, O. A., Barns, A. M., Prescott, G. R., Greaves, J. & Chamberlain, L. H. Endoplasmic reticulum localization of DHHC palmitoyltransferases mediated by lysine-based sorting signals. *J. Biol. Chem.* **286**, 39573–39584 (2011).
374. Jennings, B. C. *et al.* 2-Bromopalmitate and 2-(2-hydroxy-5-nitro-benzylidene)-benzo[b]thiophen-3-one inhibit DHHC-mediated palmitoylation in vitro . *J. Lipid Res.* **50**, 233–242 (2009).
375. Davda, D. *et al.* Profiling targets of the irreversible palmitoylation inhibitor 2-bromopalmitate. *ACS Chem. Biol.* **8**, 1912–1917 (2013).
376. Kang, R. *et al.* Neural palmitoyl-proteomics reveals dynamic synaptic palmitoylation. *Nature* **456**, 904–909 (2008).
377. Edmonds, M. J., Geary, B., Doherty, M. K. & Morgan, A. Analysis of the brain palmitoyl-proteome using both acyl-biotin exchange and acyl-resin-assisted capture methods. *Sci. Rep.* **7**, 1–13 (2017).
378. Humphreys, K. L., Eng, T. & Lee, S. S. Stimulant medication and substance use outcomes: a meta-analysis. *JAMA psychiatry* **70**, 740–9 (2013).
379. Zuvekas, S. H. & Vitiello, B. Stimulant medication use in children: A 12-year perspective. *Am. J. Psychiatry* **169**, 160–166 (2012).

380. Mazei-Robison, M. S. *et al.* Anomalous Dopamine Release Associated with a Human Dopamine Transporter Coding Variant. *J. Neurosci.* **28**, 7040–7046 (2008).
381. Jones, S. R., Gainetdinov, R. R., Wightman, R. M. & Caron, M. G. Mechanisms of amphetamine action revealed in mice lacking the dopamine transporter. *J. Neurosci.* **18**, 1979–1986 (1998).
382. Sitte, H. H. & Freissmuth, M. Amphetamines, new psychoactive drugs and the monoamine transporter cycle. *Trends in Pharmacological Sciences* **36**, (2015).
383. Tomlinson, M. J. *et al.* Identification of the benztropine analog [125I]GA II 34 binding site on the human dopamine transporter. *Neurochem. Int.* 1–12 (2018). doi:10.1016/j.neuint.2018.08.008
384. Sitte, H. H., Reither, H., Singer, A. & Pifi, C. Carrier-Mediated Release, Transport Rates, and Charge Transfer Induced by Amphetamine, Tyramine, and Dopamine in Mammalian Cells Transfected with the Human Dopamine Transporter. *J. Neurochem.* **71**, 1289–1297 (1998).
385. Volz, T. J., Hanson, G. R. & Fleckenstein, A. E. The role of the plasmalemmal dopamine and vesicular monoamine transporters in methamphetamine-induced dopaminergic deficits. *J. Neurochem.* **101**, 883–888 (2007).
386. Tulloch, L. B. *et al.* The inhibitory effect of phospholemman on the sodium pump requires its palmitoylation. *J. Biol. Chem.* **286**, 36020–36031 (2011).
387. Singaraja, R. R. *et al.* Palmitoylation of ATP-binding cassette transporter A1 Is essential for its trafficking and function. *Circ. Res.* **105**, 138–147 (2009).
388. Gu, H. M., Li, G., Gao, X., Berthiaume, L. G. & Zhang, D. W. Characterization of palmitoylation of ATP binding cassette transporter G1: Effect on protein trafficking and function. *Biochim. Biophys. Acta - Mol. Cell Biol. Lipids* **1831**, 1067–1078 (2013).
389. Khelashvili, G. *et al.* Spontaneous Inward Opening of the Dopamine Transporter Is Triggered by PIP₂-Regulated Dynamics of the N-Terminus. *ACS Chem. Neurosci.* **6**, 1825–1837 (2015).
390. Khelashvili, G. *et al.* Computational modeling of the N-terminus of the human dopamine transporter and its interaction with PIP₂-containing membranes. *Proteins Struct. Funct. Bioinforma.* **83**, 952–969 (2015).
391. Buchmayer, F. *et al.* Amphetamine actions at the serotonin transporter rely on the availability of phosphatidylinositol-4,5-bisphosphate. *Proc. Natl. Acad. Sci.* **110**, 11642–11647 (2013).
392. Berthiaume, L. & Resh, M. D. Biochemical characterization of a palmitoyl

- acyltransferase activity that palmitoylates myristoylated proteins. *J. Biol. Chem.* **270**, 22399–22405 (1995).
393. Hancock, J. F., Magee, A. I., Childs, J. E. & Marshall, C. J. All ras proteins are polyisoprenylated but only some are palmitoylated. *Cell* **57**, 1167–1177 (1989).
 394. Mumby, S. M., Kleuss, C. & Gilman, A. G. Receptor regulation of G-protein palmitoylation. *Proc. Natl. Acad. Sci.* **91**, 2800–2804 (2006).
 395. Navarro-Lérida, I. *et al.* A palmitoylation switch mechanism regulates Rac1 function and membrane organization. *EMBO J.* **31**, 534–551 (2012).
 396. Alland, L., Peseckis, S. M., Atherton, R. E., Berthiaume, L. & Resh, M. D. Dual myristylation and palmitoylation of Src family member p59(fyn) affects subcellular localization. *J. Biol. Chem.* **269**, 16701–16705 (1994).
 397. Bahouth, S. W. & Nooh, M. M. Barcoding of GPCR trafficking and signaling through the various trafficking roadmaps by compartmentalized signaling networks. *Cell. Signal.* **36**, 42–55 (2017).
 398. Block, E. R. *et al.* Brain Region-Specific Trafficking of the Dopamine Transporter. *J. Neurosci.* **35**, 12845–58 (2015).
 399. Segal-Salto, M., Sapir, T. & Reiner, O. Reversible cysteine acylation regulates the activity of human palmitoyl-protein thioesterase 1 (PPT1). *PLoS One* **11**, 1–18 (2016).
 400. Lehtovirta, M. Palmitoyl protein thioesterase (PPT) localizes into synaptosomes and synaptic vesicles in neurons: implications for infantile neuronal ceroid lipofuscinosis (INCL). *Hum. Mol. Genet.* **10**, 69–75 (2001).
 401. Greaves, J. & Chamberlain, L. H. S-acylation by the DHHC protein family. *Biochem. Soc. Trans.* **38**, 522–524 (2010).
 402. Bartels, D. J., Mitchell, D. A., Dong, X. & Deschenes, R. J. Erf2, a Novel Gene Product That Affects the Localization and Palmitoylation of Ras2 in *Saccharomyces cerevisiae*. *Mol. Cell. Biol.* **19**, 6775–6787 (1999).
 403. Kim, S. J. *et al.* Palmitoyl protein thioesterase-1 deficiency impairs synaptic vesicle recycling at nerve terminals, contributing to neuropathology in humans and mice. *J. Clin. Invest.* **118**, 3075–3086 (2008).
 404. Veit, M., Söllner, T. H. & Rothman, J. E. Multiple palmitoylation of synaptotagmin and the t-SNARE SNAP-25. *FEBS Lett.* **385**, 119–123 (1996).
 405. Jennifer Greaves, Gerald R. Prescott, Yuko Fukata, Masaki Fukata, Christine Salaun, and L. H. C. The Hydrophobic Cysteine-rich Domain of SNAP25 Couples with Downstream Residues to Mediate Membrane Interactions and Recognition by DHHC Palmitoyl Transferases. *Mol. Biol. Cell* **20**, 1845–1854 (2009).

406. Greaves, J., Gorleku, O. A., Salaun, C. & Chamberlain, L. H. Palmitoylation of the SNAP25 protein family: Specificity and regulation by DHHC palmitoyl transferases. *J. Biol. Chem.* **285**, 24629–24638 (2010).
407. Greaves, J. & Chamberlain, L. H. Differential palmitoylation regulates intracellular patterning of SNAP25. *J. Cell Sci.* **124**, 1351–1360 (2011).
408. Chamberlain, J. G. and L. H. Dual Role of the Cysteine-String Domain in Membrane Binding and Palmitoylation-dependent Sorting of the Molecular Chaperone Cysteine-String Protein. *Mol. Biol. Cell* **17**, 4748–4759 (2006).
409. Greaves, J., Salaun, C., Fukata, Y., Fukata, M. & Chamberlain, L. H. Palmitoylation and membrane interactions of the neuroprotective chaperone cysteine-string protein. *J. Biol. Chem.* **283**, 25014–25026 (2008).
410. Veit, M., Becher, A. & Ahnert-Hilger, G. Synaptobrevin 2 is palmitoylated in synaptic vesicles prepared from adult, but not from embryonic brain. *Mol. Cell. Neurosci.* **15**, 408–416 (2000).
411. Chapman, E. R. *et al.* Fatty Acylation of Synaptotagmin in PC12 Cells and Synaptosomes vesicle membrane once . They possess short amino-terminal intravesicular domains and large residues at the transmembrane-cytoplasmic domain border followed by a highly basic region brane span. *Biochem. Biophys. Res. Commun.* **332**, 326–332 (1996).
412. Heindel, U., Schmidt, M. F. G. & Veit, M. Palmitoylation sites and processing of synaptotagmin I, the putative calcium sensor for neurosecretion. *FEBS Lett.* **544**, 57–62 (2003).
413. Kang, R. *et al.* Presynaptic trafficking of synaptotagmin I is regulated by protein palmitoylation. *J. Biol. Chem.* **279**, 50524–50536 (2004).
414. Runkle, K. B. *et al.* Inhibition of DHHC20-Mediated EGFR Palmitoylation Creates a Dependence on EGFR Signaling. *Mol. Cell* **62**, 385–396 (2016).
415. Ingram, S. L., Prasad, B. M. & Amara, S. G. Dopamine transporter-mediated conductances increase excitability of midbrain dopamine neurons. *Nat. Neurosci.* **5**, 971–978 (2002).
416. Ebersole, B. *et al.* Effect of C-Terminal S-palmitoylation on D2 dopamine receptor trafficking and stability. *PLoS One* **10**, 1–23 (2015).
417. Cartier, E. *et al.* Rare Autism-Associated Variants Implicate Syntaxin 1 (STX1 R26Q) Phosphorylation and the Dopamine Transporter (hDAT R51W) in Dopamine Neurotransmission and Behaviors. *EBioMedicine* **2**, 135–146 (2015).
418. Resh, M. D. Targeting protein lipidation in disease. *Trends Mol. Med.* **18**, 206–214 (2012).
419. Cho, E. & Park, M. Palmitoylation in Alzheimer’s disease and other

- neurodegenerative diseases. *Pharmacol. Res.* **111**, 133–151 (2016).
420. Hull, R. N., Cherry, W. R. & Weaver, G. W. The origin and characterization of a pig kidney cell strain. *In Vitro* **12**, 670–677 (1976).
 421. Gu, H., Wall, S. C. & Rudnick, G. Stable expression of biogenic amine transporters reveals differences in inhibitor sensitivity, kinetics, and ion dependence. *J. Biol. Chem.* **269**, 7124–7130 (1994).
 422. Yang, M. Projected number of people with Parkinson disease in the most populous nations, 2005 through 2030. *Neurology* **68**, 384–6 (2002).
 423. Lorraine V Kalia, A. & Lang, ony E. Parkinson's Disease. *Lancet* **386**, 869–912 (2015).
 424. Matzuk, M. M. & Saper, C. B. Preservation of hypothalamic dopaminergic neurons in Parkinson's disease. *Ann. Neurol.* **18**, 552–555 (1985).
 425. M.H., P. *et al.* Mutation in the α -synuclein gene identified in families with Parkinson's disease. *Science (80-)*. **276**, 2045–2047 (1997).
 426. Blochberger, A. & Jones, S. Parkinson's disease clinical features and diagnosis. *Clin. Pharm.* **3**, 361–366 (2011).
 427. Scherman, D. *et al.* Striatal dopamine deficiency in parkinson's disease: Role of aging. *Ann. Neurol.* **26**, 551–557 (1989).
 428. Postuma, R. B. *et al.* Identifying prodromal Parkinson's disease: Pre-Motor disorders in Parkinson's disease. *Mov. Disord.* **27**, 617–626 (2012).
 429. T.K., K. *et al.* The spectrum of nonmotor symptoms in early Parkinson disease. *Neurology* **80**, 276–281 (2013).
 430. Ibarretxe-Bilbao, N. *et al.* Olfactory impairment in Parkinson's disease and white matter abnormalities in central olfactory areas: A voxel-based diffusion tensor imaging study. *Mov. Disord.* **25**, 1888–1894 (2010).
 431. Carlos H. Schenck, Scott R. Bundlie, M. W. M. Delayed Emergence of a Parkinsonian Disorder in 38% of 29 Older Men Initially Diagnosed with Idiopathic Rapid Eye Movement Sleep Behavior Disorder. *Neurology* **46**, 388–393 (1996).
 432. Iranzo, A. *et al.* Rapid-eye-movement sleep behaviour disorder as an early marker for a neurodegenerative disorder: a descriptive study. *Lancet Neurol.* **5**, 572–577 (2006).
 433. R.D., A. *et al.* Frequency of bowel movements and the future risk of Parkinson's disease. *Neurology* **57**, 456–462 (2001).
 434. Savica, R. *et al.* Medical records documentation of constipation preceding Parkinson disease: A case-control study. *Neurology* **73**, 1752–1758 (2009).
 435. Ishihara, L. & Brayne, C. A systematic review of depression and mental

- illness preceding Parkinson's disease. *Acta Neurol. Scand.* **113**, 211–220 (2006).
436. Santamaria, J., Tolosa, E. & Valles, A. Parkinson's disease with depression: A possible subgroup of idiopathic parkinsonism. *Neurology* **36**, 1130–1133 (1986).
 437. Connolly, B. S. & Lang, A. E. Pharmacological treatment of Parkinson disease: A review. *JAMA - J. Am. Med. Assoc.* **311**, 1670–1683 (2014).
 438. Ferreira, J. J. *et al.* Summary of the recommendations of the EFNS/MDS-ES review on therapeutic management of Parkinson's disease. *Eur. J. Neurol.* **20**, 5–15 (2013).
 439. Hely, M. A., Morris, J. G. L., Reid, W. G. J. & Trafficante, R. Sydney Multicenter Study of Parkinson's disease: Non-L-dopa-responsive problems dominate at 15 years. *Mov. Disord.* **20**, 190–199 (2005).
 440. Hely, M. A., Reid, W. G. J., Adena, M. A., Halliday, G. M. & Morris, J. G. L. The Sydney Multicenter Study of Parkinson's disease: The inevitability of dementia at 20 years. *Mov. Disord.* **23**, 837–844 (2008).
 441. Wood-Kaczmar, A., Gandhi, S. & Wood, N. W. Understanding the molecular causes of Parkinson's disease. *Trends Mol. Med.* **12**, 521–528 (2006).
 442. Noyce, A. J. *et al.* Meta-Analysis of Early Nonmotor Features and Risk Factors for Parkinson Disease. *Ann. Neurol.* **72**, 893–901 (2012).
 443. Bose, A. & Beal, M. F. Mitochondrial dysfunction in Parkinson's disease. *J. Neurochem.* **1802**, 216–231 (2016).
 444. Tansey, M. G. & Goldberg, M. S. Neuroinflammation in Parkinson's disease: Its role in neuronal death and implications for therapeutic intervention. *Neurobiol. Dis.* **37**, 510–518 (2010).
 445. Miyazaki, I. & Asanuma, M. Dopaminergic neuron-specific oxidative stress caused by dopamine itself. *Acta Med. Okayama* **62**, 141–150 (2008).
 446. Nirenberg, M. J., Vaughan, R. A., Uhl, G. R., Kuhar, M. J. & Pickeli, V. M. The Dopamine Transporter Is Localized to Dendritic and Axonal Plasma Membranes of Nigrostriatal Dopaminergic Neurons. *J. Neurosci.* **76**, 436–447 (1996).
 447. German, D. C., Manaye, K., Smith, W. K., Woodward, D. J. & Saper, C. B. Midbrain Dopaminergic Cell Loss in Parkinson's Disease: Computer Visualization. *Ann. Neurol.* **26**, 507–514 (1989).
 448. Uhl, G. R., Hedreen, J. C. & Price, D. L. Parkinson's Disease: Loss of Neurons from the Ventral Tegmental Area Contralateral to Therapeutic Surgical Lesions. *Neurology* **35**, 1215–1218 (1985).

449. Cerruti, C., Walther, D. M., Kuhar, M. J. & Uhl, G. R. Dopamine transporter mRNA expression is intense in rat midbrain neurons and modest outside midbrain. *Mol. Brain Res.* **18**, 181–186 (1993).
450. Uhl, G. R., Walther, D., Mash, D., Faucheux, B. & Javoy-Agid, F. Dopamine Transporter Messenger RNA in Parkinson's Disease and Control Substantia Nigra Neurons. *Ann. Neurol.* **35**, 494–498 (1994).
451. Hurd, Y. L., Pristupa, Z. B., Herman, M. M. & Kleinman, J. E. The Dopamine Transporter and Dopamine D2 Receptor Messenger RNAs Are Differentially Expressed in Limbic- and Motor-related Subpopulations of Human Mesencephalic Neurons. *Neuroscience* **63**, 357–362 (1994).
452. Freed, C. *et al.* Dopamine Transporter Immunoreactivity in Rat Brain. *J. Comp. Neurol.* **349**, 340–349 (1995).
453. Revay, R., Vaughan, R., Grant, S. & Kuhar, M. J. Dopamine Transporter Immunohistochemistry in Median Eminence, Amygdala, and Other Areas of the Rat Brain. *Synapse* **22**, 93–99 (1996).
454. Uhl, G. R. Hypothesis: The Role of Dopaminergic Transporters in Selective Vulnerability of Cells in Parkinson's Disease. *Ann. Neurol.* **43**, 555–560 (1998).
455. Bové, J. & Perier, C. Neurotoxin-based models of Parkinson's disease. *Neuroscience* **211**, 51–76 (2012).
456. Soto-Otero, R., Mendez-Alvarez, E., Hermida-Ameijeiras, A., Munoz-Patino, A. M. & Labandeira-garcia, J. L. Autoxidation and Neurotoxicity of 6-Hydroxydopamine in the Presence of Some Antioxidants: Potential Implication in Relation to the Pathogenesis of Parkinson's Disease. *J. Neurochem.* **74**, 1605–1612 (2000).
457. Yelena Glinka, M. Gassen, M. B. H. Y. Mechanism of 6-Hydroxydopamine Neurotoxicity. *J. Neural Transm.* **50**, 55–66 (1997).
458. Saner, A. & Thoenen, H. Model Experiments on the Molecular Mechanism of Action of 6-Hydroxydopamine. *Mol. Pharmacol.* **7**, 147–154 (1971).
459. Borisenko, G. G., Kagan, V. E., Hsia, C. J. C. & Schor, N. F. Interaction between 6-Hydroxydopamine and Transferrin: "Let My Iron Go". *Biochemistry* **39**, 3392–3400 (2000).
460. Ben-Shachar, D., Eshel, G., Finberg, J. & Youdim, M. The Iron Chelator Desferrioxamine (Desferal) Retards 6-Hydroxydopamine Induced Degeneration of Nigrostriatal Dopamine Neurons. *J. Neurochem.* **56**, 1441–1444 (1991).
461. Glinka, Y., Tipton, K. F. & Youdim, M. B. H. Nature of Inhibition of Mitochondrial Respiratory Complex I by 6-Hydroxydopamine. *J. Neurochem.* **66**, 2004–2010 (1996).

462. Glinka, Y., Tipton, K. F. & Youdim, M. B. H. Mechanism of Inhibition of Mitochondrial Respiratory Complex I by 6-Hydroxydopamine and its Prevention by Desferrioxamine. *Eur. J. Pharmacol.* **351**, 121–129 (1998).
463. D. Hernandez-Baltazar, L.M. Zavala-Flores, A. V.-O. The 6-hydroxydopamine model and parkinsonian pathophysiology: Novel findings in an older model. *Neurol. (English Ed.)* **32**, 533–539 (2017).
464. Ransom, B. R., Kunis, D. M., Irwin, I. & Langston, J. W. Astrocytes convert the parkinsonism inducing neurotoxin, MPTP, to its active metabolite, MPP+. *Neurosci. Lett.* **75**, 323–328 (1987).
465. W.J. Brooks, M.F. Jarvis, G. C. W. Astrocytes as a Primary Locus for the Conversion of MPTP into MPP+. *J. Neural Transm.* **76**, 1–12 (1989).
466. Cui, M. *et al.* The organic cation transporter-3 is a pivotal modulator of neurodegeneration in the nigrostriatal dopaminergic pathway. *Proc. Natl. Acad. Sci. U. S. A.* **106**, 8043–8048 (2009).
467. Inazu, M., Takeda, H. & Matsumiya, T. Expression and functional characterization of the extraneuronal monoamine transporter in normal human astrocytes. *J. Neurochem.* **84**, 43–52 (2003).
468. Moriyama, Y., Amakatsu, K. & Futai, M. Uptake of the neurotoxin, 4-methylphenylpyridinium, into chromaffin granules and synaptic vesicles: A proton gradient drives its uptake through monoamine transporter. *Archives of Biochemistry and Biophysics* **305**, 271–277 (1993).
469. Speciale, S. G., Liang, C. L., Sonsalla, P. K., Edwards, R. H. & German, D. C. The neurotoxin 1-methyl-4-phenylpyridinium is sequestered within neurons that contain the vesicular monoamine transporter. *Neuroscience* **84**, 1177–1185 (1998).
470. Lotharius, J. & O'Malley, K. L. The Parkinsonism-inducing Drug 1-Methyl-4-phenylpyridinium Triggers Intracellular Dopamine Oxidation. *J. Biol. Chem.* **275**, 38581–38588 (2000).
471. Blum, D. *et al.* Molecular Pathways Involved in the Neurotoxicity of 6-OHDA, Dopamine and MPTP: Contribution to the Apoptotic Theory in Parkinson's Disease. *Prog. Neurobiol.* **65**, 135–172 (2001).
472. Schapira, A. H. V. Evidence for Mitochondria1 Dysfunction in Parkinson's Disease-A Critical Appraisal. *Mov. Disord.* **9**, 125–138 (1994).
473. Qureshi, H. Y. & Paudel, H. K. Parkinsonian neurotoxin 1-methyl-4-phenyl-1,2,3,6-tetrahydropyridine (MPTP) and α -synuclein mutations promote tau protein phosphorylation at Ser262 and destabilize microtubule cytoskeleton in Vitro. *J. Biol. Chem.* **286**, 5055–5068 (2011).
474. Cappelletti, G., Maggioni, M. G. & Maci, R. Influence of MPP+ on the state of tubulin polymerisation in NGF- differentiated PC12 cells. *J. Neurosci. Res.* **56**, 28–35 (1999).

475. Serra, P. A., Pluchino, S., Marchetti, B., Desole, M. S. & Miele, E. The MPTP mouse model: Cues on DA release and neural stem cell restorative role. *Park. Relat. Disord.* **14**, 189–193 (2008).
476. Choi, S. J. *et al.* Changes in neuronal dopamine homeostasis following 1-methyl-4-phenylpyridinium (MPP⁺) exposure. *J. Biol. Chem.* **290**, 6799–6809 (2015).
477. Cohen, G. Oxy-Radical Toxicity in Catecholamine Neurons. *Neurotoxicology* **5**, 77–82 (1984).
478. Javitch, J. a, D'Amato, R. J., Strittmatter, S. M. & Snyder, S. H. Parkinsonism-inducing neurotoxin, N-methyl-4-phenyl-1,2,3,6 - tetrahydropyridine: uptake of the metabolite N-methyl-4-phenylpyridine by dopamine neurons explains selective toxicity. *Proc. Natl. Acad. Sci. U. S. A.* **82**, 2173–2177 (1985).
479. Bezard, E. *et al.* Absence of MPTP-induced neuronal death in mice lacking the dopamine transporter. *Exp. Neurol.* **155**, 268–273 (1999).
480. Obata, T. Dopamine efflux by MPTP and hydroxyl radical generation. *J. Neural Transm.* **109**, 1159–1180 (2002).
481. Richards, T. L. & Zahniser, N. R. Rapid substrate-induced down-regulation in function and surface localization of dopamine transporters: Rat dorsal striatum versus nucleus accumbens. *J. Neurochem.* **108**, 1575–1584 (2009).
482. Saunders, C. *et al.* Amphetamine-induced loss of human dopamine transporter activity: an internalization-dependent and cocaine-sensitive mechanism. *Proc. Natl. Acad. Sci. U. S. A.* **97**, 6850–5 (2000).
483. Gulley, J. M., Doolen, S. & Zahniser, N. R. Brief, repeated exposure to substrates down-regulates dopamine transporter function in *Xenopus* oocytes in vitro and rat dorsal striatum in vivo. *J. Neurochem.* **83**, 400–411 (2002).
484. Chi, L. & Reith, M. E. A. Substrate-Induced Trafficking of the Dopamine Transporter in Heterologously Expressing Cells and in Rat Striatal Synaptosomal Preparations. *J. Pharmacol. Exp. Ther.* **307**, 729–736 (2003).
485. Kokoshka, J. M., Vaughan, R. A., Hanson, G. R. & Fleckenstein, A. E. Nature of methamphetamine-induced rapid and reversible changes in dopamine transporters. *Eur. J. Pharmacol.* **361**, 269–275 (1998).
486. Sandoval, V., Riddle, E. L., Ugarte, Y. V., Hanson, G. R. & Fleckenstein, A. E. Methamphetamine-Induced Rapid and Reversible Changes in Dopamine Transporter Function: An In Vitro Model. *J. Neurosci.* **21**, 1413–1419 (2018).
487. Furman, C. A. *et al.* Dopamine and Amphetamine Rapidly Increase

- Dopamine Transporter Trafficking to the Surface: Live-Cell Imaging Using Total Internal Reflection Fluorescence Microscopy. *J. Neurosci.* **29**, 3328–3336 (2009).
488. Gorentla, B. K. & Vaughan, R. A. Differential effects of dopamine and psychoactive drugs on dopamine transporter phosphorylation and regulation. *Neuropharmacology* **49**, 759–768 (2005).
 489. Zahniser, N. R. & Sorkin, A. Rapid regulation of the dopamine transporter: Role in stimulant addiction? *Neuropharmacology* **47**, 80–91 (2004).
 490. Staal, R. G. & Sonsalla, P. K. Inhibition of brain vesicular monoamine transporter (VMAT2) enhances 1-methyl-4-phenylpyridinium neurotoxicity in vivo in rat striata. *J. Pharmacol. Exp. Ther.* **293**, 336–342 (2000).
 491. Staal, R. G., Hogan, K. A., Liang, C. L., German, D. C. & Sonsalla, P. K. In vitro studies of striatal vesicles containing the vesicular monoamine transporter (VMAT2): rat versus mouse differences in sequestration of 1-methyl-4-phenylpyridinium. *J. Pharmacol. Exp. Ther.* **293**, 329–335 (2000).
 492. Eiden, L. E. & Weihe, E. VMAT2: A dynamic regulator of brain monoaminergic neuronal function interacting with drugs of abuse. *Ann. N. Y. Acad. Sci.* **1216**, 86–98 (2011).
 493. Schuldiner, S., Steiner-Mordoch, S., Yelin, R., Wall, S. C. & Rudnick, G. Amphetamine derivatives interact with both plasma membrane and secretory vesicle biogenic amine transporters. *Mol. Pharmacol.* **44**, 1227–1231 (1993).
 494. Caudle, W. M. *et al.* Reduced Vesicular Storage of Dopamine Causes Progressive Nigrostriatal Neurodegeneration. *J. Neurosci.* **27**, 8138–8148 (2007).
 495. Neve, K. A., Janowsky, A., Eshleman, A. J. & Henningsen, R. A. Release of dopamine via the human transporter. *Mol. Pharmacol.* **45**, 312–316 (1994).
 496. Groves, P. M. & Linder, J. C. Dendro-Dendritic Synapses in Substantia Nigra: Descriptions Based on Analysis of Serial Sections. *Exp. Brain Res.* **49**, 20–217 (1983).
 497. Wilson, C. J., Groves, P. M. & Fifkova, E. Monoaminergic Synapses, Including Dendro-dendritic Synapses in the Rat Substantia Nigra. *Exp. Brain Res.* **30**, 161–174 (1977).
 498. Groves, P. M., Wilson, C. J., Young, S. J. & Rebec, G. V. Self-Inhibition by Dopaminergic Neurons. *Science (80-)*. **190**, 522–529 (1975).
 499. Geffen, L. B., Jessell, T. M., Cuello, A. C. & Iversen, L. L. Release of dopamine from dendrites in rat substantia nigra. *Nature* **260**, 258–260 (1976).

500. Falkenburger, B. H., Barstow, K. L. & Mintz, I. M. Dendrodendritic Inhibition Through Reversal of Dopamine Transport. *Science* **293**, 2465–2470 (2001).
501. Hoffman, A. F. & Gerhardt, G. A. Differences in pharmacological properties of dopamine release between the substantia nigra and striatum: An in vivo electrochemical study. *J. Pharmacol. Exp. Ther.* **289**, 455–463 (1999).
502. Curtin, K. *et al.* Methamphetamine/amphetamine abuse and risk of Parkinson's disease in Utah: A population-based assessment. *Drug Alcohol Depend.* **146**, 30–38 (2015).
503. Lappin, J. M., Darke, S. & Farrell, M. Methamphetamine use and future risk for Parkinson's disease: Evidence and clinical implications. *Drug Alcohol Depend.* **187**, 134–140 (2018).
504. Garwood, E. R., Bekele, W., McCulloch, C. E. & Christine, C. W. Amphetamine exposure is elevated in Parkinson's disease. *Neurotoxicology* **27**, 1003–1006 (2006).
505. Callaghan, R. C., Cunningham, J. K., Sykes, J. & Kish, S. J. Increased risk of Parkinson's disease in individuals hospitalized with conditions related to the use of methamphetamine or other amphetamine-type drugs. *Drug Alcohol Depend.* **120**, 35–40 (2012).
506. Bizzozero, O. A., Bixler, H. A. & Pastuszyn, A. Structural determinants influencing the reaction of cysteine-containing peptides with palmitoyl-coenzyme A and other thioesters. *Biochim. Biophys. Acta - Protein Struct. Mol. Enzymol.* **1545**, 278–288 (2001).
507. Konno, S. *et al.* A Chemoproteomics Approach to Investigate Phosphopantetheine Transferase Activity at the Cellular Level. *ChemBioChem* **18**, 1855–1862 (2017).
508. James, A. M. *et al.* Non-enzymatic N-acetylation of Lysine Residues by AcetylCoA Often Occurs via a Proximal S-acetylated Thiol Intermediate Sensitive to Glyoxalase II. *Cell Rep.* **18**, 2105–2112 (2017).
509. Percher, A. *et al.* Mass-tag labeling reveals site-specific and endogenous levels of protein S-fatty acylation. *Proc. Natl. Acad. Sci.* **113**, 4302–4307 (2016).